WIND-POWERED MEMBRANE DESALINATION OF BRACKISH WATER

Gavin Lawrence Park, MEng

Submitted for the degree of Doctor of Philosophy

Heriot-Watt University

School of Engineering and Physical Sciences

Department of Mechanical Engineering

Edinburgh, United Kingdom

May 2012

Abstract

This thesis presents a detailed investigation of the technical feasibility, challenges and performance issues associated with the direct-connection of a wind turbine to a membrane (wind-membrane) system for treating brackish water in remote communities. The direct-connection of these two technologies negates the reliance on energy storage in batteries, which are traditionally used, but result in reduced system efficiency and increased life-cycle costs. Furthermore, the lack of knowledge of the safe operating window in which transient operation of membrane systems is beneficial or tolerable can be addressed.

The impact of wind speed fluctuations on the performance of the wind-membrane system (using a BW30-4040 membrane and feed waters of 2750 and 5500 mg/L NaCl) showed that the performance deteriorated most under fluctuations at low average wind speeds with high turbulence intensity and long periods of oscillation. Therefore, the main challenge of operating with renewable energy is not the size of the fluctuations, but the effect of the power switching off. Further examination of the impact of wind intermittency (over one hour intervals with intermittent periods from 0.5 – 3 min) showed that the increase in permeate concentration was highest at off-times < 60 s, highlighting the potential for improved performance using short-term energy buffering.

The safe operating window and the key constraints to safe operation were determined for several membranes and feed water concentrations to establish the optimum operating strategy for the wind-membrane system. Supercapacitors were used to expand the safe operating window by providing energy during periods of intermittency and enhancing the power quality delivered to the membrane system by absorbing wind fluctuations. When tested over 24 hours using real wind speed data (average 6 m/s), the wind-membrane system produced 0.78 m^3 of water with an average permeate concentration of 240 mg/L NaCl and average specific energy consumption (SEC) of 5.2 kWh/m^3. With the addition of supercapacitor storage, the system performance improved significantly with 0.93 m^3 of water produced with an average permeate concentration of 170 mg/L NaCl and SEC of 3.2 kWh/m^3.

Acknowledgements

As with most people, this PhD has been a defining experience for me, both from an intellectual and a personal point of view. There are many people whom I would like to thank for making this PhD a success, for valuable assistance along the way and for the essential aspect of moral support. Thank you to my supervisors Bryce Richards (Heriot-Watt University) and Andrea Schäfer (University of Edinburgh) for making this PhD possible and for providing guidance throughout this exciting research. Your knowledge and experience have been invaluable and I appreciate the standards that you uphold.

Special thanks to Jack Gilron (external) and Matt Dunnigan (internal) for agreeing to be my PhD viva examiners and for the thorough and interesting discussion.

I would like to thank the Scottish Enterprise for funding the use of their wind tunnel facility at the Energy Technology Centre and TUV NEL for their technical support and consultation throughout the period of testing. My thanks to Ronald Millar and Curtis Abbott for all of their technical support and consultation throughout this project. I have happy memories of setting up wind turbines and carrying heavy lead acid batteries in the wind and rain together! I would like to thank the MSc and MEng students whom I have worked with and who have contributed to this research: Olivier Bertrand, Thomas Pietzsch, Sean Reid, Donagh Goulding, Pauline Trancart and Shin Ding Huang. A very special mention for Pierre Besson, I hope we have many more adventures together!

My heartfelt thanks goes to Laura Richards who has been an excellent colleague and an even better friend, I wish you all the very best for your future. Special thanks to Dave Ross for all of our interesting chats and your support over the years. I have also been fortunate enough to meet and work with Pas who has been very generous with his technical expertise and is a true friend. To Rebecca, Mark, Kris, Ash, Em, Ian, Ginny and the Malta crew, thanks for your friendship and the fun times.

My particular thanks to a small group of very special people. To my family for all of their love and support. Most importantly to Bren, my lovely, banterful companion for whom words cannot express my gratitude, you are precious to me.

ACADEMIC REGISTRY
Research Thesis Submission

Name*:*	Gavin Lawrence Park		
School/PGI:	Engineering and Physical Sciences, Department of Mechanical Engineering		
Version: *(i.e. First, Resubmission, Final)*	Final	Degree Sought (Award **and** Subject area)	PhD Mechanical Engineering

Declaration

In accordance with the appropriate regulations I hereby submit my thesis and I declare that:

1) the thesis embodies the results of my own work and has been composed by myself
2) where appropriate, I have made acknowledgement of the work of others and have made reference to work carried out in collaboration with other persons
3) the thesis is the correct version of the thesis for submission and is the same version as any electronic versions submitted*.
4) my thesis for the award referred to, deposited in the Heriot-Watt University Library, should be made available for loan or photocopying and be available via the Institutional Repository, subject to such conditions as the Librarian may require
5) I understand that as a student of the University I am required to abide by the Regulations of the University and to conform to its discipline.

* *Please note that it is the responsibility of the candidate to ensure that the correct version of the thesis is submitted.*

Signature of Candidate*:*		Date:	

Submission

Submitted By *(name in capitals):*	GAVIN LAWRENCE PARK
Signature of Individual Submitting:	
Date Submitted:	

For Completion in the Student Service Centre (SSC)

Received in the SSC by *(name in capitals):*			
1.1 Method of Submission *(Handed in to SSC; posted through internal/external mail):*			
1.2 E-thesis Submitted (**mandatory for final theses)**			
Signature:		Date:	

Please note this form should bound into the submitted thesis.

Updated February 2008, November 2008, February 2009, January 2011

Contents

List of Tables

List of Figures

Glossary of Terms

Acronyms

EPR – equivalent parallel resistance in supercapacitors (represents current leakage)

ESR – equivalent series resistance in supercapacitors (represents internal resistance)

DAQ – data acquisition system

IEC standard – international electrotechnical commission standards for wind turbines

MCS – microgeneration certification scheme for producing electricity from renewables

MDGs – millennium development goals

MF – microfiltration

MPPT – maximum power point tracker controller for connecting wind turbine to pump

NF – nanofiltration

NGOs – non-governmental organisations

PV – photovoltaic

RE-membrane – renewable energy-powered membrane system

RO – reverse osmosis

ROSA – reverse osmosis system analysis software (Dow Water & Process Solutions)

SEC – specific energy consumption (kWh/m^3)

SOC – state of charge of supercapacitors in terms of available energy (%)

TDS – total dissolved solids in water (mg/L)

TI – turbulence intensity of the wind (-)

TMP – transmembrane pressure (bar)

UF – ultrafiltration

UI – usability index (-)

Wind-membrane – wind-powered membrane system

WHO – world health organisation

WHO guideline – world health organisation drinking water guideline value

Nomenclature

A – amplitude of wind speed fluctuations (m/s)

$A_{membrane}$ – surface area of membrane module (m^2)

A_{swept} – swept surface area of wind turbine blades (m^2)

c – ionic concentration of the feed water (mol/L)

c_w – scale factor for Weibull distribution

C – NaCl concentration of feed, permeate or concentrate stream (mg/L)

C_{bank} – rated capacitance of supercapacitor bank (F)

C_{eff} – aerodynamic conversion efficiency of wind turbine (%)

C_{module} – rated capacitance of supercapacitor module (F)

d – hydraulic diameter of membrane flow passage (m)

D – salt diffusion coefficient in bulk solution (m^2/s)

E_{bank} – energy stored in supercapacitor bank (Wh)

EC – measured electrical conductivity of feed, permeate or concentrate stream (µS/cm)

g – gravitational acceleration (9.81 m/s^2)

H – static pressure head developed by pump (m)

$I_{avg.}$ – average discharge current of supercapacitor bank (A)

I_{pp} – current of pump motor (A)

J_0 – pure water flux measured using deionised water ($L/m^2.h$)

J_s – solute flux ($mg/m^2.h$)

J_v – total volume flux ($L/m^2.h$)

k_d – mass transfer coefficient (m/s)

k_{ec} – conversion factor for electrical conductivity (EC) into NaCl concentration (C)

k_w – shape factor for Weibull distribution

L_p – permeability coefficient for solvent flux ($L/m^2.h.bar$)

$N_{parallel}$ – number of supercapacitor modules in parallel

N_{series} – number of supercapacitor modules in series

Δp – pressure difference between discharge and suction sides of pump (Pa)

$p(U)$ – probability that wind speed will exceed a certain value for Weibull distribution

ΔP – measured transmembrane pressure (bar)

$P_{hydraulic}$ – hydraulic power transferred by pump to the water (W)

P_s – diffusive salt permeability of membrane (m/s)

P_{shaft} – mechanical shaft power supplied by pump motor to pump (W)

P_{wt} – power output from wind turbine (W)

Q – feed flowrate from pump (L/h)

R – retention of NaCl (%)

R_{bank} – internal resistance of supercapacitor bank (μΩ)

R_c – ideal gas constant (0.082 L.bar.K^{-1}.mol^{-1})

Re – Reynolds number (-), for mass transport calculation

Sc – Schmidt number (-), for mass transport calculation

Sh – Sherwood number (-), for mass transport calculation

Δt – amount of energy storage time provided by supercapacitor bank (s)

t_{off} – length of time with zero power (min)

t_{on} – length of time with power on (min)

T – operating temperature of the feed water (K)

T_{ws} – period of oscillation of wind speed fluctuations (s)

u – flow velocity through membrane (m/s)

U – mean wind speed (m/s)

U_z – mean wind speed at hub height z (m/s)

v – kinematic viscosity (m^2/s)

$v(t)$ – wind speed during specific time period (m/s)

V_{max} – maximum voltage output from wind turbine (V_{DC})

V_{pp} – voltage of pump motor (V_{DC})

V_R – rated voltage of supercapacitor bank (V_{DC})

Y – recovery ratio for the membrane (%)

z – hub height of wind turbine (m)

z_0 – surface roughness index for log law

Greek symbols

π – osmotic pressure of feed, permeate or concentrate stream (bar)

β – concentration polarisation modulus (-)

δ – boundary layer thickness (m)

η_{pump} – pump efficiency (%)

ρ_a – air density (kg/m^3)

ρ_w – water density (kg/m^3)

$\Delta\sigma$ – standard deviation of wind speed data set (m/s)

Subscripts

b – bulk solution

c – concentrate solution

m – membrane surface

p – permeate solution

pp – pump motor

sc – supercapacitor bank

v – suction side of pump

wt – wind turbine

Publications resulting from this thesis (to date)

G.L. Park, A.I. Schäfer, B.S. Richards, Renewable energy powered membrane technology: Supercapacitors for buffering resource fluctuations in a wind-powered membrane system, Renewable Energy (accepted with minor corrections April 2012).

G.L. Park, A.I. Schäfer, B.S. Richards, The effect of intermittent operation on a wind-powered membrane system for brackish water desalination, Water Science and Technology, 65 (2012) 867-874.
Presented at the Small Sustainable Solutions for Water (SSS 4 WATER) Conference in Venice, Italy, 18 – 22 April 2011.

G.L. Park, A.I. Schäfer, B.S. Richards, Renewable energy powered membrane technology: The effect of wind speed fluctuations on the performance of a wind-powered membrane system for brackish water desalination, Journal of Membrane Science, 370 (2011) 34-44.

G.L. Park, A.I. Schäfer, B.S. Richards, Potential of wind-powered renewable energy membrane systems for Ghana, Desalination, 248 (2009) 169-176.
Presented at the Water and Sanitation in International Development and Disaster Relief (WSIDDR) International Workshop in Edinburgh, Scotland, 28 – 30 May 2008.

Chapter 1

Introduction

There is a clear need for reliable and affordable water treatment systems that can remove microbial and chemical pollutants from groundwater in off-grid locations. Renewable energy-powered membrane (RE-membrane) systems are promising technologies for the production of potable water in such regions as they exhibit low energy consumption, reliable contaminant removal and modularity. This means they can make efficient use of the local renewable energy resource while meeting the requirements according to the groundwater characteristics and size of the community. Wind turbine-powered (wind-membrane) systems provide a particularly feasible option in many areas of the world that have a good wind resource with average wind speeds of 5 m/s or more. The main challenges associated with the use of wind power are the inherent fluctuations and intermittency of the resource that can cause reduced power quality and transient operation of the membrane system. The effect of transient operation on membrane systems is not well understood and there has been little detailed experimental research performed in this area. Therefore, a systematic investigation of the impact of wind variability and short-term energy buffering on the safe operating window of wind-membrane systems is a significant step towards their implementation.

1.1 Motivation for this research

"The trouble with water – and there is trouble with water – is that they're not making any more of it. They're not making any less, mind, but no more either. There is the same amount of water in the planet now as there was in prehistoric times. People, however, they're making more of – many more,

> *far more than is ecologically sensible – and all those people are utterly dependent on water for their lives (humans consist mostly of water), for their livelihoods, their food, and increasingly, their industry. Humans can live for a month without food but will die in less than a week without water. Humans consume water, discard it, poison it, waste it, and restlessly change the hydrological cycles, indifferent to the consequences: too many people, too little water, water in the wrong places and in the wrong amounts". Marq de Villiers, scientific writer and journalist, 2001 [1].*

As a result of the worldwide water crisis, the United Nations declared the years 2005 to 2015 to be the International Decade for Action 'Water for Life' [2]. The primary goal of this effort is to fulfil international commitments regarding water and related issues by 2015. This includes the Millennium Development Goals (MDGs), one of which aims to reduce by half the proportion of people without sustainable access to safe drinking water and to stop the unsustainable exploitation of water resources [3]. This target has a deadline of 2015 and progress is evaluated on baseline statistics from 1990. The latest MDGs report, published in 2011 with data from 2008, shows that although many areas of the world are ahead of schedule for meeting the MDGs, there are still 884 million people without access to improved water sources, 84 % of whom live in rural areas (Figure 1.1) [3]. The situation is worst in sub-Saharan Africa, where urban dwellers are 1.8 times more likely to have access to safe drinking water than those living in rural areas. Even if the MDGs for water were to be achieved by 2015, there will still be 700 million people without access to safe drinking water [4]. The fact that an estimated 3900 children die every day from diseases related to unsafe drinking water and inadequate sanitation highlights the ongoing severity of this humanitarian crisis and the requirement for a concerted effort by all parties to end this silent injustice [5].

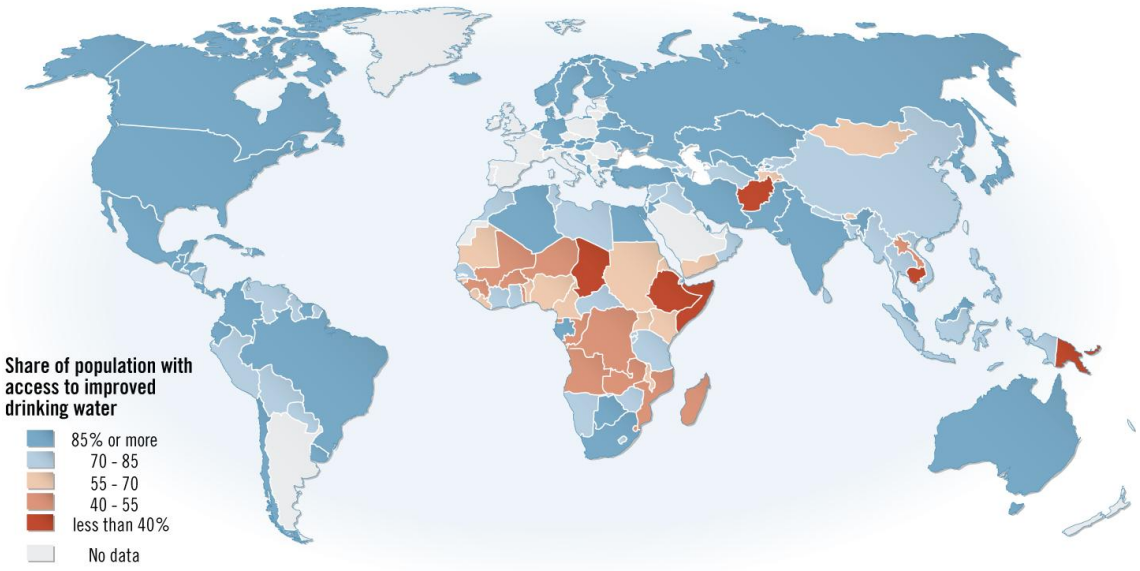

Figure 1.1: Share of population with sustainable access to a safe and easily accessible drinking water supply (2008) [6].

The very nature of rural communities, located away from population centres means that they generally experience reduced management of water supplies and less likelihood of water infrastructure and services [7]. This often results in the use of untreated natural sources (groundwater, lakes, rivers and rainwater) that are often unsafe due to the presence of microbial or chemical pollutants [8]. Community-level water supply solutions are unable to exploit economies of scale resulting in a high cost of water that is generally unfeasible in poorer regions [7]. These problems are compounded by the fact that rural areas are generally not considered during central energy planning, with 1.5 billion people having no access to electricity, 85 % of whom live in rural areas in developing countries [9]. This highlights the requirement for off-grid or energy independent water treatment systems that are able to remove microbial and chemical pollutants [10].

There are several key factors that should be considered when developing a secure and suitable water supply for a rural community [11]:

i. the water quality meets the World Health Organisation (WHO) guidelines regarding contaminants and is therefore safe to drink [12];
ii. there is a reliable supply throughout the year even during periods of drought and high demand;

iii. the supply is accessible to the whole community and within a reasonable distance (~ 1 km); and
iv. the water supply is affordable to all and can be maintained by the community.

1.1.1 Groundwater potential

In developing countries, drinking water is often taken directly from surface water sources without any treatment, resulting in unsafe water due to the presence of viruses, bacteria, protozoa or larvae [13]. These are known to cause about two dozen different infectious diseases that are potentially fatal. Groundwater is often the main alternative to treated surface water, where filtering through layers of soil and rock means it doesn't require disinfection as it is generally free of suspended particles, larger parasites and protozoan cysts [8, 14].

Groundwater is contained beneath the surface of the earth in rocks and soil and constitutes 97 % of global fresh water [15]. The widespread uptake of groundwater is considered the most affordable and sustainable method of providing access to a secure water supply in rural areas [11]. Boreholes of 80 – 100 m in depth are required to reach deep water aquifers and there are many regions where cheap drilling and successful deployment of handpumps have allowed communities to access good quality groundwater. In rural India, a concerted effort by non-governmental organisations (NGOs) and competition between entrepreneurs has reduced the cost of a borehole drilled into hard rock then lined to 10 m and fitted with an India Mark II handpump to £850 [8]. The main advantages of using groundwater in rural areas are as follows [11]:

i. it can be found in most environments and unlike surface water or rainwater is less affected by drought and seasonal variations;
ii. it is generally protected from microbial pollutants which are the main cause of water borne diseases in developing countries [13]; and
iii. it can normally be located close to the point of use, therefore allowing incremental and low cost development while providing a solid platform for management by the local community.

The main concerns associated with the use of groundwater are: i) depletion due to overdraft; ii) waterlogging and salinisation due to inadequate drainage; and,

iii) pollution by agricultural, industrial and other human activities [15, 16]. Contamination of groundwater can be caused by the presence of naturally occurring chemicals (particularly arsenic and fluoride), or shallow wells and boreholes being located near to sources of contamination [7]. Contamination of shallow groundwater aquifers is becoming an increasingly widespread problem in developing countries as a result of rapid industrialisation, expansion of urban populations and intensive agriculture [14]. The leaching of nitrogen rich fertilisers and pesticides from agricultural activities results in an estimated 3 million people being poisoned by pesticides every year causing approximately 220,000 deaths [17]. Figure 1.2 illustrates the extent of the global brackish groundwater resource and its origins resulting from seawater intrusion along coastal regions, dissolved chemical elements and pollution by human activities.

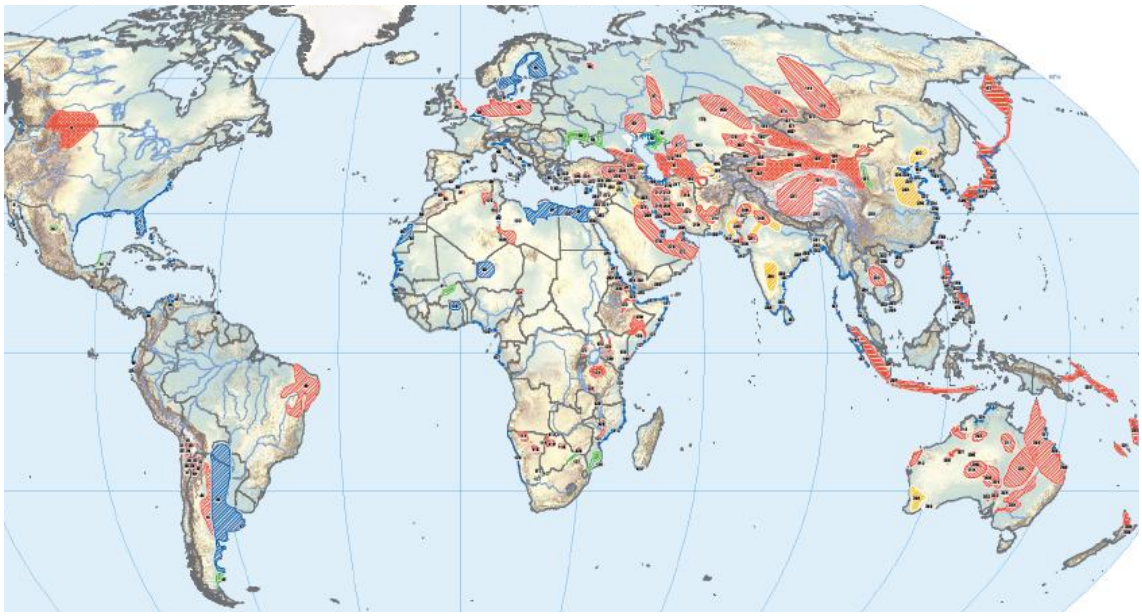

Figure 1.2: Global overview of brackish groundwater occurrence and its origins (2009). Blue shaded regions have resulted from seawater intrusion, red regions from dissolved chemical elements and yellow regions from pollution [18].

The characteristics of groundwater are highly variable as they depend on a complex combination of the local geology, geomorphology/weathering and rainfall patterns (current and historical) [11]. This results in a wide variation in the quantity, quality, accessibility and recharge rate of the groundwater resource. The main chemical solutes (99 %) in natural groundwater are made up of nine chemical elements: sodium, calcium,

magnesium, potassium, bicarbonate, chloride, sulphate, nitrate and silicon [11]. These occur as a result of the chemical reactions between weak carbonic acid (produced from rainwater and carbon dioxide) and minerals from the underlying rocks. While the above chemicals give the groundwater its hydrochemical characteristics, it is the remaining 1 % of chemical constituents that can make the water unsafe for human consumption [11]. To minimise the effects of these chemicals, the WHO has set guideline values for the maximum acceptable concentrations of antimony, arsenic, barium, boron, cadmium, chromium, copper, fluoride, lead, manganese, mercury, molybdenum, nickel, selenium and uranium [12].

Arsenic and fluoride are the most prevalent naturally occurring chemical pollutants and can lead to skin diseases, cancer (arsenic poisoning) or crippling (fluorosis) [7]. These two chemicals alone affect an estimated 100 million people in developing countries [8]. The rapid deployment of shallow boreholes in southern Bangladesh and West Bengal has caused over-extraction and resulted in arsenic leaching from geological strata due to significant lowering of the water table [8]. As a result of this, 1.5 million people out of an estimated 28 – 35 million people in Bangladesh who consume drinking water with elevated levels of arsenic are suffering from skin lesions [19]. Contamination of groundwater by arsenic has also been found in Argentina, Bangladesh, Chile, China, India, Mexico, Thailand and the United States. Fluorosis is caused by the excessive intake of fluoride and there are more than 20 countries worldwide that have a widespread problem with this disease [14]. In China alone, elevated levels of fluorosis have resulted in over 26 million people suffering from dental fluorosis and 1 million from skeletal fluorosis [19].

To compound the problems associated with water quality, a combination of climate change, over-extraction and population growth (6.85 billion in 2010 to 7.52 billion by 2020) is causing increased stress on the earth's limited fresh water reserves [20]. There is strong evidence to suggest that climate change will have an increased impact on groundwater supplies in the future [21]. Rising sea levels may disrupt the freshwater/saline water boundary resulting in increased groundwater salinisation, while prolonged dry periods may lead to higher salt concentrations due to slower rates of recharge. Through a combination of over-extraction, reduced recharge rates and rising

sea levels, brackish water occurrence is expected be an increasing problem even in inland aquifers [21].

1.1.2 Potential of renewable energy-powered membrane systems

There is a growing awareness of the inextricable link between water and energy in modern society as they are both essential to maintain a high quality of human life [22]. The treatment and distribution of potable water depends on low-cost energy and the production of energy requires large volumes of water [23, 24]. With a plentiful and low-cost supply of energy, there can also be a plentiful supply of water by pumping from deep water aquifers, treating municipal discharges or desalinating brackish and sea water to a potable standard. The conventional method of using fossil fuels to produce potable water is not only unsustainable, it results in a worsening of the water scarcity problem as further emissions contribute to climate change causing increased scarcity that in turn requires advances in energy production and exacerbates the current crisis [22]. Therefore, the use of renewable energy is the only sustainable way of providing the required energy to provide potable water and avoid further contribution to the deterioration of the environment. A detailed study of the life cycle assessment of desalination technologies integrated with renewable energy technologies showed that wind-powered plants (150 kW and 2 MW) would produce 75 % less CO_2 emissions than an equivalent fossil fuel powered plant [25]. The remaining 25 % of emissions associated with the wind turbine were a result of fabrication, construction, transportation and decommissioning of the plant.

RE-membrane systems offer one of the most promising options for removing salts as well as microbial and chemical pollutants from groundwater for communities in remote or off-grid locations [7, 26, 27]. The potential market for small-scale RE-membrane systems is potentially very large, with several thousand islands and countless small communities worldwide that have water quality problems and less than 100 inhabitants [28]. Brackish water is most often found in groundwater rather than surface water and it occurs due to naturally saline aquifers, seawater intrusion or anthropogenic influences such as overuse and irrigation [29]. On islands, brackish water often occurs in a transition zone where fresh water from rainfall and surface runoff floats on top of the seawater [30]. Overuse of the fresh water results in further seawater intrusion and

expansion of the brackish water transition zone. Many small communities are located in arid or coastal regions with an abundance of renewable energy resources [23, 31]. The use of an autonomous water treatment system provides stability and security where grid connections are often non-existent or unreliable due to weak grid infrastructure and frequent power cuts [32].

The minimum energy consumption for large-scale seawater reverse osmosis (RO) plants is currently 3.7 kWh/m^3 including all of the pumping requirements and energy recovery [33]. By comparison, the energy requirements of brackish water plants are often in the region of 1 kWh/m^3 or less, depending on the scale of plant, feed water concentration and whether energy recovery is used. A cost comparison of a typical large-scale brackish water RO plant with a seawater RO plant showed that the cost of water was four times higher for the seawater plant [29]. This was caused by the energy consumption of the seawater plant being five times greater due to increased pumping requirements as well as the increased membrane replacement costs due to shorter lifetime caused by the increased rate of fouling associated with seawater [29].

From a social point of view, the integration of RE-membrane systems into communities enforces socioeconomic development by using local resources while avoiding dependence on an external supply of energy [23]. However, their integration into rural communities needs to be carefully managed as new technology is often associated with political status amongst the men which conflicts with the tradition of women being responsible for water management [28]. When projects are not fully integrated into communities such that there is a sense of ownership and responsibility, they often end in failure, therefore further studies on the social aspects of these technologies need to be carried out [34]. Some of the other key issues that prevent membrane systems from being successful in rural communities are the annual maintenance requirements and the lack of trained personnel to carry them out [7]. Governments and NGOs often install systems and then leave without providing the necessary education or setting up an appropriate means of organisation and control to ensure that they can continue to operate. Therefore, any membrane systems that are developed for use in rural communities must take these other non-technical factors into account in order to have any hope of providing a successful solution.

Apart from membrane based desalination, there are several thermal-based processes commonly used for autonomous small-scale desalination systems in remote regions; namely solar stills, solar membrane distillation and solar multiple effect humidification [35]. These thermal based systems are ideal for coupling with solar thermal technologies. However, the main advantage of membrane desalination systems is that they have lower energy consumption, which is ideal for coupling with the electrical output of wind turbines or solar PV modules. The specific energy consumption (SEC), defined as the ratio of the energy required per unit volume of permeate produced is the main gauge of the energy requirements for desalination processes. Membrane technologies require only half as much energy as thermal technologies with values of 1.5 – 4 kWh/m^3 achievable for small-scale brackish water systems [33, 36, 37]. The energy requirements of the plant are of vital importance as they determine the scale of the renewable energy generator required, which translates directly into the capital cost and therefore the cost of water.

The key advantages of using membrane technologies over the other thermal-based processes can be summarised as follows [38, 39]:

i. ability to remove a wide range of contaminants with different membranes;
ii. flexible with regards to water quality and quantity;
iii. highly modular design allows uncomplicated plant design and opportunity for scaling up if required;
iv. no requirement for chemicals;
v. rapid start-up sequence; and
vi. compactness, requiring limited installation space.

These benefits mean that it is relatively straightforward to size and design the RE-membrane system according to the characteristics of the local groundwater, number of inhabitants and the available energy resource. The main challenge associated with the implementation of directly-coupled systems is the optimum matching of the intermittent renewable energy resource with the constant energy demand of the desalination process [35]. This challenge forms the basis for this research and is detailed further in Sections 1.3 – 1.6.

Unfortunately, the wide-scale integration of renewable energy sources with desalination systems has been slow, with less than 1 % of the total installed capacity worldwide utilising renewable energy in comparison to conventional fossil fuel powered plants [40]. This has mainly been due to the increased capital costs associated with renewable energy and the unpredictable nature of the resource, making them uncompetitive with fossil fuels. However, a detailed cost analysis by Bilton *et al.* [36] showed that the feasibility of using RE-membrane systems to treat brackish water in rural locations is often more cost-effective than the equivalent diesel powered system due to rising fossil fuel prices. This was found to be dependent on the renewable energy resource, water salinity and the locality of the site. When the energy resource was poor or the feed water salinity was high, as in the case of seawater, these community-scale RE-membrane systems were not able to achieve a break-even point during their lifetime [36].

Wind energy is the second most widely used renewable energy source for desalination plants after solar energy, which is often used as it provides a much more predictable power output that is well matched to daily water consumption. [41]. However, many high altitude and coastal regions often have a good wind resource as shown in Figure 1.3. The wind speed data in Figure 1.3 is given at a height of 80 m, which is much greater than the height used for small-scale wind power generation (~ 8 m). By allowing for this difference in height, regions that are shaded dark yellow to red would theoretically have a sufficient wind resource of $\geq$ 5 m/s. The resource would also depend on the local topographical and ground cover variations which have a significant impact on the wind speed but cannot be shown on a map of this scale (5 km resolution). Regions that suffer from high levels of unsafe drinking water (Figure 1.1), with brackish groundwater reserves (Figure 1.2) and an adequate wind resource (Figure 1.3) include: sub-Saharan Africa (particularly the horn of Africa), Afghanistan, Mongolia and Papau New Guinea. In these regions with good wind resources, the use of wind-membrane systems can be much more cost effective than the equivalent solar PV powered system for treating brackish water [42, 43]. By applying a mix of renewable energy technologies to provide the energy for membrane desalination systems, this RE-membrane technology can be used all over the globe according to the energy resource in each geographical location.

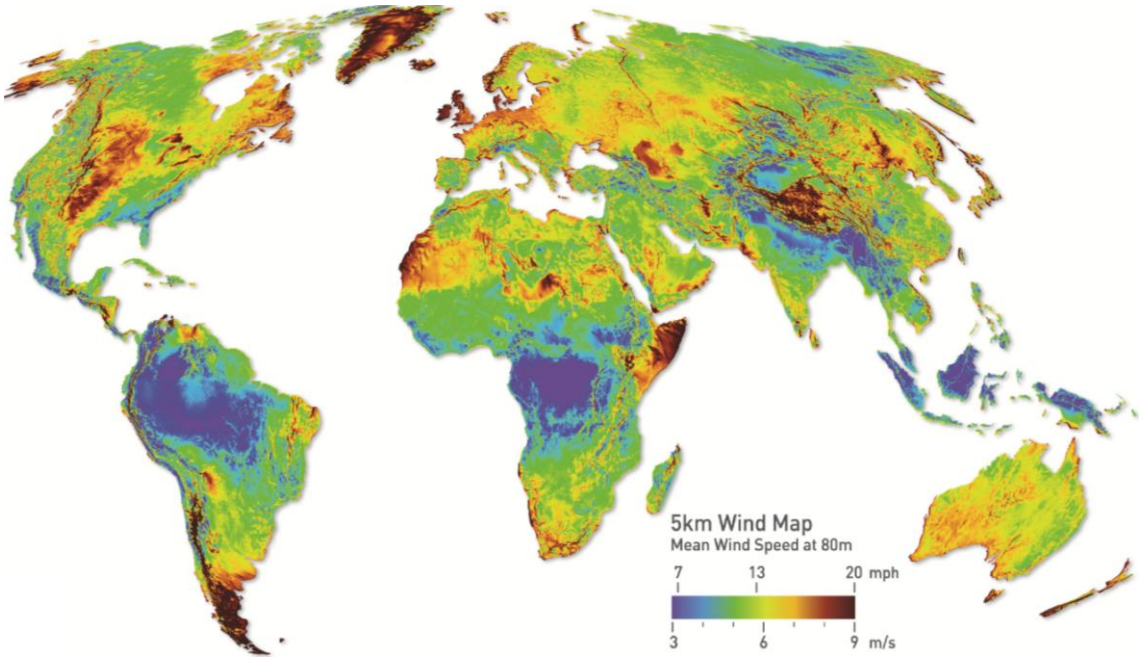

Figure 1.3: Global wind speed resource at a height of 80 m [44]. Regions that are dark yellow to red would have sufficient resource for small-scale wind power generation as they would have an average wind speed ≥ 5 m/s at a height of 8 m.

1.2 Membrane technology

1.2.1 Principles of operation

Membranes were initially developed for water treatment in the late 1960s, where they were first used for brackish water desalination [29]. These early reverse osmosis (RO) membranes required operation at high pressure and were designed to produce very good quality permeate, however this was at the expense of elevated energy consumption [45]. Improvements in membrane materials were required to increase permeability before RO membranes could be applied to seawater desalination. Nanofiltration (NF) membranes were then developed in the 1980s to provide increased water permeability with lower rejection of solutes and reduced energy consumption [46]. Since then, there have been dramatic improvements in membrane materials and technologies resulting in improved performance and reduced costs, such that RO membranes now dominate the worldwide desalination market [29]. The development of ultra-low pressure membranes means that RO desalination is now approaching the minimum theoretical limit of the pressure required to separate water from a salt solution (Section 1.2.2) [33]. The majority of this development however, has been focussed on large-scale water and wastewater treatment

and membrane technology is still largely inaccessible for small-scale systems in developing countries [7].

The principle of RO depends upon applying a hydrostatic pressure in excess of the osmotic pressure of the feed water to reverse the natural action of osmosis [29]. The positive difference in pressure across the membrane creates a concentration gradient that forces the water through the membrane, while salts are retained and concentrated in the concentrate stream. The driving force for water flux through the membrane is the difference between the hydraulic pressure provided by the pump and the trans-membrane osmotic pressure caused by the concentration difference [47]. The driving force for solute permeation is entirely a result of the concentration difference across the membrane. Therefore, the permeate salinity is controlled by the ratio of the water flux to the solute flux, which creates the apparent rejection of solutes.

The solution-diffusion theory describes the transport process through RO membranes according to three separate phases [48]. Water molecules from the feed water adsorb onto the surface of the membrane, then diffuse across the concentration gradient through the membrane and desorb to form the permeate flow. The flowrate through the membrane is dependent upon several factors including the porosity of the membrane; the fraction of void space within the module that can contain liquid; and the tortuosity, which is the ratio of the distance that a molecule must travel through the membrane to the membrane thickness [29]. There are no perfect membranes; therefore salt diffusion also occurs through the membrane with flux dependent on the concentration gradient and temperature of the feed water. RO membranes are able to reject the smallest contaminants (monovalent ions), with typical retention of 95 – 99 % for dissolved salts, inorganic molecules, and organic molecules with a molecular weight > 100 Da [49]. Figure 1.4 illustrates the range of membrane filtration technologies commercially available and their respective pore sizes. Both NF and ultrafiltration (UF) membranes are characterised by the molecular cut-off weight at which the membrane retains 90 % of the solute in solution, which is 250 – 2000 Da for NF and 2000 – 500,000 Da for UF, respectively [29].

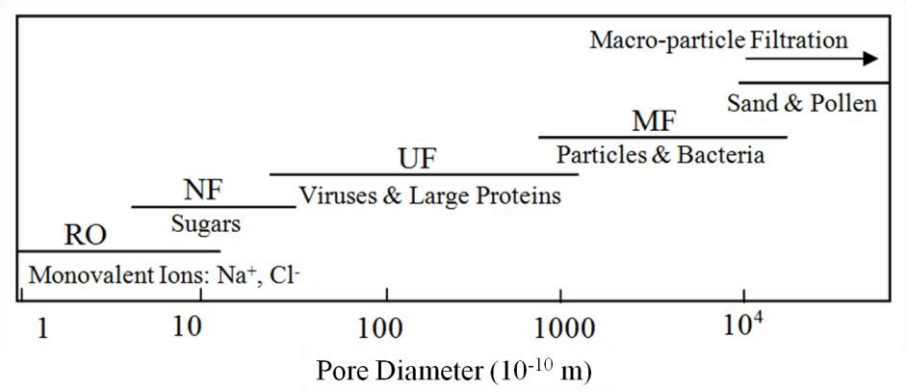

Figure 1.4: The range of pore diameter sizes for commercially available membrane filtration technologies [50].

As mentioned above, NF membranes are characterised by their molecular cut-off weight, and they get their name from the fact that they reject particles in the scale of 1 nm [49]. They can provide effective removal of divalent ions such as magnesium sulphate with typical retention of 90 – 98 %. However, the retention of monovalent ions like chloride salts is much more variable with typical values between 20 – 80 % [49]. The lower retention of monovalent ions distinguishes NF membranes from RO membranes, and gives NF the advantage of lower osmotic pressure and the ability to operate at lower pressures (typically 3.5 – 16 bar) with less energy consumption. NF membranes can also be used to remove fluoride (retention ~ 75 %), arsenic (~ 99 % for both III and V), nitrate (~ 75 %) and certain pesticides (40 – 95 %) depending on the membrane module [45]. They have a wide range of applications but are typically used for removing colour and organic carbon from surface water, removing hardness from groundwater (instead of using lime) and reducing total dissolved solids (TDS) [45].

RO/NF membranes are most commonly available as spiral wound modules with the membrane sheets wound around a perforated central tube that is used to collect the permeate flow (Figure 1.5) [29]. Hollow fibre, tubular and plate-and-frame modules are also available, but spiral wound modules have dominated the market because of their high surface area to volume ratio, increased robustness and permeability [51, 52]. These modules are generally operated in crossflow mode by using a pressurised feed stream that flows parallel to the surface of the membrane as shown in Figure 1.5. A proportion of the feed flow (measured as the recovery ratio) passes through the membrane as permeate, leaving behind the rejected particles in the concentrate stream. The continual

flowrate parallel to the membrane surface ensures that rejected particles are flushed away as concentrate and do not accumulate within the membrane module [49].

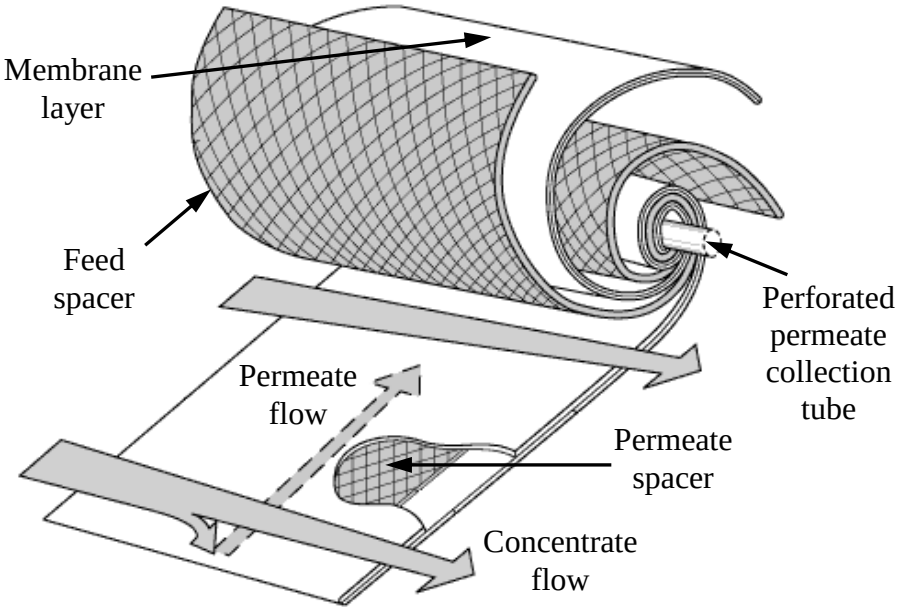

Figure 1.5: Construction of a spiral wound membrane module used for RO and NF membranes illustrating the flow of feed and permeate streams when operated in crossflow mode [49].

RO/NF membranes are thin film composite structures made up of three layers: a thin polyamide layer on the outer surface, a microporous polysulfone interlayer and a polyester support web [49]. Feed channel spacers, as shown in Figure 1.5, are required to keep the membrane layers apart and form flow channels to enhance mass transfer at the membrane surface, therefore their geometry is crucial to the performance of the membrane module [51].

The development of ultra-low pressure RO membranes has allowed them to bridge the gap between RO and NF by operating at similar pressures to NF for the treatment of brackish water [53]. Detailed experimental analysis of NF has shown that they can provide similar retention to RO membranes for many organic contaminants with the advantage of increased productivity and reduced overall costs [54]. Pilot and full-scale experimental results with a NF membrane (NF90) showed overall retention of 83 % for neutral compounds and 99 % for ionic compounds. The main difference between the NF and low pressure brackish water RO membrane (BW30LE) was the improved retention

of RO for several small organic contaminants [54]. Therefore, the selection of an RO or NF membrane should be based on the local water characteristics, the desired water recovery (or productivity), and the required permeate concentration for a particular contaminant [55].

The main factors that will affect the performance of the chosen membrane system can be summarised as follows [56]:

i. feed water salinity/contaminants and effectiveness of the pre-treatment;
ii. characteristics of the membrane (permeability, size, number, arrangement);
iii. operating conditions (pressure, flowrate, temperature, water recovery);
iv. efficiency of components (pumps, motors, energy recovery devices); and
v. degree of scaling/fouling and ability to clean the membrane.

1.2.2 Energy requirements

The RO industry has typically separated natural waters into two broad categories based on their salinity; brackish water (1000 – 10,000 mg/L) or seawater (> 10,000 mg/L), and applied either brackish or seawater RO membranes to these applications [29]. To gain an idea of the difference in the energy requirements, the osmotic pressure (π, bar) of an ideal solution can be calculated using the van't Hoff formula [57]:

$$\pi = c.R_c.T\,, \qquad (1.1)$$

where c is the ionic concentration of the feed water (mol/L), R_c is the ideal gas constant (0.082 L.bar.K^{-1}.mol^{-1}) and T is the operating temperature (K). This yields a theoretical approximation for the mechanical pressure required to overcome the natural osmotic pressure of a saline solution as 0.76 bar for every 1000 mg/L NaCl [55]. Therefore, without taking into account membrane resistance and concentration polarisation effects, the minimum pressure required for brackish water desalination is in the range 0.76 – 7.6 bar according to the feed water salinity. By comparison, a minimum pressure of 23 – 26 bar is required to overcome the natural osmotic pressure of seawater. However, in reality, merely achieving the osmotic pressure of the feed water would result in very low permeate flux, therefore much higher operating pressures of 3 – 30 bar and 60 – 80 bar are commonly used for brackish and seawater desalination, respectively [29].

The required operating pressure has a direct impact on the SEC, the size of the renewable energy generator, and the cost of water. This means that RE-membrane systems often have different design criteria to conventional membrane plants [58]. Rather than designing for the maximum efficiency in terms of high pressure, water flux, recovery and solute rejection, the most important factor tends to be the energy requirements. For any membrane system, the SEC will achieve a minimum value when there is maximum permeate production for a minimum pressure difference [47]. The limitation is that the water recovery increases according to the pressure, resulting in an optimum recovery which delivers a balance of productivity to the losses caused by osmotic pressure build-up. The importance of optimising the operating parameters in favour of energy efficient operation is vital for reducing the cost of water.

1.2.3 Technological challenges

One of the main limitations of RO/NF membrane systems is fouling; defined as the decline in performance caused by insoluble rejected matter accumulating on the surface of the membrane [47]. This problem is more commonly associated with surface waters rather than groundwater and can result in the need for pre-treatment, as well as increased operating pressure to maintain performance and frequent chemical cleaning. If fouling is not controlled, it can result in reduced membrane lifetime and performance with increased water costs. External fouling of membranes can be minimised by pre-treatment, optimised operating conditions and regular cleaning of the membranes [47]. In contrast, internal fouling, caused by physical compaction and chemical degradation, is largely irreversible and ultimately affects the lifetime of the membrane module. The main fouling prevention measure for RO/NF membranes is through feed water pre-treatment [7].

Conventional pre-treatment methods for RO/NF generally use acid addition, coagulant/flocculent addition, disinfection and media/cartridge filtration [29]. Although these techniques have been widely used, variations in feed water quality can result in less effective removal of colloids and suspended particles, resulting in fouling of the membrane. To allow for feed water variations, many new installations have started to use membranes with larger pore sizes (microfiltration (MF), UF and sometimes NF) to replace the conventional means of pre-treatment [29]. In particular, UF membranes have

been widely used and are an effective means of pre-treatment as they can remove the majority of waterborne pathogens including bacteria, particles and colloidal matter [59, 60]. UF membranes are seen to offer the best compromise between contaminant removal and permeate production while also allowing backwash cleaning [29]. MF membranes are used to provide higher flux and removal of larger particulate matter, while NF membranes can be used to remove dissolved contaminants and colloidal material for seawater RO pre-treatment [29].

The main fouling problem in brackish water RO/NF membrane systems is salt precipitation and the subsequent membrane scaling [29]. Scaling occurs due to the precipitation of sparingly soluble inorganic compounds from the feed water within the membrane, and causes reduced permeability, increased energy consumption and shorter membrane lifetime [61]. Examples of sparingly soluble salts that may become supersaturated and precipitate on the membrane are calcium carbonate, barium sulphate, silica and calcium phosphate. Depending on the water recovery and retention of the RO/NF membrane module, dissolved salts in the feed water can be concentrated 4 – 10 times in the concentrated stream.

The risk of membrane scaling can be increased by the action of concentration polarisation at high water recovery, resulting in high concentrations of sparingly soluble salts at the membrane surface [61]. Concentration polarisation is caused by a boundary layer of higher salt concentration than the bulk solution that forms at the membrane surface due to the rejection of dissolved salts and the water flux through the membrane [55]. This causes increased osmotic pressure; reduced driving pressure across the membrane and therefore less water flux; and, an increased risk of scaling. Concentration polarisation is increased at high permeate flux with correspondingly low crossflow velocity [61]. It is considered to be one of the major factors that causes non-linearity between the driving pressure and resulting permeate flux, particularly with full-scale RO modules [52, 62].

A key operating challenge from a practical and environmental point of view is the disposal of the concentrate stream. If UF has been used for feed water pre-treatment, the concentrate stream will be physically disinfected [60]. Depending on the raw water quality and water recovery, the concentrate could be used for household applications

that do not involve ingestion or for maintaining livestock [60]. The majority of coastal desalination plants discharge the concentrate stream into the ocean which causes several environmental problems due to the increased temperature, salinity and the concentration of chemicals and organic material in the outflow [63]. For most inland desalination plants, the main methods for concentrate disposal are brine wells, land application and evaporation ponds. These are either not always available, unsustainable or involve the use of large areas of land. A more sustainable method for reducing brine volumes that does not require large areas of land is to use the drying power of the wind [63, 64]. This technology, called Wind-Aided Intensified eVaporation (WAIV) operates by passing the concentrate stream over vertical hydrophilic surfaces that are positioned parallel to the wind direction. Experimental testing over several months showed that evaporation rates of 90 % of those from open water surfaces could be achieved at a much smaller footprint with packing density of 20 m^2 per m^2 of surface area [64]. WAIV provides an alternative solution to separate the salts from the brine, allowing for a more environmentally sustainable disposal option.

1.3 Wind power generation

Wind is driven by solar energy (0.7 % of the 173 000 TW total solar energy) that generates varying thermal conditions in air masses, causing atmospheric pressure differences and the resulting formation of jet streams in the upper atmosphere (12 km height) [41]. The jet streams transfer energy to a boundary layer near the earth's surface where the wind characteristics are determined by the latitude, regional geography and roughness of the ground [65]. This means that the wind utilised by wind turbines is highly variable, both according to the geographical location and the moment in time [66]. The available energy in the wind exhibits a cubic relationship to the wind speed, highlighting the importance of the wind turbine location and the potential impact of wind variability on the power output from wind turbines.

The distribution of energy content of wind turbulence is described by the Van der Hoven wind speed spectrum shown in Figure 1.6 [67]. The units for the y-axis (m^2/s^2) are obtained by multiplying the power spectral density of the wind by the angular frequency. This spectrum shows a clear distinction between long-term wind speed fluctuations caused by the passage of weather systems (synoptic variations) or time of

day (diurnal) and short-term fluctuations caused by turbulence [66, 67]. There is a 'spectral gap' observed in the region between two hours and ten minutes where there is little energy between the synoptic-diurnal region and the turbulent region. This gap is attributed to the lack of any physical process that could cause wind speed fluctuations in that range of frequency [67]. The turbulent region occurs over time periods ranging from five seconds up to ten minutes with a peak at one minute. Turbulence causes fluctuations in power output that have a negative effect on the quality of power delivered by a wind turbine, therefore these short-term fluctuations are considered to be more significant than long-term variability for the implementation of wind energy systems [68].

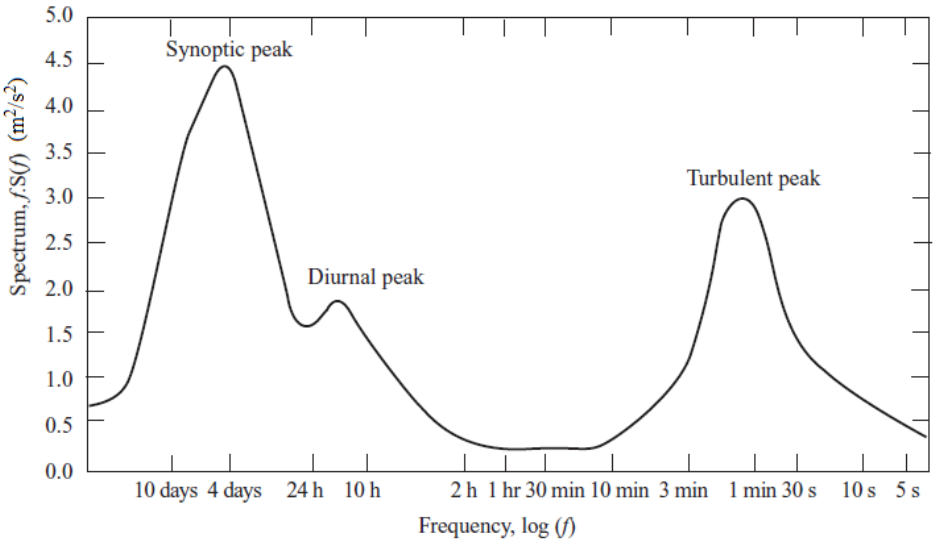

Figure 1.6: The variation of wind speed fluctuations and frequency based on data from Brookhaven, New York by van der Hoven [66].

The power output from a wind turbine (P_{wt}, W) is calculated as:

$$P_{wt} = \tfrac{1}{2} C_{eff} \cdot \rho_a \cdot A_{swept} \cdot U^3, \qquad (1.2)$$

where C_{eff} is the aerodynamic conversion efficiency of the wind turbine, ρ_a is the air density (kg/m^3), A_{swept} is the swept surface area of the wind turbine blades (m^2) and U is the mean wind speed (m/s). There is a theoretical maximum wind turbine efficiency that was calculated by Betz to be 59 %, as it is impossible to create a wind turbine rotor that

can extract all of the wind power and cause the wind to stop within the swept area [65]. Wind turbines extract energy from the wind using either aerodynamic drag with many blades (windmills) or aerodynamic lift using airfoil shaped blades (wind turbines). The relationship between the number of blades (solidity of the wind turbine) and the aerodynamic conversion efficiency is shown in Figure 1.7.

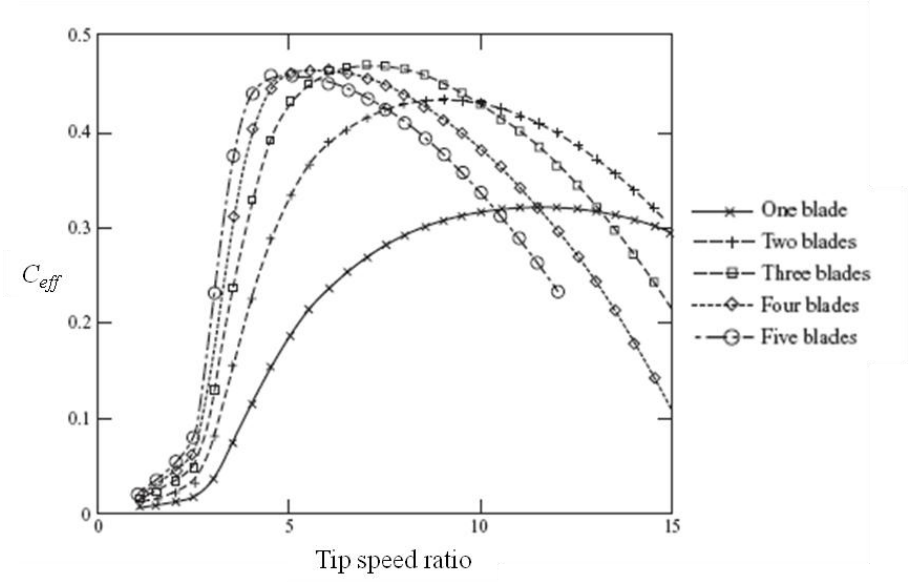

Figure 1.7: The relationship between wind turbine efficiency (C_{eff}) and the number of blades [66]. Tip speed ratio is the ratio of the rotational velocity of the blade tip to the wind speed.

Wind turbines are often designed using 3 blades as this provides the highest aerodynamic efficiency over a relatively wide range of rotational speeds (tip speed ratio) [66]. In contrast, windmills utilise up to 20 blades, resulting in a lower aerodynamic efficiency with a very narrow operating range. The advantage of using more blades is that they are able to provide high torque at low rotational speeds, allowing the windmill to extract energy at low wind speeds. Some small wind turbines also utilise more blades to increase the amount of energy extracted at low wind speeds, particularly for battery charging applications. In terms of real wind turbine efficiency, large wind turbines have maximum efficiencies of 45 %, and small-scale wind turbines are commonly in the region of 30 % efficiency [41]. Small wind turbines generally have higher aerodynamic efficiency losses as they do not have the facility to adjust the pitch angle of the blades and the cost of blade manufacturing is considered to be of greater importance than the aerodynamic efficiency.

Small-scale wind turbines are technically classified as 'micro-wind turbines' if they have a swept blade area of < 25 m^2, and therefore a maximum rated power of 6 kW [69]. These wind turbines are considerably different to large-scale designs as they are built to be more reliable and maintenance free, also they generally don't have a gearbox as they operate at high rotational speeds [65]. The majority of small wind turbines use a permanent magnet generator that can operate at variable speed and is directly-driven by the wind turbine rotor. The main components used in the majority of small wind turbines are shown in Figure 1.8. Furling of the wind turbine using a tail connected to the rotor achieves power control by turning the wind turbine rotor out of the wind at high wind speed, thereby reducing the swept area and preventing damage. The design and testing process used for selecting the wind turbine used in this research is given in Section 2.2.

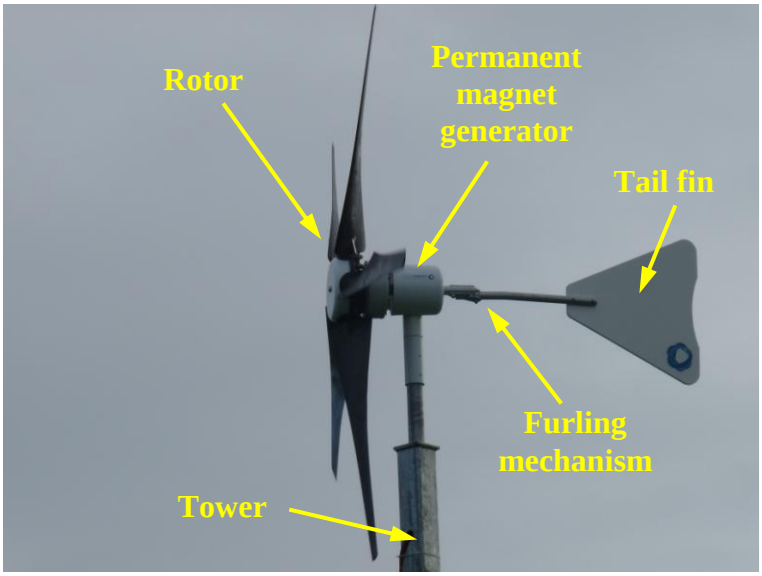

Figure 1.8: The main components of a small wind turbine.

Although there has recently been a dramatic increase in the uptake of small-scale wind turbines, their power output is strongly site dependent and often falls short of the predictions of the manufacturers [69]. There are several reasons for this, many of which stem from the fact until recently (2010), there has been no standard method required from the manufacturers when publishing the power curves for their wind turbines. Therefore, wind turbines have power ratings based on high wind speeds (~ 12 m/s) that are rarely seen in real locations, especially on the low (~ 8 m) towers used for small-scale systems. Additionally, the use of low towers means that the wind turbines are

impacted by increased turbulence due to nearby obstacles and frictional effects. The minimum recommended average wind speed for a small-scale wind turbine site is generally considered to be 5 m/s, and this has also been suggested as the minimum cost-effective wind speed for wind-membrane systems [38, 69].

As part of the UK government's incentive to promote the uptake of small-scale renewable technologies with the Feed-in Tariffs, a scheme where homeowners and businesses earn a fixed tariff for every kWh generated using renewable energy technologies, they introduced the Microgeneration Certification Scheme (MCS) in April 2010 [70]. The objective of the MCS accreditation scheme was to ensure that both manufacturers and installers of small-scale renewable technologies had conformed to a rigorous set of standards, therefore providing eligibility for consumers to access the Feed in Tariff. The MCS scheme includes small-scale wind turbines with power outputs up to 50 kW. The process of accreditation involves verifying design calculations, certifying the manufacturing process and field testing of a prototype wind turbine. It is hoped that having a list of accredited wind turbines should help to reduce the inaccuracy of wind turbine power curves and overestimation of their annual power outputs. However, currently there are only 13 different MCS accredited wind turbines, of which 9 have power ratings > 10 kW, 3 are rated at 5 – 6 kW and the smallest has a 2.4 kW rating [70]. The certification process costs about £100,000, taking anywhere from 9 – 18 months, and must be performed by an accredited certification body, of which there are only 13 [71]. This is a large investment for many small wind turbine companies and may help to explain why there are so few MCS accredited turbines, and none with power ratings < 2.4 kW.

It is hoped that by achieving MCS accreditation, many of the reliability issues that have been prevalent within the small wind turbine industry will be addressed [70]. There have recently been a series of trials performed on small wind turbines that highlighted these reliability issues [72]. A one year trial of 12 different small wind turbines (≤ 6 kW) was performed during 2008 – 2009 in the Netherlands. The wind turbines were installed on 12 m towers, with an average wind speed of 3.8 m/s over the period of testing. During the field testing, 3 of the wind turbines broke down and testing could not be continued, however, the reasons for failure were not provided. During the Warwick Wind Trials Project, 26 different small wind turbines were installed in different urban

locations throughout the UK between 2007 – 2008 [73]. The objective of these tests was to determine the energy production from small wind turbines installed within urban environments. The results showed that wind turbines generally perform poorly in the urban environment due to high turbulence and low average wind speeds. During the test period, two of the wind turbines experienced blade failures and a further wind turbine had a failure in the tail mechanism. These failures were attributed to the recent development of the small wind turbine industry within the UK, and therefore a lack of adequate durability testing [73].

An alternative option for small-scale wind-membrane systems is the utilisation of mechanical windmills that produce a mechanical power output. Windmills were the first form of wind turbine and are characterised by having many blades (up to 20) that provide a high starting torque and low rotational speed [65]. They are useful for extracting power at low wind speeds, but exhibit reduced efficiency as the wind speed increases and generally require a gearing system to utilise the mechanical energy. The increased power output at low wind speeds and efficiency gain by not converting to electrical energy are distinct advantages, however these need to be weighed against the increased costs and reduced flexibility when compared to conventional wind turbines. Further discussion and examples of wind-membrane systems are given in Section 1.5.1.

1.4 Pumping system

The pumping system is one of the key components of any membrane system as it generates the feed flowrate and pressure required to operate the membranes, and determines the main energy requirements from the renewable energy generator. As the pump is critical to the operation and performance of the membrane system, it is essential that it provides efficient and dependable service with minimal maintenance and long operational lifetime. Apart from these factors, the choice of pump will also depend on the following criteria [74]:

i. the feed water characteristics and type of membrane used, as these determine the feed pressure requirements;
ii. the feed flowrate as determined by the desired yield of the membrane plant and the chosen recovery ratio; and

iii. the quality of the energy supply, particularly where renewable energy is concerned due to the impact of low power caused by fluctuations and intermittency on the efficiency of the pumping system.

The performance of a pump is described by the following parameters: flowrate (capacity), pressure (static pressure head), hydraulic power, efficiency and rotational speed [74]. The flowrate generated by the pump is proportional to the rotational speed of the pump, impeller diameter (for centrifugal pumps), volumetric displacement and the number of pistons or plungers (for positive displacement pumps).

The static pressure head (H, m) developed by the pump is due to the difference in pressure between the discharge and suction sides of the pump (Δp, Pa) and is calculated using:

$$H = \frac{\Delta p}{\rho_w . g}, \tag{1.3}$$

where ρ_w is the water density (kg/m^3) and g is the gravitational acceleration (9.81 m/s^2). The static pressure head can be converted to an operating pressure using 10 m = 1 bar, and has been done throughout the following discussion to simplify the analysis for membrane systems. It is vital that the maximum pressure rating of a pump is not exceeded as results have shown that even an excess pressure of 1.5 bar has resulted in up to an 80 % reduction in the lifetime of the pump [75].

The hydraulic power ($P_{hydraulic}$, W) transferred by the pump to the water is calculated as:

$$P_{hydraulic} = \Delta p . Q, \tag{1.4}$$

where Δp is the pressure difference (Pa) between the discharge and suction sides of the pump and Q is the flowrate (m^3/s).

The pump efficiency (η_{pump}) is defined as the ratio of the hydraulic power output gained by the fluid to the mechanical shaft power (P_{shaft}, W) supplied by the pump motor to the pump:

$$\eta_{pump} = \frac{P_{hydraulic}}{P_{shaft}} \tag{1.5}$$

When comparing different systems, it is necessary to examine the calculation of efficiency and whether it is based upon the whole pumping system including electronics, the pump and motor, or the mechanical shaft power delivered to the pump. The above calculation is for the overall pump efficiency and includes the hydraulic losses (friction and acceleration of fluid), mechanical losses (transmission and bearings) and volumetric losses (fluid leakage) within the pump. The mechanical shaft power is calculated after taking into account the efficiency losses caused by the pump motor and associated electronics.

The main sources of information regarding the coupling of small-scale renewable energy with pumping (RE-pumping) systems are either solar PV or mechanical windmill powered water pumping systems. These are both mature technologies that have been developed to provide stand-alone water pumping as an alternative to diesel or petrol powered systems. All of the pumps used for RE-pumping and RE-membrane systems can be divided up into either dynamic (also known as kinetic) pumps or positive displacement pumps [74]. The four pumps commonly used are centrifugal (dynamic), diaphragm, piston and positive cavity (all positive displacement) pumps [75]. Detailed analysis and comparison of the pumps that could be used for small-scale RE-membrane systems are given below.

1.4.1 Centrifugal pumps

The main type of dynamic pump is the centrifugal pump, which has long been the most commonly used pump worldwide due to its robustness, simplicity and cost-effective design [74]. A centrifugal pump consists of a pump casing with bearings and seals that houses an impeller mounted on a rotating shaft as shown in Figure 1.9. The rotation of the impeller transfers kinetic energy to the fluid which is then converted into potential

energy (pressure) by guiding the fluid into a gradually increasing volume (volute) within the pump casing. The velocity at the edge of the impeller determines the amount of energy transferred to the fluid, and can be increased by higher rotational speeds or increasing the diameter of the impeller [74].

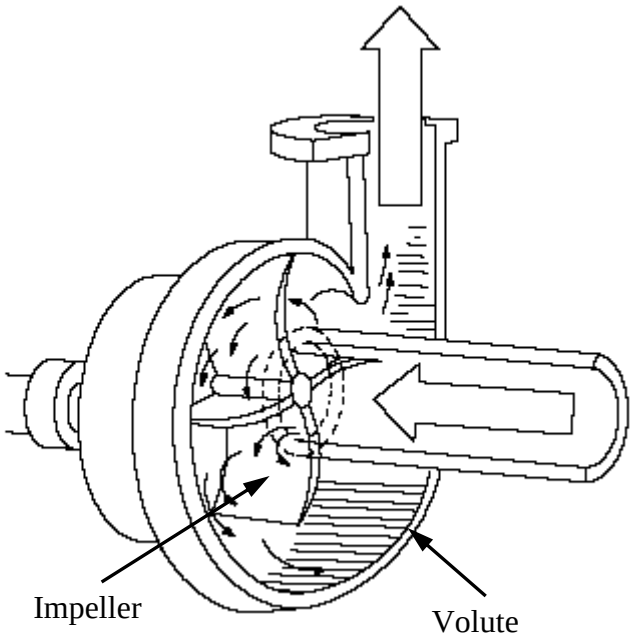

Figure 1.9: Diagram of a centrifugal pump showing the passage of water from the suction to discharge sides of the pump and the main components [76].

Centrifugal pumps are ideal for high flowrate systems with relatively low to medium pressure requirements when compared to positive displacement pumps [74]. These pumps are commonly used in large-scale desalination plants as they are very reliable and have low operating costs. They require low maintenance and are resistant to wear as they do not have mating surfaces to deteriorate. The efficiency of centrifugal pumps is generally in the range of 30 – 60 %, with larger capacity pumps providing the higher end of the efficiency range. To achieve maximum efficiency, the rotational speed of the pump rotor must be matched to the optimum flow/pressure operating point according to the impeller design. This results in a limited operating range due to significantly decreased efficiency when the operating pressure is different to the design specification [4]. Centrifugal pumps also have a minimum flowrate constraint, where mechanical damage can occur if the pump is operated below this value for extended periods. For

these reasons, 'first generation' centrifugal pumps have largely been replaced by 'second generation' positive displacement pumps for more efficient pumping with small-scale renewable energy systems [77].

To highlight the efficiency improvement of 'second generation' pumps, a comparison of progressive cavity, diaphragm, and piston pumps was made with a 'first generation' centrifugal pump, all of which were designed for PV-powered water pumping [77]. The pumps had power ratings from 75 – 400 W and were tested over their full range of operation in terms of pressure and flowrate. Details of the manufacturers were not provided. While the 400 W centrifugal pump was able to provide high flowrates over a wide range from 700 – 3600 L/h, the low efficiency of 10 – 28 % and pressure range of 0.5 – 3.5 bar were relatively poor. By comparison, a 400 W progressive cavity pump was able to operate at much higher efficiency of 55 – 75 %, while providing a pressure range of 4.5 – 12 bar and flowrates of 700 – 2500 L/h. The 75 W diaphragm pump and 100 W piston pump had much lower power ratings and exhibited similar performance in terms of pressure range (1 – 6 bar) and flowrate (180 – 900 L/h), however the diaphragm pump operated with higher efficiency (15 – 50 %) compared to the piston pump (10 – 32 %). This study highlighted the improved performance of the new generation of PV-powered pumping systems in terms of high efficiency and pressure, particularly in the case of the progressive cavity pump.

1.4.2 Positive displacement pumps

Positive displacement pumps operate by moving a fixed volume of water from the inlet to the discharge side of the pump during each stroke or revolution [74]. The flowrate is directly proportional to the speed of oscillation or rotation and is not affected by pressure fluctuations on either the suction or discharge side of the pump due to the fixed volume of water displaced during each pump stroke. Positive displacement pumps have the ability to provide higher operating pressures at the expense of lower flowrates when compared to centrifugal pumps for the same power rating. The other key advantage of positive displacement pumps over centrifugal pumps is that they are able to operate with higher efficiency over wider speed and pressure ranges, which is particularly useful for coupling with renewable energy generators providing a variable power supply [4].

Positive displacement pumps can be divided up into either reciprocating or rotary pumps according to their operation [74]. Reciprocating pumps use a crankshaft to transfer the rotational drive power to a plunger, piston or diaphragm oscillating within a cylinder. Rotary pumps use rotating screws, lobes, gears or rollers that are directly connected to the drive shaft from the motor. Rotary pumps can provide higher efficiency than reciprocating pumps at low flowrates as they are designed to operate at low rotational speeds to reduce wear caused by the erosive action of the pumping fluid on the small clearances that need to be maintained.

Progressive cavity pumps, also known as Moineau, helical screw or eccentric screw pumps have seen dramatic growth within the last 10 years for solar PV powered water pumping applications [75]. These pumps use an eccentric single helix rotor that rotates within a flexible stator with double internal helixes as shown in Figure 1.10. The difference in the pitch angle between the rotor and stator forms sealed cavities that travel along the stator from the suction side to the discharge side with the rotation of the rotor giving smooth axial fluid flow [78]. There is a continuous seal developed between the rotor and stator that pumps the fluid at a flowrate proportional to the rotational speed of the pump. The pressure developed by the pump is proportional to the length of the rotor and stator. Every revolution of the rotor sweeps the full surface of the stator thus minimising the build up of deposits and making it ideal for potable water applications [79]. Flexible shafts have been developed to bend according to the rotation of the rotor and reduce wear of components by overcoming cyclic oscillations caused by the off-centre rotation of the rotor [78].

Progressive cavity pumps are generally used to provide higher flowrates and pressures than diaphragm pumps and piston pumps, and therefore often require higher power ratings [80]. These pumps require a relatively high starting torque due to the static friction of the pump, particularly after several hours without operation, as water is required to provide the lubrication between the rotor and stator [81]. Therefore, the motor will not rotate until there is sufficient power to overcome the required starting torque and associated frictional losses. For this reason, capacitors are often used as part of a ‘booster’ circuit to store the energy until it is sufficient to provide the necessary spike in current required to start up the pump [77].

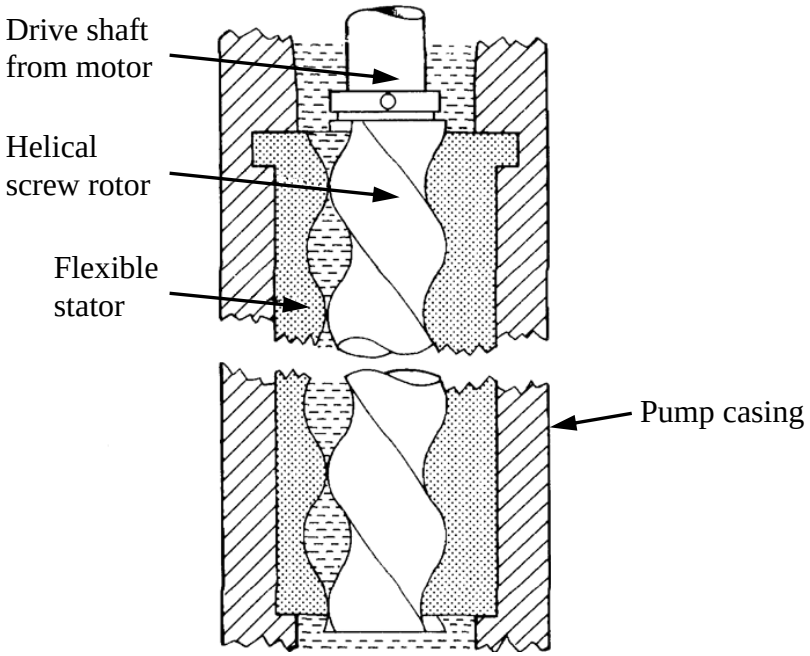

Figure 1.10: Cross-section schematic of a progressive cavity pump showing the helical screw rotor and flexible stator [82].

Diaphragm pumps (Figure 1.11) are used for very small-scale PV pumping systems as they can operate at low power (<200 W) while providing flowrates of up to 960 L/h at low to moderate pumping pressures of up to 7 bar [80]. The DC motors used for PV-powered diaphragm pumps generally have a voltage range of 12 – 40 V_{DC} and a maximum voltage of 50 V_{DC}. This voltage range would have to be taken into account when trying to couple the pump to a small wind turbine generator to avoid electrical damage and reduced lifetime of the pump motor caused by excessive voltages. According to the manufacturers, diaphragm pumps require maintenance and new parts every 1 – 2 years of operation [75, 80]. This involves replacing the diaphragm, bearing surfaces and motor end assembly (including carbon brushes). Apparently this maintenance is a relatively straightforward procedure requiring simple tools that returns the pump close to its new condition [77].

Performance and lifetime tests of four different diaphragm pumps connected to a 160 W PV array were tested experimentally by Vick *et al*. [80]. Two of the pumps were high pressure/low flow pumps (7 bar/240 L/h): SHURflo Model 9325 and Sun Pumps Model SDS-D-228. The other two were low pressure/high flow pumps (3 bar/720 L/h): Robison Model BL40Q and Sun Pumps Model SDS-Q-128. The experiments were

performed using underground water sumps of 4 m depth with a back pressure valve to simulate a pressure range of 2 – 15 bar. Readings of solar irradiance, voltage, current, pressure, flowrate and temperature were taken and averaged every minute using a datalogger. The results showed that the SHURflo pump produced higher flowrates than the Sun Pumps high pressure pump at both low pressure (2 bar) and high pressure (7 bar) conditions. The maximum efficiency of the SHURflo pump was 48 % at 7 bar pressure, which was 30 % higher than the Sun pumps pump. At low pressure, the improved performance was due to the higher capacity of the SHURflo pump by using three pistons and chambers compared to two used by the Sun Pumps pump. At high pressure, the performance increase was caused by the higher DC power restriction of the SHURflo controller which allowed up to 35 % more power to the pump. The performance comparison of the low pressure/high flow pumps showed that the Sun Pumps low pressure pump produced higher flowrates at low power (<100 W), but this was attributed to the lack of controller on the Robison pump.

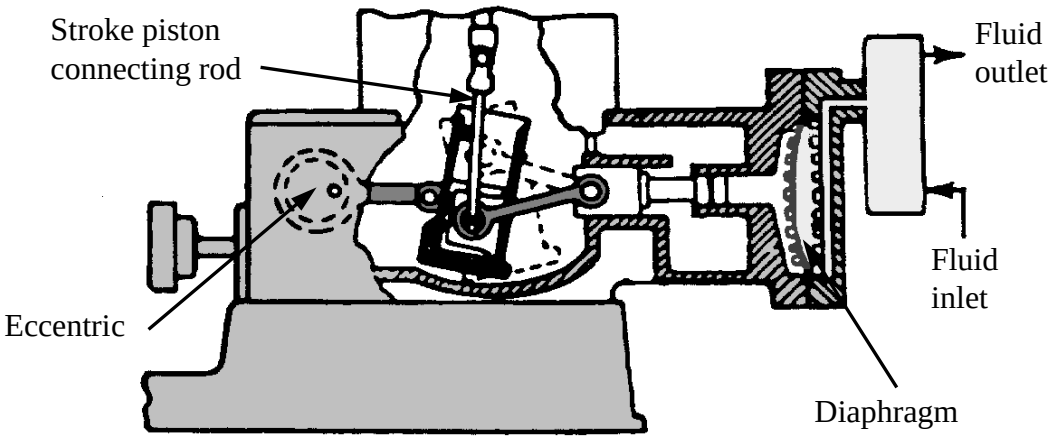

Figure 1.11: Cross-section schematic of a diaphragm pump showing the main components, the passage of water and the connection of the diaphragm to the piston and cylinder [83].

The lifetime test for the four different diaphragm pumps was performed by testing the pumps to failure at their maximum rated pumping depths. The SHURflow pump failed after only 1.33 years while the Sun Pumps high pressure pump had a lifetime of 2.4 years before failure. The Robison pump failed after only 0.75 years and the Sun Pumps low pressure pump ran for 1.95 years before the controller failed due to excessive

voltage. The other three pump failures were caused by worn diaphragm seals, highlighting the requirement of regular servicing of diaphragm pumps to replace these seals. As mentioned above, maintenance of diaphragm pumps is required every 1 – 2 years to enable a long service life [75, 80]. Further development of more robust diaphragm seals is therefore required before high pressure (7 bar) and high flow diaphragm pumps can be implemented on a large scale. Previous testing of low pressure/low flow diaphragm pumps by the same authors showed operating lifetimes of over 6 years within the limitations of 3 bar maximum pressure [84]. These pumps could only be used for membrane systems that operated at low pressure (< 3 bar), and therefore very low feed water concentrations.

The above authors also tested a progressive cavity pump using 320, 480 and 640 W PV arrays over a pressure range from 5 – 10 bar [80]. The pump was a Grundfos 3SQF rated at 1500 W with voltage input from 35 – 300 V_{DC} or single phase AC. The pump was able to produce flowrates of up to 500 L/h with hydraulic efficiency 40 – 60 %. Testing of the Grundfos pump with the three different PV array sizes and pressures of 5, 7.5 and 10 bar over 3 years showed no measurable degradation in performance. These recent tests further highlight the added capability of progressive cavity pumps over diaphragm pumps in terms of longer operational lifetime and the ability to provide higher operating pressures.

1.4.3 Pump motors

The type of motor used to provide the drive to the pump can be either DC or AC, depending on the size and application of the membrane system [4]. Permanent magnet brushless DC motors are commonly used for small-scale renewable energy applications as they are highly efficient (~ 90 %) and do not require power conditioning to utilise the DC output from the renewable energy generator. Squirrel-cage AC induction motors are used for larger pumping systems (> 10 kW) as they are cheap and robust, however they require complex control systems or inverters which are an additional cost and reduce the overall efficiency. For these reasons, DC motors are much more commonly used in small-scale renewable energy systems [4]. Permanent magnet brushless DC motors (Figure 1.12) use permanent magnets to produce the magnetic field, thereby reducing the power losses consumed in the windings associated with wound-field DC motors.

Brushless DC motors require electronic commutation to sense the rotor position and provide the current in the correct sequence. While the commutation electronics are an additional cost, brushless motors require very little maintenance apart from preventing ingress of water and dust, to provide operational lifetimes of 10 – 20 years [74]. Brushed motors on the other hand, require motor brushes to be replaced periodically every 2000 – 4000 hours or 2 years [85].

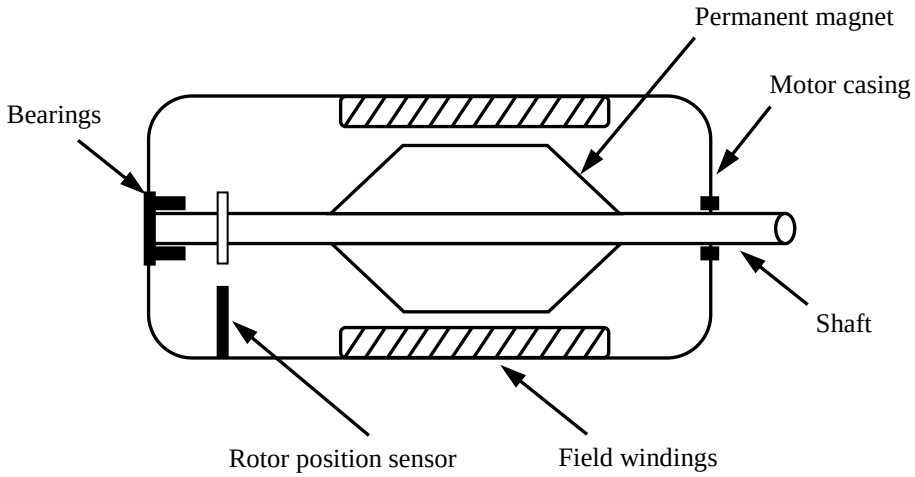

Figure 1.12: Cross-section schematic of a permanent magnet brushless DC motor, as commonly used in small-scale renewable energy applications (adapted from [4]).

The commutation of brushless DC motors is generated by Hall effect sensors that detect the position of the rotor and send pulses back to the controller [81]. The rotational speed of the motor is then controlled by the voltage applied by the controller to the stator windings. Maximum power point tracker (MPPT) controllers are required for matching the power output from the wind turbine or PV array to the DC motor in order to drive the positive displacement pump [4]. This is because the current from the renewable energy generators varies linearly according to the wind speed or solar radiation, where the pump motor requires a high start-up current followed by a constant current to provide a given torque proportional to the pumping pressure [85]. The low cost MPPT controller can perform this conversion with 95 % efficiency and the transistors in the controller can also be used for commutation of the brushless DC motor to avoid further efficiency losses.

In summary, positive displacement pumps appear to be the most suitable pumps for small-scale RE-membrane systems as they combine the characteristics of high efficiency and pressure with low flowrates over a wide operating range, which are difficult to achieve with centrifugal pumps. Specifically, the combination of progressive cavity pumps with brushless DC motors appears to provide the most efficient pumping system that fulfils the pressure and flowrate requirements with low maintenance and relatively long operational lifetime. The same conclusion on the potential of progressive cavity pumps due to their improved efficiency over a wide pressure range was made by the ADU-RES group following detailed energy consumption modelling of six membrane systems that were designed and tested with renewable energy [86].

The combination of a progressive cavity pump with a brushless DC motor was utilised in the design of the membrane system used for this research (specifications in Section 2.1.3) following several design iterations that started off with a rotary vane pump (detailed in Section 2.1.2).

1.5 Development of small-scale wind-membrane systems

To allow detailed comparison of small-scale membrane technology and specific systems, it is important to define their capacity (permeate volume produced per day). This is because medium (25 – 400 m^3/day) and large-scale (> 400 m^3/day) membrane systems are designed to produce high volumes of water at minimal cost by utilising economies of scale [87]. By comparison, small-scale systems are generally designed for rural communities with the most important criteria being energy consumption, simplicity of operation, robustness and minimal maintenance requirements (Section 1.2.2). Small-scale membrane systems are generally defined as those that produce up to 25 m^3/day fresh water, which is sufficient for a typical rural community of up to 4000 people [87]. This figure correlates with the WHO guidelines for drinking water quality that state that the minimum daily drinking-water consumption should be 2 L per adult, although a minimum of 7.5 L is seen as necessary for hydration and incorporation into food in most circumstances [12].

The majority of the small-scale wind-membrane systems that have been developed to date either used the electrical output from a horizontal axis wind turbine with energy

storage in batteries [88-92], or the mechanical output from mechanical windmills with a pressure vessel as the buffer for fluctuations [58, 93]. While the use of deep-cycle lead acid batteries can enable uninterrupted operation, they result in increased capital and operating costs as well as lower system efficiency and decreased robustness [94, 95] (further details provided in Section 1.7.1). There have also been several wind-membrane systems that were developed without the use of energy storage, such that the wind fluctuations had a direct effect on the power input to the membrane system. The lack of knowledge and information regarding transient operation of membrane systems (Section 1.6) has meant that directly-connected systems have mostly either been simulated using modelling [96, 97], or tested under laboratory conditions [98-101]. There have been some directly-connected wind-membrane installations, namely the 'Drinking with the wind' project in the Caribbean [102], and the SDAWES installation in the Canary Islands [103-105], both of which were for seawater desalination. Further analysis and details of these wind-membrane systems are given in Section 1.5.1.

Both the electrical and mechanical wind-membrane systems require the output from the wind turbine to drive a pump in order to raise the pressure of the feed water so that it can pass through the membrane filtration system. The required pressure of the feed water is closely linked to the performance of the membrane system and the quality of the feed water. Details of the small-scale wind-membrane systems that have been developed are shown in Table 1.1. The table demonstrates how RO systems designed for seawater desalination (36 g/L) require an operating pressure of up to ten times that of systems designed for brackish water desalination (1-10 g/L).

One of the most important criteria for determining the feasibility of these systems is the SEC (kWh/m^3), as this will invariably impact the cost of water and the repayment period for the plant. The SEC demonstrates the water productivity and power consumption, which translates into the required wind turbine output and membrane surface area. The recovery represents how much clean water (permeate) is produced compared to the feed flow. In the case of brackish desalination systems, low recovery ratios (10-25%) are often used to reduce scaling of the RO membrane [58, 93]. This means that four to ten times as much feed water compared to permeate must be pumped through the system for any given output, which also increases the SEC.

Table 1.1: Overview of mechanical ($_m$) and electrical small-scale wind-powered membrane filtration units (brackish and seawater). The large-scale wind-membrane system designed by ENERCON has been included to allow comparison.

Location	TDS (g/L)	Pressure (bar)	Salt Retention (%)	Recovery (%)	Permeate (m^3/d)	Wind Turbine (kW)	Energy Storage	SEC (kWh/m^3)	Ref.
Curacao	35	40	98	20	5	3 $_m$	None	5.2	[106]
Hawaii	3	5-7	97	20	4	2 $_m$	Pressure vessel	3.5*	[93]
Australia	4	6-11	86	9	0.2	1 $_m$*	Pressure vessel	11*	[58]
UK	32	40-50	98	20-50	4	2.5	None	5	[107]
Colombia	35	5.5	99	12.5	0.4	0.9	None	15*	[99]
Germany	36	80	—	27*	6	6	Battery bank	11	[90]
Greece	36	58	99*	15	0.6-1	0.9 (hybrid PV)	Battery bank	16.9*	[91]
Israel	4	14-16	98	50	3	0.6 (hybrid PV)	Battery bank	13*	[92]
Spain	36	40-60	99*	40	20-50*	26	None	5.7*	[100]
Spain	36	60	99*	33	25	230	Flywheel	6.9	[104]
ENERCON, Germany	36	70	—	25	180-1440	1200	Diesel generator	2-2.5	[108]

*Calculated by current author †Simulated results

The cost of water from membrane plants varies considerably according to the size of the plant, feed water concentration, energy source and energy requirements for the particular installation. The Ashkelon seawater RO plant in Israel is the largest in the world, producing 330,000 m^3/day of permeate from seawater (40,700 mg/L) to supply 13 % of the country's domestic demand [29]. Including all of the plant and labour costs, the cost of water from the Ashkelon plant is 0.4 £/m^3. A further comparison of 12 other

large-scale (> 3500 m^3/day) seawater RO plants showed the cost of water to be in the range of 0.5 – 1.26 £/m^3, with the cost increasing as the plant size decreased [29]. By comparison, the brackish feed water (~500 mg/L) Metropolitan plant in California produces 700,000 m^3/day of fresh water at a cost of 0.1 £/m^3 [29]. The difference in water cost between these systems is mainly a result of much higher capital costs for the seawater RO systems (up to five times higher) and increased energy consumption due to the high pressure requirements of seawater RO.

When comparing the cost of water from small-scale RE-membrane systems, there are a much wider range of costs quoted that mostly depend on the investment costs due to plant size, type of components used, salinity of the feed water and some site specific factors like the renewable energy resource [28]. The ProDes report stated that investment costs were disproportionately high for small capacity RE-membrane systems (< 5 m^3/day), resulting in high water costs, typically 3 – 6 £/m^3 [28]. Some other figures quoted by authors following overviews of small-scale membrane systems were 1.3 – 4.2 £/m^3 by Papadakis *et al.* [32], and 2.3 – 8.3 £/m^3 by Ghermandi and Massalem [109]. These water costs are significantly higher than those quoted for large-scale plants, however small-scale membrane systems can provide a secure option in remote locations where the alternatives (bottled water or water delivered by boats or trucks) are often limited and costly. For example, field work in Ghana showed that the cost of trucking water in was between 2.9 – 3.5 £/m^3, and this will continue to rise with the cost of fossil fuels [110].

As autonomous small-scale membrane systems will have their own renewable energy supply and operate with minimal maintenance or chemicals, the main operating costs are expected to be the replacement costs of the membrane modules. The expected membrane lifetimes quoted for stand-alone systems range from 1 – 3 years [30, 58, 111], however none of these predictions are based on long-term studies. For their brackish water FilmTec membranes, Dow quote an operational lifetime of 1 – 2 years for membranes operated at low recovery (< 30 %) with a preventative cleaning by regularly opening the concentrate valve to flush the membrane [49]. By comparison, an assessment of several large-scale brackish water RO plants showed typical membrane lifetimes of between 5 – 7 years [29]. Longer lifetimes were found in systems with lower feed water concentrations, which was attributed to less fouling and lower pressure

operation. This highlights the lack of knowledge and understanding on the membrane lifetime for small-scale systems. The technical challenge in the design of RE-powered RO/NF membrane systems is in allowing variable operating conditions that provide the necessary quality and quantity of water at low SEC, while reducing the likelihood of scaling or damage to the membrane modules.

1.5.1 Design and performance of wind-membrane systems

The following section provides a detailed examination of small-scale wind-membrane systems that have been developed in the past and the key outcomes resulting from their operation. This was considered to be an essential step for identifying gaps in the literature and determining the most important factors to consider when designing the wind-membrane system for this work.

An electrically driven wind-membrane system for seawater desalination (35,000 mg/L) was designed and tested at the Centre for Renewable Energy Systems Technology (CREST) at Loughborough University in 2002 [101, 107]. The design was initially modelled in Matlab before building a prototype system to validate the theoretical results. The system was set up to operate from three different power outputs for experimentation purposes; a 2.5 kW Proven wind turbine, a wind turbine simulator, or the grid. The wind turbine simulator was constructed using the Proven wind turbine generator connected to a variable speed induction motor with a flywheel to account for the difference in rotor inertia. The use of the simulator would allow the RO system to be tested independently of the wind turbine, but unfortunately was not commissioned in time to obtain any results. There was no battery storage included, meaning that the instantaneous wind speed had a direct effect on the fresh water production.

The pumping system used for the CREST design utilised a medium and a high-pressure pump that were controlled separately to maximise the use of wind energy and control the flow of water (Figure 1.13). The system also made use of a Clark pump to recover energy from the concentrate stream and increase the overall system efficiency (further details in Section 1.6.2). Preliminary experimental results obtained using the wind turbine were based on the rotational speed of the turbine since the anemometer was damaged. The results showed that if the permeate flow was discontinued for any

significant length of time (not formally assessed), the pressure would drop considerably and the permeate concentration would overshoot to high values when the system was restarted before returning to normal. This was attributed to natural osmosis occurring at levels below the osmotic pressure. Therefore, it was deemed to be important to keep the feed water flowing to avoid spikes in the permeate concentration. An adequate control mechanism was also required to reduce the likelihood of surges in pressure and flow and avoid damage to the RO membrane.

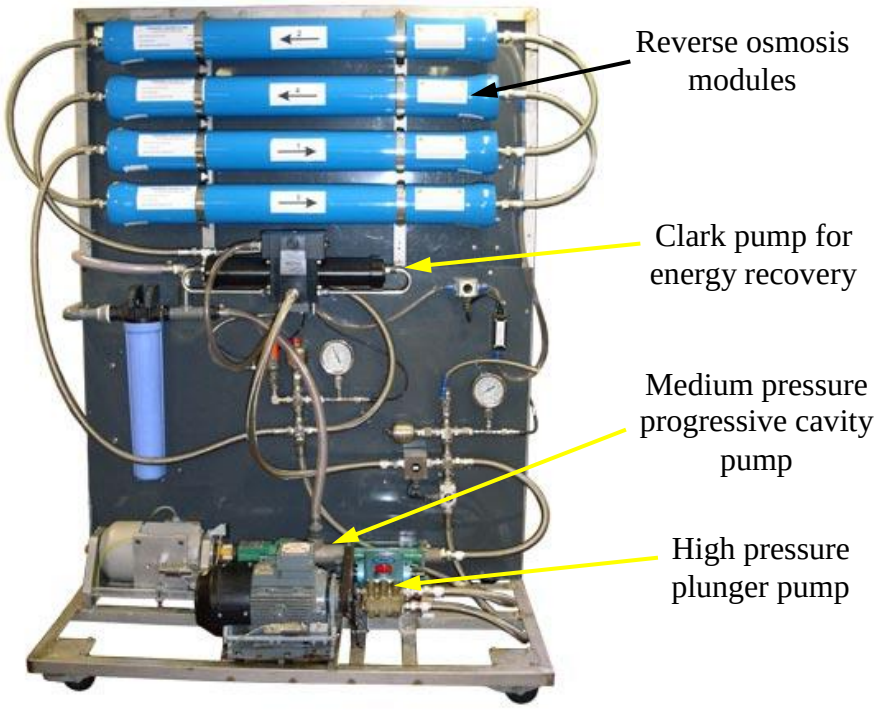

Figure 1.13: Main components of the small-scale membrane system for seawater desalination developed by CREST, Loughborough [107].

An economic analysis was performed on the CREST wind-membrane system to determine the cost of water based on an expected system lifetime of 20 years and an average water production of 9.6 m^3/day [107]. The total capital cost of the system was £33,000, including £15,000 for the wind turbine, tower and installation costs. There was a degree of uncertainty in the operation and maintenance costs, which were taken to be £1500 per year including £1000 for annual replacement of membranes. The net present value of the system was calculated to be £51,000, resulting in an estimated cost of water of 0.8 £/m^3. This exceptionally low cost of water was based on an average wind speed of 9.5 m/s over the lifetime of the plant, which is significantly higher than the average

wind speed of 5 m/s achieved during testing. Using the more conservative average wind speed of 5 m/s would result in a water cost of 2 £/m³, which would be more realistic in practice. Compared to the typical water costs from small-scale systems discussed in Section 1.5, this is still excellent and highlights the energy efficient design of this system (comparatively low SEC in Table 1.1). This research project concluded that the Proven 2.5 kW wind turbine was not adequate for the RO system because of its low power output at average wind speeds, therefore a larger wind turbine should be used.

The effect of varying wind speed, battery storage and RO operating pressure on the performance of a RO plant powered by a small wind turbine was modelled in early work by Infield [88]. Modelling was performed using the European Wind Diesel Modelling Package and the system consisted of a 5 kW wind turbine powering a 3 kW RO unit with a maximum flowrate of 260 L/h. Much of the research considered the optimal use of battery banks at varying operating pressures and wind speeds. One of the main issues was the lack of information regarding the amount of cycling that can be handled by RO units before mechanical fatigue starts to occur. The results of the modelling showed that the amount of system operating time increases with wind speed, particularly above 4 m/s. For mean wind speeds greater than 6 m/s, the system was seen to operate continuously. Energy storage in batteries was deemed to be desirable to facilitate system operation at low wind speeds, increase the average operating time and reduce the risk of fatigue due to on/off cycling of the system. Operation at lower pressures allowed better use of the wind resource as there was less electrical load on the wind turbine, therefore allowing it to operate at lower wind speeds. This does not mean that RO units should be operated at pressures much lower than their design pressure, but that units should be sized according to the available wind resource.

A hybrid seawater desalination system (36,000 mg/L) that operates using wind turbines and a photovoltaic (PV) array was developed by the Centre for Renewable Energy Systems (CRES) in Greece [91, 112]. The wind turbine and PV array were installed in 2001, while the membrane plant was added in 2004 (Figure 1.14). The power requirements for the plant were met by a 4 kW PV array and a 900 W wind turbine (Whisper H40) connected to a 1850 Ah battery bank. The PV array and the wind turbine were used to charge the battery bank which acted as an energy buffer and provided stable power to the RO unit. The battery bank was prevented from overcharging using a

charge controller and a dump load. A data measurement and control program was developed in Visual Basic that operated the RO plant according to the state of charge in the battery bank. The length of daily run-time provided by the battery bank depended on the renewable energy resource available, varying between 5 hours in winter and 8 hours in summer. A 3 kW inverter was used to supply AC power to a 2.2 kW motor that drove the positive displacement high pressure pump (Danfoss APP1.0). The RO process was performed using a pair of 2" FilmTec SW30-2540 spiral wound modules connected in series. The pre-treatment system consisted of carbon filters for de-chlorination and cartridge filters for polishing (25 μm) and (5 μm) filtration. The use of constant power allowed the RO plant to be operated under steady-state conditions with a feed pressure of 58 bar and recovery of 15 %, producing 130 L/h over the daily run-time provided by the battery bank.

Figure 1.14: Photos of the CRES system showing the 900 W wind turbine (Whisper H40) and 130 L/h seawater RO plant [112].

The performance of the CRES system was given using average values rather than detailed performance curves or analysis [91, 112]. While low permeate concentrations of 150 mg/L were produced, the SEC was very high at 16.5 kWh/m^3. The high energy consumption was most probably due to the lack of any energy recovery device and the relatively low recovery ratio, which limited the flow of permeate. These factors combined with high capital costs, only 5 – 8 hours of operation per day and high replacement costs for membranes (3 years), battery bank (5 years) and pumps/inverters

(10 years) resulted in a very high water cost of 20 £/m^3. An analysis of the problems encountered by the CRES system was performed after 5 years of continuous operation of the power supply system (wind turbine, PV array and battery bank) and 3 years for the membrane plant [112]. No maintenance had been required for the wind turbine, PV array or the battery bank. However, after only two years of operation, the 3 kW inverter overheated and was replaced with a 4 kW inverter, costing £ 3000. No issues were reported for the positive displacement pump or the performance of the membrane plant. The other problems encountered were related to short-circuiting of sensors and cable damage due to rodents and high winds.

A mechanical windmill-driven design was set up on Coconut Island off the coast of Hawaii, where the windmill was used to mechanically drive a pump and raise the pressure of the feed water for brackish water desalination (3500 and 2700 mg/L) [93]. Figure 1.15 shows a schematic diagram of the plant with the windmill (Dempster, 4.3 m diameter), brackish water desalination subsystem and feedback control. A hydraulic accumulator (300 L) was used to regulate the pressure and flowrate, thereby buffering the fluctuations and increasing the system efficiency (further details in Section 1.6.2). The feedback control mechanism was developed to adjust the feed pressure and flowrate according to the available pressure in the hydraulic accumulator using data acquisition and a series of solenoid valves. This enabled the membrane system to be operated under low wind speeds of up to 4 m/s.

A FilmTec low pressure RO membrane module (details not given) was used for desalinating the brackish feed water over the pressure range from 5.2 – 6.9 bar. The windmill was able to generate 200 – 800 W of mechanical power with average wind speeds of 4 – 8 m/s. The cylinder pump attached to the windmill provided feed flowrates of 480 – 1020 L/h over this wind speed range. With a feed water concentration of 3500 mg/L, the membrane plant operated with recovery of 19 % and retention of 97 %, producing an average of 160 L/h of permeate with low concentration < 100 mg/L. With feed water of 2700 mg/L, the recovery and retention increased to 23 % and 98 %, respectively. The average SEC was 3.5 kWh/m^3, which is comparatively very good for such a small-scale system (Table 1.1). On the second day of experimentation, when the feed water concentration of 2700 mg/L was used, the wind speed was fluctuating in the range of 2 – 8 m/s. At one point, when the wind speed

dropped to 2 m/s, the plant shut down for a period of ~ 5 min until the wind speed increased to 4 m/s, which was sufficient to re-charge the hydraulic accumulator. During this period of shut-down, the feed flowrate reduced to zero while the pressure remained at the minimum value of 5.2 bar. There was minimal impact upon the quality of the permeate caused by this period of intermittency due to the action of the hydraulic accumulator (discussed further in Section 1.6.2).

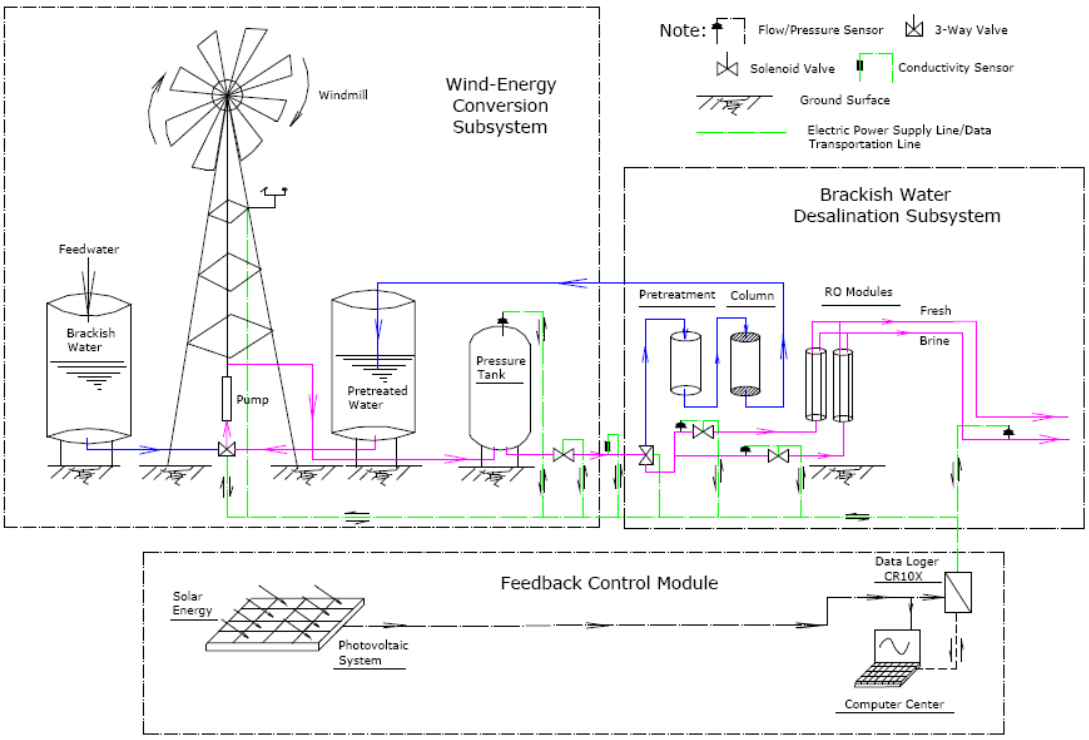

Figure 1.15: Schematic diagram of the mechanical windmill-driven brackish water RO plant installed on Coconut Island, Hawaii [30].

An analysis of the overall energy efficiency of the mechanical windmill system was performed based on the ratio of the energy available in the wind to the hydraulic power generated by the cylinder pump, giving an average efficiency of 35 % [93]. The energy efficiency decreased with increasing wind speeds from 45 % at 5 m/s to 20 % at 7 m/s. The reasons for this decrease in efficiency were not given, but presumably it could be due to the reduction in aerodynamic efficiency of the windmill at higher wind speeds coupled with leakage losses in the cylinder pump. The windmill-powered RO plant was operated for a period of 3 months, during which time it underwent 460 on/off cycles (average 5 on/off cycles per day) due to low wind speeds or intermittent wind

availability. Throughout the period of testing, there was no decrease observed in the performance of the membranes, nor any damage caused to any of the components. Further development of the windmill system has enabled dual working pressure for separate feed water pre-treatment (1.4 – 3.4 bar) and RO desalination (4.8 – 7.2 bar), while all of the electrical requirements for sensors are now provided by solar PV [30]. A larger pilot plant is planned using a 6 m diameter windmill that can provide significantly increased pressure of 40 bar and feed flowrates of up to 700 L/h. A preliminary cost assessment of the planned design was performed by scaling up from the existing system assuming the same overall efficiencies. By scaling up in this manner, the average permeate production would increase from 4 m^3/day to an estimated 13.3 m^3/day. The preliminary cost calculations estimated the cost of water to be 0.9 £/m^3, which seems exceptionally low for a small-scale system (Section 1.5). It remains to be seen whether this is achievable in practice, as these calculations were based on linear scaling up and average values.

A windmill (Aermotor, 4 m diameter) was also used as the power source for a RO desalination unit that was tested with three brackish feed water concentrations in Australia for 13 months [58]. The system included a hydraulic accumulator (36 L) to store feed water under pressure, and keep the feed flowrate and pressure within an acceptable range (further details in Section 1.6.2). A small diesel or portable gasoline pump was used during periods of low energy input and high demand. The membrane system was set up to operate at low recovery (< 15 %) to reduce the risk of fouling in an attempt to prolong membrane lifetime and reduce maintenance requirements. With a feed water concentration of 2000 mg/L, the system produced 291 L/day of permeate at 9.7 % recovery and 352 mg/L. With a higher feed concentration of 4000 mg/L, the productivity was 197 L/day at 9.1 % recovery and salinity of 564 mg/L. Performance with the highest feed water concentration of 6000 mg/L was marginal, with 151 L/day at an average concentration of 1142 mg/L and 9.3 % recovery. The minimum power requirement for driving the RO system was 150 W, and this was achieved at wind speeds of 4.5 m/s. When the wind speed dropped below this value, the system relied on the energy stored in the hydraulic accumulator (length of storage time not given). The power output from the windmill increased sharply between 2 – 5 m/s and levelled off above 8 m/s, making the system ideal for low wind speed regimes. A cost comparison showed that wind-powered RO is economically viable in comparison to similar

technologies at production rates of 500 L/day or more. However, at the time of publication (1992), it was still more economical to transport water 30 – 40 km than desalinate using RO technologies and pumping with diesel equipment, highlighting the need for continued development of small-scale RO systems.

Another more recent windmill-powered RO project called 'Drinking with the wind' was designed and tested by Heijman *et al.* [102, 106]. The objective of this project was to design, manufacture and test a prototype of a mechanically powered RO system with straightforward mechanical controls and no form of energy storage. A prototype system was set up on the island of Curacao in the Caribbean in 2007. The windmill (Molins de Vent, M5015) had a 5 m diameter rotor installed at a hub height of 15 m. The power output from the windmill was between 250 – 2500 W over the wind speed range 4 – 9 m/s. The mechanical drive from the windmill was transferred via a belt drive to a Danfoss high-pressure piston pump (APP1.5) and energy recovery motor (APM1.2), as shown in Figure 1.16. By using a direct-drive shaft connecting the piston pump to the energy recovery motor and sizing the motor with 20 % less volume than the pump, a maximum recovery of < 25 % was maintained. To protect the pump from damage caused by running dry, a 30 L buffer tank was installed at 10 m above the membrane plant to provide water to the pump during low winds. The buffer tank was connected to a mechanically actuated brake to stop pump operation when the tank emptied. A permeate storage tank of 25 m^3 was sized to store water during periods of low wind, providing up to 5 days of autonomous storage.

The membrane plant used 4 seawater RO membranes connected in series (Hydranautics, SWC1-4040) that were operated at feed pressures between 30 – 50 bar and feed flowrates 600 – 760 L/h depending on the available wind speed. Preliminary results were presented showing three days of experimental data with the windmill-powered RO system operating under fluctuating wind conditions with corresponding fluctuations in feed pressure and flowrate. At an average wind speed of 7 m/s, the membrane system produced 5 m^3 of water per day with permeate concentration 800 – 1000 mg/L and an average SEC of 5.2 kWh/m^3. Minimum average wind speeds of > 6.5 m/s were required to produce permeate with concentrations within the WHO guidelines [12]. The minimum wind speed required for the pump to overcome the osmotic pressure (30 bar) of the seawater was 4.5 m/s, however the permeate concentration of ~2000 mg/L was

double the WHO guideline limit. Based on these short-term results, the authors concluded that it was possible to operate the membrane system with fluctuations in pressure and flowrate. Again, further long-term testing would be required to provide an ageing study on the membrane modules. The cost of water from this system was estimated at 2 £/m^3, however details of the calculations were not provided.

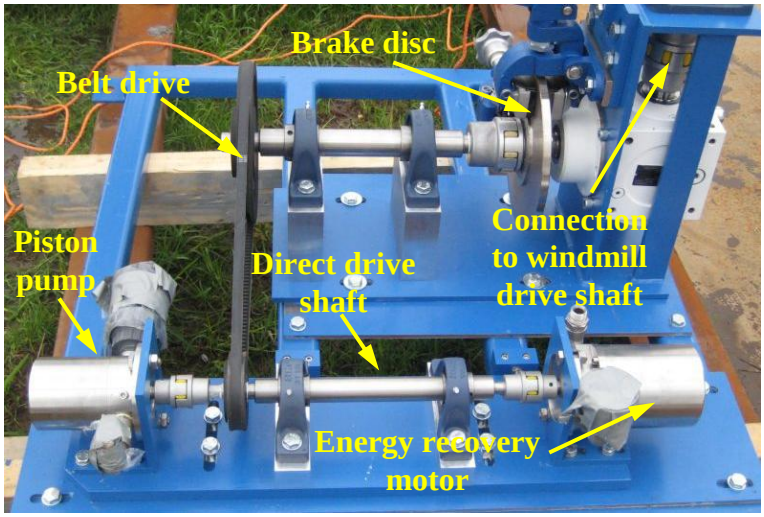

Figure 1.16: Main components of the mechanical transmission system on the 'Drinking with the wind' pilot plant installed on the island of Curacao [102].

A relatively large-scale project for testing a wind-membrane system was set up as part of the 'seawater desalination by an autonomous wind energy system' (SDAWES) project in the Canary Islands [103-105]. This project, including design and installation, was carried out over 6 years (1996 – 2002) with experimental testing and analysis performed for 2 years [105]. The membrane plant was powered by two 230 kW wind turbines (Enercon GmbH, E-30), although the energy requirements of the membrane plant were much lower (26 kW) (Figure 1.17). These oversized wind turbines were used as Enercon was part of the SDAWES project and there were no smaller wind turbines available with the required technical characteristics. Two wind turbines were required to investigate the potential problems associated with controlling a stand-alone wind farm. The power output from the wind turbines was used to set up an isolated grid using a flywheel (inertia 677.5 kg.m^2) that was powered by a 100 kW motor. The flywheel was used to supply the grid frequency and voltage reference while providing temporary energy storage during periods of low wind speeds. Once a wind speed of 6 m/s had been

achieved for 5 min, the power output from the wind turbines was used to accelerate the flywheel up to 52 Hz to provide the stand-alone electrical grid. The blade angle of the wind turbines was then adapted to supply the correct amount of power according to the power requirements of the membrane system and associated electronics. The time required to achieve the required frequency of 52 Hz depended on the available wind speed, with 26 min required at an average wind speed of 5.3 m/s.

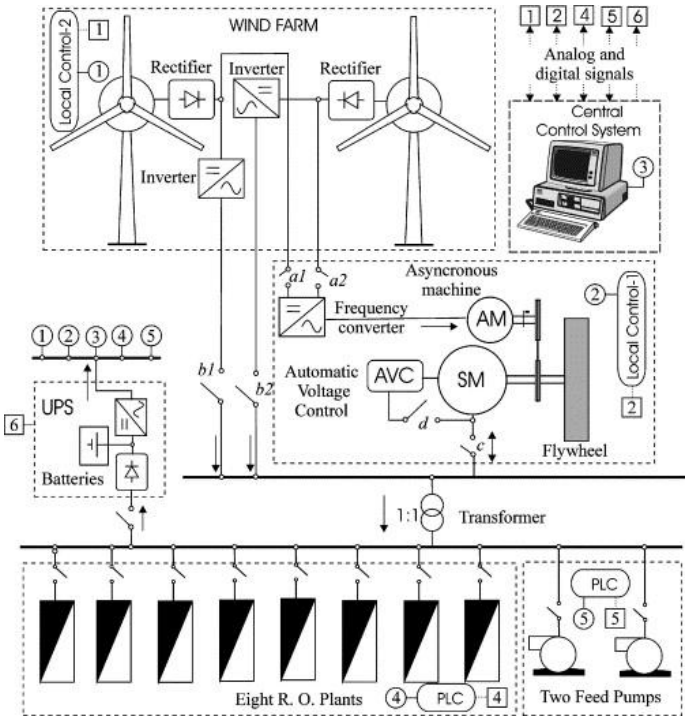

Figure 1.17: Schematic diagram showing the main components of the SDAWES wind-membrane system for seawater desalination installed in Gran Canaria [104].

The membrane system for the SDAWES project was comprised of eight seawater RO plants, each with a production capacity of 25 m^3/day [103]. The pumping system consisted of two 13 kW plunger pumps (CAT, 2537), able to provide feed flowrates of 40 m^3/h, that were operated alternately every 30 min. The membrane plants were operated at a feed pressure of 62 bar and recovery of 33 %, providing water with an average SEC of 6.9 kWh/m^3. Each plant consisted of 9 membrane modules (Hydranautics, SWC-4040) with motorised solenoid valves at the high pressure pump inlets to allow controlled pressure increase when the plants were started up. The membrane plants were connected to the grid and started up one at a time according to the power available from the wind turbines. When the wind speed dropped, a control

system was used to balance the energy supply/consumption and prevent the grid frequency dropping below 48 Hz. The strategy was to change the pitch angle of the wind turbines to capture more energy, decelerate the flywheel to provide more energy to the membrane plants, and then if necessary, gradually disconnect the membrane plants.

The start-up and shut-down procedures for the membrane plants in the SDAWES system were examined to determine the impact on the quality and quantity of permeate produced and the effect on the operating lifetime of components [104]. Two procedures were examined; the first involved disconnecting the membrane plants in the inverse order in which they were connected, so the first plant connected would be the last plant to be disconnected. The second procedure was used to try and achieve a uniform number of cycles for each plant by using a ring strategy in which the order the plants were connected was the same order they were disconnected. From start-up, the RO plants required an average time of 38 s for the flowrate to stabilise and 900 s before the permeate conductivity reduced from an initial value of 950 µS/cm to the stabilised value of 650 µS/cm. Fluctuations in the grid frequency from 52 Hz to 49 Hz resulted in feed pressure fluctuations of 5 % (61 bar to 58 bar) with minimal impact upon the permeate quantity and quality. The fluctuations caused an 8 % reduction in the permeate flowrate (970 L/h to 890 L/h) and 3 % increase in the permeate conductivity (905 µS/cm to 933 µS/cm). After approximately 2 years of testing, there was no deterioration of any of the components in the membrane plant due to cycling on/off during periods of low wind speeds (number of plant cycles not provided). However, as the standard working lifetime of the RO membranes was 5 years, prolonged testing would be required to establish whether intermittent operation impacted upon their lifespan.

1.6 Transient operation of membrane systems

1.6.1 The impact of transient operation

As mentioned previously, the main challenges associated with the use of wind turbines in directly-connected membrane systems are the intermittency and fluctuations of the wind resource which occur due to turbulence and gusts over short periods of time (seconds to a few minutes) and mass air movements over long periods of time (tens to hundreds of hours) [113]. The direct connection of a wind turbine to a RO system with no form of energy storage will inevitably result in large fluctuations in pressure and/or

flowrate. This presents a considerable challenge for wind-membrane systems as membranes are designed to operate under constant operating conditions with no abrupt pressure or crossflow variations in order to minimise the potential for excessive mechanical stresses on the membrane module [114].

As with many materials, membranes experience plastic creep under constant pressure and temperature conditions; therefore the combination of fluctuating pressure and flowrate with cycling on/off is expected to cause material fatigue [115]. Rahal and Infield [115] suggested that an upper limit should be applied to the cycling on/off frequency of the membrane system to prevent deterioration of membrane system performance and lifetime. However, the impact on both the short-term performance parameters and the degree of fatigue damage caused by repetitive cycling of RO modules is not known and has not yet been investigated under either energy fluctuations or intermittent operation. The likely performance deterioration caused by the cycling on/off of membrane systems is due to reduced permeate quality and the potential for increased wear on the pump and motor [98, 116, 117]. The reduction in permeate quality is caused by low flux combined with the continual diffusion of salt across the membrane during a period of intermittency. Again, these problems have only been stated and are not backed up by studies that quantify the overall impact of fluctuations or intermittency on RE-membrane system performance.

An important factor for directly-powered systems is that the variability and unpredictability of the wind resource may result in the water demand not being met [101]. In order to overcome this problem, most of the small-scale wind-powered systems that have been developed utilised electrical energy storage in batteries [88-92] or mechanical storage in a pressure vessel [58, 93]. An alternative method for overcoming the intermittency of wind is to store the potable water, which greatly reduces the capital and maintenance costs of these systems and avoids the drawbacks associated with use of lead-acid batteries (see Section 1.7.1 for details).

There have been several wind-membrane systems that operated successfully under varying flowrate and pressure with no form of energy storage [98-100, 104, 106, 107, 118]; however, the transient operation of these systems under fluctuations and the extent to which these fluctuations can be managed or exploited is not well understood. This is

because these experimental studies have either focussed on the initial feasibility of a directly-connected system [98-100, 118] resulting in minimal conclusive data; or the design and setup of a prototype wind-membrane installation [104, 106, 107] that has resulted in the analysis of a specific segment of data or an overview of performance. Therefore, further analysis necessitates a systematic investigation of the effect of fluctuations and intermittency on membrane systems in order to understand the underlying mechanisms, determine their impact on performance and establish the most appropriate control strategy.

The details and analysis of the prototype wind-membrane systems that have been set up in the past are detailed in Section 1.5.1. The feasibility studies on wind-membrane systems that suggest that membranes can operate under fluctuating conditions within a safe operating window and without deteriorating are detailed below.

Some of the earliest recorded work on the direct-connection of renewable energy to membrane systems was performed by Lising and Alward in the 1970s [98]. This research investigated the impact of fluctuations in flowrate on a brackish water RO membrane system to determine its compatibility with the transient power output from a windmill. Laboratory experiments were performed using a variable speed motor drive connected to a progressive cavity pump that could produce feed flowrates of 270 L/h at 40 bar. Experiments were performed using a feed water concentration of 3500 mg/L NaCl at constant system pressure of 40 bar with sinusoidal fluctuations in feed flowrate. The sinusoidal variation in feed flowrate was assumed due to the windmill's high moment of inertia, which caused shaft speed variations to be smoothed with sudden changes in wind speed. Two test runs were completed on the system over 7 days, each with a constant period of oscillation of 90 s and average feed flowrate of 175 L/h. The peak-to-peak amplitude of sinusoidal fluctuation in flowrate was set at 105 L/h for the first test and 77 L/h for the second. During the second test, the pump was stopped for 30 seconds to repair a leak which caused high conductivity of the permeate flow upon restarting the system. This short period of intermittency allowed saline water to permeate through the membrane, requiring two days for the conductivity of the permeate to return to its original value. This time period of two days was also required for the permeate conductivity to stabilise when the membrane system was initially turned on. It is assumed that the recovery time of two days was a result of the

membrane technology available at the time (1971), and significant advances in technology since then should result in less lag time. The conclusion of this work was that small amplitude variability in feed flow velocity had very little effect upon the quantity or quality of potable water, provided the flowrate was not reduced to zero at any point, therefore wind-membrane systems were considered to be technically feasible.

Pestana *et al.*[100] performed a study of seawater RO membranes subject to fluctuations of pressure and flowrate to determine the possibility of operation within a safe operating window. The drive system for the plant was provided by a 26 kW three-phase AC motor connected to a positive displacement piston pump capable of providing a pressure range of 7 – 85 bar and flowrates up to 13,600 L/h (Figure 1.18). The speed of the AC motor was adjusted using a 30 kW variable speed inverter (Telemacanique Altivar). The membrane plant consisted of six seawater RO membranes (Koch Fluid Systems TFC 2822-SS) installed in series within a 6 m long pressure vessel. These membranes were spiral wound modules with a surface area of 27.9 m^2 that were able to supply up to 800 L/h of permeate with retention of 99.8 %. By varying the speed of the pump motor and adjusting the regulating valve on the concentrate stream, the membrane plant was subjected to the full range of pressure (30 – 60 bar) and flowrates (5000 – 10,000 L/h) as specified by the manufacturer. The results showed the reduction of permeate concentration with increasing pressure and the relationship of the input power, operating pressure, recovery and permeate flowrate over the full range of operation. As would be expected, the recovery and the permeate flowrate both increased with increasing pressure and input power. Detailed results were not provided, but the conclusion was that the optimal control strategy for reducing the energy consumption would be to maintain the recovery within the narrow range (40 – 43 %) specified by the manufacturer of these seawater RO membranes. This would require a control system that adjusted the recovery according to the available power. The membrane plant used for these results had been operated for more than 7000 hours over a wide range of pressure and flowrate. This led the authors to conclude that membranes can function under fluctuations without deteriorating, although additional information would be required for an ageing study.

Figure 1.18: Photo of the membrane plant used by Pestana *et al.* [100] to investigate the possibility of using a range of pressure and flowrates within a safe operating window.

To prove the technical feasibility of transient operation of RO with renewable energy, Gocht *et al.* [118] examined the impact of varying the feed pressure on the permeate flux and salt retention. The experiments were performed by increasing the pressure linearly at a rate of 180 bar/min and in steps from 10 – 60 bar. Unfortunately, details of the experimental setup or results were not presented. Nevertheless, the authors determined that there was nothing to rule out the transient operation of a RO membrane system. The recommended operating strategy for transient operation was to increase the operating pressure and feed flowrate according to increasing power, while ensuring that the crossflow velocity within the membrane module remained high, presumably to reduce the risk of membrane scaling. Overall in the literature there is little known about both the short and long-term consequences of fluctuations and intermittency on RO membrane systems, especially at the lower pressures used for brackish water desalination [60, 94, 101]. Furthermore, the safe operating window in which fluctuations are beneficial or tolerable has not yet been determined.

As a further consideration, it is well known that introducing fluid instabilities in the region of concentration polarisation will result in increased performance because the induced turbulence disturbs the polarisation layer [119, 120]. To examine the effect of cyclic operation on RO membranes, Al-Bastaki and Abbas [121] performed experiments in which the pressure was varied according to an asymmetric square wave

about a constant mean value. This method is known as the bang-bang cyclic strategy as it produces the most abrupt disturbance in the boundary layer. The experimental setup consisted of a 1.3 kW pump, a DOW FilmTec membrane (details not provided) and a 300 L feed tank with feed water concentration of 10,000 mg/L NaCl. Experiments were performed over a period of 30 minutes using two average pressures of 40 and 50 bar. At each average pressure, two amplitudes of fluctuation (5 and 10 bar) and five different time periods (5, 7, 10, 13 and 15 minutes) were investigated. The results showed that cyclic operation of this nature resulted in a higher average flux than under steady-state conditions for all of the amplitudes and time periods investigated. In addition, the flux increased with increasing amplitude and decreasing period of fluctuation of the operating pressure. This highlighted that square wave fluctuations with high frequency and amplitude were the most effective at disturbing the boundary layer and improving the productivity of the RO membrane. Analysis of the SEC and permeate concentration showed that the cyclic operation had no detrimental impact on either of these performance parameters. These results indicate that there could be possible benefits to be gained from the inherent fluctuations in a wind-membrane system, although there has been very little work performed in this area.

1.6.2 Operation under fluctuations within a safe operating window

The concept of a safe operating window for the transient operation of RO membrane systems with wind power was first proposed by Feron [96] in 1985. By examining the feasibility of the direct-connection of these technologies, two observations were made regarding the changes that would occur to the normal operation of the plant:

i. there would be irregular operation according to the availability of the wind, and
ii. operation with fluctuations in power according to the instantaneous wind speed.

It was decided that irregular operation would not cause any major problems as long as the cycling on/off of the plant was controlled such that the rate of pressure change and the frequency of cycling did not cause any damage to the membranes. The operation with fluctuations however, required further investigation because of the operational characteristics of membranes that require them to operate within a set range of pressure and flowrate conditions as defined by the manufacturers to avoid damage to the modules. The constraints arising from the membrane characteristics that define the safe operating window are illustrated in Figure 1.19. These constraints were determined to be as follows:

i. the maximum feed water pressure as determined by the mechanical strength of the materials used in the membrane;
ii. the maximum concentrate flowrate due to mechanical deterioration at high concentrate flowrates;
iii. the minimum concentrate flowrate due to precipitation of salts at high recovery and subsequent membrane fouling; and
iv. the maximum permeate concentration for a particular contaminant according to the WHO drinking water guidelines [12]. The guideline value for NaCl is 1000 mg/L (further details in Section 2.5.5). Low pressure can cause the permeate to exceed the guideline value as the salt concentration in the permeate is inversely proportional to the difference between the applied pressure and the osmotic pressure gradient.

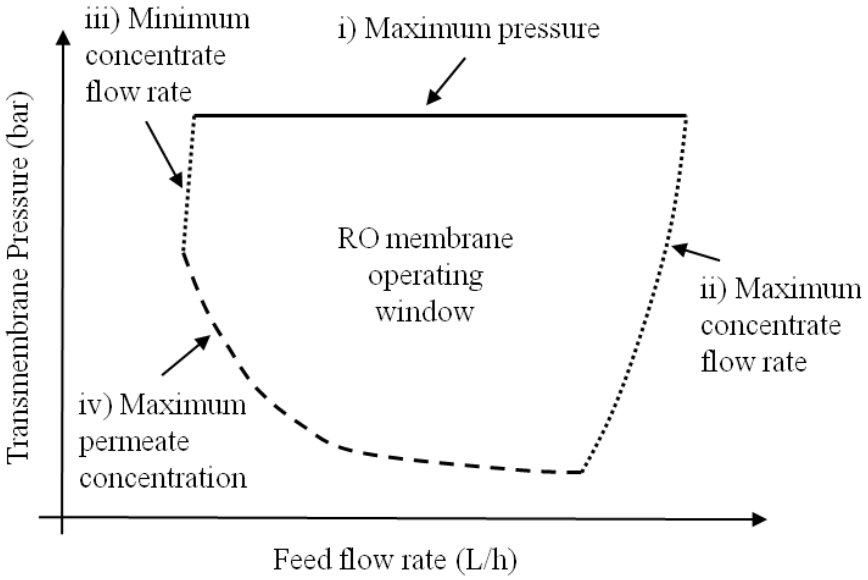

Figure 1.19: Safe operating window for a membrane as proposed by Feron [96], showing the maximum allowable range of operating conditions due to the manufacturer's specifications and the maximum permeate concentration (adapted from [96]).

Based on the above operational constraints, a membrane system should be able to operate within the safe operating window by adjusting the flow and pressure (hydraulic power) according to the electrical input power [107]. Feron went on to produce mathematical models describing the manner in which a RO plant could deal with the variability of wind power [96]. The two suggested methods of adapting the RO plant

were to vary the membrane area or allow transient operation within the constraints of the safe operating window. The conclusion was that neither option was economically beneficial as it either involved under-utilisation of expensive membrane area or a relatively minor increase in productivity for the increased complexity of the plant.

While the work by Feron [96] has since been referred to by several authors [97, 99-101], there is no record of a detailed experimental investigation or verification of an operating strategy for transient operation of RO plants within a safe operating window. Modelling work was performed by Miranda and Infield [101] on the wind-membrane system for seawater desalination described in Section 1.5.1. The objective was to maximise the energy extracted from the wind and the water output from the membrane system using a model of the whole system in Matlab-Simulink. The membrane system was designed to use two positive displacement pumps (medium and high pressure) to allow independent control of the feed flowrate and pressure at any point within the safe operating window. By controlling the variable speed drives (inverter coupled with induction motor) that powered the pumps, the speed of the pumps could be controlled to maximise the performance according to the available wind speed. However, further details on how this operating strategy could be applied were not provided, and the requirement for having two pumps, motors and inverters would prove costly. Another modelling exercise was performed by Moreno *et al.* [99] used the Dow FilmTec modelling package (ROSA) to determine the operating limits of a membrane module for a wind-powered plant. The limits were given as the minimum concentrate flowrate and the maximum feed flowrate, which are caused by ionisation and polarisation of the membrane. Based on this analysis, the minimum operating pressure and feed flowrate required to produce adequate permeate quality were identified. While preliminary experiments were performed using the operating constraints, these were aimed at verifying the steady-state ROSA analysis and detailed results were not provided.

Pohl *et al.* [97] performed some detailed modelling work using ROSA to investigate the use of four different operating strategies for transient operation within a safe operating window. A simple seawater RO system was modelled using a high pressure feed pump (70 % efficiency), a single-pass RO unit with four membrane modules in series and an energy recovery device (85 % efficiency). The simulation was performed using DOW FilmTec SW30-HR400i membrane modules and seawater (35,650 mg/L) at 25 °C. The

safe operating window was found by mapping out the maximum operating conditions based on the constraints given by the membrane manufacturer as defined by Feron [96]. Once this was established, the various operating strategies that could be achieved were plotted within the safe operating window as shown in Figure 1.20. The operating strategies were defined by holding one parameter constant while the others were varied within the operating window as follows:

i. constant feed pressure by varying the feed flowrate and recovery;
ii. constant permeate recovery by varying the feed pressure and flowrate to keep the ratio between them constant;
iii. constant feed flowrate by varying feed pressure and recovery; and
iv. constant concentrate flowrate by varying feed flowrate and pressure.

A comparison of the operating strategies was performed based on the steady-state operating points over the range of operation shown in Figure 1.20 [97]. Constant recovery was found to be the optimum operating strategy based on the criteria of low energy consumption, wide load range, good permeate quality and low pressure variation. Operating the RO plant with constant feed pressure, as used in conventional plants, resulted in low SEC but exhibited a narrow load range that is unsuitable for transient operation. This showed that the wide load range necessary for transient operation could only be achieved by varying the feed pressure. However, as detailed above (Section 1.6.1), the impact of pressure variations on the performance and lifetime of the membrane module is largely unknown and requires further investigation. The modelled results were not verified by practical experimentation and focussed purely on the membrane system without performance curves for the pumps and motors. Therefore, it would be necessary to perform a detailed experimental analysis to determine the accuracy of these results and the most appropriate method of implementing the chosen operating strategy.

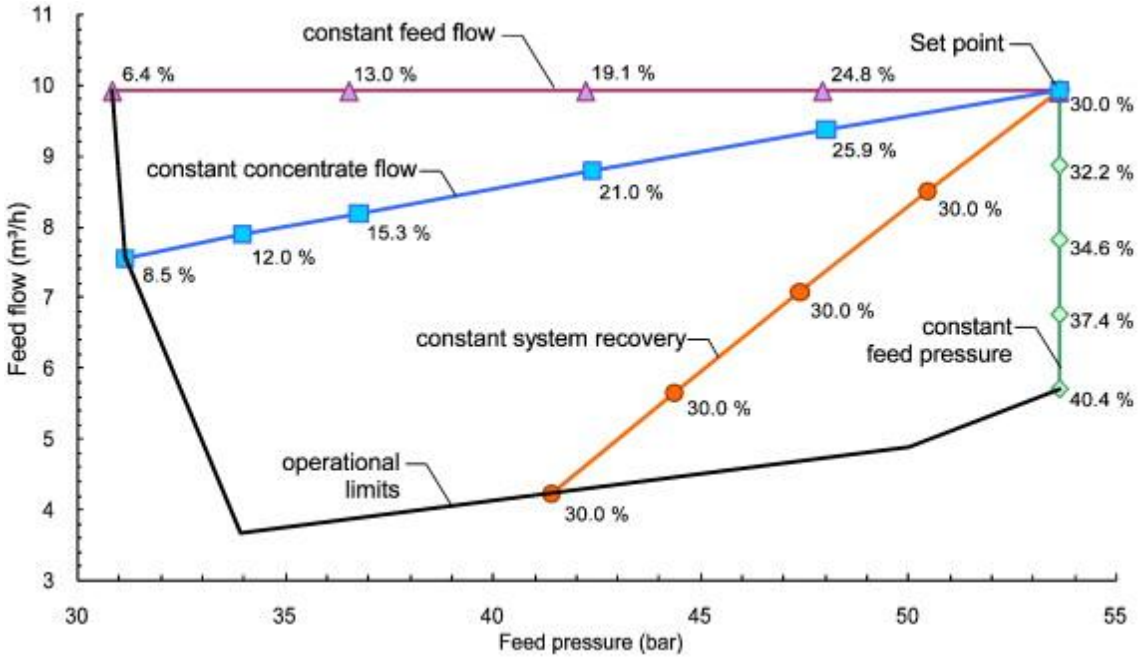

Figure 1.20: Modelling analysis by Pohl *et al.* [97] on the operating strategies that may be used for transient operation of membrane systems within the safe operating window.

Several of the mechanical windmill-powered membrane systems described in Section 1.5.1 utilised a hydraulic accumulator to reduce the variability of pressure and flowrate while providing an energy buffer for periods of low energy supply [58, 93]. Liu *et al.* [93] used a hydro-pneumatic accumulator with a bladder that was pre-charged with air to provide the energy fluctuation buffer and exert pressure on the water. The hydraulic accumulator had a volume of 300 L, which was sufficient to provide an average hydraulic detention time (storage time) of 30 min [30]. The hydraulic accumulator was operated with a feedback control mechanism to vary the pressure and flowrate according to the available wind speed. The range of operating pressure experienced by the RO membrane was restricted by the pressure tank to 5 – 7 bar. This was achieved using a series of solenoid valves that only allowed water to flow out of the pressure tank if the pressure was greater than 5 bar and relieved water from the tank at high wind speeds when the pressure exceeded the upper limit of 7 bar. On the second day of testing, when the wind speed dropped below 4 m/s and there was insufficient power being generated by the windmill (< 200 W), the membrane system relied on the hydraulic energy contained within the accumulator. During the ~30 min of storage time provided by the accumulator, the feed pressure dropped from 7 bar to 5 bar, and the feed flowrate dropped from 850 L/h to 0 L/h.

The hydraulic accumulator used by Robinson *et al.* [58] was operated under the same principle with a restricted pressure range of 6 – 11 bar, but did not used a feedback control mechanism for system operation. The hydraulic accumulator was operated continuously for 13 months of testing without any problems or maintenance required. Unfortunately, the amount of operational time provided by this hydraulic accumulator was not provided and was impossible to determine from the data provided. It is assumed that due to its small volume of 36 L, the hydraulic retention time would have been on the order of a few minutes, based on the size of the accumulator used by Liu *et al.* [93].

The simplicity of hydraulic accumulators is ideally suited to the mechanical output of a windmill system, and in conjunction with solenoid valves, they appear to allow dependable operation within a pre-determined operating window [58, 93]. The expected operational lifetime of a hydraulic accumulator is typically 12 years, with a well maintained bladder expected to last for the lifetime of the pressure vessel [122]. Regular maintenance is required to top up the gas in the bladder as they are not completely gas tight due to leakage rates that vary according to the bladder material [78]. This maintenance helps to uphold the performance of the hydraulic accumulator as well as reducing the risk of damage to the bladder. Maintenance periods are generally dependent on the leakage rate of the bladder, but are normally required every couple of months. This requires the availability of the appropriate gas (normally nitrogen) and a compressor. The use of solenoid valves to control the lower pressure limitation from the hydraulic accumulator should not impact upon the lifetime of the system as solenoid valves are standard industrial items that are generally considered to be robust and dependable. An experimental analysis on the robustness of 21 different solenoid valves showed operational lifetimes of 0.8 – 5 million cycles before failure [123]. The regular maintenance of the pressure in the bladder could therefore prove to be the main reason why it would be difficult to use hydraulic accumulators in remote locations; however this would require further investigation. Particularly in an electrically-based system, this form of hydraulic energy buffering would need to be compared against the numerous alternatives available in the form of electrical energy buffering or storage.

The energy losses across a RO membrane are caused by the pressure drop between the feed and concentrate flows and the viscous losses due to the driving force through the membrane module [95]. As this pressure drop is generally small (~ 0.5 bar), there can

be significant energy available in the brine stream. However, there are very few options for recovering the energy from the brine stream on small-scale RO systems, particularly over the low pressure range used for brackish water desalination [95]. Therefore, most small-scale systems are designed without energy recovery by using a valve to provide the necessary back-pressure on the concentrate stream. While cost effective, this method is wasteful of the energy available in the brine stream (up to 70 % losses for seawater RO) and can result in high SEC [95].

Constant recovery operation can be achieved using a piston pump that operates as an energy recovery device by recovering energy from the pressurised brine stream [95, 124-126]. These devices were first presented by Keefer *et al.* [124] in 1985 with the specific purpose of allowing transient operation of membrane systems with renewable energy sources. They operate by recycling the energy available in the brine stream to assist in pumping of the feed water. The cylinders in the energy recovery pump have a piston rod to pump the feed water coupled with a displacer piston where the concentrate brine is admitted to provide the majority of the driving force required to reciprocate the piston (Figure 1.21). The ratio of the swept volumes of the piston rod and displacer piston to the pump cylinders are used to determine the water recovery ratio of the system. The operating pressure and permeate flowrate both vary linearly with the pump speed which allows reduced energy consumption at part load.

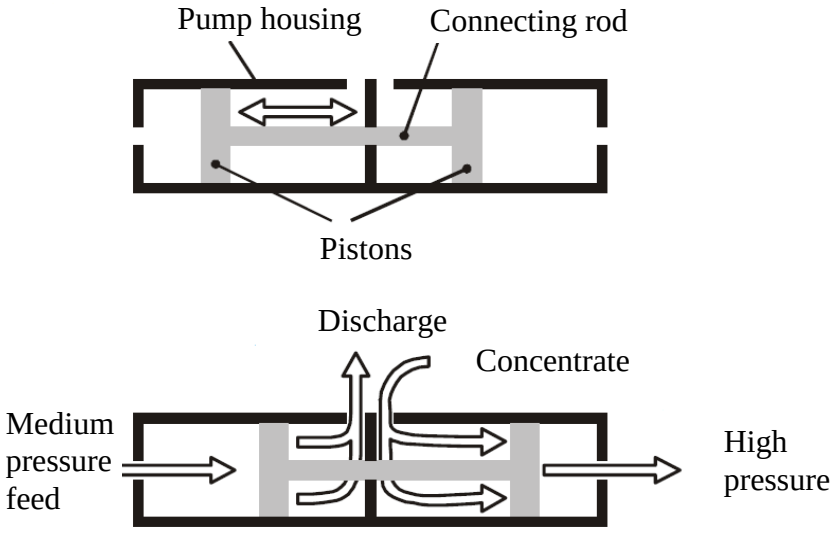

Figure 1.21: Cross-section schematic showing the basic operation of a Clark Pump (adapted from [127]).

Further development of the constant recovery piston pump has resulted in the commercial deployment of several devices including the Solarflow (Murdoch Environmental Technology Centre and Solco, Australia) [126] and the Clark pump (Spectra Watermakers, USA) [95]. The Solarflow is designed to provide 400 L/day of potable water with recovery ratios of either 16 or 25 %, however detailed results showing transient operation of this device have not been provided and preliminary laboratory testing showed low pump efficiency of only 15.5 %, calculated as the ratio of hydraulic power out to electrical power input [126]. Several problems were encountered during field testing of a previous prototype of the Solarflow pump in Australia, including fouling of the MF pre-filters and cracking of the pump case [128]. Although the prototype was tested in 2000, and the Solarflow system has now reached commercial production, updated information on the reliability problems could not be found. The Clark pump exhibited excellent short-term performance with efficiencies of 90 – 97 % over a wide operating range [95], however field testing showed that it was not robust and deteriorated when used for extended periods [129]. Aside from the reliability problems of the above piston pumps, there is also a need for a pressure recovery system for small-scale membrane plants that can operate down to the low pressures used for brackish water desalination (4 – 12 bar).

1.7 Potential of short-term energy storage

As described already, the main challenge associated with the implementation of RE-membrane systems is the intermittency and fluctuations of the renewable energy resource. Directly-coupled systems without energy storage can have higher efficiency, but the variable and unpredictable nature of the resource can cause lower permeate quality and productivity, resulting in the water demand not being met. While potable water can be stored for several days to overcome long term periods of intermittency, this does not address the negative impact of reduced power quality on the average quality and quantity of the permeate.

For energy storage over time periods of a few seconds to several minutes, a detailed investigation by the INVESTIRE network highlighted supercapacitors, lithium-ion batteries and flywheels as the best short-term energy storage mediums in terms of technology [130]. The objective of the research was to identify competitors to lead-acid

batteries for large-scale grid penetration of distributed energy systems. However, by performing a cost assessment including energy losses and the costs of maintenance and replacement, lead-acid batteries were found to be more cost effective than the above technologies [130]. While supercapacitors have long been recognised as ideal for situations that require short-term energy storage with long cycle life-time, high power density, deep cycle stability and maintenance free operation; they have poor energy density [131-133]. The following sections will highlight the relative merits of these technologies in order to explain why supercapacitors were chosen for the wind-membrane system.

1.7.1 Lead-acid batteries

The most common energy storage technology implemented in off-grid RE-membrane systems is lead-acid batteries [88-92], which are relatively cheap and readily available [134]. Lead-acid batteries are ideal for long-term energy storage due to their high energy density, round-trip efficiency (85 – 90 %) and low self discharge rate of 2 % of rated capacity per month [133]. The main disadvantage associated with lead-acid batteries is their lifespan, characterised by low cycle lifetime (500 – 1800 cycles) and reduced life caused by deep discharging or operation at high temperatures [133, 134]. When connected to RE systems that supply a daily load, typical lifetimes are between 3 – 5 years [135] and in extreme circumstances only 2 years [95]. To reduce the capital costs and the operation and maintenance costs associated with batteries, several RE-membrane systems have overcome the challenge of longer term fluctuations and intermittency by storing the permeate water in a tank [98-102, 118]. However, this does not address the effects of reduced power quality and frequent system shut-down, or potential damage to the pump motor and RO membrane [88, 101] caused by the short term variability of the RE resource.

1.7.2 Flywheel energy storage

Flywheels store kinetic energy in a rotating mass that is supported by magnetic bearings and housed within a vacuum to minimise frictional losses [136]. Low speed flywheels can be built with steel rotors and conventional bearings, however energy losses would be higher [133]. Energy is stored by accelerating the flywheel using an electric motor with surplus electricity, which increases the velocity according to the inertia of the mass

and the amount of energy available [133]. The energy stored by the flywheel is then proportional to the rotational speed squared [137]. By applying a torque and decelerating the flywheel, energy can be retrieved by powering the electric motor as a generator.

Flywheels can be designed to operate at low speeds (6000 rpm) or high speeds (50,000 rpm) and can achieve these speeds in a matter of minutes [133]. This technology has high time-dependent efficiency (90 – 95 %) and a long cycle life (10,000 – 100,000) with typical lifetimes from 15 – 20 years [134]. These devices are ideal for rapid pulses in power (<15 s) with a very short response time on the order of milliseconds [137]. The disadvantages of flywheels are that they have a high daily discharge rate of 55 – 100 % per day and a high capital cost due to the precision engineering required for advanced composite materials and low friction bearings [134, 136]. This means that flywheels are only useful for short-term energy storage with maximum storage times of up to a day [130]. For these reasons, flywheels are much more appropriate for power conditioning or smoothing, rather than storing energy for any significant length of time [133, 134].

1.7.3 Supercapacitor use for renewable energy buffering

Supercapacitors are energy storage devices that operate by building up positive and negative charge within an electrolytic solution, as opposed to the chemical reaction used in batteries [138]. They are also referred to as ultracapacitors or electrochemical double layer capacitors and are one of the most promising devices for buffering short term fluctuations from RE sources [130, 139]. While high power batteries such as lithium-ion are more appropriate for longer periods of time (10 – 15 min), supercapacitors are much better suited to situations where they are charged/discharged over periods of 1 – 2 min [140]. The charge/discharge process of supercapacitors is highly reversible, allowing them to undergo hundreds of thousands of cycles at a much higher rate than batteries [134]. Supercapacitors have a high round-trip efficiency between 84 – 98 %, and typical operating lifetimes of 8 – 12 years [131, 134, 141, 142]. However, one of the main disadvantages of supercapacitors is the high self-discharge rate compared to batteries, which has been quoted as 0.5 – 40 % after 24 hours, depending on the state of charge (SOC) [134].

Supercapacitors have been used in parallel with batteries to extend battery lifetime by reducing the number of charge/discharge cycles and buffering the peak currents in the battery [133, 135, 143-146]. A synergy exists between both technologies where high power or current pulses can be met by the supercapacitors while long-term energy requirements are provided by the battery [135, 144]. There are also numerous examples of the application of supercapacitors to large-scale grid-connected RE systems to smooth fluctuations, provide power during intermittency and re-start turbines when the grid fails [137, 139, 144, 147]. Experimental research using a 3 kW wind turbine simulator with power output fluctuations (0 – 700 W) demonstrated the ability of supercapacitors to buffer wind fluctuations over short periods of time (300 s) [148]. Although the power reduced to zero on several occasions, the ability of the supercapacitor bank to buffer intermittency was not examined in that study [148]. By installing supercapacitor storage in a 500 W wind turbine system, the availability of the system was increased by over 30 % at wind speeds higher than 5 m/s during a three hour period [149]. The results showed that the system performance deteriorated at wind speeds less than 5 m/s due to insufficient power from the wind turbine [149]. These applications highlight the feasibility of coupling supercapacitors with RE-membrane systems to improve their performance with the inherent short term fluctuations and intermittency of the resource.

1.8 Thesis objectives and research questions

One of the key outcomes of the recent European funded ProDes project was a roadmap for the promotion of desalination powered by renewable energy [28]. This report highlighted some of the key technical barriers to the wide-scale deployment of RE-membrane systems as follows:

i. the majority of RE-membrane systems are combinations of components that are developed independently resulting in poor reliability and increased water costs;
ii. the development of desalination focuses on large-scale systems resulting in a lack of appropriate technology for small-scale systems;
iii. desalination technology has been designed for constant power usage which could result in increased capital and maintenance costs for RE-membrane systems due to frequent replacement of membrane modules; and

iv. RE-membrane systems are considered to be more suitable for small-scale community led projects and are therefore not being commissioned by water authorities who consistently use centralised and familiar technologies.

These barriers emphasise the lack of detailed design knowledge, technical experience and experimental data from RE-membrane systems within the wider desalination community. This shortage of information results in a lack of confidence in their operation and low possibility for large-scale deployment as they are viewed as only being suitable for a niche market. The main aim of this PhD research is to systematically examine the challenges and performance issues associated with a wind-membrane system, and in doing so help to address this shortage of knowledge and experience. This information can then be used to improve the feasibility of this technology by determining appropriate strategies for robust operation.

The detailed literature review given above highlighted several issues as both important and lacking information, and therefore they require further investigation for the implementation of wind-membrane systems. The main challenges faced by wind-membrane systems are the inherent fluctuations and intermittency of the resource that can cause reduced power quality and transient operation of the membrane system. This means that the membrane module will be subject to fluctuations in pressure and flowrate, having been designed to operate under constant hydrodynamic conditions. While there have been several wind-membrane systems that operated under varying flowrate and pressure conditions, the transient operation of these systems under fluctuations, and the extent to which these fluctuations can be managed or exploited is not well understood.

An important consideration for wind-membrane systems is that the unpredictability of the wind resource may result in the water demand not being met. Storing the potable water is an efficient method of dealing with the wind variability and reduces the capital and maintenance costs associated with long-term energy storage. Based on the characteristics of wind speed fluctuations, lead-acid batteries are an inefficient method of energy storage resulting in increased operation and maintenance costs. Supercapacitors provide a promising alternative and are ideal for buffering short-term wind variability while providing long operational lifetime. Their potential for providing

improved power quality to improve performance and reduce the number of on/off cycles requires further investigation.

Concentration polarisation and the subsequent risk of membrane scaling are the main causes of reduced performance and membrane lifetime in brackish water RO/NF membrane systems. The safe operating window for the wind-membrane system should therefore avoid high water recovery to reduce the impact of concentration polarisation. To operate a membrane plant over a wide load range it is necessary to vary the feed pressure. Constant recovery operation appears to be a good operating strategy based on the criteria of low energy consumption, wide load range, good permeate quality and low pressure variation. However, the robustness of piston pumps for this purpose is still an issue and other operating strategies should be explored.

By implementing a systematic approach to the characterisation and impact of wind speed fluctuations and intermittency, the following research questions were developed to determine the feasibility and performance of wind-membrane systems:

i. What are the steady-state operating characteristics of the wind-membrane system over a range of wind speeds with brackish feed water? This information was used to map out the operating range of the system and provide a baseline for comparison with further experiments on the impact of wind speed fluctuations and intermittency (Chapter 3).
ii. What is the relationship between wind speed fluctuations and membrane system performance, and to what extent can these be beneficial or detrimental within a safe operating window? This was necessary to understand the specific dynamics of the system and determine the magnitude of fluctuations that can be tolerated while producing permeate within the guidelines for safe drinking water quality (Chapter 4).
iii. Why is wind intermittency so detrimental to membrane system performance and what are the impacts on the average permeate quality and quantity? By understanding the dynamics of cycling the membrane system on/off, the potential for short-term energy storage was determined (Chapter 5).
iv. What is the potential for supercapacitors to expand the safe operating window of the wind-membrane system by buffering short-term wind speed fluctuations and intermittency? This information was used to establish whether supercapacitors

could enhance the short-term performance of wind-membrane systems and provide an improved alternative to the commonly used lead-acid battery (Chapter 6).

v. How is the safe operating window for the wind-membrane system affected by the type of membrane module and feed water concentration, and what are the constraints to safe operation? The optimum operating strategy for transient operation of the wind-membrane system was then determined before examining the performance of the system subject to real wind speed fluctuations over 24 hours (Chapter 7).

Chapter 2

Materials and methods

This chapter provides details of the equipment, experimental design and techniques used throughout this research. A description of the membrane system and specifications for the performance of the progressive cavity pump and membrane modules are provided. The methodology for selecting the appropriate wind turbine for the membrane system involved detailed wind tunnel and outdoor testing in accordance with the IEC 61400 standards, and is useful for the design of future wind-membrane systems. The design process for sizing a supercapacitor bank for the wind-membrane system is also described in depth to provide a framework for other systems to utilise short-term energy storage. Experiments were designed to eliminate the uncontrolled variables and complexity inherent in real wind conditions, resulting in the use of sinusoidal fluctuations to characterise wind turbulence and square waves to represent intermittency. This experimental design was used to provide a comprehensive foundation (Chapter 3 – Chapter 5) for examining the effectiveness of supercapacitor energy buffering (Chapter 6) and the impact of real wind (Chapter 7) on the performance of the wind-membrane system.

2.1 Membrane system

2.1.1 System overview

The wind-powered desalination system (wind-membrane) used throughout this research was a single-stage RO/NF membrane system powered by a small wind turbine. All of

the components for the membrane system were mounted on a 4WD double-axle trailer as shown in Figure 2.1. The wind turbine system was designed using a free-standing tower with a portable base that could be pegged into the ground. This transportable system was designed to allow for field testing in remote areas. For the purposes of laboratory work, a wind turbine simulator (based on the wind turbine generator) was designed by the author and used as the power input to the membrane system (see Section 2.3).

The membrane system is now in its 6th prototype development stage, having undergone several iterations and field testing in Australia with UF for pre-treatment of the feed water [60]. It was sized to supply up to about 1000 L of fresh water per solar day from brackish groundwater sources, which is sufficient for a small community (approximately 50 people) [60, 94]. The system was designed to operate without storing energy in batteries as they result in increased capital and operating costs as well as lower system efficiency and decreased robustness [94, 95] (detailed in Section 1.7.1). Instead, by storing the permeate water in a tank, the challenge of meeting the water demand with variable and unpredictable power can be overcome [98-102, 118].

Figure 2.1: Photograph of the trailer-mounted membrane system in the laboratory at Heriot-Watt University.

The main components of the membrane system including the membrane housing, progressive cavity pump and permanent magnet brushless DC motor are shown in Figure 2.2. The main power requirement was a 300 W progressive cavity pump that

drew water through a micro filter (suction pressure of -0.3 bar) before pumping it through the RO/NF membrane (up to 12 bar). Figure 2.2 also shows the pressure, flowrate and conductivity sensors that were used on the feed, permeate and concentrate streams to measure the transient performance of the membrane system.

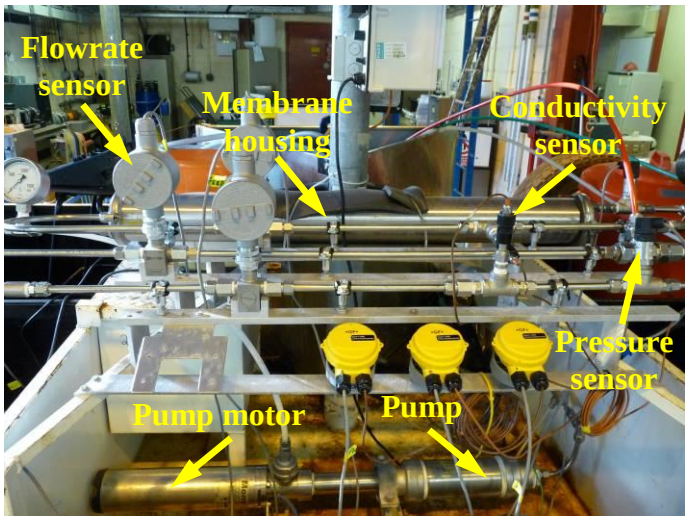

Figure 2.2: Main components of the membrane system including membrane housing, progressive cavity pump and permanent magnet brushless DC motor. Pressure, flowrate and conductivity sensors used on the feed, permeate and concentrate streams to measure transient performance at a reading rate of 1 Hz.

A polypropylene 1μm micro filter with cartridge volume of 1.2 L (SupaGard) was used to filter out larger particles (> 1 μm) to prevent damage to the pump and RO/NF membrane. This replaced the UF pre-treatment stage that was used for previously reported field results with this system [60, 94], as the UF membranes were not required when using synthetic feed water made with de-ionised water and NaCl. The micro filter was immersed in a 300 L feed tank (feed volume 130 L) with permeate and concentrate flows continuously recycled back into the feed tank to maintain a constant feed concentration. Most of the wetted parts in the system were constructed from marine grade stainless steel (316) to reduce the risk of corrosion when using saline feed waters.

A schematic diagram of the system illustrating the main components and placement of sensors for measuring performance is shown in Figure 2.3. The three main methods of controlling the wind-membrane system were i) the power input; ii) the regulating valve

on the concentrate stream (pressure) and iii) the maximum pump motor speed (this set the maximum voltage and therefore power consumed by the pump motor).

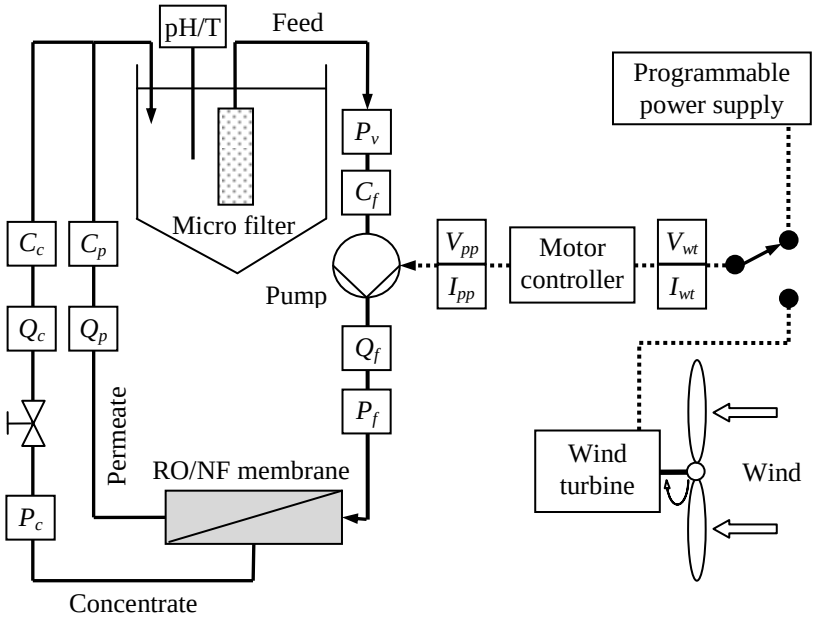

Figure 2.3: Schematic diagram of the wind-membrane system with electrical connections (dotted lines) and water flow (solid lines) for the components of the wind-membrane system: programmable power supply; wind turbine; motor controller; micro filter; RO/NF membrane; pump; *P*: pressure transducers; *Q*: flow sensors; *C*: conductivity sensors; *V*: voltage sensors; *I*: current sensors; pH/T: pH and temperature sensor.

To accurately determine the transient operation of the system under fluctuations, all of the parameters (pressure, flowrate, conductivity, temperature, pH, current, voltage) were taken at a reading rate of 1 Hz using a datalogger (dataTaker, DT800). A LabVIEW (version 8.2.1) interface was used for viewing instantaneous system performance and downloading the data. The specifications and response times for all of the sensors used to measure the performance of the membrane system are provided in Table 2.1.

Table 2.1: Specifications of the sensors used for measuring the performance parameters of the membrane system. For the specific location of sensors, see Figure 2.3.

Measurement parameter	Sensor position	Manufacturer (type)	Model No.	Operating range (units)	Accuracy	Response time	Ref.
Flowrate	Feed	Omega (turbine)	FTB9512	30 – 600 (L/h)	± 0.5 %	1 s	[150]
	Permeate/ Concentrate		FTB9510	16.5 – 300 (L/h)			
Conductivity	Feed/ Permeate	Georg Fischer (inline electrode)	3-2821 (Cell: 1 cm^{-1})	10 – 10,000 (µS/cm)	± 2 %	1 s	[151]
	Concentrate		3-2822 (Cell: 10 cm^{-1})	100 – 200,000 (µS/cm)			
Pressure	Feed	Burkert (mechanical transmitter)	8323	0 – 1 abs (bar)	± 0.5 %	0.1 ms	[152]
	Permeate/ Concentrate			0 – 16 (bar)			
Voltage	Wind turbine/ Motor controller	Omega (signal conditioner)	DRF-VDC	0 – 200 (V_{DC})	± 0.2 %	0.7 ms	[153]
Current			DRF-IDC	0 – 5 (A_{DC})	± 0.3 %	0.7 ms	[154]
pH	Feed tank	Georg Fischer (protected bulb)	2717	0 – 14 log(L/mol)	± 0.3 %	5 s	[155]
Temperature	Feed tank	Omega (thermocouple probe)	KTSS	-200 – 900 (°C)	± 0.75 %	1 s	[156]

2.1.2 Previous research performed with the membrane system

As mentioned in Section 2.1.1, the membrane system used for this PhD research is currently in its 6th prototype development stage, having gone through several previous iterations in terms of the pumping system, design and other components. The initial design utilised two Dankoff Solar Slowpumps, model 1322 for the high pressure pump and model 2507 for the recycle pump to recover energy from the concentrate stream [157]. The high pressure pump was a rotary vane pump with a maximum operating

pressure of 13 bar and a relatively constant feed flowrate of 114 – 90 L/h over the pressure range from 0.6 – 13 bar. The pump exhibited low efficiency (calculated as 20 – 22 % by the author) with power consumption of 168 W (11.2 A, 15 V_{DC}) at 13 bar. Field testing of this system was performed in April 2002 at a remote location in New South Wales, Australia with feed waters of 2000 mg/L NaCl added to rainwater, 150 mg/L dam water and 3500 mg/L borehole water [157]. The results showed that when the operating pressure was increased from 9 bar to 10 bar, there was a large increase in the SEC from 2.2 kWh/m^3 to 3.5 kWh/m^3 with no change in the permeate flowrate. This was because the permeate flowrate produced by the rotary vane pump was virtually independent of the operating pressure. Therefore, the additional power requirements for increasing the pressure resulted in a direct increase in the SEC. When tested with borehole water of salinity 3500 mg/L, the minimum SEC of 8 kWh/m^3 was achieved at operating pressure of 6 – 7 bar. Further testing of the Dankoff 1322 pump showed that the SEC decreased with increasing pressure up to 7 bar, beyond which the SEC increased due to reduced permeate flow caused by pump and salinity limitations [158]. The restrictions of this pump with regards to feed flowrate resulted in high recoveries at medium pressure (> 7 bar) due to the pumps inability to maintain high cross-flow velocity.

Previous tests were performed using the current membrane system with six Zenon ZW10 UF membranes for pre-treatment and four different RO/NF membranes with a real brackish groundwater (5300 mg/L TDS, 8290 µs/cm) using a constant power source [60]. The operating window of the system under steady-state conditions (pressure from 4 to 12 bar and feed flowrates 300, 400 and 500 L/h) showed that safe operation could be achieved for this highly brackish groundwater with NF90, ESPA4 and BW30 membranes but not with TFC-S [60]. The system was further tested by direct connection (no energy storage) to a PV array (300 W from two 24V_{DC} panels) over several solar days [94]. The results showed that the RE-membrane system (using a BW30-4040 membrane) operated under fluctuations in solar irradiance of 500-1200 W/m² (125 – 300 W) with minimal effect on the permeate quality, although further testing below 500 W/m² (< 125 W) would be required to determine its operation under heavy cloud [94]. In addition, the fluctuations shown over a typical solar day during these experiments [94] showed an average rate of change of 1 % per second (based on data with a 5 s sampling rate) whilst wind fluctuations over a typical day were

calculated to vary by 12 % per second (calculated using high resolution data in Section 2.5.4). Therefore, using a wind turbine to power the membrane system requires a separate investigation to determine the effect of higher frequency fluctuations in power associated with wind energy and their impact on the safe operating window.

2.1.3 Progressive cavity pump and motor

The 300 W progressive cavity pump (Mono Pumps, Australia, SM022, specifications shown in Table 2.2) was developed for use with solar power as it has the advantage of being able to operate at very low power (~ 40 W). These pumps use an eccentric single helix rotor that rotates within a flexible stator with double internal helixes. The difference in the pitch angle between the rotor and stator forms sealed cavities that travel along the stator from the suction side to the discharge side with the rotation of the rotor giving smooth axial fluid flow [78]. There is a continuous seal developed between the rotor and stator that pumps the fluid at a flowrate proportional to the rotational speed of the pump. The pressure developed by the pump is proportional to the length of the rotor and stator. Every revolution of the helical rotor sweeps the full surface of the stator thus minimising the build up of deposits and making it ideal for potable water applications [79]. Flexible shafts have been developed to bend according to the rotation of the rotor and reduce wear of components by overcoming cyclic oscillations caused by the off-centre rotation of the helical rotor [78].

The power output from the wind turbine was used to directly power the pump and associated electronics, which were the only power requirements for the membrane system. The pump used a permanent magnet brushless DC motor rated at 300 W with maximum voltage and current of 180 V_{DC} and 3 A, respectively. The motor controller electronics included a MPPT (inputs: 30 – 100 V_{DC}, 0 – 5 A) that was designed to maximise the power output from a 48 V_{DC} PV array, and the required controller for the brushless DC motor. The MPPT had a microprocessor to continuously adjust the voltage from the renewable energy generator according to the demands of the motor controller [79]. An electric commutator was used to determine the rotor position of the motor by sensing back EMF voltages to minimise wear, rather than using brushes as used in conventional DC motors. The energising sequences for the motor phases were then determined by a microprocessor according to the rotor position. In order to reduce

pump and motor wear at low speeds, the power was shut off for approximately 1 min if it dropped below 40 W for more than 3 s, before attempting to restart the pump.

Table 2.2: Progressive cavity pump and motor specifications according to the manufacturer (Mono Pumps, Australia, SM022) [79]. Note that the pump used was custom built (based on this design) with titanium rotor and a shorter flexible shaft, however details of the changes to performance could not be obtained.

Specification	Value
Power rating (W)	300
Nominal torque rating (Nm)	0.7
Nominal speed at rated power (rpm)	3000
Flowrate at rated power (L/h)	1200*
Maximum discharge pressure (bar)	15*
Efficiency at nominal torque rating (%)	85
Input voltage range (V_{DC})	0 – 180
Operating frequency range (Hz)	0 – 100
Maximum current (A)	3
Total length (mm)	1025
Outside diameter (mm)	93
Mass (kg)	18

* Note that values are for the pump only and do not include the rest of the membrane system.

The performance curves for the pump are shown in Figure 2.4 as a function of volumetric flowrate. The equations used for calculating the static pressure head and pump efficiency are provided in Section 1.4. The pump efficiency calculation requires knowledge of the shaft power transferred from the pump motor, which is the electrical power input to the pumping system subject to efficiency losses in the motor. For these calculations, the efficiency of the brushless DC motor was assumed to be constant at 85 % (Table 2.2) over the operating range as efficiency curves could not be obtained. These performance measurements were taken on the membrane system using the regulating valve on the concentrate stream to simulate water head, hence shown as equivalent head (Figure 2.4A). The range of equivalent head (m) covered the total operating range of the membrane system with system pressure from 2 – 14 bar. The pump efficiency (Figure 2.4B) of 30 – 55 % was consistent with other published experimental data for progressive cavity pumps [80, 81] (Section 1.4.2).

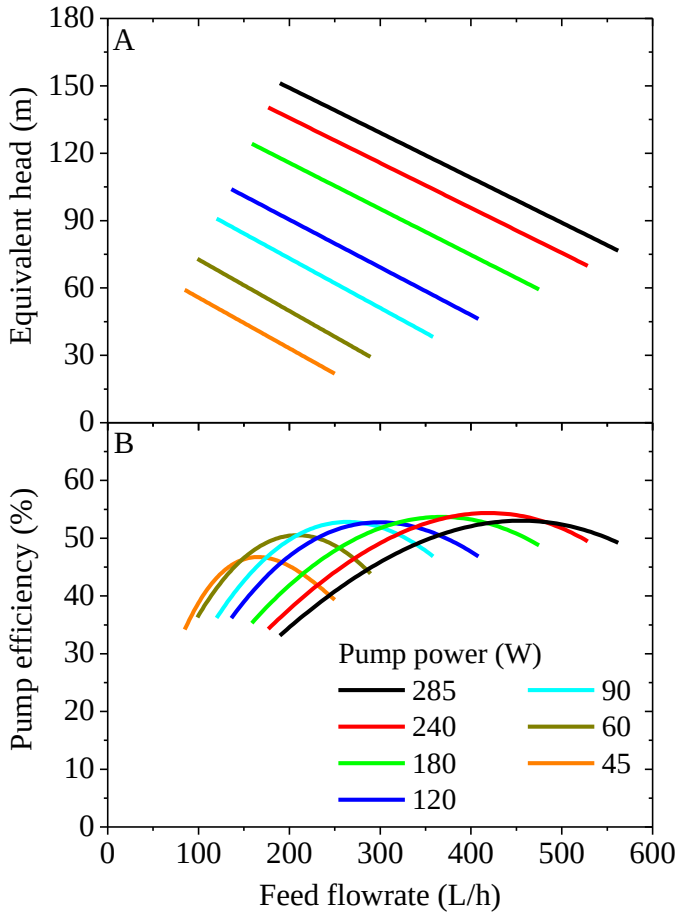

Figure 2.4: Performance curves for the 300 W progressive cavity pump: equivalent head (A) and hydraulic efficiency (B) as a function of volumetric flowrate.

2.1.4 Membrane modules

The choice of RO/NF membrane module for use in the membrane system is determined by the characteristics of the groundwater and the contaminants that need to be retained, and is therefore location dependent. As described in Section 1.2.1, NF membranes have high retention of divalent ions (90 – 98 %) and variable retention of monovalent ions (20 – 80 %), whereas RO membranes retain dissolved salts and inorganic molecules with high retention (95 – 99 %) [49]. The disadvantage of RO membranes is that their reduced permeability results in lower flux and higher energy consumption. Therefore, there is a balance to be struck between using a RO membrane to retain the majority of salts and contaminants and using a NF membrane to reduce the cost of water while retaining specific salts and contaminants.

The low pressure RO/NF membranes used for this work are specifically designed for brackish water desalination and exhibit high sodium chloride retention even when operated at low pressure (typically 4 – 12 bar) [49]. The ability to operate effectively at low pressures is ideal for coupling with small renewable energy generators in order to provide the necessary energy required for desalination. This is an important point as operation of the membrane system at the standard test conditions given by the manufacturer (Table 2.3) would require significant energy input and therefore a much larger renewable energy generator and pump than used for the wind-membrane system. This is because RE-membrane systems have significantly different design criteria compared to large-scale grid connected membrane plants to minimise the size of renewable energy generator required (discussed further in Chapter 3).

Table 2.3: Membrane performance characteristics at standard test conditions (25 ˚C, pH 8) according to the manufacturer [49].

Product	Description	Module dimensions			Permeate flowrate (L/h)	Stabilised salt retention (%)
		Diameter, mm (inch)	Length, mm (inch)	Active area, m² (ft²)		
BW30-4040	Brackish water reverse osmosis membrane element	99 (3.9)	1016 (40)	7.2 (78)	380 (Using 2000 mg/L NaCl at 15.5 bar and 15 % recovery)	99.5
NF90-4040	Nanofiltration element	99 (3.9)	1016 (40)	7.6 (82)	320 (Using 2000 mg/L $MgSO_4$ at 4.8 bar and 15 % recovery)	99.5

A low pressure RO membrane (aged BW30-4040) was used for the bulk of the experimental work (Chapter 3 – Chapter 6), while a new BW30-4040 and NF90-4040 membrane module were additionally used for the safe operating window analysis (Chapter 7). The BW30-4040 membrane is described by the manufacturer as a high rejection RO element for brackish water desalination that is typically applied to feed waters with up to 10,000 mg/L NaCl. The NF90-4040 is a NF membrane for 90 % salt removal, high removal of iron, pesticides, herbicides and total organic carbon and generally applied to feed waters up to 2000 mg/L NaCl [49]. The membrane

performance characteristics at standard test conditions according to the manufacturer are shown in Table 2.3.

The performance of the membrane modules at the standard set-point conditions used for the wind-membrane system are given in Table 2.4 for comparison. The aged BW30 was used for field trials in Australia in 2005 [60, 94] and extensive laboratory testing from 2008 to the present date. There has been a reduction in the retention and an increase in the permeate flowrate and therefore recovery compared to a new BW30 membrane module. However, this aged membrane module continues to produce permeate with concentration < 600 mg/L from a feed water of 5500 mg/L NaCl, well within the WHO guideline value of 1000 mg/L [12], which is why it continues to be used. The performance of the aged BW30 is described in detail in Chapter 3 – Chapter 6.

Table 2.4: Measured membrane performance characteristics according to standard set-point conditions of 240 W pump motor power, TMP of 10 bar and feed flowrate 250 L/h using feed water concentration 5500 mg/L NaCl.

Module	Retention (%)	Recovery (%)	Permeate flowrate (L/h)
BW30-4040	97.0	28	72
Aged BW30-4040*	92.0	30	90
NF90-4040	91.6	45	135

*Membrane used for field trials with real water in Australia (2005) and extensive lab testing using synthetic water (2008 – 2011).

2.1.5 Water quality and analysis

Feed waters were prepared using deionised tap water (3 µS/cm, grade 2 – 3 according to ISO 3696) and general purpose grade NaCl (> 99 % NaCl, Fisher Scientific, UK). Feed water salinities of 2750 mg/L, 5500 mg/L and 10,000 mg/L NaCl at temperature of 13 ±0.5 °C and pH of 6.8 ±0.2 were used. These feed water salinities were chosen to represent a range of typical salinity levels from brackish groundwater reserves [34] and to provide a basis for comparison with previous experimental results from field trials in Australia that were performed using feed water of 8290 µS/cm (5300 mg/L TDS) [60].

The conductivity of the feed, permeate and concentrate streams were measured using conductivity electrodes (GF Signet) at a reading rate of 1 Hz. The measured electrical conductivity, *EC* (µS/cm) was converted into NaCl concentration (*C*, mg/L) using:

$$C = k_{ec} \,.\, EC \,, \qquad (2.1)$$

where the conversion factor k_{ec} = 0.625 was determined using a calibration curve for NaCl dissolved in deionised water at 13°C.

An air bubbling system was used to ensure homogenous mixing and the temperature of the feed water was maintained at 13 ±0.5 °C by constant circulation through a water chiller system. This feed water temperature was chosen to reflect a typical groundwater temperature as would be found in regions with a temperate climate. The temperature of groundwater responds to seasonal variations in the heat from the sun at depths of up to 25 m and is generally within 7 °C of the mean annual air temperature whilst on average 1 – 2 °C higher [159].

2.1.6 Concentration polarisation calculations

The following methodology was used to determine the extent of concentration polarisation and its impact on the performance of the membrane system. The effects of concentration polarisation are best described using a schematic of the boundary layer achieved under steady-state conditions as shown in Figure 2.5.

The net driving force for water permeation across the membrane is determined by the difference between the trans-membrane applied pressure (ΔP, bar) and the trans-membrane osmotic pressure ($\Delta\pi$, bar) between the membrane surface and permeate. According to the solution diffusion model, the flux of water can be considered equal to the total volume flux (J_v, L/m^2.h), and is determined as [47]:

$$J_v = L_p \left(\Delta P - \Delta\pi\right), \qquad (2.2)$$

where L_p is the permeability coefficient for the solvent flux (L/m^2.h.bar). L_p relates the flux of water through the membrane to the applied pressure and can be measured experimentally using deionised water by assuming $\Delta\pi$ = 0 bar [160].

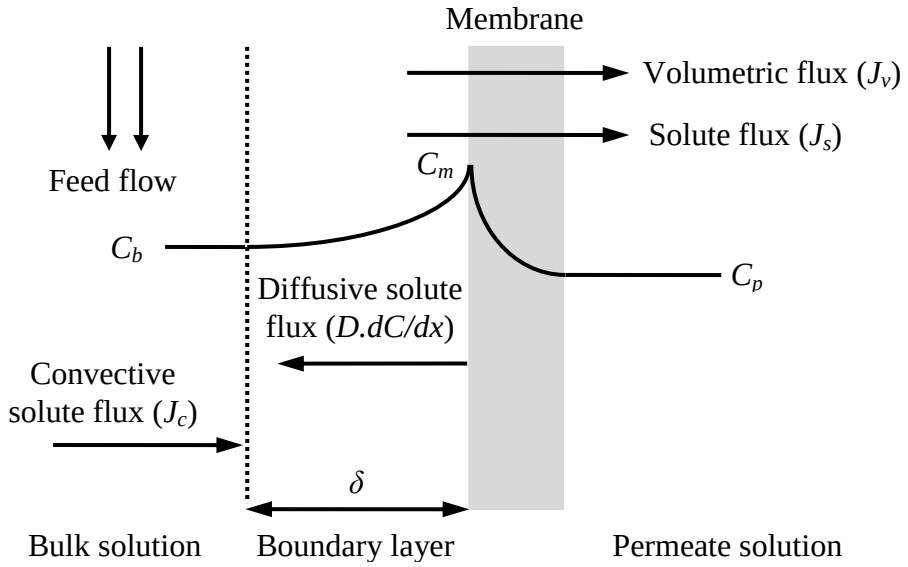

Figure 2.5: Schematic representation of concentration polarisation (adapted from [161]).

The net driving force for the solute flux (J_s, mg/m^2.h) is due to the concentration gradient across the membrane (ΔC, *mg/L*) based on the difference in concentration between the membrane surface and the permeate:

$$J_s = P_s \,.\, \Delta C \,, \tag{2.3}$$

where P_s is the diffusive salt permeability of the membrane (m/s).

The stagnant film model is commonly used in the analysis of concentration polarisation assuming one-dimensional steady-state conditions [162]. By performing a mass balance on an element of fluid in the boundary layer (Figure 2.5) and equating convective solute flow towards the membrane with back-diffusion flow, the following differential equation can be determined [163]:

$$J_s = C_p \,.\, J_v = C \,.\, J_v - \frac{dC}{dx}\,, \tag{2.4}$$

where C is the solute concentration in the boundary layer at distance x from the membrane surface. Solving this differential equation over a boundary layer thickness δ (m) gives:

$$ln\left(\frac{C_m - C_b}{C_b - C_p}\right) = \frac{J_v \,.\, \delta}{D} = \frac{J_v}{k_d}\,, \tag{2.5}$$

where k_d is the mass transfer coefficient (m/s) and the subscripts m, b and p refer to membrane surface, bulk solution and permeate, respectively. Therefore, the concentration modulus (β) that determines the extent of concentration polarisation can be calculated as:

$$\beta = \frac{C_m - C_p}{C_b - C_p} = exp\left(\frac{J_v}{k_d}\right), \tag{2.6}$$

The concentration polarisation modulus will increase by increasing the applied pressure (higher permeate flux), decreasing the Reynolds number (reduced mass transfer and less turbulent conditions) and increasing the bulk concentration (higher difference in osmotic pressure) [164]. The mass transfer coefficient is defined as:

$$k_d = \frac{D}{\delta}\,, \tag{2.7}$$

where D is the salt diffusion coefficient in the bulk solution (m^2/s). The most common methods for determining the mass transfer coefficient utilise hydrodynamic correlations based on the dimensionless Sherwood (*Sh*) number. The Sherwood number describes the ratio between mass transport by convection and diffusion near the membrane surface [61]. It is determined using the Reynolds (*Re*) and Schmidt (*Sc*) numbers as follows [163, 165]:

$$Sh = \frac{k_d \,.\, d}{D} = a_1 \left(\frac{du}{\nu} \right)^{a_2} . \left(\frac{\nu}{D} \right)^{a_3} = a_1 \,.\, Re^{a_2} . Sc^{a_3}, \qquad (2.8)$$

where d is the hydraulic diameter of the membrane flow passage (m), u is the flow velocity through the membrane (m/s), ν is the kinematic viscosity (m^2/s), a_1 is a numerical constant characterising the geometry of the flow channel, a_2 is the Reynolds number exponent and a_3 is the Schmidt number exponent in the mass transfer correlation. The parameter values of a_1, a_2 and a_3 used in the literature vary significantly and are highly dependent on channel geometry and hydrodynamic conditions, thus they cannot be applied uniformly to different systems or different operating conditions. Therefore, a more straightforward experimental technique for determining the mass transfer coefficient was proposed by Sutzkover *et al*. [163]. This calculation is based on the decrease in permeate flux resulting from the higher osmotic pressure of a salt solution as compared to pure water flux. The mass transfer coefficient is calculated as:

$$k_d = \frac{(J_v)_{salt}}{ln\left(\frac{\Delta P}{\pi_b - \pi_p} . \left(1 - \frac{(J_v)_{salt}}{(J_v)_{water}} \right) \right)}, \qquad (2.9)$$

where $(J_v)_{salt}$ is the permeate flux ($L/m^2.h$) with salt water, $(J_v)_{water}$ is the pure water flux, π_b and π_p are the osmotic pressures (bar) of the bulk and permeate solutions, respectively.

2.1.7 Experimental setup

To examine the effect of energy fluctuations and determine the safe operating window for the wind-membrane system, it was necessary to standardise the setup of the variable input parameters to the membrane system. This was required to allow accurate comparison of the results between different sets of experiments and to simplify the analysis of the safe operating window. Aside from changing the membrane module and feed water characteristics (concentration and temperature), the following input parameters could be used to control the operating characteristics of the membrane system:

i. varying the input power to the membrane system using either the wind turbine simulator (Section 2.3) or a programmable power supply (Agilent Technologies, E4350B);
ii. adjusting the position of the regulating valve on the concentrate stream (performed before the start of each experiment but not during operation); and
iii. altering the maximum pump motor power using the speed regulating dial. Note that this feature was not used for any of the results presented as the impact was a restriction on the operating range of the pump. The pump motor speed was set to the maximum position for all experimental results.

As there were essentially two variables (input power and position of regulating valve) that could both alter the feed pressure and flowrate, a set-point was required to ensure consistency between experiments. The set-point was always determined at a constant input power of 240 W. This input power had traditionally been used when the membrane system was operated with solar PV, as it corresponded to a solar irradiance of 1000 W/m^2, as used in the standard test conditions for PV modules. However, this value of power had other advantages as it allowed the pump to operate at almost full capacity, ensuring rapid stabilisation of the membrane system and providing a good starting point for calibrating all of the sensors.

To simplify the description of the set-point, the impact of both the input power and the position of the regulating valve (set-point pressure) on the performance of the membrane system are illustrated in Figure 2.6. Each set-point pressure resulted in a different curve of TMP (Figure 2.6A) and feed flowrate (Figure 2.6B) according to the input power. To compare system performance under fluctuations and intermittency, all of the experiments in Chapter 3 – Chapter 6 were set up using 240 W input power with the regulating valve adjusted to provide 10 bar TMP and feed flowrate of 250 L/h (red lines in Figure 2.6). Once this set-point was achieved, experiments were performed with variable power which had a direct impact upon both the TMP and feed flowrate as shown in Figure 2.6. In Chapter 7, the set-point pressure was varied from 4 – 12 bar (or within the maximum operating range) to determine the safe operating window for the wind-membrane system. To ensure consistency and simplify the analysis, the operating window was described using set-point pressure lines, which were all determined at 240 W input power as shown in Figure 2.6.

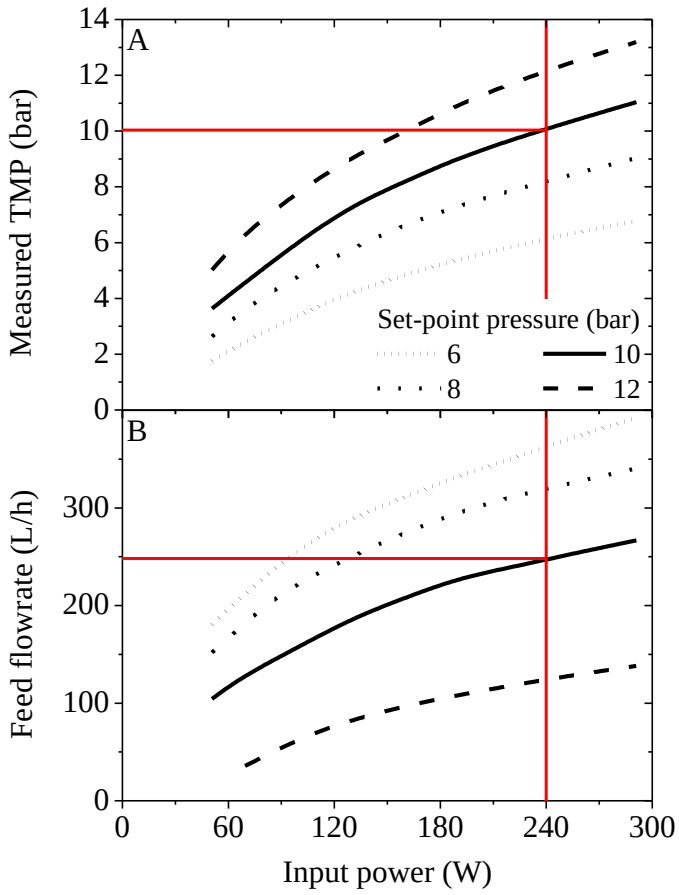

Figure 2.6: The use of set-point pressure (set using regulating valve on concentrate stream) to set the hydraulic inputs to the membrane system from the pump in terms of (A) transmembrane pressure (TMP) and (B) feed flowrate at 240 W input power. The standard set-point of 10 bar used for experimental work in Chapter 3 – Chapter 6 is highlighted by the red lines.

The standard set-point was also used to verify the pure water flux (J_0) of the membranes using deionised water (J_0 = 25 L/m².h for BW30 and J_0 = 70 L/m².h for NF90) regularly (at least every 3 days) throughout the period of testing to ensure that the membrane performance was consistent before and after each series of experiments.

Membrane specific parameters were calculated using the following relationships (location of sensors shown in Figure 2.3):

$$\Delta P = \left(\frac{p_f + p_c}{2} \right) - p_p \qquad (2.10)$$

$$J_v = \frac{Q_p}{A_{membrane}} \tag{2.11}$$

$$Y = \left(\frac{Q_p}{Q_f} \right).100\% \tag{2.12}$$

$$R = \left(1 - \frac{C_p}{C_f} \right).100\% \tag{2.13}$$

$$\text{SEC} = \frac{I_{pp} . V_{pp}}{Q_p} \tag{2.14}$$

where, ΔP is measured trans-membrane pressure (bar), p is relative pressure (bar; where $p_p = 0$), J_v is flux (L/m².h), Q is flowrate (L/h), $A_{membrane}$ is membrane area (m²), Y is recovery (%), R is retention of NaCl (%), C is concentration (mg/L), SEC is specific energy consumption (kWh/m³), I_{pp} is current (A) and V_{pp} is voltage of the pump motor (V).

2.2 Wind turbine selection

2.2.1 Matching wind turbine to membrane system

Matching the wind turbine to the membrane system is one of the main design challenges for a directly-connected system. Having chosen the pump motor based on the required pressure and flowrates for the membrane system, the wind turbine must be sized to meet this demand according to the available wind resource and the wind turbine power curve. As mentioned previously, the wind resource is highly variable and site specific. The fact that small wind turbines are generally placed on low towers to minimise construction costs means they experience much lower average wind speeds and are susceptible to turbulence caused by obstacles and frictional effects. Another challenge is that there are only 13 MCS accredited small wind turbines (Section 1.3) so the vast majority of the wind turbine power curves are not produced according to a standard and are often rated at high wind speeds that are rarely experienced in the field. This makes it very difficult

to accurately predict performance without testing the wind turbine and using high resolution wind speed data. The wind turbine was selected based on the power requirements of the pump motor and associated electronics as detailed in Section 2.1.3, as well as the performance and cost of the wind turbine. The process of choosing the most appropriate wind turbine for this application is shown below using a feasibility study for operating the wind-membrane system in Accra, Ghana.

2.2.2 Initial feasibility study for operation in Ghana

In order to complete a comprehensive wind turbine comparison and predict the performance of the wind-membrane system in a realistic environment, a study was carried out to determine the potential for implementation in Ghana. This West African country was chosen as links have been made with Kwame Nkrumah University of Science and Technology and water samples were taken from various boreholes and wells across the country in 2007 [110]. A recent study showed that in Ghana only 62 – 70 % of people in urban areas and 35 – 40 % of people in rural areas have access to treated water [166]. An undesirable consequence of the fact that Ghana has the largest gold mining industry in West Africa has been the contamination of water supplies by contaminants such as arsenic [167]. There are also many water sources in the North of the country that have high levels of fluoride, giving rise to dental and skeletal fluorosis [168].

A comparison of eight small wind turbines available in the UK was performed using average monthly wind speed data from a previously published study [169]. The average monthly wind speed values were based on the daily mean value at a height of 2 m above the ground from readings taken close to Accra. The log law [113] was used to give the wind speeds at a height (U_z) of 8 m (z), which is a more realistic hub height for a small wind turbine using the following equation:

$$U_z = U_{ref} \cdot \left(\frac{\ln\left(z / z_0 \right)}{\ln\left(z_{ref} / z_0 \right)} \right), \qquad (2.15)$$

where U_{ref} is the wind speed at 2 m (z_{ref}), and z_0 is the surface roughness index. A roughness index of 0.1 m was used to describe this terrain which was characterised by countryside with trees and hedges [113]. The variation in the average monthly wind speed in Accra at a hub height of 8 m is shown in Figure 2.7A, where the average wind speed was 4.3 m/s with a range 3.8 – 5.4 m/s. The wind speed characteristics are better analysed using the Weibull distribution, which calculates the probability (*p(U)*) that the wind speed will exceed a certain value [113]:

$$p(U) = \left(\frac{k_w}{c_w}\right).\left(\frac{U}{c_w}\right)^{k_w-1}.exp\left(-\left(\frac{U}{c_w}\right)^{k_w}\right), \qquad (2.16)$$

where k_w is the shape factor, c_w is the scale factor and U is the mean wind speed (m/s). A Weibull shape factor of 3 was used, as this is typical of areas that experience the trade winds. The scale factor can be calculated empirically using the shape factor:

$$c_w = U.\left(0.568 + \frac{0.433}{k_w}\right)^{-\frac{1}{2}} \qquad (2.17)$$

The Weibull distribution for Accra (Figure 2.7B) showed that a high shape factor results in a curve with a sharp peak, indicating less wind speed variation. In general, the average wind speed data for Accra showed an adequate wind speed velocity with little variation, which could be well suited to wind energy production. The Weibull distribution (Figure 2.7B) was used to calculate the annual energy production in Accra of eight different small-scale wind turbines available in the UK. The annual energy output calculations were based on the power curves for each of the wind turbines (Figure 2.8) as detailed by the manufacturers [170]. Further details of the wind turbine performance specifications are provided in Table 2.5.

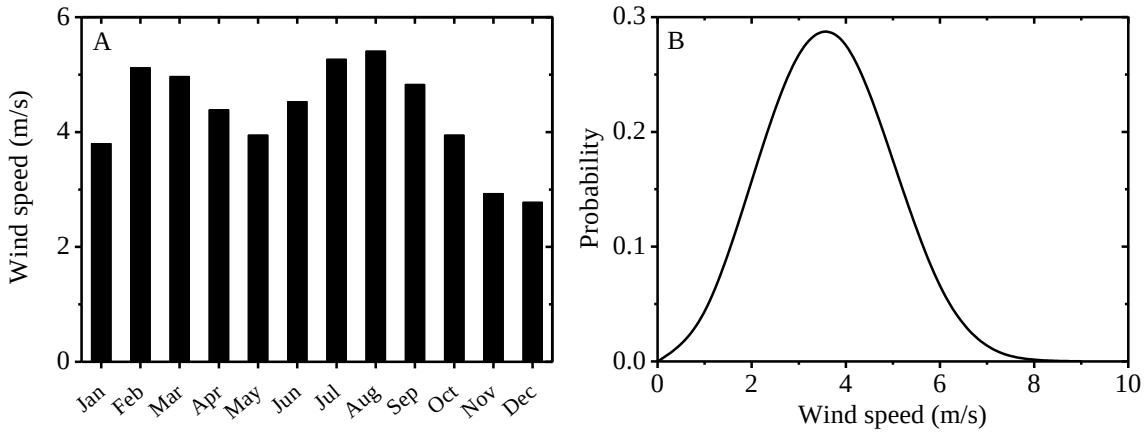

Figure 2.7: Average monthly wind speed (A) and Weibull distribution (B) (where k_w = 3) at 8 m hub height for Accra, Ghana (1991) (adapted from SolEnergiCentret [169]).

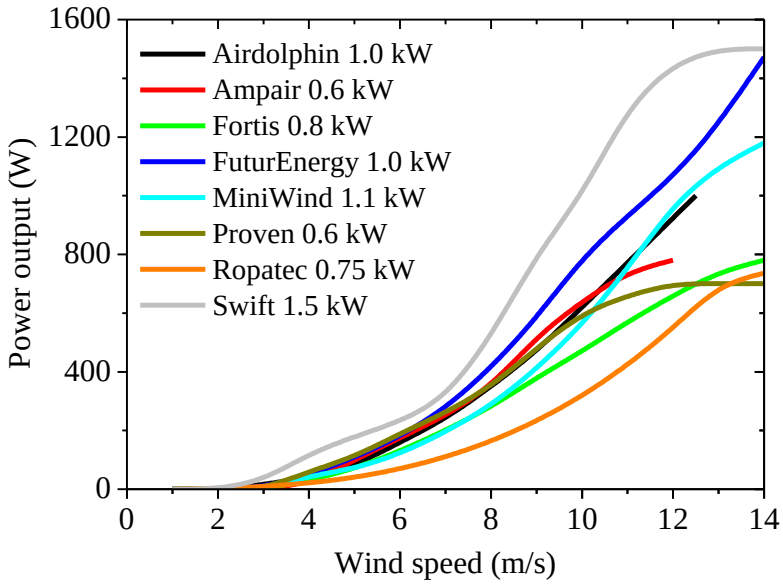

Figure 2.8: Power curves for eight small wind turbines available in the UK rated at ≤ 1.5 kW, based on manufacturers data from [170].

Table 2.5: Performance comparison of eight small wind turbines available in the UK, rated at ≤ 1.5 kW. Manufacturers specifications taken from [170] and calculated values based on wind resource data for Accra, Ghana from [169] as illustrated in Figure 2.7.

	Manufacturers Data						Calculated based on one year			
Manufacturer	Rated Power (kW)	Rated Speed (m/s)	Cut-in Wind Speed (m/s)	Blade Diameter (m)	Generator Output (V_{DC})	Approx Cost Installed (£k)	Capacity Factor (%)	Energy Production (kWh)		Cost of Energy (£/kWh)
							8 m	4 m	8 m	8 m
Airdolphin	1.00	12.5	2.5	1.0	25	6.5	8	425	710	9.2
Ampair	0.60	11.0	3.0	1.7	48	3.1	13	389	580	5.3
Fortis	0.80	14.0	3.0	2.2	24	6.2	8	320	590	10.5
FuturEnergy	1.00	12.5	3.2	1.8	48	2.4	9	490	830	2.9
MiniWind	1.10	12.0	3.8	1.8	48	3.0	6	343	580	3.6
Proven Energy	0.60	12.0	2.5	2.6	48	8.5	15	531	810	10.5
Ropatec	0.75	14.0	2.0	1.5	48	3.8	5	207	340	11.2
Swift	1.50	12.0	2.3	2.1	240*	7.0	10	836	1250	5.6

*Voltage is V_{AC}

The total annual energy production and the capacity factor for each of the eight wind turbines is shown in Figure 2.9. The capacity factor is defined as the ratio of energy generated over the year to the energy that the wind turbine would produce at its rated power over the same time period. The Proven Energy wind turbine had the highest capacity factor giving a good indication of how efficiently it could operate in the given wind conditions. The Swift wind turbine produced up to twice the amount of energy of some of the other turbines, and initially this seemed to be an obvious result due to a higher rated output of 1.5 kW compared to power ratings of ≤ 1.1 kW for the others.

When the wind turbine hub height was increased from 4 to 8 m, the annual energy output from the wind turbines increased by 50 – 80 % (Table 2.5). This shows why it is beneficial to obtain high laminar wind speeds by mounting the wind turbine as high as feasibly possible. At lower average wind speeds, it is apparent that the cut-in wind speed (when the turbine starts to generate power) and the initial steepness of the power curve have a large effect on the total energy output. This is highlighted by the fact that

although the MiniWind turbine was rated at 1.1 kW, it had a high cut-in speed (3.8 m/s) and relatively shallow power curve (Figure 2.8) that produced similar energy production to the Ampair 600 W wind turbine. While the Proven Energy wind turbine appeared to have the best overall performance according to the capacity factor, once cost was taken into consideration (Table 2.5), it became apparent that the 1 kW FuturEnergy wind turbine was the most cost-effective wind turbine for this specific application.

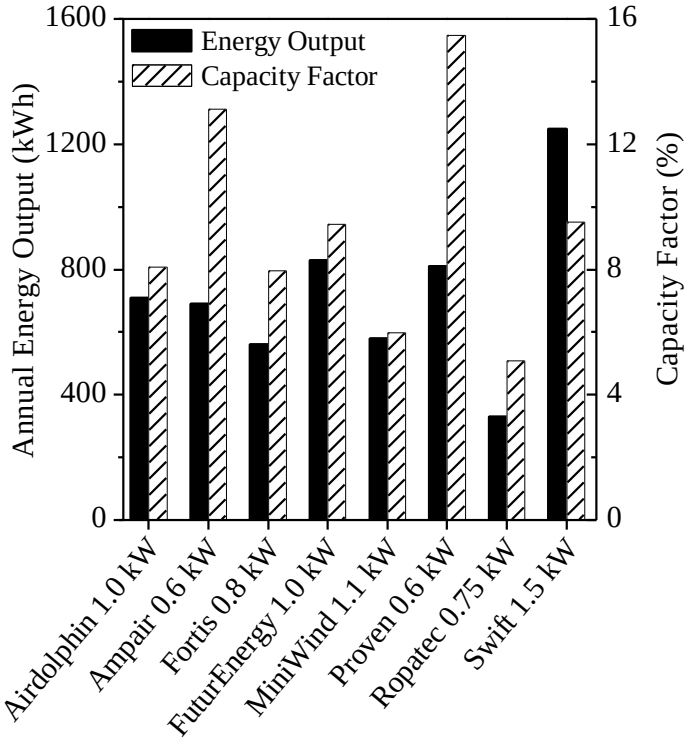

Figure 2.9: Performance comparison of eight small wind turbines using calculated annual energy output and capacity factor at 8 m hub height for Accra, Ghana (1991). Calculations performed using wind resource data from [169] and wind turbine data from [170].

The FuturEnergy wind turbine had improved performance at lower wind speeds by using five blades as a result of the higher starting torque at low tip speed ratio obtained by using increased solidity [66]. An additional design consideration was that the DC/DC converter as part of the MPPT for the existing membrane system was designed to operate with 48 V_{DC} from PV modules. By using the FuturEnergy wind turbine which had a 48 V_{DC} output, no further electronics or modifications were required. It must be noted that this performance comparison was based on a situation where the average annual wind speed is relatively low for wind energy production. This was deemed to be

useful for the membrane system where the low power performance would be crucial for maintaining high productivity.

2.2.3 Wind tunnel analysis

To assess the real performance of the FuturEnergy wind turbine (theoretical performance given in Table 2.5), the wind turbine was tested under controlled conditions using a wind tunnel. The wind tunnel (TUV NEL, East Kilbride, UK) had a cross-section of 3.2 m (width) × 3 m (height) and could produce wind speeds up to 13.3 m/s using a bank of nine fans that were switched selectively to create steady-state conditions or controlled fluctuations in wind speed. The wind turbine was mounted in the centre of the airflow and the wind speed was measured using a cup anemometer (A100L2, Vector Instruments) that was placed 1.5 m upstream of the wind turbine rotor as shown in Figure 2.10.

Figure 2.10: FuturEnergy wind turbine and cup anemometer mounted in wind tunnel for power performance testing (TUV NEL, East Kilbride, UK).

The power performance curves for the FuturEnergy wind turbine over a range of resistance loads (5 – 50 Ω) are shown in Figure 2.11. The first thing to note is that the maximum power output from the wind turbine was ~ 550 W, only half of the rated power of the wind turbine (1 kW at 12.5 m/s) given by the manufacturer [171]. The power curve given by the manufacturer was significantly higher than the measured

performance over the whole range of operation. Details of how this power curve was measured could not be obtained from the manufacturer. Some plausible methods include modelling or the use of a test bed assembly with a variable speed motor drive.

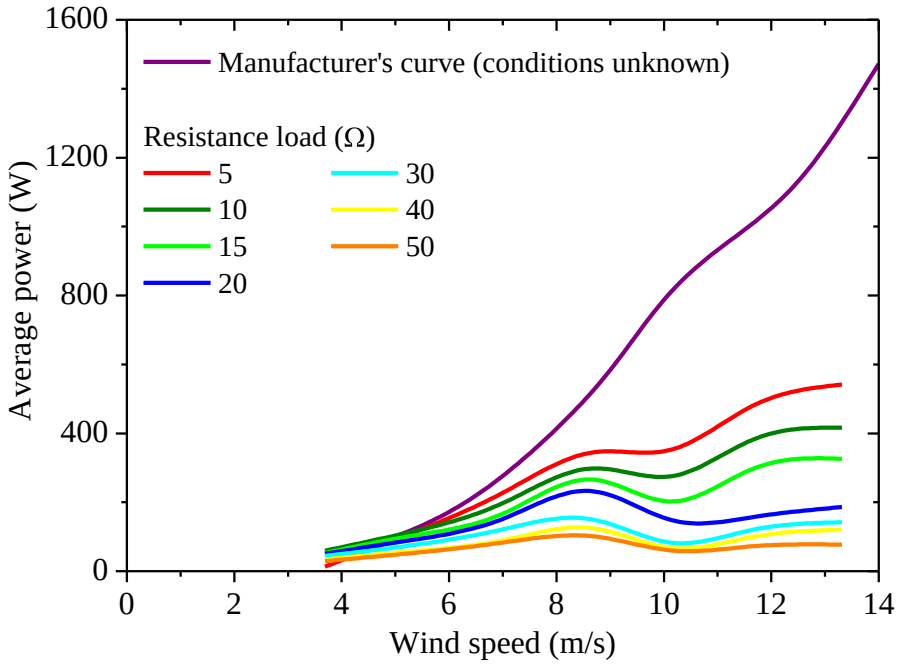

Figure 2.11: FuturEnergy wind turbine power curve provided by the manufacturer [171] compared to power curves measured in the wind tunnel with a range of resistance loads (5 – 50 Ω).

These results highlight the discrepancy between the theoretical performance and the measured performance of small wind turbines. An additional observation was the furling of the wind turbine observed at wind speeds of >8.7 m/s. This self-protection mechanism that is used on small wind turbines to turn the blades of out of high winds to avoid excessive electrical or mechanical loading was thought to be the main reason for the large difference between the theoretical and measured performance. As the wind turbine was intended to supply power to the 300 W pump motor on the membrane system, this wind turbine was deemed to be a suitable match at realistic average wind speeds of 5 – 8 m/s.

2.2.4 Outdoor testing

Power performance measuring of the wind turbine was carried out according to the international standard technical specification (IEC 61400-12-1) [172]. This was done over a period of one month (August 2010) on Heriot-Watt campus to verify the wind tunnel experiments and provide further data on the real operating characteristics of the wind turbine. Figure 2.12 shows the location of the test site on Heriot-Watt campus and a wind rose for the sight highlighting the prevailing south-westerly winds that are common in Edinburgh [173]. Extended testing of the wind turbine could not be carried out due to the proximity of the site to Edinburgh airport and the resulting planning regulations. However, a one month period was sufficient to gain experience of setting up the wind turbine and to provide an overview of the wind turbine performance in real wind conditions. The wind turbine was mounted on an 8 m stand-alone tower along with weather measurement instrumentation for wind speed and direction, barometric pressure, temperature and humidity as shown in Figure 2.13. All of the specifications and response times for the sensors used for the wind turbine performance measurements are provided in Table 2.6.

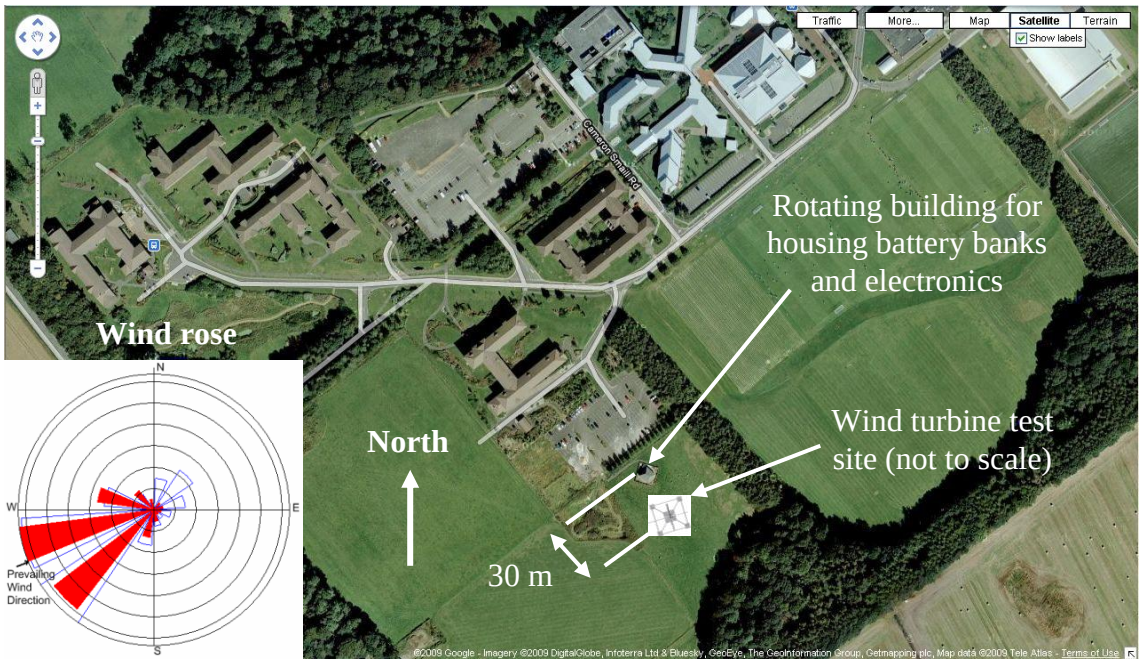

Figure 2.12: Wind turbine test site in a field on Heriot-Watt campus with a wind rose showing the prevailing SW wind resource.

Figure 2.13: Outdoor power performance testing of FuturEnergy wind turbine on Heriot-Watt campus for three weeks, August 2010.

Table 2.6: Specifications of the sensors used for power performance testing of the FuturEnergy wind turbine. See Figure 2.13 for a photo of the wind turbine setup.

Measurement parameter	Sensor position	Manufacturer (type)	Model No.	Operating range (units)	Accuracy	Response time	Ref.
Wind speed	Hub height, 4m from turbine	Vector Instruments (anemometer)	A100L2	0.1 – 75 (m/s)	± 2 %	0.15 s	[174]
Wind direction	1.5 m below hub height	Vector Instruments (wind vane)	W200P	360° (angle)	± 1 %	–	[175]
Voltage		Omega (signal conditioner)	DRF-VDC	0 – 200 (V_{DC})	± 0.2 %	0.7 ms	[153]
Current	Junction box, 4 m below hub height	Powertek	CTH – Type 2	0 – 40 (A_{DC})	± 1 %	0.7 ms	[176]
Air pressure		Campbell Scientific (barometer)	CS100	600 – 1100 (mb)	± 0.2 %	0.1 s	[177]
Temperature/ Humidity	Shield, 3 m below hub height	Vaisala (probe)	HMP50	-40 – 60 °C 0 – 98 %	± 3 %	15 s	[178]

The cup anemometer (Vector Instruments, A100L2) was mounted at hub height, 1.5 m above the wind vane (Vector Instruments, W200P), and both were placed on a boom

4 m away from the turbine rotor according to the regulations given in the IEC standard [172]. All of the measurement parameters taken from the sensors given in Table 2.6 were recorded at a reading rate of 0.2 Hz using a datalogger (dataTaker, DT600).

Over the course of testing, three different load configurations were tested: 48 V_{DC} battery charging, 12 V_{DC} battery charging and direct connection to a 3 kW (18 Ω) immersion element for water heating (Aqualoy, 27”). These loads were used to test the wind turbine operation for typical domestic applications. A charge controller (Xantrex, C40) was used to protect the battery banks from overcharging by diverting excess power to a dump load. Each of the load configurations was tested for a period of at least five days to enable the wind turbine power curves to be determined over a sufficient time period and range of wind speeds as shown in Figure 2.14.

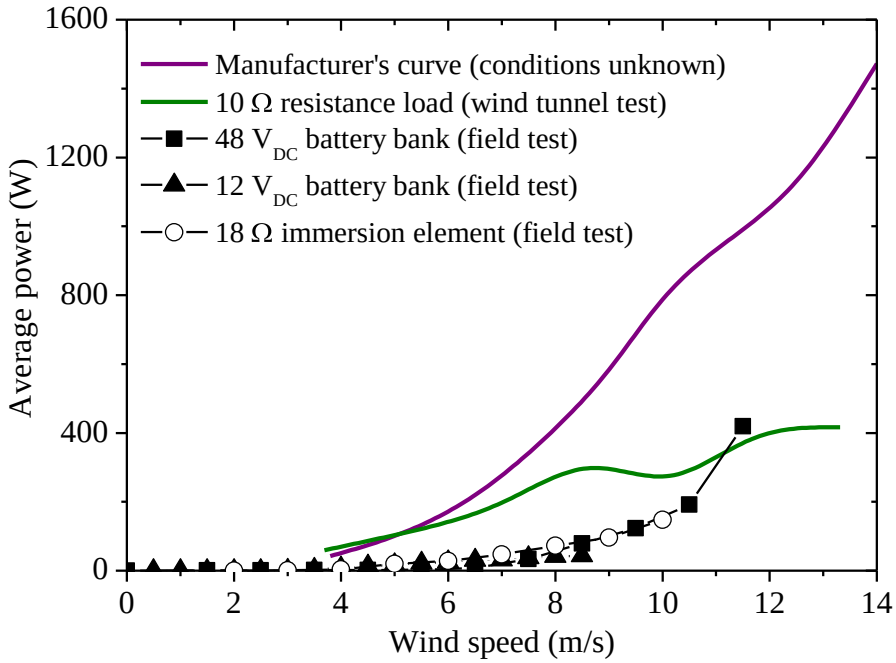

Figure 2.14: Real wind turbine performance curves compared to wind tunnel test (10 Ω) and manufacturer’s data [171].

As demonstrated in Figure 2.14, the power output from the wind turbine was significantly lower than predicted by the manufacturer or observed in the wind tunnel experiments (Section 2.2.3). This was caused by the low wind speeds throughout the period of testing as shown in Figure 2.15. The regions with missing data were a result of poor battery performance in the datalogger or periods when the load on the wind turbine

was being changed. Even though there was a predominantly South Westerly wind, the average wind speed over the period of testing was 2.89 m/s. The accuracy of this data was verified by cross-checking with the local meteorological station less than 1 mile away at Gogarbank, where the average wind speed was 3 m/s over the same period of time. The average wind speed for Edinburgh is 4.2 m/s, calculated according to 10 years of historical data averaged over 10 min intervals from 1999 – 2008 [173]. On average, the probability distribution for Edinburgh showed that 72.5 % of the wind speeds were > 3 m/s, highlighting the poor average wind speeds obtained during the period of testing. However, the outdoor power performance testing did verify that the wind tunnel performance was more accurate than the performance curve given by the manufacturer. The maximum power output from the wind turbine was 420 W at 11 m/s when connected to the 48 V_{DC} battery bank, this was consistent with the wind tunnel tests for a 5 – 10 Ω resistance load at the same wind speed. As the outdoor testing did not yield satisfactory power performance curves, the results of the wind tunnel experiments were used for characterising the wind turbine and the design of the wind turbine simulator.

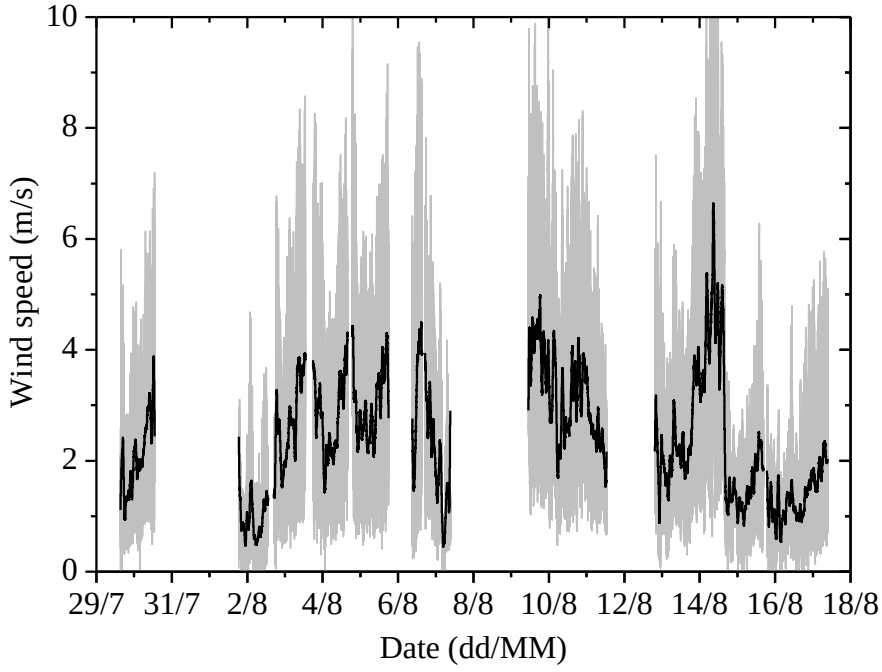

Figure 2.15: Wind speed data (0.2 Hz) during the power performance measurements at 8 m hub height. Black line shows smoothed data.

2.3 Wind turbine simulator

In order to perform real wind speed experiments in the laboratory with the membrane system, a wind turbine simulator was designed using the FuturEnergy wind turbine generator with the blades removed (Figure 2.16). The wind turbine simulator was designed using a geared induction motor (Nord, SK51E-160M/4) with a 10/1 speed reduction (range 300 – 1000 rpm) that was controlled using a vector frequency inverter (Nord, SK700E-112-340-A). The geared motor was rated at 6.7 kW (de-rated from 11 kW by 10/1 speed reduction) and could therefore be used for testing larger wind turbines. The power output characteristics of the simulator were modelled on the wind tunnel experiments described in Section 2.2.3. Real wind turbine behavior was simulated by using the motor to apply the torque that the blades would give and allowing the wind turbine generator to spin accordingly. Compensation for the blades being removed was applied to the accelerating torque by calculating the moment of inertia of the blades and subtracting it from the applied torque.

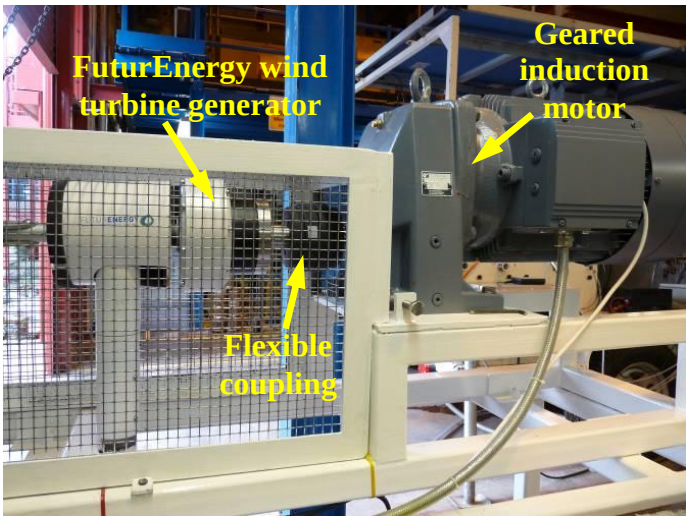

Figure 2.16: Wind turbine simulator with FuturEnergy wind turbine inside the safety cage (left) and geared induction motor (right).

The control of the wind turbine simulator and supply of wind speed data to the frequency inverter were carried out using a LabVIEW interface (Figure 2.17). A data acquisition system (DAQ, National Instruments, NI USB-6008) was required to interface with the frequency inverter to control the output speed and measure the rotational speed, acceleration, torque and power in order to calculate the required torque. An optical encoder was designed to measure the rotational speed and

acceleration of the wind turbine generator in order to calculate the applied torque. A paper strip with black and wide strips was attached to the generator and a photo-interrupter (Kingbright, KTIR0821DS) was used to sense the movement of the strips. The torque controller calculated the motor torque which should be applied by first calculating the required torque given the input wind speed and the rotational speed of the wind turbine generator. By comparing this value with the actual torque output of the motor, the inverter speed was adjusted to compensate for any difference. This control loop for the frequency inverter was executed every 20 ms to maintain a high degree of accuracy.

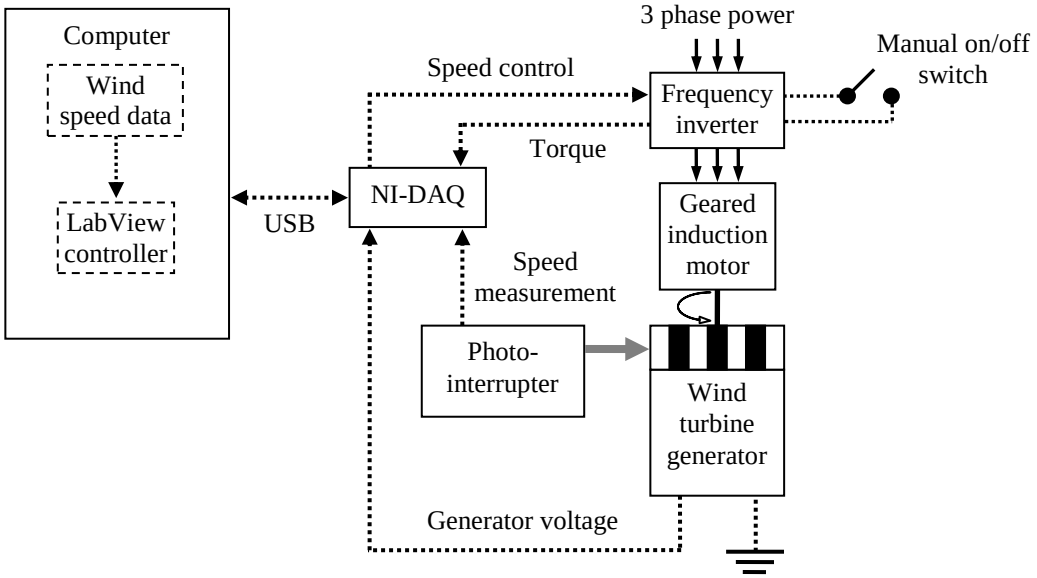

Figure 2.17: Block diagram of the wind turbine simulator (adapted from Reid [179]).

The wind turbine simulator was calibrated under steady-state and fluctuating conditions using the results of the wind tunnel tests (Figure 2.11). These particular results were used as the power curve given by the manufacturer and the field testing results did not provide accurate performance curves (Figure 2.14). Figure 2.18 shows a comparison of the wind turbine performance from the wind tunnel experiments with the calibrated performance curve of the wind turbine simulator. Initially, the wind turbine simulator produced a higher power output than the wind tunnel experiments due to inaccuracy in the measurement of the inertia of the wind turbine rotor. However, further calibration by reducing the acceleration torque provided by the motor to the wind turbine generator

yielded a much more accurate performance curve as shown in Figure 2.18. Furling of the wind turbine at wind speeds ≥ 8.7 m/s was incorporated into the wind turbine simulator to achieve realistic performance over the whole wind speed range. To prevent the wind turbine generator from overheating at high rotational speeds, the wind turbine simulator was given a maximum torque rating at wind speeds of ≥ 13.3 m/s. Therefore, higher wind speeds resulted in a constant power output from the wind turbine generator.

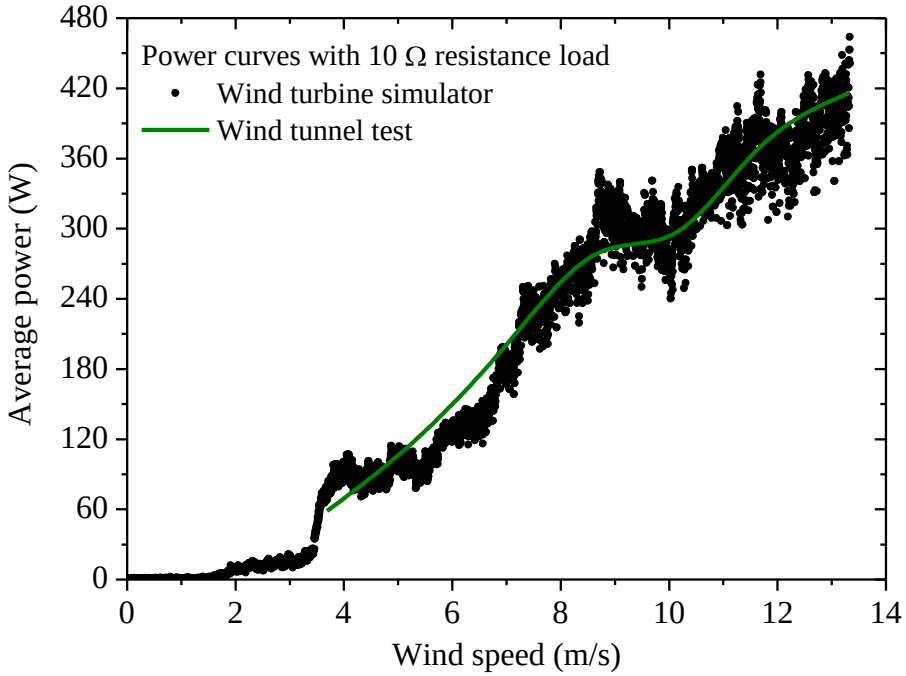

Figure 2.18: Power performance curve of the wind turbine simulator compared to results of the wind tunnel experiment from Figure 2.11.

To determine the accuracy of the wind turbine simulator under wind speed fluctuations, a further performance comparison was made with wind tunnel experiments where sinusoidal wind speed fluctuations were induced with the wind turbine directly-connected to the membrane system. (described in Section 2.5.3). Figure 2.19A shows the sinusoidal wind speed fluctuations that were produced in the wind tunnel experiments and used as the input to the wind turbine simulator. The membrane system was set up to provide the same load to the wind turbine simulator using the set-point conditions (Section 2.1.7) and a feed water of 5500 mg/L NaCl.

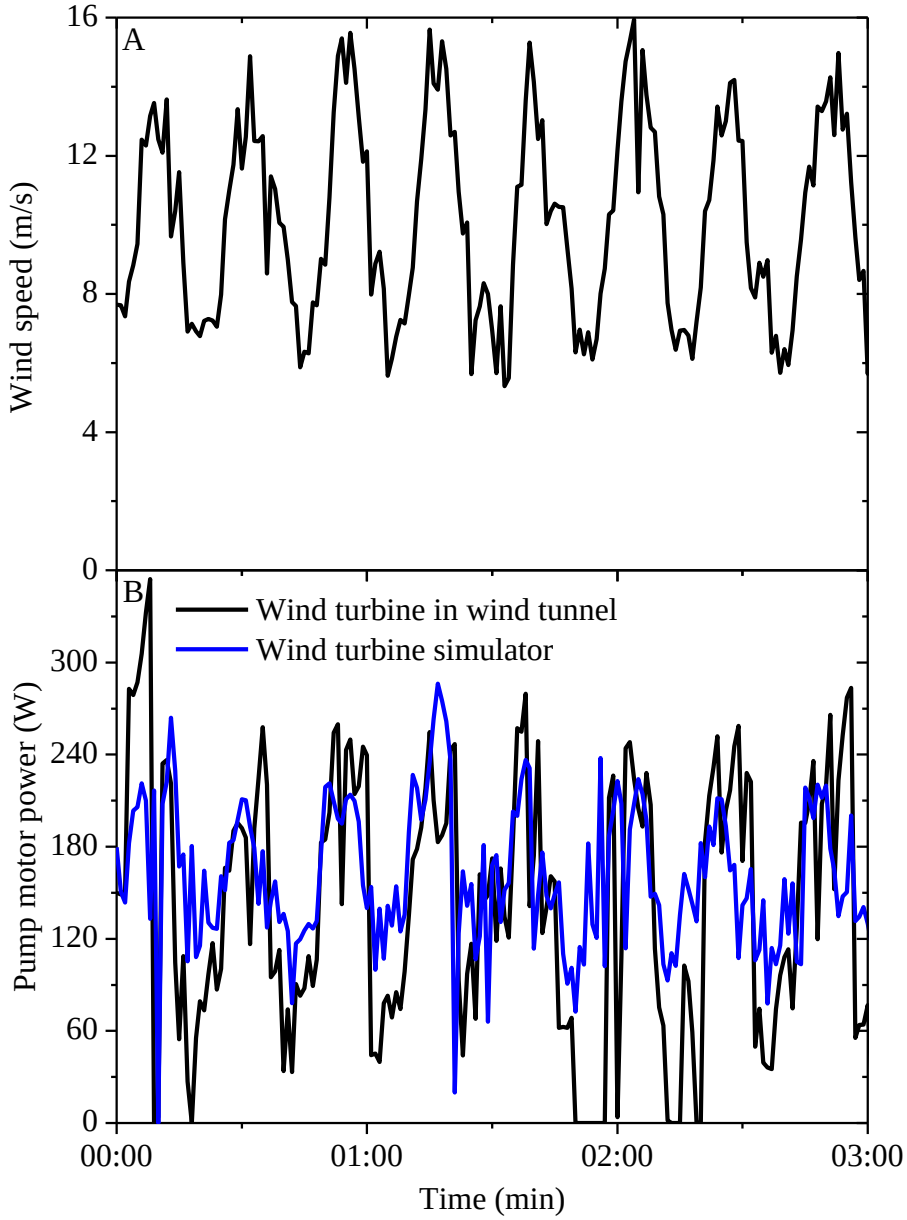

Figure 2.19: Comparison of the performance under wind speed fluctuations (A) of the wind turbine mounted in the wind tunnel and the wind turbine simulator by means of the power supplied to the pump motor on the membrane system (B).

The comparison of the pump motor power supplied under sinusoidal wind fluctuations in the wind tunnel with the wind turbine simulator connected to the membrane system is shown in Figure 2.19B. The performance of the wind turbine simulator generally followed the same trend as the wind tunnel experiments under fluctuating wind speed conditions and exhibited high consistency under accelerating conditions (increasing wind speed). The difference in the pump motor power, particularly at low wind speeds,

was caused by the slower response time of the simulator. This was a result of the braking time required to decelerate the wind turbine generator, gearbox and motor when the wind speed dropped. Further improvements in the accuracy of the wind turbine simulator under fluctuations could not be achieved and were attributed to the deceleration time required. These fluctuation experiments were performed at a 30 s period of oscillation, which is at the higher frequency end of the wind speed spectrum, where the most common fluctuations occur at 1 min intervals [67] (described in Section 1.3). Therefore, the accuracy of the wind turbine simulator should increase with oscillation periods > 30 s, although a lack of wind tunnel data did not allow verification.

2.4 Supercapacitor bank sizing

The motivation for using supercapacitors as a short-term energy storage medium for buffering wind fluctuations and intermittency was described in Section 1.7. The methodology for sizing the supercapacitor banks according to the renewable energy generator and length of storage time required was essential to prevent damage to the wind turbine generator or pump motor. This procedure to size supercapacitor banks could be used for other RE-membrane systems.

2.4.1 Series connection and voltage balancing

One of the main limitations of supercapacitors is caused by the electrolyte, which determines the maximum voltage-stability of the cells [131]. This is generally limited to 1 – 3 V_{DC} in order to avoid electrolysing the electrolyte. Unlike batteries, supercapacitors are damaged by the electrolyte gassing or drying up [180, 181]. The supercapacitors used for this work utilised an organic electrolyte which has the advantage of a much higher operating voltage (2.7 V_{DC}) compared to an aqueous electrolyte (1 V_{DC}), and can provide increased energy density [131, 136, 182]. As a result of the low rated voltage of supercapacitors, they generally have to be stacked in series to provide a useable operating voltage for higher voltage applications. For this reason, supercapacitors in pre-connected and sealed modules with balancing electronics are common and were used for this work.

The number of supercapacitors used in series to form the bank is determined by the terminal voltage of the charging system or application, in this case the wind turbine

generator and membrane system (60 V_{DC}). The total size or capacitance of the bank is then increased by adding rows in parallel [183]. Increasing the total capacitance or energy storage of the supercapacitor bank has the same effect as a low pass filter, where the size of energy storage is proportional to the time constant and results in improved smoothing out of the fluctuations in power [184].

To ensure even voltage distribution between the supercapacitors connected in series and to minimise losses due to leakage, supercapacitors require a voltage balancing system. The voltage within the supercapacitors varies for two reasons; slight variance in capacitance and different current leakage rates within individual cells [185]. The variation due to capacitance results in lower voltage in cells with higher capacitance and higher voltage in cells with lower capacitance as the current is uniform and voltage is proportional to the charging current and capacitance [185]. Once the cells are balanced, the leakage rate results in increased voltage imbalance within the cells. The supercapacitors used in this work were supplied with an active balancing system that used linear voltage-balancing to allow cell-to-cell leakage according to the imbalance of the cells, therefore no additional circuitry was required [186].

2.4.2 Sizing for the wind-membrane system

For these experiments, modular (15 V_{DC}) supercapacitors (Maxwell BOOSTCAP BPAK0058 E015 B01, specifications shown in Table 2.7) were chosen to allow for expansion and experimentation with the optimum supercapacitor bank size. As mentioned above, these modules had the cells enclosed in durable packaging for safety with integrated balancing electronics to ensure the cell-to-cell voltage was balanced when connected in series and the leakage current was minimised [186]. Within each supercapacitor, the cells are stacked in series in order to increase the voltage because of the low voltage stability (1 – 3 V_{DC}) of the electrolyte [131]. This also extends the useable voltage range, which varies linearly according to the present state of charge.

Table 2.7: Supercapacitor module specifications according to the manufacturer [187].

Specification	Value
Capacitance, C_{module} (F)	58
Rated voltage, V_R (V_{DC})	15
Operating temperature range (°C)	-40 to +65
Life test (years)	10 years at rated voltage and 25 °C
Cycle test (cycles)	500,000
Maximum energy (Wh/kg)	3.63
Power density (W/kg)	3,000
Leakage current (mA)	1.0
Internal resistance (mΩ)	19.0
Dimensions (mm)	216 x 69 x 38
Mass (kg)	0.566

The rated voltage of the supercapacitor modules (15 V_{DC}) was determined by the number of cells in series and the electrochemical stability of the organic electrolyte. While it was possible to operate the modules above this voltage (up to 16.7 V_{DC}), the increased performance is obtained at the expense of decreased lifetime [188]. In extreme over-voltage circumstances, failure of the device can occur resulting in venting of gas, dramatic temperature increase (up to 200 °C) and weight loss of approximately 30 % [131]. Although not used here, resistors or zener diodes should be connected in parallel with the supercapacitors or the SOC monitored for long term operation in order to keep the voltage within the safe operating range [180].

The following design steps were used to size the supercapacitor bank (values given in Table 2.7) [188]:

i. The maximum voltage output from the wind turbine (V_{max} ~ 60 V_{DC}) determined the maximum charging voltage and therefore the size of the supercapacitor bank based on the rated voltage of the supercapacitor modules (V_R). The number of supercapacitor modules in series (N_{series}) was calculated using:

$$N_{series} = \frac{V_{max}}{V_R}, \tag{2.18}$$

where N_{series} was determined as 4 for this system.

ii. The total amount of charge stored was determined by the capacitance of the supercapacitor bank (C_{bank}, Farads (F)) as:

$$C_{bank} = C_{module} \cdot \frac{N_{parallel}}{N_{series}}, \qquad (2.19)$$

where C_{module} is given in Table 2.7, N_{series} was 4 and the number of rows in parallel ($N_{parallel}$) was varied from 1 – 3 (therefore C_{bank} = 14.5, 29, 43.5 F) to increase the amount of system run-time and therefore determine the most appropriate size of energy storage for the system.

iii. Two efficiency losses associated with supercapacitors are the equivalent parallel resistance (EPR) and the equivalent series resistance (ESR). The EPR represents a current leakage path within the supercapacitor that limits the long term capabilities of the device. This value was given as 1 mA by the manufacturer (Table 2.7) and was dependent upon the charge voltage and ambient temperature. Experiments showed the typical energy loss due to current leakage to be 1 – 2 % per day. The ESR is important for charge/discharge efficiency as it represents the material resistances of the electrode and electrolyte that result in internal heating [182]. The ESR depends on the number of cells in series or parallel. Increasing cells in parallel reduces the resistance whereas more cells in series increases the resistance. The resistance of the supercapacitor bank (R_{bank}) was calculated using:

$$R_{bank} = \mathrm{ESR} \cdot \frac{N_{series}}{N_{parallel}}, \qquad (2.20)$$

with the resistances of the 4x1 – 4x3 supercapacitor banks being 76, 38 and 25 μΩ, respectively. As mentioned previously, the energy losses due to the ESR typically resulted in cycle efficiencies of 84 – 98 % [131, 134, 141, 142].

iv. In order to get an indication of the amount of storage time (Δt) available from the supercapacitor bank, the following equation was used:

$$\Delta t = \frac{C_{bank}}{I_{avg}} . \left(\Delta V - I_{avg} . R_{bank} \right), \quad (2.21)$$

where I_{avg} is the average discharge current and ΔV is the voltage difference between V_{max} (60 V_{DC}) and the minimum operating voltage (31.2 V_{DC}). This equation could be used for charging or discharging. For an average discharge current of 5.3 A, this would give a discharge time of 78 s for a 4x1 supercapacitor bank (4 supercapacitors in series, 1 row in parallel). The average discharge current was calculated as the time-averaged current supplied to the load while discharging the supercapacitors. As discussed earlier, this length of time would be ideal for improving the power quality from the wind turbine by buffering turbulent wind speed fluctuations that frequently occur at periods of one minute [67].

v. The energy (Wh) stored in the supercapacitor bank (Figure 2.20) was proportional to the charge voltage (V) squared where:

$$E = \tfrac{1}{2} C_{bank} . V^2 \quad (2.22)$$

Therefore, it was possible to use 75 % of the electrical energy stored in the supercapacitor bank by discharging to half of its maximum voltage (60 V_{DC}) [131]. Although supercapacitors have no lower operating threshold and can be discharged to zero volts, most DC/DC converters have a minimum voltage which limits the use of energy [182]. In this particular application, the DC/DC converter limited the minimum voltage to 31.2 V_{DC} to provide an adequate operating voltage to the pump motor (detailed in Section 2.1.3). This was equivalent to a minimum SOC of 27 %, as calculated using Equation 2.23.

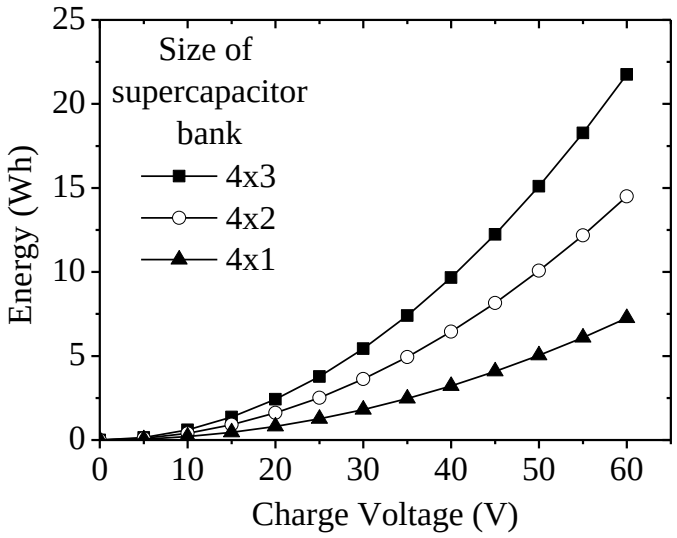

Figure 2.20: Energy available from the supercapacitor bank according to the charge voltage and the size of bank or number of parallel rows.

vi. The SOC of the supercapacitor bank is a useful measure of the available energy as a percentage of the banks maximum energy capacity (E_{max}) [182], calculated as:

$$\text{SOC} = \left(\frac{E_{bank}}{E_{max}} \right).100\%, \tag{2.23}$$

where the energy was calculated using Equation 2.22 with 60 V_{DC} for E_{max} and the supercapacitor bank charge voltage for E_{bank}.

2.4.3 Connection to wind-membrane system

The connection of the supercapacitor bank to the wind turbine simulator and the membrane system is shown in Figure 2.21. The output from the wind turbine generator along with all of the system electronics, supercapacitor bank and the pump motor for the membrane system were direct current (DC). The supercapacitor charging current from the wind turbine simulator (I3) was measured at a reading rate of 1 Hz along with all of the various membrane parameters and current/voltage either side of the motor controller. It should be noted that the voltage at V3 was governed by the SOC of the supercapacitor bank and therefore equal to V1. The membrane system load of 210 W corresponds to the set-point of 240 W including the average efficiency of the motor electronics (~ 86 %).

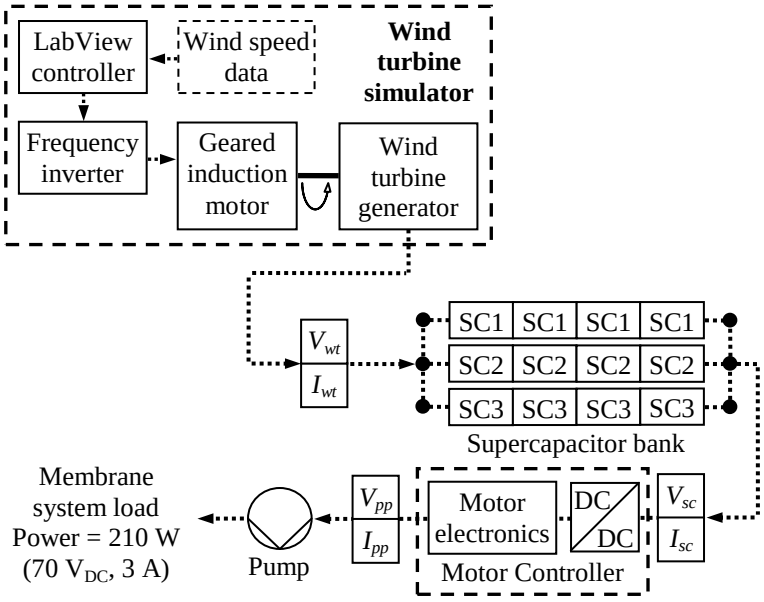

Figure 2.21: Schematic diagram of the supercapacitor bank attached to the wind-membrane system including wind turbine simulator, control electronics, motor controller and membrane system load with current sensors (*I*) and voltage sensors (*V*). Subscripts *wt*, *sc* and *pp* are for wind turbine, supercapacitor bank and pump motor, respectively. Further details of the wind turbine simulator are given in Figure 2.17 and a schematic of the membrane system is shown in Figure 2.3.

The voltage output from a supercapacitor varies linearly during the discharge process; therefore a DC/DC converter was required in order to provide the appropriate voltage to the pump motor (Figure 2.21). The DC/DC converter was integrated into the control electronics for the pump motor as part of a MPPT. By drawing more current as the voltage of the bank decreased (60 – 31.2 V_{DC}), the DC/DC converter was able to provide constant voltage input to the pump motor (~ 70 V_{DC}).

The supercapacitor bank was charged directly by the wind turbine simulator without the use of control electronics. However, the use of an inductance as a charge buffer could improve the charging efficiency, as this is closely related to the SOC [145]. An additional consideration is that once completely discharged a supercapacitor is equivalent to a short circuit for the charging source [189]. This is only a concern when the supercapacitors are completely uncharged, when new or unused for longer than several months, depending on the SOC. During normal operation the minimum SOC of

the supercapacitors was constrained by the DC/DC converter to 27 %. For the initial charge, a pulse charge power supply was used to manage the high initial charge current.

2.5 Experimental design

A series of experiments was designed to systematically examine the operation of the wind-membrane system under both steady-state and fluctuating conditions. These experiments provided a basis for understanding the impact of wind fluctuations and intermittency while also determining the safe operating window, optimum operating strategy and overall performance of the membrane system. The experimental inputs included step functions in power (steady-state), sinusoidal fluctuations (simulated wind fluctuations), square wave fluctuations (simulated wind intermittency) and real wind speed fluctuations (wind data). Experimental procedures are described in detail below.

2.5.1 Steady-state conditions

Constant power experiments were used to determine the steady-state operating characteristics of the membrane system (Section 3.2) to form a baseline for comparison with results obtained using fluctuations. These experiments were also necessary for determining the charge/discharge characteristics of the supercapacitor bank (Section 6.1) and for obtaining the safe operating window for different membranes and feed waters (Section 7.1).

The wind turbine simulator (Section 2.3) or the programmable power supply was used to provide power in the range 0 – 300 W, corresponding to the power output of the wind turbine obtained over the wind speed range 0 – 14 m/s and the rated power of the pump motor (300 W). Note that this covered the whole range of wind speed performance from zero-power up to high wind speeds. The power was held constant for 20 min during each step from 40 – 300 W, corresponding to average wind speeds of 4 – 14 m/s, respectively (Figure 2.22). A standard test time of 20 min is commonly used for performance measurements with FilmTec membrane elements to allow stabilisation of the performance parameters [49].

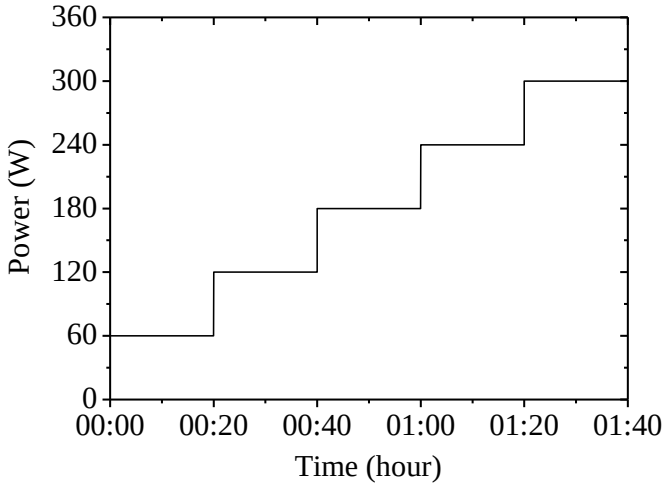

Figure 2.22: Constant power experiments for determining steady-state operating characteristics of the membrane system and the safe operating window and charging/discharging characteristics of the supercapacitor banks.

Depending on the power available, between 30 s – 5 min were required for stable conditions to be achieved; therefore the average performance values were taken over a 15 min period. The system was run for 20 min at the start and end of each experiment using the set-point conditions described in Section 2.1.7 (10 bar system pressure and 250 L/h feed flowrate at 240 W input power). This allowed the membrane parameters to stabilise while allowing the user to bleed off any air trapped in the system (using the regulating valve on the concentrate stream) and ensuring that the system performance was uniform before and after each experiment.

2.5.2 Controlled fluctuations and intermittency

Wind speed variations consist of short-term fluctuations related to turbulence or gusts and longer term fluctuations due to large movements of air. Short term fluctuations caused by turbulence over time periods of up to an hour can vary significantly and are generally the most important for the utilisation of wind energy systems [137]. These fluctuations are taken to be the stochastic variations in wind speed averaged over a period of ten minutes [113], therefore this is the length of time used in this work. Wind turbulence intensity (TI) is the basic measure of turbulence and can be seen as random wind speed fluctuations imposed on the mean wind speed. TI is represented as the

dimensionless ratio (-) of the standard deviation of the wind speed to the mean wind speed [113] as given by:

$$TI = \frac{\sigma_U}{U}, \tag{2.24}$$

where σ_U is the standard deviation of the wind speed (m/s) and U is the mean wind speed (m/s) over a ten minute period, henceforth referred to as the average wind speed. TI is generally in the range of 0.1 – 0.4, with the highest values occurring at the lowest wind speeds [113].

Wind speed fluctuations are often approximated by a sinusoidal wave in order to simplify practical experiments [98] and theoretical analysis [191]. The wind speed during a time period *v(t)* is then defined as

$$v(t) = U + A.\sin\left(2\pi.\frac{t}{T_{ws}}\right), \tag{2.25}$$

where A is the amplitude of fluctuation (m/s) and T_{ws} is the period of oscillation (s).

An experimental plan was designed to take into account the random fluctuations of wind in a controlled manner in order to eliminate the uncontrolled variables and complexity inherent in real wind. The range of periods of oscillation, TI and length of time with zero-power were chosen to represent real wind fluctuations. The effects of wind were divided into fluctuations and intermittency to allow more detailed analysis. Intermittency was taken to be any period of time where the membrane system shut down due to insufficient power. The experimental procedure was carried out as follows:

i. Simulated fluctuations (Chapter 4): oscillating power experiments (Figure 2.23A) lasted for a period of 10 min with the parameters of average power, peak-to-peak amplitude and period of oscillation varied one at a time to cover the full range of operation: (i) average power from 60 – 240 W; (ii) peak-

to-peak amplitude from 0 W (steady-state conditions) – 340 W (extreme fluctuations); and (iii) period of oscillation from 15 – 90 s.

ii. Intermittent operation (Chapter 5): power step experiments (Figure 2.23B) were used to turn the power off for varying lengths of time and test the effect of off-time on permeate quality and the system stabilisation time. The experiments were performed over one hour with six on/off cycles with the following variables: (i) peak-to-peak amplitude over the range 60 – 300 W with minimum value at 0 W and ii) length of time with zero-power (t_{off}) from 0.5 – 3 min. Six periods of zero-power were chosen as this was the maximum number that allowed the permeate quality to return to its original value once the power had been switched on (t_{on}) within a one hour period over the range of t_{off} up to 3 min.

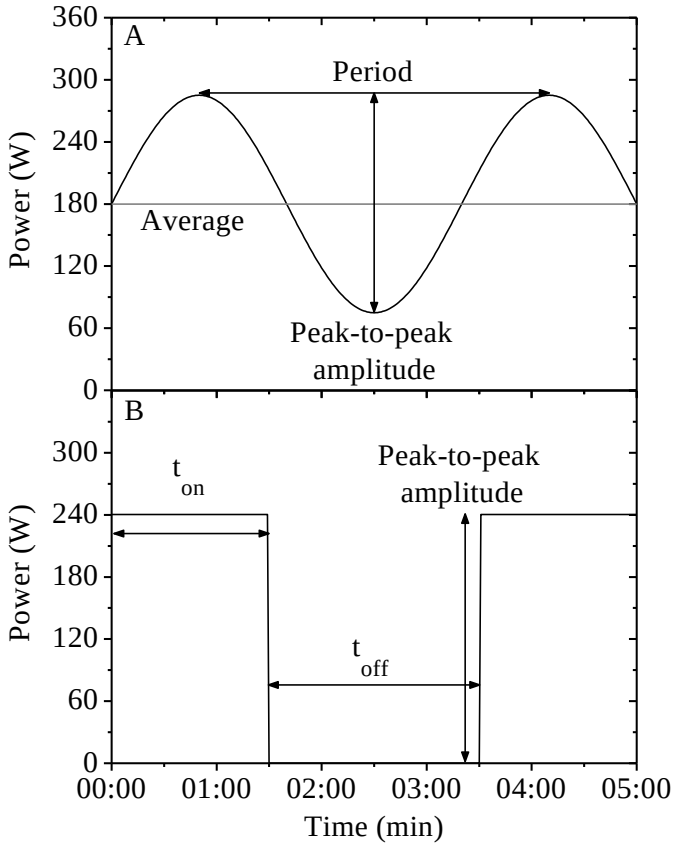

Figure 2.23: Power inputs for experiments performed on the wind-powered membrane system using the wind turbine simulator or programmable power supply; (A): simulated fluctuations and (B): intermittent operation.

The experimental procedure described above was also used to analyse the performance of the system using supercapacitor energy storage (Chapter 6). The wind turbine simulator was used over the wind speed range from 4 – 14 m/s in increments of 2 m/s for each of the three sizes of supercapacitor bank as follows:

i. Simulated fluctuations with supercapacitors (Section 6.3): oscillating wind speeds with varying periods of oscillation from 15 s – 20 min were tested over a range of turbulence intensities (0.1 – 0.6). The wide range of periods was important to fully examine the performance of the supercapacitors and the effects on the permeate quality and quantity.

ii. Intermittent operation with supercapacitors (Section 6.2): square wave wind speed inputs were used to establish how effectively the supercapacitor banks could prevent system shut-down during intermittent operation. The square waves were used to turn the power off over a range of time periods (0.5 – 5 min). An upper limit of 5 min was used as this was the maximum membrane system run-time for the largest size of supercapacitor bank.

2.5.3 Wind tunnel testing

The experiments performed in the wind tunnel were used to assess the performance of the wind turbine when directly-connected to the membrane system (Section 4.3) and to provide data for setting up the laboratory-based wind turbine simulator (Section 2.3). Controlled steady-state and sinusoidal wind fluctuations were performed by selective switching of the fans in the wind tunnel (described in Section 2.2.3). Wind speeds were held for a period of 20 min before being increased in steps (3.7, 5.3, 7.0, 8.7, 10.1, 11.7, 13.3 m/s) by increasing the speed of the fans in the wind tunnel. A range of wind turbulence intensities from 0.3 to 0.6 were tested at average wind speeds of 3.7, 5.3, 7.0, 8.7 and 10.1 m/s within the constraints of the wind tunnel (maximum wind speed 13.3 m/s). The experiments were performed over 10 min (standard length of time used in wind turbulence measurements) with an oscillation period of 30 s, and repeated once for verification. These parameters were chosen to correspond with the simulated wind experiments described in Section 2.5.2 to allow direct comparison.

The relationship between TI and the peak-to-peak amplitude used in the experiments described in Section 2.5.2 is illustrated in Figure 2.24. The peak-to-peak amplitude varied linearly with the TI until the maximum power constraint of the pump motor (300 W) was exceeded.

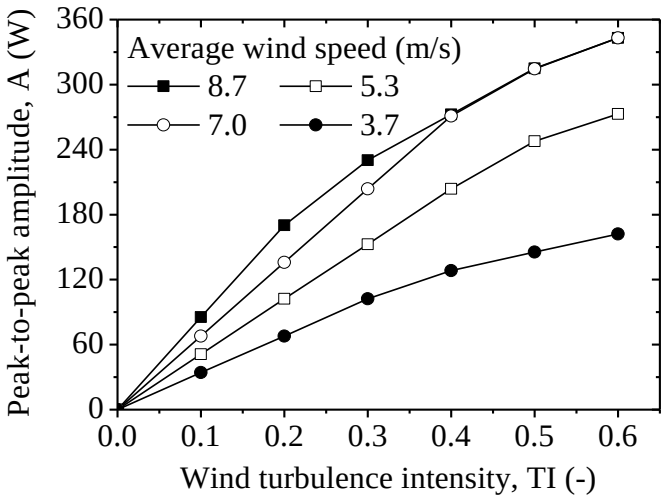

Figure 2.24: Relationship between TI and the peak-to-peak amplitude of power oscillation used in experiments with the programmable power supply.

2.5.4 Real wind speed data testing

Real wind speed data was used as the input to the wind turbine simulator (described in Section 2.3) to determine the performance of the wind-membrane system in a real wind environment over 24 hours (Section 7.3). The wind speed data was obtained from measurements taken near the town of Emden on the North Sea coastline of Germany [68]. This high quality data was measured using an ultrasonic anemometer at 20 m hub height and a sampling frequency of 4 Hz over 275 hours in October 1997. The log law (Equation 2.7) was used to make the data applicable for a small wind turbine system by reducing the hub height from 20 m to 8 m. A 24 hour segment of the wind speed data exhibiting a wide range of wind speeds with distinct high and low regions, turbulence and gusts was chosen to provide a realistic but challenging test for the wind-membrane system. The data was chopped to change it from 4 Hz to 1 Hz and make the file sizes more manageable for the 24 hour experiments. A sampling rate of 1 Hz is also used as standard when examining wind turbulence [113]. Further details of the wind speed data

including the average wind speed and range are given in the experimental results (Section 7.3).

2.5.5 Usability index for determining safe operating window

The safe operating window is essential to ascertain if a water treatment system is operating efficiently and is performing the task for which it was designed; to remove the contaminants from the water. In order to analyse the operation of the membrane system while it is subject to fluctuations of pressure and flowrate, a new measure of performance was developed. This was deemed necessary because fluctuations in power resulted in rapid changes in the flux whilst the permeate concentration took longer to respond due to diffusion. Using the permeate concentration as the main performance indicator does not take into account the periods of low flux when the permeate quality may be within the guideline value, but in reality the system is not operating effectively as there is little water being produced. The general trend in permeate quality was to follow an exponential decay with increasing flux under steady-state conditions. However, the presence of wind fluctuations caused a time lag to changes in the permeate concentration. This phenomenon occurred because fluctuations in power had an immediate effect on the flux, but a delayed impact on the permeate quality due to the time taken for diffusion of salts (discussed further in Section 4.3). The proposed usability index (UI) is dimensionless (-) and equates good system performance to a high flux with a permeate stream that meets the required guideline value for a particular chemical or contaminant as defined by the following relationship:

$$\mathrm{UI} = \left(\frac{J}{J_0} \right) . \left(\frac{C_{guideline} - C_p}{C_{guideline}} \right), \tag{2.26}$$

where C is concentration (mg/L). The UI has a maximum value of 1 (when passing deionised water through the system) and depending on the solutes involved, will generally be in the range of $-1 \leq \mathrm{UI} \leq 1$. A UI of 0 indicates that there is no flux, whereas a negative value shows that the concentration of the permeate stream is not compliant with the guideline value and the system is functioning outside the safe operating window. The UI can also be 0 when the permeate quality is equal to the guideline value. This would normally only occur at low flux as the permeate

concentration follows an exponential decay with increasing flux. Another situation where this could occur would be when starting up the system after a period of intermittency, when the permeate quality may pass through the guideline value momentarily before achieving stabilisation. Therefore, in order to provide an accurate and complete understanding of the system performance, the UI should be used in conjunction with the SEC to highlight both the productivity and the energy consumption of the membrane system. The pure water flux, J_0 was 25 L/m^2.h for the BW30 membrane and 70 L/m^2.h for the NF90. The solute of interest for this research was sodium chloride (NaCl), with a WHO guideline value of 1000 mg/L [12]. The palatability of drinking water at concentrations > 1000 mg/L may be objectionable to consumers; however this is not a health-based guideline. The UI is a useful indicator of system performance but should be used in conjunction with the SEC for a more detailed analysis of the operating window.

2.6 Conclusions

The components and experimental setup of the wind-membrane system have been described in detail including the performance of the progressive cavity pump and the membrane modules. The availability of low pressure (4 – 12 bar) brackish water membrane modules has allowed for the design of the membrane system using a small (300 W) progressive cavity pump that can operate at very low power (40 W). This is advantageous for the use of renewable energy technologies, where the amount of power required corresponds directly to the size of the renewable energy generator and the capital cost. Operation at low power is also important for utilising the power output from the wind turbine generator at low wind speeds and maintaining productivity.

Matching the wind turbine correctly to the membrane system according to the power requirements of the pump motor was the main challenge faced in the system design. By choosing the pump motor according to the required pressure and flowrate, the wind turbine was sized to meet the power requirements according to the available wind resource and the power curve of the wind turbine. This involved a detailed feasibility study of several wind turbines as well as wind tunnel characterisation and outdoor testing (Section 2.2). The requirement for detailed investigation is largely due to the variability of the wind resource and the fact that there was no rigid standard used by

manufacturers for predicting the performance of small wind turbines. There is a new MCS accreditation process introduced in 2010 that should help with the power prediction of small wind turbines (detailed in Section 1.3). However, so far there are only 13 certified wind turbines [70], all of which are > 2.4 kW and would therefore be too large for this membrane system. All or part of this methodology could be used in the design of future stand-alone wind-powered systems.

In order to perform controlled laboratory experiments with the wind turbine connected to the membrane system, a wind turbine simulator was designed (Section 2.3). The wind turbine simulator consisted of a geared induction motor connected to the wind turbine generator with the blades removed. The performance of the simulator was based on experimental results with the wind turbine mounted in a wind tunnel (Section 2.2.3), where provision was made for the inertia and furling of the wind turbine. The simulator performance with the membrane system exhibited comparable performance to the wind tunnel experiments and provided an excellent means for testing the wind-membrane system with controlled fluctuations in Chapter 4, supercapacitors in Chapter 6 and wind data in Chapter 7.

The calculations required for sizing a supercapacitor bank and connection to the wind-membrane system have been detailed to allow other membrane systems to utilise temporary energy buffering. Supercapacitors can provide improved power quality by buffering fluctuations and short periods of intermittency (several minutes) in the power source. Detailed background information on supercapacitors and the motivation for using them is provided in Section 1.7, while the results of the experiments using supercapacitors with the wind-membrane system are given in Chapter 6.

By separating the impact of wind variability into fluctuations and intermittency, and representing these using sinusoidal and square wave power inputs, the complexity inherent in real wind was removed. This allowed a detailed experimental methodology to be designed to characterise the wind-membrane system over the full range of wind speeds and understand their impact on performance. The use of robust sensors to measure pressure, flowrate, conductivity, temperature, pH, current and voltage was essential for accurately determining the transient nature of the wind-membrane system when subjected to fluctuating power.

The following chapter describes the performance of the wind turbine when connected to the membrane system from the wind tunnel experiments. The steady-state performance of the membrane system is described in detail to provide a comprehensive foundation for further chapters detailing the impact of wind fluctuations, intermittency, supercapacitor energy storage and real wind.

Chapter 3

Steady-state system performance

The challenge posed by the inherent variability of the wind resource and the inconsistency of data given by wind turbine manufacturers required a detailed investigation for the direct coupling of the wind turbine to the membrane system. The performance of the wind turbine when directly-connected to the membrane system was determined over a wide range of wind speeds using a wind tunnel. The power output from the wind turbine was then used to map out the operating range of the membrane system and determine the relationship between power and membrane performance. These results were used to provide a basis for determining the impact of wind speed fluctuations on the membrane system performance in further work.

3.1 Power performance of wind turbine and membrane system

The design process used for choosing the most appropriate wind turbine and testing of the turbine in the wind tunnel and outdoors are detailed in Section 2.2. As a result of coupling the wind turbine to the membrane system, the power output from the turbine had a direct effect on the operation of the pump motor, and therefore the pressure and flowrate in the membrane system. The relationship between wind speed and the power output from the wind turbine was determined using the wind tunnel as detailed in Section 2.5.3. Up to a wind speed of 7 m/s the relationship of power output with wind speed was linear (Figure 3.1). At higher wind speeds a combination of wind turbine furling and the power restrictions of the pump motor caused the wind turbine power curve to level off at a maximum value of 300 W. Wind turbine furling is a self-

protection mechanism that turns the blades out of the wind during high winds to avoid excessive electrical or mechanical loading. Furling was observed at wind speeds of 8.7 m/s and above, which was much lower than expected based on the rated power given by the manufacturer (1 kW) and resulted in much less power being generated. The difference between the wind turbine and pump motor power curves was caused by the control electronics between the wind turbine and the pump motor which have an average efficiency of 86 %.

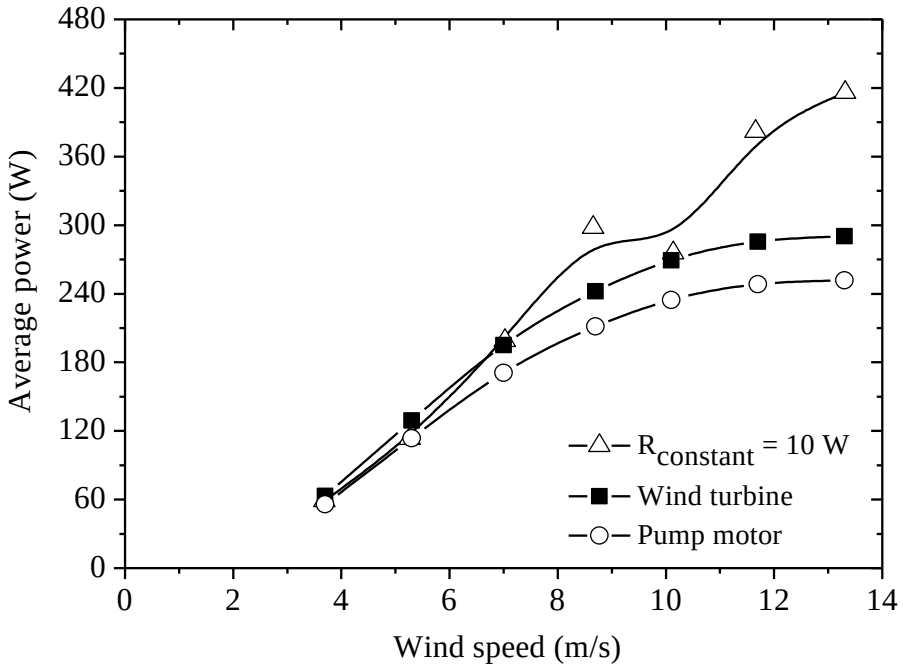

Figure 3.1: Wind turbine power curve at constant load (Figure 2.11) and with the wind turbine connected to the membrane system.

The constant resistance curve in Figure 3.1 illustrates why this particular wind turbine was chosen for coupling with the membrane system. A low cut-in wind speed (2.3 m/s) was observed as a result of the high torque generated with having five blades as opposed to three. Importantly, this resulted in much more energy being produced at low wind speeds when compared with other small wind turbines (as shown in Figure 2.8). A resistance of 10 Ω is shown as this best represented the load of the membrane system and illustrates that the power generated was a good match for this pump motor. However, the resistance of the membrane system changed with the power available as shown by the mismatch between the curves. This was most evident at wind speeds

above 7 m/s where the wind turbine curve departed from the constant resistance curve due to the higher load from the pump motor which varied in the range 10 to 25 Ω.

3.2 Operating characteristics under steady-state conditions

The operation of the membrane system under steady-state conditions was used to determine the performance of the aged BW30-4040 membrane module and provide a baseline for comparison with fluctuations in power. Details of the experimental setup and set-point for the membrane system are given in Section 2.5.1. Experiments were performed with feed water concentrations of 2750 mg/L and 5500 mg/L NaCl to allow comparison. The TMP (Figure 3.2A) increased with wind power and was independent of the feed water concentration as it was controlled by the valve on the concentrate stream which was set at the start of each experiment. This was a non-linear relationship and was seen to level off above 240 W due to lower efficiency in the region of the rated power of the pump motor (300 W) and the restriction of the control valve. It should be noted that the effective TMP was reduced by the osmotic pressure in the membrane boundary layer and was therefore dependent on the salt concentration of the feed as well as operating conditions. The effective TMP reduction due to the osmotic pressure of the feed water was calculated as 2.2 bar for 2750 mg/L and 4.4 bar for 5500 mg/L without taking into account the effect of concentration polarisation.

At low pressure, permeate flux and recovery are controlled by mass transfer mechanisms and therefore exhibit a linear dependence on the effective TMP [52]. The flux deviates from a linear dependence on TMP at higher pressure due to thermodynamic restrictions where the osmotic pressure of the concentrate stream can be equal to the TMP and the net driving pressure is reduced to zero. The flux (Figure 3.2B) and the recovery (Figure 3.2C) both followed the same trend as the TMP, highlighting the mass transfer controlled performance. The values of flux and recovery were lower for the higher feed concentration due to the lower effective TMP mentioned above. In order to validate this, the osmotic pressure was subtracted from the TMP to give the effective TMP and the flux calculated to be equal to the effective TMP multiplied by a constant (C = 1.96) for both feed waters.

The retention (Figure 3.2D) increased with the available power to a maximum value of 92 % for both of the feed waters at 180 W with 2750 mg/L NaCl and 300 W with 5500 mg/L NaCl. The retention was below the expected value according to the manufacturer due to the operating conditions and the age of the membrane, which was used for field trials in Australia in 2005 [60, 94] and for extensive laboratory experiments since then. Whilst the flux was consistent with previous experiments, the maximum retention under these operating conditions has reduced from 96 % [192] to 92 % over time (Figure 3.2D). It is well known that increased feed water temperature results in higher flux and lower retention due to the increased rate of diffusion of water and salts through the membrane [193]. Analysis of this membrane using modelled data (ROSA 7.2, Dow Water and Process Solutions) showed a 10 % increase in flux and 1 % reduction in retention when the feed water temperature was increased from 13 to 25 °C, as shown in Table 3.1.

The permeate NaCl (Figure 3.2E) decreased with increasing power and leveled off at a minimum value of 226 mg/L and 466 mg/L with feed waters of 2750 mg/L and 5500 mg/L NaCl, respectively. As would be expected, the concentrate NaCl (Figure 3.2F) followed the opposite relationship to the permeate and increased with the available power. With respect to a safe operating window, the permeate NaCl (Figure 3.2E) was within the WHO guideline value over the full range of operating conditions with a feed water of 2750 mg/L NaCl. With a feed water of 5500 mg/L NaCl, a minimum of 120 W (TMP of 6.6 bar) was required to produce permeate within the guideline value.

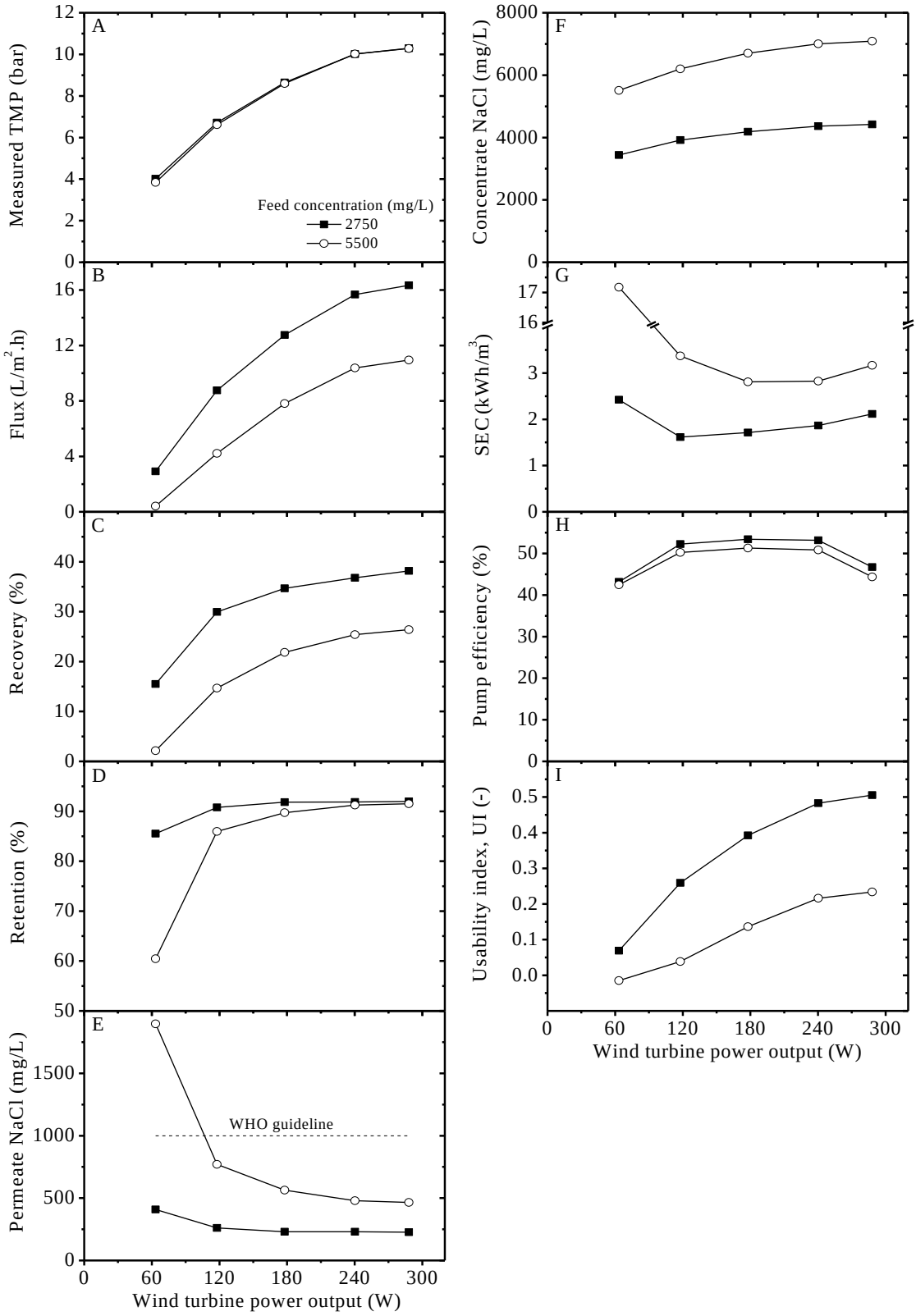

Figure 3.2: Steady-state performance of the wind-membrane system using constant power from a programmable power supply for feed waters of 2750 and 5500 mg/L NaCl.

The SEC (Figure 3.2G) exhibited high values at low power as most of the energy was used to overcome the osmotic pressure and little permeate was produced. This decreased to a minimum value of 1.6 kWh/m^3 (2750 mg/L) and 2.8 kWh/m^3 (5500 mg/L) before increasing again at high power. The minimum value was achieved for the two feed waters at a flux of 8 L/m².h, after which the SEC increased due to the pump operating close to its limit. This is illustrated in Figure 3.2H by the drop in the pump motor efficiency above 240 W. It can therefore be concluded that the most energy efficient operating point for the membrane system was at a flux of 8 L/m².h which was achieved at 120 W with a feed water of 2750 mg/L NaCl and at 180 W with a feed of 5500 mg/L.

The pump efficiency was calculated using the standard equation for efficiency (given in Section 1.4) as the ratio of the hydraulic power output to the shaft power supplied by the motor to the pump. This calculation was performed assuming constant efficiency of the brushless DC motor (85 %) over the whole operating range as discussed in Section 2.1.3. There was a reduction in the pump efficiency (Figure 3.2G) observed with the higher feed water salinity due to the increased density of the feed water. The maximum efficiency of ~ 44 % was achieved at 180 W for both feed waters. The UI (Figure 3.2H) achieved a maximum value of 0.51 and 0.23 for the feed waters of 2750 mg/L and 5500 mg/L NaCl, respectively. The low values of UI obtained with a feed water of 5500 mg/L NaCl show that the system was operating within the guideline value but with higher concentration and lower permeate flux (Figure 3.2B) when compared to a 2750 mg/L feed water.

3.2.1 Effect of operating conditions on system performance

It should be noted that the FilmTec BW30-4040 module was being operated below the test conditions given by the manufacturer (Table 2.3). The different operating conditions along with the age and deterioration of the membrane explain the significant difference in performance in terms of permeate flowrate and retention [49]. This is because systems designed to operate in remote regions with renewable energy generally have different design criteria to those used for conventional systems (Section 1.2.2). Rather than designing for the maximum water flux with high pressure, recovery and salt rejection, the most important factors for designing these systems are the energy

requirements and the need for robust long term operation [58]. As shown above, the operating pressure (Figure 3.2A) has a significant impact on the energy consumption (Figure 3.2G), therefore higher operating pressure would require a larger pump and renewable energy generator. The need for minimal maintenance operation means that these membrane systems are often run at low recovery (< 30 %) to reduce the requirement of using antiscalants [49]. As a result of operation at low pressure and low recovery, smaller pumps can be used which generate lower feed pressure and flowrates.

To demonstrate the impact of the operating conditions on the energy requirements, some modelling was performed using the membrane system analysis software provided by the manufacturer (ROSA 7.2) as shown in Table 3.1.

Table 3.1: Analysis of simulated system performance using manufacturer's standard test conditions (2000 mg/L NaCl; applied pressure 15.5 bar; 25 °C; 15 % recovery) and the test conditions contained in this work compared to experimental results. Simulation was performed assuming constant pump efficiency (ROSA 7.2, Dow Water and Process Solutions).

Parameter	Simulation				Experiment
	Standard test conditions	5500 mg/L feed and standard test conditions	5500 mg/L feed and our test conditions (at 25 °C)	5500 mg/L feed and our test conditions (at 13 °C)	5500 mg/L
Inputs					
Pre-stage ΔP (bar)	-0.9	-0.9	-0.24	-0.24	-0.24
Feed NaCl (mg/L)	2000	5500	5500	5500	5500
Feed temp. (°C)	25	25	25	13	13
Feed flow (L/h)	2530	1750	300	300	300
Feed pressure (bar)	15.5	15.5	10	10	10
Pump efficiency (%)	43.2	43.2	43.2	43.2	43.2
Outputs					
Permeate flow (L/h)	380	280	101	77	75
Flux (L/m².h)	52.4	38.2	14.1	10.7	10.4
Retention (%)	99.4	99.2	97.6	98.7	91.3
Recovery (%)	15	15	33.9	26.0	25.4
Power (W)	2520	1840	190	190	210
SEC (kWh/m³)	6.6	6.7	1.9	2.5	2.8
UI (-)	0.84	0.59	0.49	0.40	0.22

If a larger pump was obtained with the same efficiency, then the power required to operate the membrane at the test conditions given by the manufacturer would be 2520 W with an SEC of 6.6 kWh/m³ using a feed water of 2000 mg/L. In order to operate the system at 15.5 bar and 15 % recovery using a feed water of 5500 mg/L, 1840 W would be required and a flux of 38.2 L/m².h would be produced with an SEC of 6.7 kWh/m³. This would require a much larger wind turbine at significant cost when compared to the maximum value of 300 W required for operating the current system. It should be noted that larger systems may have more energy efficient pumps and employ energy recovery (generally at higher pressure), which would result in much lower SEC. The situation shown here is unique to small-scale brackish water systems where energy recovery is not really feasible due to the relatively low pressures used. The data in Table 3.1 also illustrates the effect of operating conditions on the UI. By using lower feed concentrations at higher pressure and feed flowrate, the UI approaches unity. However, the cost of operating at these conditions must be weighed against the amount of energy required.

The membrane system used throughout this research was primarily designed for experimental testing to investigate the coupling of a membrane system with a renewable energy supply to provide drinking water in remote areas. The design utilised a single 4 inch industrial membrane module with pressure, flowrate and conductivity sensors at all of the relevant stages. The use of a single membrane allowed a simplified analysis with the ability to take detailed performance readings in order to analyse the transient operation of the system. The membrane system was tested in Australia using real brackish groundwater with 4 inch BW30, NF90, ESPA4 and TFC-S membrane modules to compare their performance over a wide operating range [60], as described previously in Section 2.1.2. Further experimental testing was performed with the BW30 module using energy from a solar PV array to determine the impact of fluctuations in solar irradiance on the performance of the membrane system [94]. To provide continuity to the experimental work and allow for comparison with previous experimental results, the design of the membrane system was not altered for coupling with the wind turbine system used in this work. However, if this prototype system were to be commercialised, the performance could be improved through the use of 2.5 inch membrane modules as opposed to the 4 inch modules currently used. It is worth noting at this point that the use of more than one membrane module does provide several challenges both from an

experimental point of view and for providing drinking water in remote areas. The use of multiple modules increases the complexity of the system and requires additional sensors in order to understand the system performance. The remote area criteria (Section 1.2.2) specify that membrane systems designed for isolated locations should be cost effective and require minimal maintenance. Therefore, any performance enhancement gained by adding further membrane modules would have to be weighed against the added complexity of the plant.

As a result of the small size of the pumping system, the required cross flow velocities to operate the 4 inch membrane modules within the acceptable operating range specified by the manufacturers could not be provided. The specifications given by the membrane manufacturer state that the minimum concentrate flowrate should be > 450 L/h and the maximum recovery should not exceed 30 % [49]. The pumping system provided concentrate flowrates of 50 – 350 L/h depending on the operating parameters, which was significantly lower than the recommended level. The impact of operating at low crossflow velocities is a reduction in the mass transfer coefficient (see calculations in Section 2.1.6) that results in a higher accumulation of salts near the membrane surface due to concentration polarisation. This results in lower driving pressure due to the higher osmotic pressure at the membrane surface with increased likelihood of membrane scaling and fouling. By using three 2.5 inch membrane modules in series, the same membrane area as a single 4 inch module could be achieved while reducing the level of concentration polarisation. To investigate the impact of using 2.5 inch modules, some simulation work was carried out using these modules and compared to experimental results obtained using 4 inch modules, as shown in Table 3.2.

The results in Table 3.2 show that the use of three 2.5 inch membrane modules in series could provide significantly improved performance of the membrane system. By using the 2.5 inch BW30 module, the flux could be increased by 16 % and the retention by 2 %. While with a 2.5 inch NF90 module, the flux could increase by 7 % and the retention by 3 % compared to the performance with a 4 inch module. The impact of the increased crossflow velocity and resulting mass transfer coefficient obtained with a 2.5 inch module is highlighted by the reduction in the concentration polarisation modulus. By changing from 4 inch to 2.5 inch modules the concentration polarisation for the individual membrane modules would reduce from 1.79 to 1.09, and 2.02 to 1.07

for the BW30 and NF90 membranes, respectively. The reduction in concentration polarisation would also have an impact on the energy consumption, with up to 30 % energy savings achieved through the use of 2.5 inch modules. Therefore, while the current membrane system was used to provide the basis for system development and experimental testing of the wind-membrane system, further development should investigate the use of 2.5 inch modules. These smaller modules would be more appropriate for the small pumping system and could provide higher flux with reduced concentration polarisation and energy consumption.

Table 3.2: Membrane performance comparison of experimental results with 4 inch modules compared to simulated results using 2.5 inch modules (ROSA 7.2, Dow Water and Process Solutions).

Parameter	Experimental Results			Simulation	
	BW30-4040 (Aged)	BW30-4040 (New)	NF90-4040	BW30-2540 (3 in series)	NF90-2540 (3 in series)
Inputs (same for all experiments and simulations)					
Pre-stage ΔP (bar)	-0.24				
Feed NaCl (mg/L)	5500				
Feed temp. (°C)	13				
Feed flow (L/h)	300				
Feed pressure (bar)	10				
Pump efficiency (%)	43.2				
Outputs				*Unless stated, values are system values for 3 modules in series*	
Flux (L/m².h)	10.4	9.9	19.1	11.5	20.5
Retention (%)	91.3	97.1	91.6	99.0	94.3
Recovery (%)	25.4	28.1	46.2	30.3	52.3
SEC (kWh/m³)	2.8	3.3	1.72	2.12	1.23
Concentration polarisation modulus	1.76	1.79	2.02	1.09 (module)	1.07 (module)

The SEC of the wind-membrane system needs to be as low as possible to provide the maximum productivity with minimum energy requirements in order to minimise the cost of water. Therefore, this was one of the key performance parameters for comparing the overall system performance. The minimum SEC of 1.6 kWh/m^3 with the 2750 mg/L NaCl feed water and 2.8 kWh/m^3 with the 5500 mg/L feed water that were achieved with this membrane system are excellent and highlight the relatively high efficiency of

the progressive cavity pump (discussed in Section 1.4.2). As shown in Table 1.1, there have been very few wind-membrane systems developed specifically for brackish water desalination. The SEC for the brackish water wind-membrane systems that have been developed had a very wide range from 3.5 – 13 kWh/m^3 [58, 92, 93]. The windmill-powered system developed by Liu *et al.* [93] used a FilmTec low pressure RO membrane module (specifications not provided) with feed pressure 5.2 – 6.9 bar and flowrate 480 – 1020 L/h. With a feed water concentration of 3500 mg/L, the membrane plant had an average permeate production of 160 L/h (19 % recovery) with 97 % retention, producing permeate concentrations < 100 mg/L. The average SEC of the permeate produced was 3.5 kWh/m^3, which is significantly lower than the other brackish water wind-membrane systems (Table 1.1).

The mechanical windmill-powered plant set up by Robinson *et al.* [58] had a high SEC of 11 kWh/m^3 (Table 1.1). Although this was a mechanical windmill plant, the power output and pressure/flowrate provided were very similar to the wind-membrane system used in the research presented here. The power output from the windmill was 150 W at 4.5 m/s wind speeds, which allowed feed pressure of 6 – 11 bar at flowrates of 300 L/h to be provided by the piston pump. The main cause of the relatively high SEC of this plant was the low recovery of 6 – 11 % that was used to minimise the fouling potential of the membranes.

It is also useful to compare the performance of the wind-membrane system with solar PV-powered brackish water membrane plants that have been developed [194-196]. Joyce *et al.* [194] performed experiments using a 12 V_{DC} Shurflo diaphragm pump connected to a 100 W_p or 150 W_p PV array to evaluate the possibility of a PV-powered membrane system. The plant used a spiral wound membrane module (MP-TA50-J4) with feed water concentration of 2000 – 5000 μS/cm (approx 1200 – 3200 mg/L). The feed pressure varied from 3.3 – 4.2 bar and the feed flowrate from 140 – 200 L/h depending on the power output from the PV array. While the high retention of the membrane (94 %) provided low permeate concentration of 500 μS/cm (~ 320 mg/L), the SEC was very high at 25.6 kWh/m^3. The high SEC was caused by the small size of the PV-pumping system which meant the plant was operated at relatively low pressure and flowrate, resulting in very low recovery of ≤ 2.4 %.

The SEC of larger plants is often much lower, as demonstrated by the PV-powered (3250 W_p) membrane plant tested for 3 years in Oman [195]. This system used a 200 Ah battery bank to store the energy supplied by the PV array, providing 5 – 7 hours of steady-state plant operation per day. Brackish feed water with TDS of 1850 μS/cm was supplied to 6 membrane modules (specifications not provided) at a feed pressure of 12 bar and flowrate of 720 L/h. High recovery of 65 – 70 % was achieved by dosing the feed water with antiscalants. These operating parameters provided high permeate production of 5 – 7.5 m^3/day, resulting in a low estimated SEC of 2.3 kWh/m^3.

Another PV-powered membrane plant that used energy storage in batteries was set up in Egypt for demonstration purposes [196]. A 2400 W_p PV array was used to charge a 120 Ah battery bank that supplied 550 W to the pumping system (specifications not provided). The feed water concentration was varied from 500 – 1500 mg/L to determine the impact on the performance of the membrane plant. The membrane plant was supplied as a pre-constructed unit (CWG, Manheim, R0100-TW) with two RO membranes (Hydranautics, ESPA1-4021). The feed water was supplied to the membranes at feed pressures of 5 – 8 bar and flowrates of 440 – 570 L/h. As above, high recovery of 75 % was possible due to dosing of the feed water with antiscalants. The permeate flowrate was 70 – 210 L/h with concentration of ≤ 100 μS/cm (93 % retention). These operating parameters resulted in a low SEC of 2.5 – 4.5 kWh/m^3 depending on the feed water concentration and pressure/flowrate supplied to the membranes.

The above examples highlight the importance of the overall system design and the operating conditions on the SEC of the RE-membrane plant. When energy storage is not used, it is necessary to use a pumping system that is efficient over a wide range of power inputs and can provide the necessary feed flowrate and pressure to the membrane system. This operating range allows the choice of an operating strategy that can maximise both the power output from the RE generator and the productivity of the membrane system (detailed further in Chapter 7). One of the most important initial steps in the design process is determining the most appropriate membrane according to the feed water characteristics. This fact was highlighted by a performance comparison of a BW30-4040 membrane module with a NF90-4040 module using a feed water concentration of 5000 mg/L NaCl [192]. While the retention of the BW30 module was

2.8 % higher than the NF90, the flux was 45 % lower. This resulted in a high SEC of 7.7 kWh/m^3 for the BW30 module compared to 2.2 kWh/m^3 for the NF90 module. The set operating conditions of 10 bar feed pressure and 500 L/h feed flowrate resulted in lower recovery of 19 % for the BW30 compared to 31 % for the NF90 module due to its higher permeability.

3.3 Conclusions

The steady-state performance of the wind-membrane system was characterised over the whole operating range from the minimum power required (~ 60 W achieved at 3.7 m/s) to the maximum rated power of the pump motor (~ 300 W achieved at 13.3 m/s). The power output from the wind turbine was linear from 3.7 – 7 m/s above which a combination of furling of the wind turbine and power restrictions of the pump motor caused the power curve to reach a plateau at high wind speeds. The results demonstrated that this particular wind turbine was an excellent match for coupling with the membrane system. An important outcome of this work for the design of future wind-powered systems is that it is essential to determine accurately the power curve of the wind turbine over a range of loads before coupling with the membrane system or any other directly-powered application. This will result in more efficient systems by maximising the use of power from the wind turbine and operating the directly coupled device at high efficiency. This will also reduce the risk of damage to both components caused by excessive turbine rpm and/or power output.

The steady-state operating characteristics of the membrane system were used to highlight the relationship between the power input to the system and the quality and quantity of potable water obtained. Feed waters of 2750 mg/L and 5500 mg/L NaCl were used to determine the effect of increasing salinity. The TMP, which is the driving force for the desalination process, increased with the available power from the wind turbine. This was a non-linear process due to the restrictions of the control valve on the concentrate stream and corresponding lower pump efficiency. The flux and the retention both increased with the available power as a result of higher TMP. The relationship between the effective TMP and the flux was determined empirically and shown to be governed by the osmotic pressure of the feed water. This also highlighted that there was very little concentration polarisation at the relatively low pressures used throughout

these experiments. The safe operating window for the system covered the full operating range with a feed water of 2750 mg/L NaCl and above 6.6 bar (achieved at 120 W) with 5500 mg/L due to the higher osmotic pressure.

The experimental results demonstrated that the wind-membrane system produced potable water within a safe operating window over a wide range with brackish water up to 5500 mg/L. The choice of a small pump to minimise the energy requirements and overall cost of the system provided sufficient pressure and feed flowrate for operating the membrane system effectively. These results provide a basis for comparison in the following chapters which deal with the impact of wind speed fluctuations and intermittency on the safe operating window of the wind-membrane system.

Chapter 4

Effect of wind speed fluctuations

The main aims of this study were to determine the effect of wind speed fluctuations on the performance of the wind turbine and the extent to which these can be beneficial or detrimental within a safe operating window. While several wind-membrane systems have been designed and undergone preliminary testing, a systematic investigation on the effect of fluctuations on membrane performance has never been completed. By dividing the effects of wind variability into fluctuations or intermittency, the impact upon the system dynamics was analysed in great detail. With a feed water of 2750 mg/L NaCl, the wind-membrane system produced permeate with concentration < 600 mg/L over the full range of wind speeds and fluctuations. The system performance (in terms of permeate flux and NaCl concentration) at average wind speeds of 7.0 m/s or more was unaffected by fluctuations up to a turbulence intensity of 0.4 and was independent of the period of fluctuation within this operating range. With a feed water of 5500 mg/L NaCl an average wind speed of 7.0 m/s or more was required to produce permeate within the WHO guidelines (< 1000 mg/L) under fluctuating conditions. It is concluded that this wind-membrane system can be operated within a safe operating window with large power fluctuations, but the detrimental effects of intermittent operation would require further investigation.

4.1 Effect of increasing sinusoidal period of operation

The membrane system was previously tested by direct connection (no energy storage) to a PV array (300 W from two $24V_{DC}$ panels) over several solar days [94]. The results showed that the RE-membrane system (using a BW30-4040 element) operated under fluctuations in solar irradiance of 500-1200 W/m² (125 – 300 W) with minimal effect on the permeate quality, although further testing below 500 W/m² (125 W) would be required to determine its operation under heavy cloud [94]. In addition, the fluctuations shown over a typical solar day during these experiments [3] showed an average rate of change of 1% per second whilst wind fluctuations over a typical day were calculated to vary by 12 % per second. This highlighted the need for a separate study to investigate the effect of higher frequency fluctuations in power associated with wind energy. In this Chapter a systematic investigation was conducted to determine the effect of wind speed fluctuations on the performance of the wind-membrane system.

The use of controlled sinusoidal fluctuations as the input to the membrane system in order to remove the random uncertainty inherent in real wind is detailed in Section 2.5.2. Experiments were performed using the aged BW30-4040 membrane module and feed water concentrations of 2750 mg/L and 5500 mg/L NaCl. Figure 4.1 shows the operation of the membrane system with a feed water of 2750 mg/L under controlled fluctuations using an oscillating power supply with two different periods of oscillation (15 and 90 s), constant peak-to-peak amplitude of 200 W (equivalent TI = 0.4) and average power of 120 W (equivalent average wind speed = 5.3 m/s). The TI represents the amplitude of wind fluctuations about a mean value (Section 2.5.2), and the peak-to-peak amplitude is the resulting oscillations in power from the wind turbine. The relationship between TI and peak-to-peak amplitude is described in Section 2.5.3 and illustrated in Figure 2.24. The high amplitude fluctuations shown here caused the power to switch off at longer periods as the slower oscillation in power allowed the TMP to drop to a lower level, putting a high load on the pump. The combination of high load and slowly oscillating power resulted in insufficient power to regain the system pressure and the system shut down periodically. Figure 4.1A illustrates that the power did not switch off if the input power dropped below 40 W for up to 3 s (shown at 15 s period) but longer periods of low power resulted in the power switching off. Although the TMP achieved at the minimum start-up power was 4 bar (Figure 4.1A), fluctuations

down to 3 bar (Figure 4.1B) occurred once operational within the safe operating window.

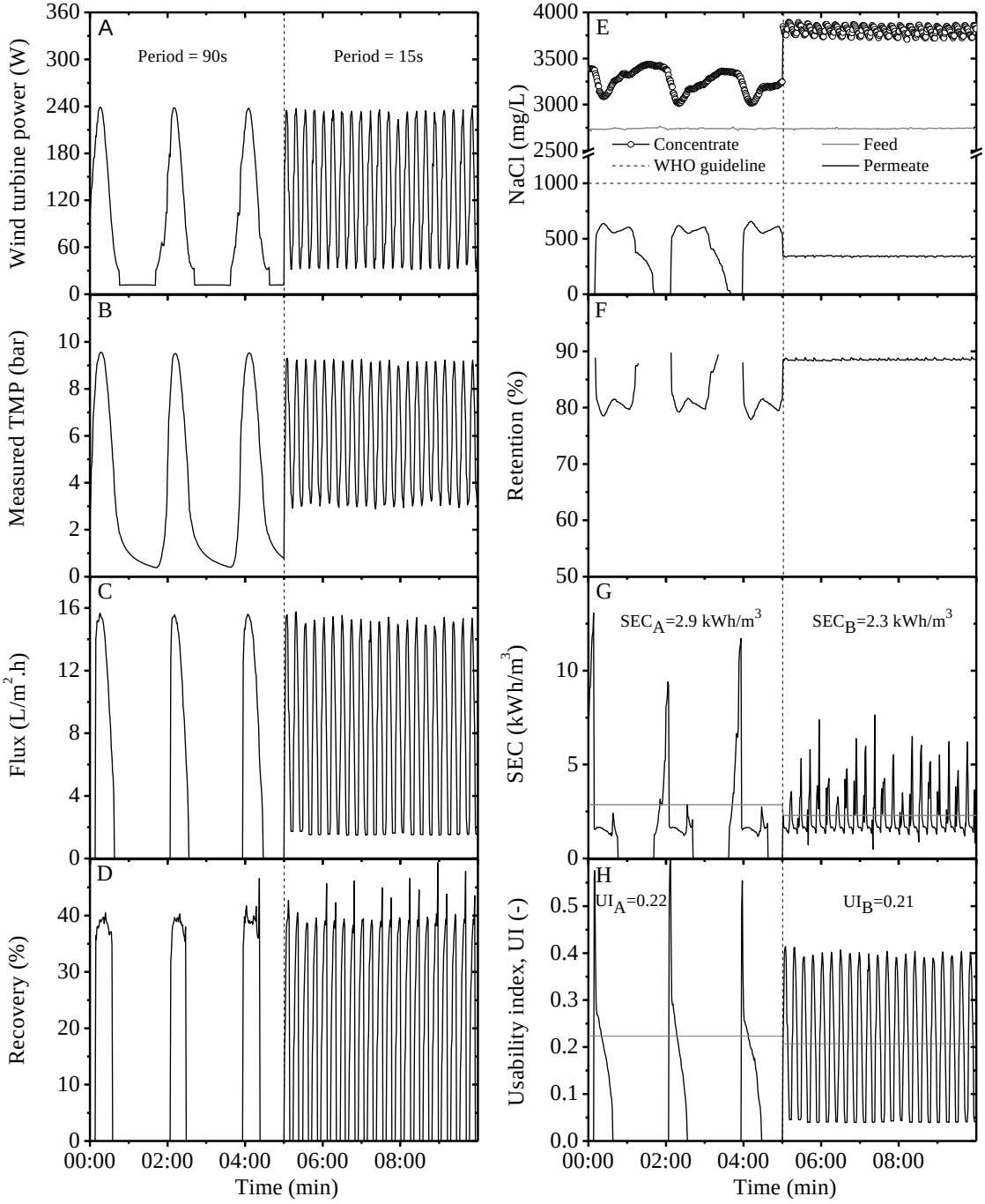

Figure 4.1: Wind-membrane system performance using oscillating power (programmable power supply) for oscillation periods of 90 s and 15 s with a feed water of 2750 mg/L NaCl (average power 120 W, amplitude 200 W).

The on/off switching of the pump at a period of 90 s caused significant deterioration in performance as demonstrated by the long periods of no flux (Figure 4.1C) and recovery (Figure 4.1D) and the higher average permeate NaCl (Figure 4.1E). The average retention (Figure 4.1F) observed at a period of 15 s was 87 % which compared well with the steady-state value of 91 % (Figure 3.2D). However the longer period of oscillation caused the average retention to drop to 82 % (Figure 4.1F). The SEC (Figure 4.1G) exhibited a large spike when the system was switched on due to the power required to achieve the flux required for desalination. This resulted in higher average SEC at 90 s period because of the power shutting off. The average SEC was calculated as the total energy consumption divided by the total permeate production and did not include the periods when the flux was zero. The average UI (Figure 4.1H) whilst water was being produced was slightly higher at 90 s period than at 15 s, but this was offset by the amount of time with no productivity.

4.2 Effect of wind turbulence intensity on system performance

The full range of experiments performed with variables of equivalent average wind speed, TI and period of oscillation are given in Table 4.1 and Table 4.2 for feed waters of 2750 mg/L and 5500 mg/L, respectively. These experiments were performed with simulated wind speed fluctuations using an oscillating power supply as described in Section 2.5.2. The values presented for the flux and permeate NaCl were the averages taken over the ten minute test period. The grey shaded areas in the table indicate experiments where the TI was sufficient to cause the power to shut off periodically. The general observation from the data, particularly at the higher average wind speeds of $\geq$ 7 m/s, was that the average permeate NaCl and flux were relatively unaffected by the TI and period of oscillation until the power started to shut off. When the TI was sufficient to cause the power to shut off, longer periods of oscillation were more detrimental to the average permeate NaCl and flux than shorter periods. Similar trends were observed with the 5500 mg/L feed water concentration (Table 4.2), although as would be expected, the performance was significantly poorer due to the increased osmotic pressure of the feed water.

Table 4.1: Performance of wind-membrane system with 2750 mg/L using oscillating power with variables of average wind speed, turbulence intensity (TI) and period of oscillation. Shaded regions show regimes where power was switching off periodically.

Average wind speed (m/s)	**Wind speed turbulence intensity**	**Period of oscillation (s)**					
		15	**30**	**45**	**60**	**75**	**90**
		Flux / **NaCl**	**Flux** / **NaCl**	**Flux** / **NaCl**	**Flux** / **NaCl**	**Flux** / **NaCl**	**Flux** / **NaCl**
3.7	0	3 / 500	3 / 500	3 / 500	3 / 500	3 / 500	3 / 500
	0.1	4 / 480	3 / 570	2 / 490	2 / 570	2 / 570	2 / 470
	0.2	4 / 500	2 / 570	1 / 500	1 / 540	1 / 670	1 / 680
	0.3	5 / 550	2 / 600	1 / 510	1 / 550	1 / 650	1 / 670
	0.4	5 / 550	3 / 500	2 / 480	2 / 300	2 / 210	1 / 110
	0.5	5 / 690	3 / 520	3 / 590	3 / 590	3 / 510	3 / 600
	0.6	6 / 540	5 / 500	5 / 540	5 / 540	5 / 540	4 / 560
5.3	0	9 / 330	9 / 330	9 / 330	9 / 330	9 / 330	9 / 330
	0.1	7 / 380	7 / 380	7 / 390	7 / 390	6 / 390	6 / 390
	0.2	8 / 380	8 / 380	8 / 380	8 / 390	7 / 390	7 / 390
	0.3	8 / 370	8 / 380	8 / 390	8 / 450	7 / 410	4 / 460
	0.4	8 / 380	8 / 390	3 / 410	3 / 430	1 / 420	1 / 410
	0.5	6 / 410	4 / 400	3 / 400	2 / 270	1 / 120	1 / 130
	0.6	6 / 400	6 / 400	6 / 410	6 / 420	5 / 420	5 / 520
7.0	0	13 / 280	13 / 280	13 / 280	13 / 280	13 / 280	13 / 280
	0.1	13 / 330	13 / 330	13 / 330	13 / 350	13 / 340	13 / 350
	0.2	13 / 330	13 / 330	13 / 310	13 / 350	13 / 340	13 / 350
	0.3	13 / 310	13 / 340	13 / 310	13 / 360	12 / 330	12 / 330
	0.4	12 / 330	12 / 340	11 / 340	11 / 350	11 / 350	11 / 350
	0.5	13 / 440	13 / 470	5 / 480	5 / 480	2 / 300	2 / 490
	0.6	11 / 370	11 / 370	11 / 360	10 / 360	10 / 360	10 / 380
8.7	0	16 / 270	16 / 270	16 / 270	16 / 270	16 / 270	16 / 270
	0.1	16 / 290	16 / 300	16 / 310	16 / 320	16 / 320	16 / 310
	0.2	16 / 310	16 / 310	16 / 310	16 / 310	16 / 310	16 / 310
	0.3	16 / 310	16 / 310	16 / 310	16 / 300	16 / 310	16 / 330
	0.4	16 / 320	16 / 320	16 / 330	16 / 320	16 / 320	16 / 330
	0.5	13 / 350	13 / 350	12 / 350	12 / 340	9 / 400	4 / 570
	0.6	14 / 360	13 / 360	13 / 360	12 / 360	12 / 360	6 / 450

Table 4.2: Performance of wind-membrane system with a feed water of 5500 mg/L using oscillating power supply and variables of average wind speed, turbulence intensity (TI) and period of oscillation. Shaded regions show regimes where power was switching off periodically.

Average wind speed (m/s)	**Wind speed turbulence intensity**	**Period of oscillation (s)**					
		15	**30**	**45**	**60**	**75**	**90**
		Flux / NaCl	**Flux / NaCl**	**Flux / NaCl**	**Flux / NaCl**	**Flux / NaCl**	**Flux / NaCl**
3.7	0	0 / 2190	0 / 2190	0 / 2190	0 / 2190	0 / 2190	0 / 2190
	0.1	0 / 0	0 / 0	0 / 0	0 / 0	0 / 0	0 / 0
	0.2	0 / 0	0 / 0	0 / 0	0 / 0	0 / 0	0 / 0
	0.3	0 / 0	0 / 0	0 / 0	0 / 0	0 / 0	0 / 0
	0.4	0 / 0	0 / 0	0 / 0	0 / 0	0 / 0	0 / 0
	0.5	0 / 0	0 / 0	0 / 0	0 / 0	0 / 0	0 / 0
	0.6	0 / 0	0 / 0	0 / 0	0 / 0	0 / 0	0 / 0
5.3	0	4 / 930	4 / 930	4 / 930	4 / 930	4 / 930	4 / 930
	0.1	4 / 1130	4 / 1130	4 / 1130	3 / 1130	3 / 1130	3 / 1130
	0.2	3 / 1130	3 / 1150	3 / 1150	3 / 1150	3 / 1170	3 / 1180
	0.3	3 / 1080	3 / 1080	3 / 1080	3 / 1110	3 / 1110	3 / 1120
	0.4	3 / 1100	3 / 1100	2 / 1100	2 / 1100	1 / 1152	1 / 1148
	0.5	2 / 1100	2 / 1100	2 / 1100	2 / 1150	1 / 1120	1 / 1161
	0.6	4 / 1150	4 / 1140	4 / 1190	2 / 1037	2 / 1171	2 / 1258
7.0	0	7 / 680	7 / 680	7 / 680	7 / 680	7 / 680	7 / 680
	0.1	7 / 690	7 / 690	7 / 690	7 / 680	7 / 690	7 / 690
	0.2	7 / 710	7 / 710	7 / 720	7 / 710	7 / 730	7 / 710
	0.3	6 / 720	6 / 720	6 / 730	6 / 700	6 / 740	6 / 760
	0.4	6 / 770	6 / 770	6 / 770	6 / 790	6 / 790	6 / 790
	0.5	7 / 770	6 / 750	3 / 500	3 / 690	1 / 890	1 / 960
	0.6	7 / 780	6 / 710	5 / 670	4 / 680	4 / 750	4 / 800
8.7	0	10 / 590	10 / 590	10 / 590	10 / 590	10 / 590	10 / 590
	0.1	10 / 430	10 / 440	9 / 440	9 / 440	9 / 440	9 / 430
	0.2	9 / 450	9 / 450	9 / 450	9 / 470	9 / 470	8 / 480
	0.3	8 / 470	8 / 480	8 / 480	8 / 470	8 / 500	7 / 500
	0.4	8 / 470	7 / 480	7 / 480	7 / 480	7 / 520	7 / 510
	0.5	8 / 490	8 / 470	8 / 470	8 / 540	5 / 520	3 / 550
	0.6	9 / 560	9 / 590	9 / 580	9 / 480	4 / 480	2 / 600

In order to better understand the combined effects of these variables, the data for 2750 mg/L from the supplementary data is illustrated in Figure 4.2 as the UI. As mentioned in the introduction (Section 1.6.1), there is evidence that fluctuations may result in increased flux compared to steady-state conditions as a result of disturbances in the polarisation layer [119-121]. The results of this study (Figure 4.2) showed that there was no increase obtained in the flux under fluctuating energy when compared with steady-state conditions (TI = 0). The exception to this was at low average wind speeds (Figure 4.2A) for reasons discussed below.

The results in Table 4.1 and Table 4.2 showed that the flux obtained at low TI was consistent with that obtained under steady-state conditions and the performance only deteriorated at high TI when the fluctuations caused the power to start cycling on/off. This does not agree with the observations of other authors (described in Section 1.6.1) that showed increased performance of membrane systems caused by fluid instabilities in the region of concentration polarisation due to the turbulence disturbing the polarisation layer [119-121]. The results obtained by Al-Bastaki and Abbas [121] showed that cyclic operation using a square wave fluctuation in pressure resulted in higher average flux than when the membrane system was operated under steady-state conditions. Furthermore, the flux increased with increasing amplitude and decreasing period of fluctuation of the operating pressure. These experiments were performed at average pressures of 40 and 50 bar with amplitudes of 5 and 10 bar and oscillating periods 5 – 15 min using a feed water concentration of 10,000 mg/L NaCl. The results showed a maximum increase of 13 % in the permeate flux with the 10 bar amplitude of fluctuation and 5 min period of oscillation [121].

There are several possible reasons why the results detailed in Table 4.1 and Table 4.2 did not agree with other research on cyclic operation of membrane systems [119-121]. The main hypothesis is that the fluctuations did not increase the flux because of the reduced effects of concentration polarisation at the relatively low pressures (< 12 bar) and feed water concentrations used (2750 mg/L and 5500 mg/L). This hypothesis is supported by the data in Table 4.2, which showed enhanced performance with fluctuations at the highest average wind speed (8.7 m/s) with the 5500 mg/L NaCl feed water. The performance was enhanced most at a low TI of 0.1, with little impact caused by increasing the period of oscillation. The fluctuation enhancement of rejection

decreased by increasing the TI and showed greater degradation with the combination of high TI and longer periods of oscillation. These results highlight that the use of fluctuations to enhance the performance of membrane systems is more apparent with increased feed concentrations and pressures due to the increased impact of concentration polarisation. The other main difference with the wind-membrane experiments was that the periods of oscillation used to represent wind fluctuations (15 – 90 s) were considerably shorter than those used by Al-Bastaki and Abbas (5 – 15 min) [121]. However, according to their results, the shortest oscillation period of 5 min resulted in the highest flux [121]. Therefore, it would be interesting for future work to try and operate the wind-membrane system using a different pump at higher TMP to determine the threshold for fluctuations that could increase the average flux.

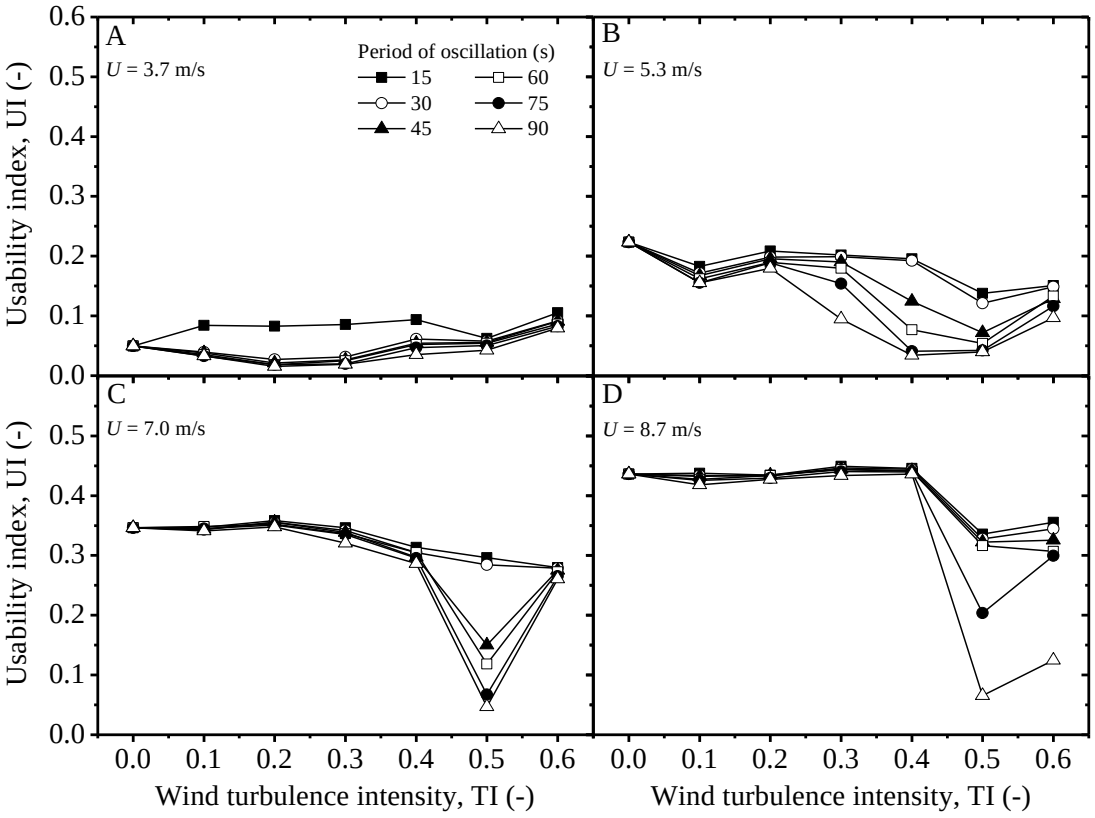

Figure 4.2: Variation of average usability index (UI) with increasing wind turbulence intensity (TI) using oscillating power (programmable power supply) for oscillation periods of 15, 30, 45, 60, 75 and 90 s with a feed water of 2750 mg/L NaCl at equivalent average wind speeds; (A) 3.7 m/s; (B) 5.3 m/s; (C) 7.0 m/s and (D) 8.7 m/s.

Although Figure 4.2A showed that fluctuations at low average wind speeds resulted in increased system performance than under steady-state conditions (TI = 0.0), it was because the fluctuations provided additional power and the system stayed turned on because of the rapid fluctuations. The effect of the power switching off at low average wind speeds is well illustrated in Figure 4.2B where higher periods of oscillation caused the power to switch off at lower values of TI resulting in a significantly reduced UI.

The performance of the system is easily understood at higher average wind speeds (Figure 4.2C and D) where the UI was independent of the period of oscillation up to TI of 0.4. Higher TI caused the system to start shutting off as shown by the drop in UI at 0.5. The rise in UI shown at TI of 0.6 was due to the additional amplitude of fluctuation providing more power to the system which reduced the stabilisation time (explained in Section 5.2). At wind speeds higher than 7.0 m/s, the fluctuations had little effect up to a TI of 0.4 which indicates that the system could operate as if under steady-state conditions under real wind speeds of 7.0 m/s or more. It should be noted that the wind-membrane system produced water within the guideline value over the whole range of wind speed fluctuations with a feed water of 2750 mg/L NaCl as shown in Figure 4.2. With a feed water of 5500 mg/L NaCl, the system required an average wind speed of 7.0 m/s or more in order to operate within the safe operating window and there was zero flux produced under all fluctuations at the lowest average wind speed of 3.7 m/s. Fluctuations at low average wind speeds caused the TMP to remain below 4 bar for significant periods of time and resulted in zero flux due to the higher osmotic pressure of this feed water. As mentioned above (Section 3.2), the osmotic pressure of the feed waters was calculated as 2.2 bar for 2750 mg/L and 4.4 bar for 5500 mg/L.

4.3 System performance with wind turbine in wind tunnel

The wind-membrane system was tested with the wind turbine in the wind tunnel for two main reasons: (i) to determine the effect of real fluctuations and (ii) to verify the results of the experiments performed with the programmable power supply. The experimental setup and procedure for these experiments is detailed in Section 2.5.3. Figure 4.3A-H shows the system operating close to its limit in terms of the maximum amplitude of fluctuations, at an average wind speed of U = 5.3 m/s and wind turbulence intensity of TI = 0.4 with a feed water of 2750 mg/L NaCl. The TI in the wind tunnel was controlled

by selectively switching a bank of nine fans to create sinusoidal wind speed fluctuations about a constant mean value (Section 2.2.3). The results showed that fluctuations in power (Figure 4.3B) were due to a complex relationship of wind speed fluctuations (Figure 4.3A), furling of the wind turbine and high loading from the membrane system at start-up. As shown in Figure 4.3B, the result was that the wind turbine power did not always follow the pattern of the wind speed.

The TMP (Figure 4.3C) varied according to the magnitude of power and the length of time for which it was available as well as the TMP starting point. Once the power was switched off, the TMP exhibited an exponential decay which assisted in absorbing the longer term fluctuations (>15 s) but not the short-term ones (<10 s). The main effect of these fluctuations was the greatly reduced flux (Figure 4.3D) which averaged 4.2 $L/m^2.h$, less than half the steady-state value of 8.8 $L/m^2.h$ obtained at the same average power (Figure 3.2B). Both the flux (Figure 4.3D) and the recovery (Figure 4.3E) demonstrated that the periods where the power was switched on compared favourably with the steady-state conditions shown in Figure 3.2B and C, but the periods of zero-power resulted in greatly reduced average system performance. In contrast, the permeate NaCl was much less affected by these fluctuations. Even under a high level of fluctuation at a low average wind speed, the permeate concentration remained well within the guideline value (Figure 4.3F). The combination of a 1 min period of zero-power (Figure 4.3B) followed by a 1.5 min period of the system cycling on/off below a TMP of 4 bar caused the permeate NaCl (Figure 4.3F) to increase but remain within the guideline value. A time lag was observed between the pressure drop and the increase in NaCl due to the period of zero-power and the time taken for diffusion of salts.

The performance of the system with regards to water quality is also shown by the average retention (Figure 4.3G) of 85 % observed during this period which compared very well with the steady-state retention of 91 % (Figure 3.2D) at the same average power. Because of the high TI and subsequent shutting on/off, the SEC averaged over the 7 min period was 1.7 kWh/m^3 with peaks of up to up to 3.4 kWh/m^3 (Figure 4.3H). This was similar to the value of 1.6 kWh/m^3 observed under steady-state conditions but illustrates how frequent turning on/off resulted in increased energy consumption. This is further highlighted by the effect of fluctuating power on the efficiency of the pump

motor. The average pump motor efficiency (not plotted) was 33 %, significantly lower than the 44 % measured under steady-state conditions (see Figure 3.2H).

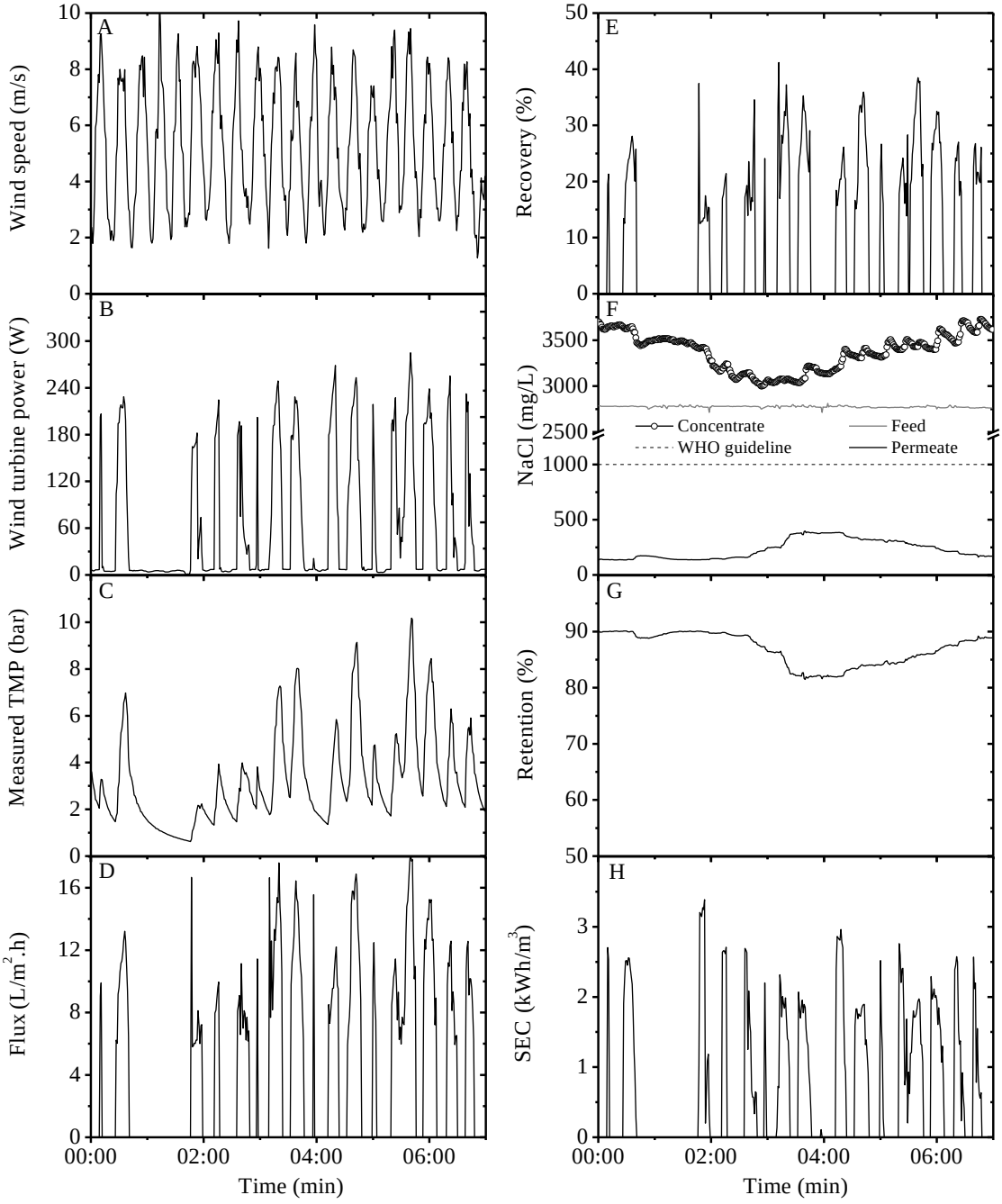

Figure 4.3: Performance of the wind-membrane system as a function of time using real wind speed fluctuations (wind tunnel) with a feed water of 2750 mg/L NaCl.

As observed in Figure 4.3A-H, the main effect of these large wind speed fluctuations was the reduced flux. Over short periods of 10 min, the largest wind fluctuations

resulted in a 50 % reduction in productivity when compared to steady-state conditions even though the permeate was within the guideline value. It should be noted that these fluctuations are at the extreme end of what any system would experience in practice. This reduction in productivity is only an indication and a long term trial would be required to determine what the overall effect of fluctuations on productivity is compared to steady-state conditions. These results verify the conclusion from the laboratory based experiments that the wind-membrane system can operate under large wind speed fluctuations within a safe operating window.

These results of the impact of fluctuations on the performance of membrane systems correspond well with other experimental studies that have been carried out (detailed in Section 1.6.1). The early research (1971) by Lising and Alward [98] was performed to investigate the impact of fluctuations in flowrate on a brackish water membrane system for coupling with a mechanical windmill. Experiments were performed using a feed water concentration of 3500 mg/L NaCl at constant system pressure of 40 bar with sinusoidal fluctuations in feed flowrate. The results showed that the performance of the RO membranes was the same under fluctuations in flowrate as under steady-state conditions, as long as the feed flowrate was not reduced to zero (i.e. a period of intermittency). Furthermore, small amplitude variations in the sinusoidal feed flowrate did not have any impact on the quality or quantity of permeate produced. Although this research was performed 40 years ago with membrane technology that has since seen significant advances, the conclusions on the impact of fluctuations were the same as those found in this research with the wind-membrane system.

Gocht *et al.* [118] performed a study to examine the impact of varying the feed pressure on the permeate flux and salt retention to determine the feasibility of transient operation of RO for use with renewable energy. Experiments were performed by increasing the pressure linearly at a rate of 180 bar/min and in steps from 10 – 60 bar. The authors determined that there was nothing to rule out the transient operation of a RO membrane system, however details of the experimental setup, results or length of operational time were not provided. Results on the pilot project set up on the island of Curacao in the Caribbean were published several months after it was set up in 2007 [102, 106] (Section 1.5.1). This windmill-powered RO project was designed for brackish water desalination using no form of energy storage. The pumping system used the Danfoss energy

recovery arrangement with a high-pressure piston pump (APP1.5) connected to an energy recovery motor (APM1.2) via a direct-drive shaft to keep the recovery within a controlled range (< 25 %). The membrane plant was operated under fluctuations in feed pressure between 30 – 50 bar and feed flowrates of 600 – 760 L/h according to the available wind speed. Only 3 days of data were provided, and the length of time over which the plant was operated was not provided. The membrane plant was able to provide permeate within the WHO guidelines at average wind speeds of > 6.5 m/s, and was seen to operate effectively at this range with fluctuating pressure and flowrates. Based on these preliminary short-term results, the authors concluded that it was feasible to operate the membrane system without any energy storage subject to fluctuations in pressure and flowrate.

There is still no detailed information on the long-term impact of fluctuations on the lifetime of the membrane or other components in the membrane system. The aged BW30-4040 membrane module used for these experiments was operated for > 250 hours under large fluctuations in pressure and flowrate without any noticeable effect on the components or the performance of the membrane. There have been some studies that reported the same result for longer periods of operation under fluctuating power, however none of these studies have lasted for the expected operational lifetime of the membrane modules (5 years) [100, 104].

The mechanical windmill-driven membrane system set up in Hawaii to desalinate brackish water (3500 and 2700 mg/L) was operated for a period of 3 months subject to fluctuations in pressure and flowrate caused by wind fluctuations [30, 93] (detailed in Section 1.5.1). Due to wind speed fluctuations of 4 – 8 m/s, the pressure varied over the range from 5.2 – 6.9 bar while the feed flowrate varied from 480 – 1020 L/h. The feed pressure and flowrate were constrained within these limits through the use of a hydraulic accumulator. As well as fluctuations in feed pressure and flowrate, the membrane plant experience 460 on/off cycles due to low wind speeds or intermittent availability. Following the 3 month period of testing, there had been no deterioration in the performance of the membrane or any of the components in the membrane plant. The research by Pestana *et al.* [100] was performed to determine the possibility of operating a RO membrane system within a safe operating window subject to fluctuations of pressure and flowrate (further details in Section 1.6.1). The membrane system was

operated over a wide range of pressure (30 – 60 bar) and feed flowrates (5000 – 10,000 L/h) by varying the power and the regulating valve on the concentrate stream. After more than 7000 hours of operation over this wide operating range, the authors concluded that membranes can function under fluctuations without deteriorating, although further testing would be required for an ageing study.

4.4 Conclusions

The operation of the wind-membrane system with no form of energy storage was described under simulated and real wind speed fluctuations from controlled experiments using a programmable power supply and a wind tunnel. In terms of a safe operating window, the membrane system was shown to produce good-quality drinking water with a feed water of 2750 mg/L NaCl over the whole range of operation with wind speeds from 3.7 m/s (system start-up) to 8.7 m/s at turbulence intensities 0.0 (steady-state conditions) to 0.6 (extreme fluctuations) and periods of oscillation from 15 to 90 s. With a feed water of 5500 mg/L, the performance was much more marginal with wind speeds of 7.0 m/s or more required to produce adequate-quality permeate under fluctuating conditions. The operation of the membrane system was influenced by the average wind speed as well as the TI (directly related to the amplitude of fluctuations) and the period of oscillation. However, at average wind speeds of 7.0 m/s or higher the performance was independent of the period of oscillation up to a TI of 0.4. In addition, within this operating range the system performance was the same under fluctuations as under steady-state conditions. The system performance was seen to deteriorate most under fluctuations that occurred at low average wind speeds with high TI and long periods of oscillation. These types of fluctuations allowed the power to shut off and the low average wind speeds meant that there was insufficient power available for the system pressure to recover to a suitable level.

This research demonstrates that membrane systems can be directly-connected to renewable energy systems (wind power presents the most extreme fluctuations) and operate effectively within a safe operating window. The main challenge associated with operation of this nature is not the size of the fluctuations but the effect of the power switching off which causes reduced flux and permeate quality. This must be controlled in innovative ways by energy buffering, careful control of the water treatment load or

disposal of the poor quality permeate in order for RE-membrane systems to be utilised. The membrane system was operated for >250 hours under large fluctuations in power without any noticeable effect on the components or the operation of the membrane. Further testing would be necessary to determine the effect of long term operation of this nature.

Chapter 5

Effect of wind intermittency

While the previous chapter dealt with the effect of wind fluctuations, this work was necessary to determine the effect of wind intermittency. Intermittent operation was taken to be any period of time when the system shut off due to insufficient power. The membrane system was tested with variables of i) amplitude from 60 – 300 W and ii) length of time with zero-power from 0.5 – 3 min. This was performed over one hour periods with six on/off cycles to simulate the system operating under intermittent operation for short periods of time when directly-connected to a small wind turbine. The results showed that the membrane system produced potable water under the majority of intermittency experiments performed. There was a relatively large increase in the average salt concentration of the permeate, especially when the system was off for shorter periods of time (0.5 – 1 min). Longer periods of zero-power (>1 min) did not have as significant an effect on the average water quality. This is important when the need for energy buffering or storage is considered for these systems as it shows the potential for improving the overall flux and water quality over the short-term.

5.1 Analysis of intermittent operation

To simplify the analysis of the impact of real wind, the behaviour of the wind-membrane system was divided up into two distinct sections dealing with i) fluctuations and ii) intermittency. Intermittent operation was taken to be any period when the membrane system shut off due to insufficient power, caused by low wind speeds. Understanding the dynamics of the membrane system when the power is turned off,

particularly with respect to diffusion, is crucial for establishing the impact on the average permeate quality. Whilst the extreme fluctuations dealt with in Chapter 4 are more commonly found in wind power, intermittence is a characteristic of all renewable energy resources and has a significant impact on the safe operating window of the membrane system.

The use of a square wave power input to the membrane system to simulate intermittent operation is detailed in Section 2.5.2. Experiments were performed using the aged BW30-4040 membrane module and feed water concentrations of 2750 mg/L and 5500 mg/L NaCl. The square wave power input is shown in Figure 5.1 with a feed water of 5500 mg/L where the power was switched off for 3 min from 240 W. As shown by line ①, when the power was switched off, the feed and permeate flowrates (Figure 5.1A) responded immediately while the concentrate stream continued to flow for several minutes due to back-pressure from the pump. The concentration of the permeate stream (Figure 5.1B) had a delayed response (~ 30 s) once the power was switched off (①). This was due to permeate water being drawn back into the membrane in order to achieve equilibrium, known as osmotic suck-back [127]. During this period the flowrate was zero as the sensor could not measure reverse flow and the conductivity measured was that of water that had already passed through the sensor. Once all of the available water had been drawn back into the membrane, the conductivity sensor on the permeate line gradually reduced to zero as there was no water remaining in the line and the sensor was exposed to air. When the power was switched back on (③) it took one min for the pressure to increase sufficiently and the permeate flow to resume (④).

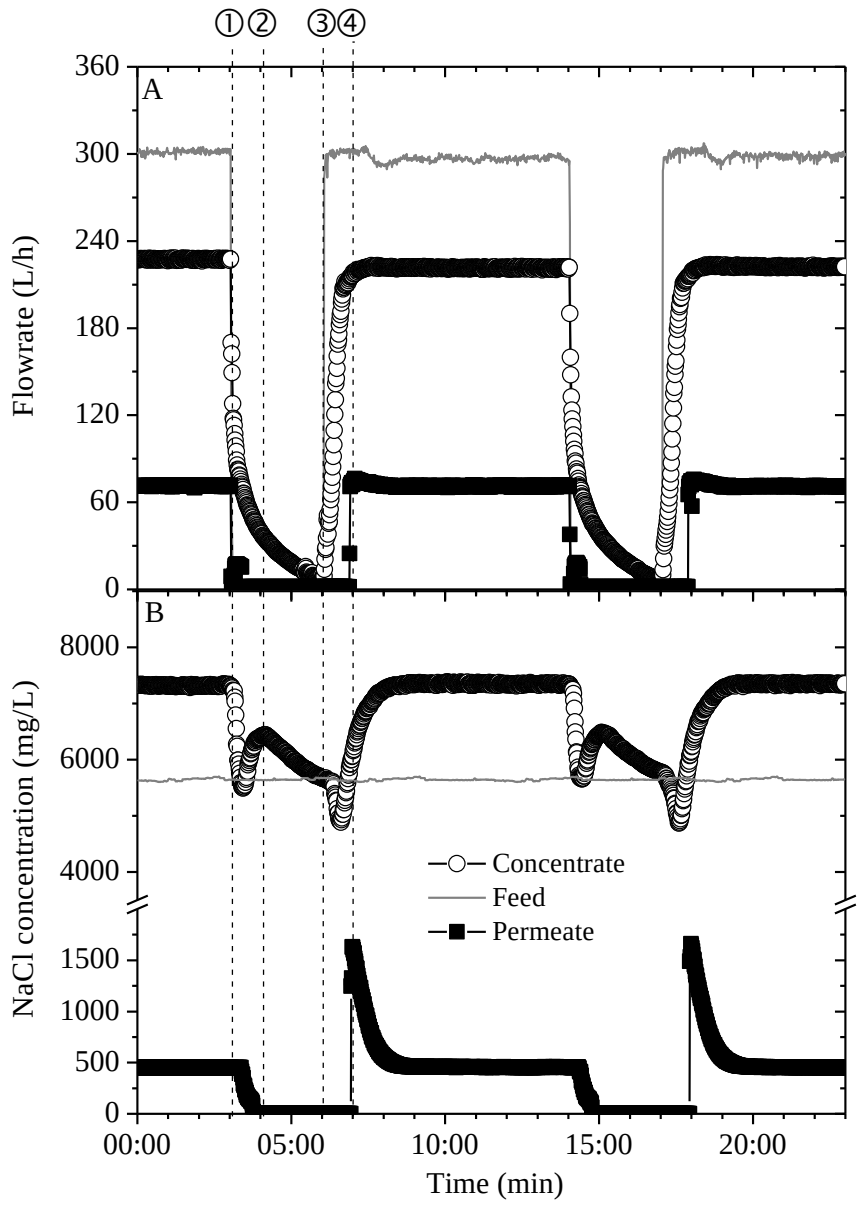

Figure 5.1: The effect of intermittent operation using a feed water of 5500 mg/L NaCl with the power switched off for 3 min from 240 W.

While the power was turned off (①-③), diffusion of salts across the membrane occurred, this is represented by a large spike in permeate concentration (④) once the system was re-started. This was caused by the permeate water being drawn back into the membrane by osmotic suck-back and providing a diffusion gradient for the continual diffusion of salt between the concentrate and permeate without any water flux to dilute the saline solution and create an apparent rejection. The concentrate stream exhibited a sharp decrease in concentration when the power was switched off (①) as the system was no longer desalinating and the concentrate concentration was the same as the feed.

This was followed by an increase (②) which showed salts from the boundary layer being washed through the system. A mass balance performed on several experiments (3% error) showed that the further drop in the concentrate concentration (between ③ and ④) was a result of diffusion of salts into the permeate stream. The net flux of NaCl across the membrane from the feed to the permeate during off-time was calculated based on experimental data as 0.46 mg/m².s for a feed water of 2750 mg/L and 0.87 mg/m².s for a feed water of 5500 mg/L NaCl. The volume of water that remained in the membrane vessel which had to be purged to return to normal conditions was 2 L ±10 %.

5.2 System stabilisation time

The stabilisation time was defined as the time required for the permeate NaCl to return to its original value once the permeate flow had resumed. In other words, this was the length of time required to flush out the poor quality permeate caused by diffusion of salts across the membrane during the period of zero flux. Figure 5.2 shows the effect on the permeate concentration of using constant power when re-starting the membrane system (240 W) following varying lengths of off-time from 0.5 – 3 min. As can be seen, the time required for the permeate concentration to stabilise following a period of intermittency was independent of the off-time.

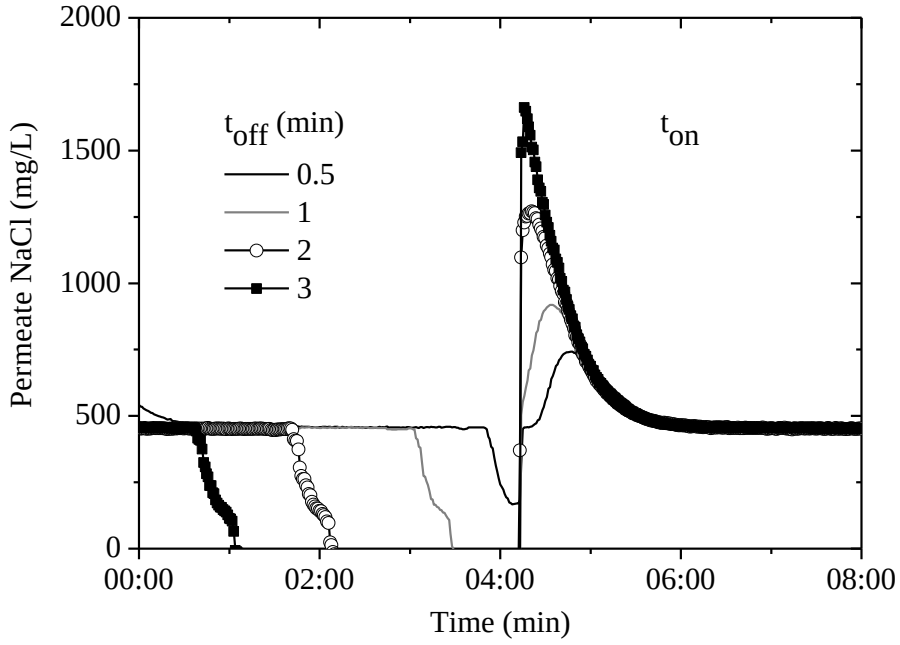

Figure 5.2: Time taken for permeate NaCl to stabilise following off-times (t_{off}) from 0-5 – 3 min with constant power during t_{on} (240 W).

Figure 5.3 demonstrates that the stabilisation time depended upon the amount of power available to re-start the system and the feed concentration. It should be noted that the permeate NaCl achievable depended on the power available as shown in Figure 3.2E, therefore the stabilisation time (Figure 5.3) was the time taken to return to this original value. The amount of power available determined the TMP, flowrate and resulting flux which purged the system of the high salinity permeate; therefore more power resulted in less time required for purging. The volume of water that remained in the membrane vessel and must be purged was measured as 2 L ±10 %. The feed concentration affected the stabilisation time as the higher feed concentration reduced the effective TMP and resulting flux due to higher osmotic pressure. The effect of feed concentration is demonstrated in Figure 5.3 by the fact that 2 min were required to achieve stability using a feed water of 5500 mg/L NaCl with 240 W of power whilst only 120 W was required to achieve stability in this time with a feed water of 2750 mg/L NaCl.

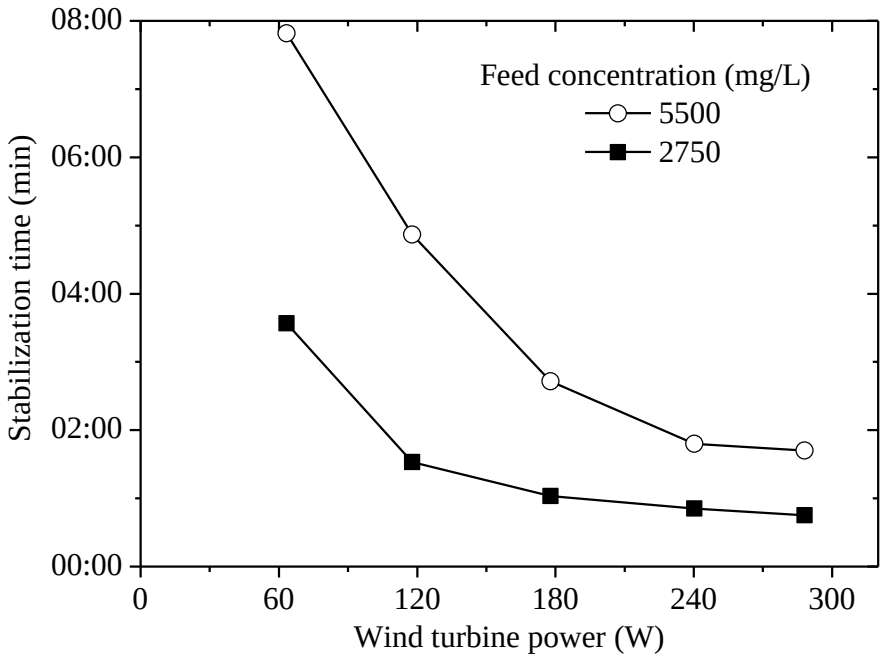

Figure 5.3: Stabilisation time of the permeate stream after a period of zero-power as a function of wind turbine power for feed waters of 2750 and 5500 mg/L NaCl.

The impact on the permeate concentration could be minimised by ensuring that sufficient power is available following a period of shutdown. For a feed water of 2750 mg/L NaCl, the system could operate with up to 3 min of down-time without the permeate exceeding the WHO guideline value. With a feed water of 5500 mg/L NaCl the minimum power required to produce permeate of adequate quality after a period of down-time was 120 W, and this must be sustained last for at least 5 min (Figure 5.3). Depending on the frequency of intermittent operation and the length of time with zero-power, it may be acceptable to allow the 2 L of high salinity permeate produced to mix with the rest of the good quality permeate that is stored. As these results have shown, this would depend very much upon the available wind resource, the salinity of the feed water and the quality of the membrane module.

5.3 Impact of wind intermittency on average water quality and quantity

To determine the effect of intermittent operation on the overall permeate quality and quantity, experiments were performed over one hour with six on/off cycles and the performance parameters averaged over this time period. The results are shown in Figure 5.4. The first point to note is that the membrane system produced water within the guideline value (1000 mg/L) at all off-times with a feed water of 2750 mg/L (Figure 5.4A), and with 5500 mg/L at power ≥120 W (Figure 5.4B). This shows the resilience of the system to periods of intermittency in terms of the water quality. The permeate concentration (Figure 5.4A and B) increased with longer off-time as a result of greater time available for diffusion of salt through the membrane. Increasing the power resulted in improved permeate concentration due to higher TMP and therefore flux (Figure 5.4C and D), which reduced the amount of time required to purge the system of the poor quality permeate water and obtain equilibrium. The permeate concentration with a feed water of 5500 mg/L was higher because of the increased osmotic pressure of the feed that offset the TMP (4.4 bar with 5500 mg/L compared to 2.2 bar with 2750 mg/L).

The change of permeate concentration with off-time showed a similar relationship for all of the experiments as shown (Figure 5.4A and B). The curve for membrane system power of 60 W showed the most obvious trend due to the reasons mentioned above and may be used to illustrate the effect of increasing the off-time. The permeate

concentration exhibited a steep slope up to an off-time of 60 s, followed by a more gradual increase for off-times of 120 s and 180 s. This was a result of the higher initial rate of diffusion due to the increased concentration gradient when the power was firstly turned off. As the salt diffused across the membrane, the concentration gradient reduced over time and the change in permeate concentration at longer off-time was not as significant. This is an interesting point as it may be more beneficial to reduce the number of intermittent periods of 60 s or less than attempt to buffer these longer periods of zero-power in order to reduce the impact of intermittency on the average permeate quality.

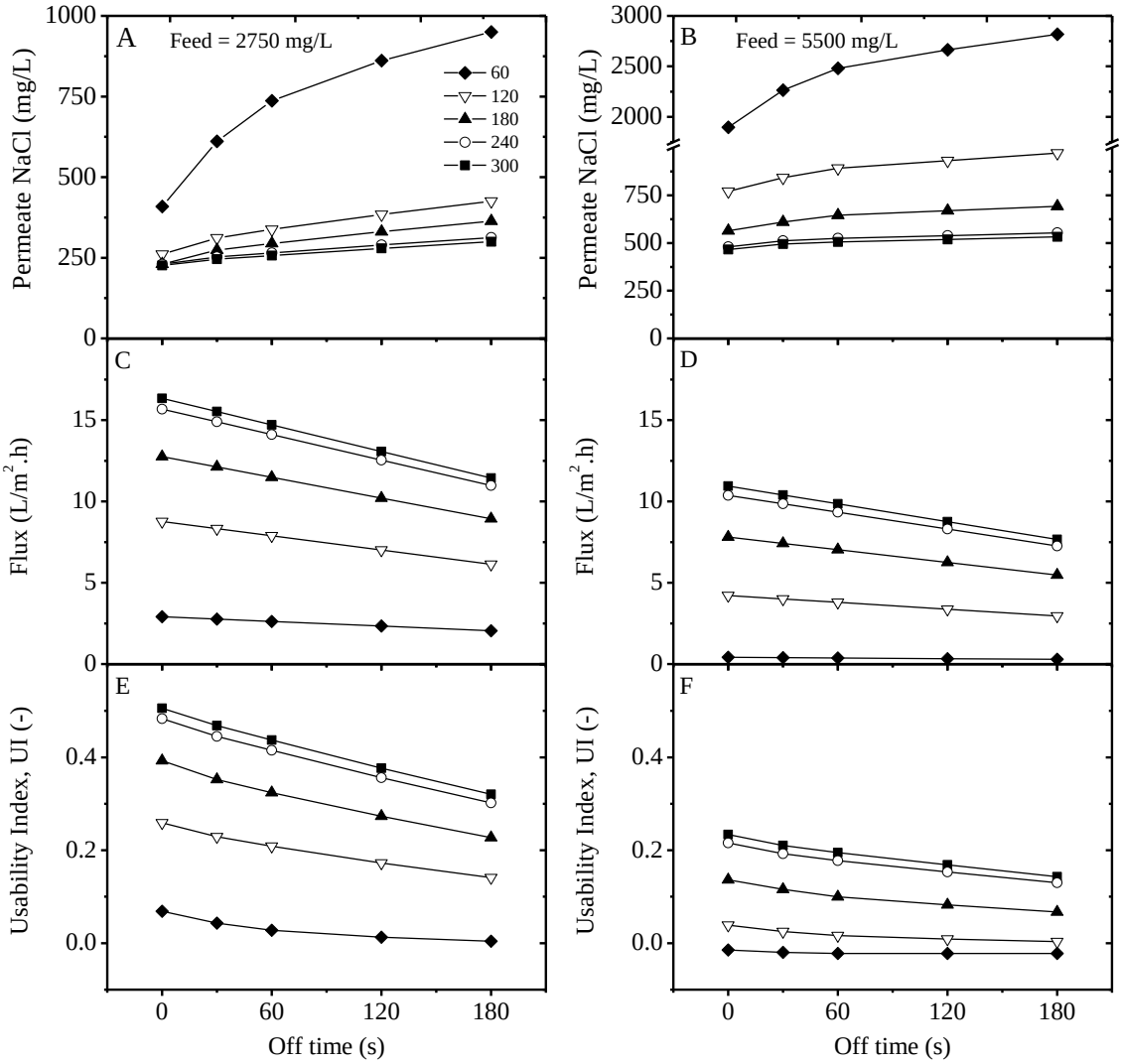

Figure 5.4: The effect of intermittent operation on membrane performance with parameters averaged over one hour with six on/off cycles and feed waters 2750 mg/L and 5500 mg/L NaCl. On/off cycling was achieved using a square wave power input with constant

peak-to-peak amplitude and off time. Each point on a line constitutes a one hour experiment with performance parameters averaged over this period A: permeate NaCl; B: flux and C: usability index (UI).

The flux exhibited a linear decrease with increasing off-time (Figure 5.4C and D) due to the periods of zero flux, and the fact that the flux returned immediately to its original value once the power was switched back on as shown previously (Figure 5.1A). There would be zero flux with an off-time of 10 min as this would be 100 % of the cycle. The UI (Figure 5.4E and F) is useful for understanding the combined impact on the permeate concentration and the flux. The graphs (Figure 5.4E and F) show that there was a more rapid decline in the UI up to 60 s (representative of the rate of change of permeate quality) followed by a more gradual reduction, which again highlights the potential for short term energy buffering. The UI was negative with a feed water of 5500 mg/L and power of 60 W (Figure 5.4F) as a result of the permeate concentration being higher than the guideline value of 1000 mg/L, which showed the system functioning outside the safe operating window. The difference in the UI obtained with feed waters of 2750 mg/L and 5500 mg/L illustrates the difference in the permeate quality and quantity that can be obtained depending on the characteristics of the feed water.

An important consideration which is not covered here due to the short time scales involved is the effect of long term intermittent operation on the pump and motor. However, short term energy buffering of 60 s would help to reduce the number of system restarts as well as improving the average permeate concentration and flux. This highlights the potential for short term electrical storage technologies such as supercapacitors to improve the performance of the wind-membrane system in terms of overall permeate quality and quantity by buffering the periods of intermittency.

This research on the short-term effects of wind intermittency on the performance of the wind-membrane system is a very important addition to the literature on RE-membrane systems. To date there is very little known about either the short-term performance impacts or the long-term lifetime effects of intermittent operation of membrane systems (detailed further in Section 1.6.1). The examination of sinusoidal fluctuations in feed flowrate by Lising and Alward [98] concluded that small amplitude variability in feed flow had very little effect upon the quantity or quality of potable water, provided the

flowrate was not reduced to zero at any point. This conclusion hints at the detrimental impact of intermittent operation in comparison to fluctuations, but no further details were provided. Some authors have stated that the likely performance deterioration caused by the cycling on/off of membrane systems would be the reduced permeate quality and the potential for increased wear on the pump and motor, however there was no evidence provided to back up these statements [116, 117]. Rahal and Infield [115] suggested that an upper limit should be applied to the cycling on/off frequency membrane systems to prevent deterioration of membrane system performance and lifetime. Again however, the impact on both the short-term performance parameters and the degree of fatigue damage caused by repetitive cycling of RO modules is unknown.

The mechanical windmill-powered brackish water desalination (3500 and 2700 mg/L) plant set up by Liu *et al*. [30, 93] in Hawaii was tested for a period of 3 months (Section 1.5.1). Throughout the period of testing, the membrane plant underwent 460 on/off cycles (average 5 on/off cycles per day) due to low wind speeds or intermittent wind availability. At the end of the test period, there was no decrease observed in the performance of the membrane modules, nor any damage caused to any of the components of the membrane plant. One of the aims of the SDAWES project (Section 1.5.1) was to examine the impact of cycling membrane plants on/off in response to the power available in the wind [104]. The objective was to determine the impact of plant cycling on the quality and quantity of permeate produced and the operational lifetime of the components of the membrane plant. There was minimal impact of the wind speed fluctuations on the permeate quality and quantity; however the fluctuations in feed pressure/flowrate were relatively small due to the oversized wind turbines and the use of energy storage with a flywheel (Section 1.5.1). The plant was tested for approximately 2 years, during which time there was no deterioration of any of the membrane plant components due to cycling on/off at low wind speeds. Unfortunately, the frequency of plant cycling or the number of cycles was not provided. As the standard operational lifetime of RO membranes was 5 years, the authors concluded that prolonged testing over a further 3 years would be required to establish whether intermittent operation impacted upon membrane lifetime.

Therefore, the results of the impact of wind intermittency on the short-term performance of membrane systems shown here will provide greater knowledge and understanding for

the design and performance of RE-membrane systems. However, there is still a need for long-term testing to determine the impact of cyclic operation on membrane lifetime and the operational lifetime of the other components in the membrane plant, particularly pumps and motors. This would require both laboratory-based ageing studies using cyclic on/off operation of membranes and long-term pilot testing of membrane plants with renewable energies.

5.4 Conclusions

The operation of the wind-membrane system was described under intermittent operation over one hour intervals with intermittent periods from 0.5 – 3 min to determine the impact on the average quality and quantity of potable water produced. The effect of on/off cycling was seen immediately in the power, TMP and flux, whereas there was a lag time associated with the permeate concentration due to the time taken for diffusion and flushing of the system. The fact that the fluctuations were seen immediately in terms of the system hydraulics is important as it means that there is no form of buffering of the fluctuations. The membrane system showed good resilience to intermittency in terms of permeate quality by producing potable water for all of the conditions except with a high feed concentration at low power (5500 mg/L NaCl at 60 W). As would be expected, increased power and less off-time resulted in a higher average permeate quality and flux over a one hour period. The amount of power available to re-start the system after a period of intermittency was important for the average permeate concentration as it determined the TMP, flowrate and flux which purged the system of high salinity permeate. Due to the concentration gradient being highest when the power was initially turned off, the increase in permeate concentration was highest at off-times up to 60 s, which highlights the potential for short term energy buffering. The following chapter investigates the use of supercapacitors to provide several minutes of energy storage in order to improve the performance of the membrane system under wind fluctuations and intermittency.

Chapter 6

Use of supercapacitors to buffer wind variability

The potential for supercapacitors to expand the safe operating window of the wind-membrane system by buffering short term wind fluctuations and intermittency is investigated. Experiments were carried out with a feed water of 5500 mg/L NaCl with three sizes of supercapacitor bank to determine the effect of increasing the short term energy storage capacity. When the wind-membrane system was powered by the supercapacitors, wind speeds of >7 m/s were required for the supercapacitor bank state of charge (SOC) to increase, otherwise they discharged gradually to a threshold value dictated by the control electronics. While the SOC of the supercapacitors was above this threshold value, the operation of the wind-membrane system was as under steady-state conditions, thereby achieving independence of the wind speed fluctuations or intermittency. It is concluded that supercapacitors are an effective method of buffering short term wind speed fluctuations to provide steady-state performance and improve the productivity of RE-membrane systems.

6.1 Charging and discharging of supercapacitor banks

6.1.1 Charging supercapacitor banks without load

The main aim of this study was to determine the effectiveness of supercapacitors in buffering short term wind speed fluctuations to provide a more stable supply of power

to the wind-membrane system. This type of operation should result in both improved water quality and quantity, as well as an expansion of the safe operating window by increasing the quality of power delivered by the wind turbine and reducing the number of intermittent periods [98, 116].

Detailed calculations for sizing of the supercapacitor bank and connection to the membrane system are given in Section 2.4. The experimental procedure for determining the charging and discharging characteristics of the supercapacitor banks involved using step function experiments (described in Section 2.5.1). These experiments were performed using the wind turbine simulator with and without the membrane system to determine the effect on the SOC and verify the amount of membrane system run-time available from each size of supercapacitor bank.

An essential part of mapping out the performance of the supercapacitors was to understand the relationship between the wind speed input to the system and the SOC of the supercapacitor bank in the absence of an electrical load. Figure 6.1 illustrates the effect of the wind speed on the charging time of the supercapacitor bank with no load attached for the three different bank sizes. Each of the charging profiles followed the same trend with increasing wind speed, which was inverse to the wind turbine power curve (Section 3.1). The rapid increase in the charging rate from 4 – 8 m/s represented the additional energy available in the wind, which is proportional to the cube of the wind speed. Furling of the wind turbine in order to protect the generator from overheating at high rotational speeds resulted in the charging time leveling off at higher wind speeds. The charging time of the supercapacitor banks was proportional to the capacitance and the ESR as shown by Equation 2.11. Hence, a longer time was required to charge a larger bank size.

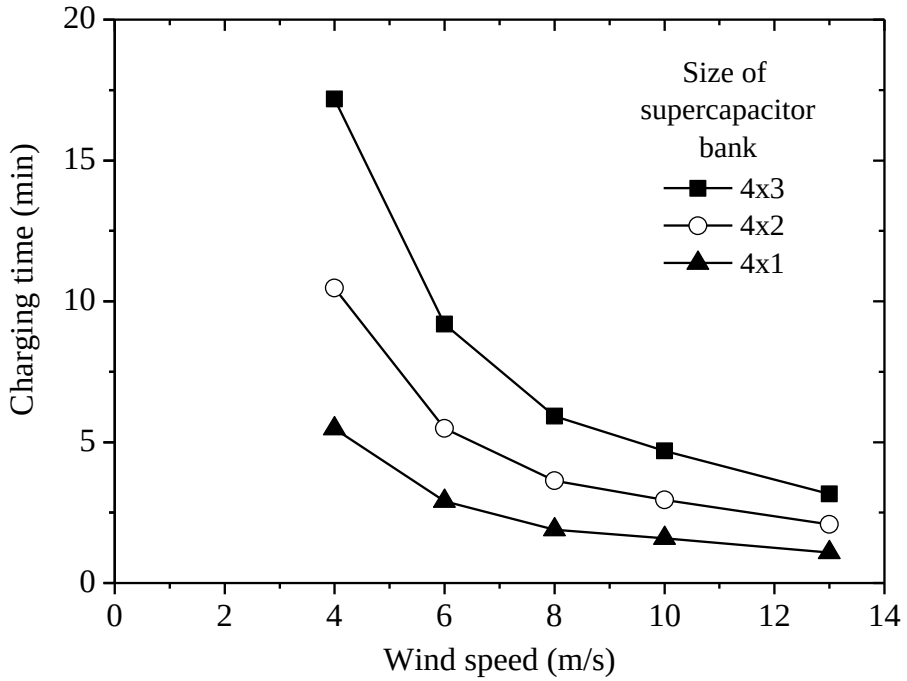

Figure 6.1: Charging time for the supercapacitor bank related to the available wind speed and the size of bank.

The SOC was the most useful measure of the amount of energy available in the supercapacitor bank and was calculated by measuring the voltage across the supercapacitors (Equation 2.13). The effect of wind speed on the SOC during the charging process over time with no load (membrane system) attached to the supercapacitor bank is shown in Figure 6.2. Higher wind speeds resulted in increased power output from the wind turbine and more charging current being provided to the supercapacitor bank causing increased rate of charge. With an average wind speed of 6 m/s (120 W), full supercapacitor charge was achieved in 3 min for 4x1 (Figure 6.2A) and 9 min for 4x3 (Figure 6.2B) supercapacitor banks.

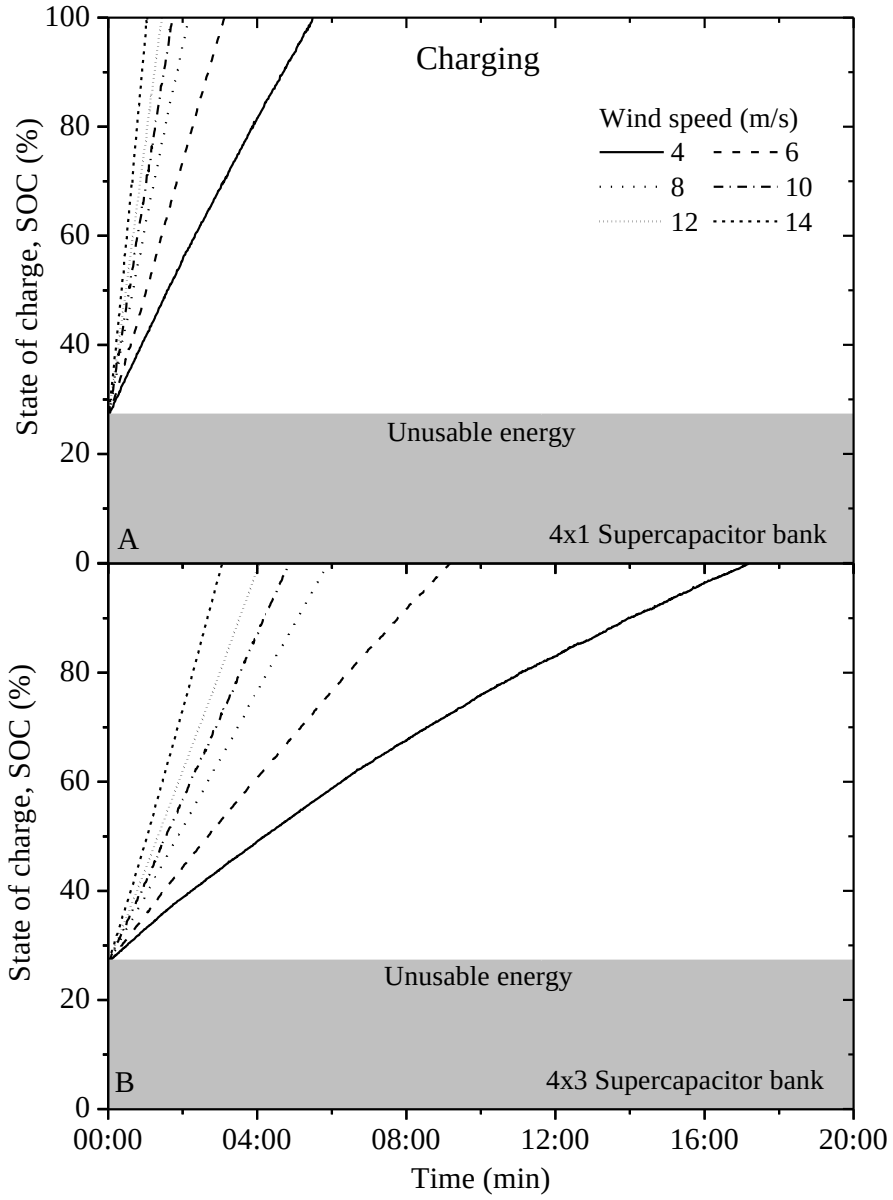

Figure 6.2: SOC of the supercapacitor bank charged by the wind turbine simulator over wind speed range 4 – 14 m/s with zero-power being drawn from the system; (A) 4x1; (B) 4x3 bank.

6.1.2 Discharging of supercapacitor banks with membrane system

The amount of membrane system run-time provided solely by the supercapacitor bank was important for verifying the effectiveness of the supercapacitors in buffering intermittent wind. The load of the membrane system was provided solely by the pump, with the maximum power consumption controlled by the set-point (240 W). The SOC of the supercapacitor banks discharging over time with the membrane system as the load and zero-power supplied by the wind turbine is shown in Figure 6.3. The discharge

time was directly related to the storage capacity of the supercapacitor bank as the power consumption of the pump was constant. The voltage and current output from the supercapacitor bank followed an exponential decay curve therefore the DC/DC converter was essential for delivering constant power to the membrane system. Full supercapacitor discharge took 1:20, 2:30 and 4:00 min for supercapacitor banks of 4x1, 4x2 and 4x3, respectively. These figures represent the maximum length of zero-power from the wind turbine during which power could be supplied by the supercapacitor banks without any detrimental effect on the operating characteristics of the membrane system.

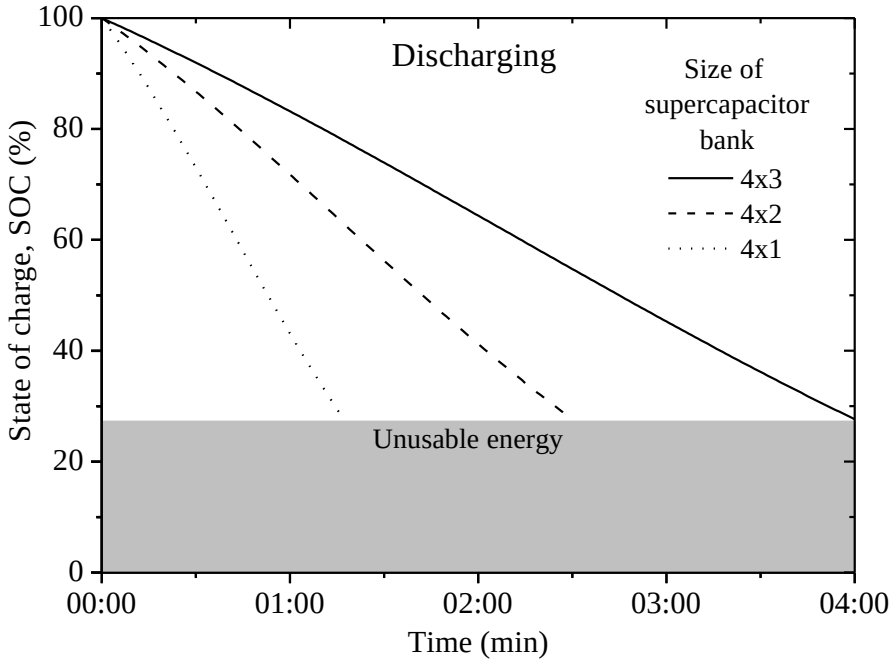

Figure 6.3: SOC of the supercapacitor banks discharged by membrane system at 240 W with no additional power being provided by the wind turbine simulator.

6.1.3 Impact of wind speed on supercapacitor charge with membrane system

Establishing the relationship between average wind speed and performance of the wind-membrane system operating with supercapacitor storage was necessary for determining the safe operating window for the system. Coupling the wind turbine and membrane system to the supercapacitor bank allowed simultaneous charging/discharging of the supercapacitor bank and operation of the membrane system under constant power. As demonstrated previously in Figure 6.1, the time required for charging the supercapacitor

banks was dependent on the wind speed. However, with the membrane system connected (Figure 6.4), wind speeds of 4 – 6 m/s resulted in more power being consumed by the membrane system (240 W) than produced by the wind turbine, causing the supercapacitor bank to discharge. The rate of discharge was related to the amount of power produced by the wind turbine therefore higher wind speeds resulted in longer discharge time. Wind speeds of >7 m/s resulted in surplus power being produced and charging of the supercapacitor bank.

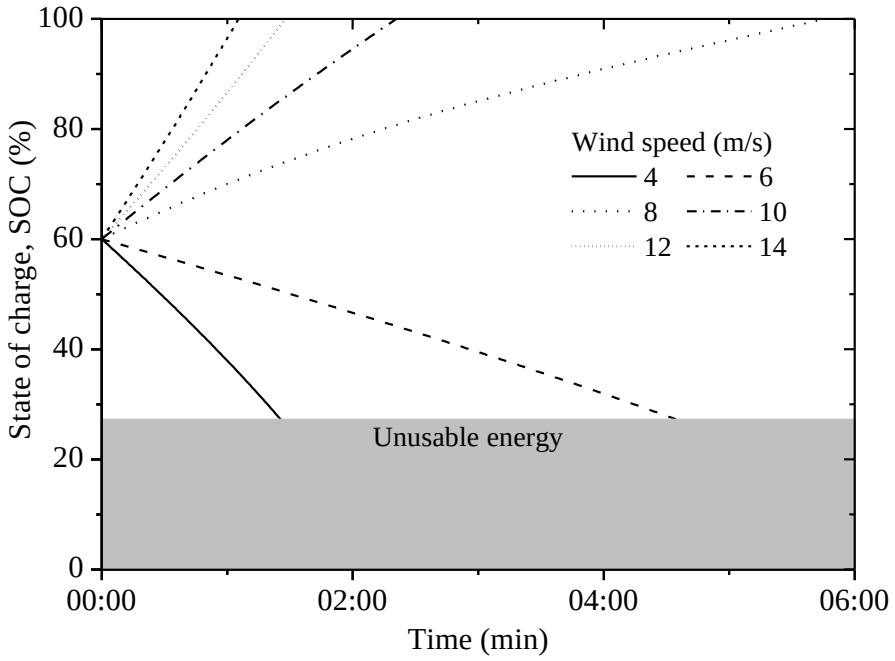

Figure 6.4: SOC of the 4x1 supercapacitor bank connected to the wind turbine simulator and membrane system over wind speeds 4 – 14 m/s.

6.2 Effect of wind intermittency on supercapacitor system performance

The results of the intermittency experiments (Chapter 5) demonstrated that intermittent operation was particularly detrimental with respect to permeate quality and quantity. The impact was most significant at shorter off times (<60 s) where the rate of change to the permeate concentration was highest due to the increased initial rate of diffusion within the membrane. By varying the period of intermittency or off-time over a range from 0.5 – 5 min, the effectiveness of supercapacitor banks in buffering the most common power-cuts associated with wind fluctuations were investigated.

The experimental methodology for examining the impact of wind intermittency and fluctuations is detailed in Section 2.5.2 and was the same method used without energy storage as shown in Chapter 4 and Chapter 5. Experiments were performed with the aged BW30-4040 membrane module and a feed water concentration of 5500 mg/L NaCl. Figure 6.5 illustrates the effect of increasing the off-time on the largest supercapacitor bank (4x3) with a wind speed of 10 m/s. This set of experiments was chosen to demonstrate the effect of intermittent operation as the longest off-time of 5 min was sufficient to cause system shut-down and demonstrate the operating range of the wind-membrane system (Figure 6.5A).

As shown in Figure 6.5B, the current output from the wind turbine fluctuated between 0 – 10 A according to the power output from the wind turbine and the SOC (Figure 6.5D), while the current drawn by the pump motor remained constant at 3 A up to 4 min off-time. The supercapacitor bank was charged and discharged according to the power available from the wind turbine while the membrane system was drawing constant power (240 W) all of the time. This is shown by the increase and decrease of the voltage of the supercapacitor bank (Figure 6.5C) and therefore the SOC (Figure 6.5D). The expected discharge time as shown in Figure 6.3 for the 4x3 supercapacitor bank was 4 min. This intermittency experiment reinforces that result by showing that the supercapacitor bank could provide power to the membrane system for a maximum off-time of 4 min of no wind while 5 min caused the SOC to reduce to the unusable threshold. By comparison, the 4x1 supercapacitor bank could provide power for periods of intermittency up to 1:20 min long and the 4x2 up to 2:30 min.

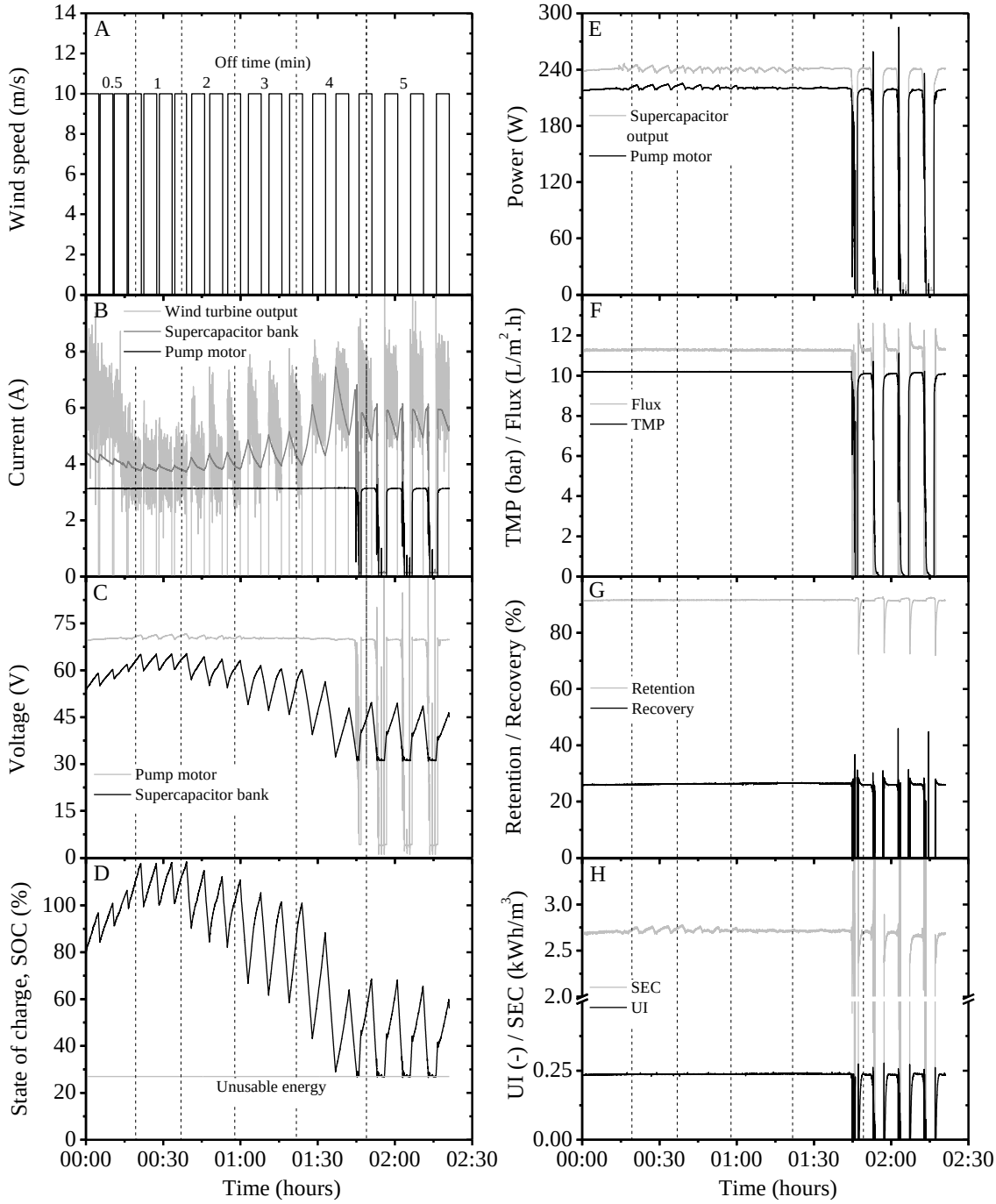

Figure 6.5: Wind-membrane system performance using 4x3 supercapacitor bank under intermittent operation with off time 0.5 – 5 min and feed water concentration 5500 mg/L NaCl.

The performance of the wind-membrane system was determined by the SOC of the supercapacitor bank, which was dependent on the availability of power from the wind turbine. When sufficient energy was available from the supercapacitor bank (SOC above unusable threshold, Figure 6.5D) the membrane system operated with constant energy and the desalination performance was as during steady-state conditions

(Figure 6.5E-H). During steady-state conditions, the TMP (Figure 6.5F) was 10 bar according to the set-point, resulting in flux of 11 L/m².h and recovery (Figure 6.5G) of 26 %. The TMP determined the driving force for the desalination process by providing the hydraulic pressure required to overcome the osmotic pressure of the feed water and boundary layer and the relatively small resistance of the membrane. At low TMP (<5.5 bar) and recovery (<10 %), the retention of NaCl was limited by the relatively high rate of NaCl diffusion in comparison to the water flux (<2.5 L/m².h). In contrast, there was increased concentration polarisation at high TMP (>10 bar) and recovery (>40 %) due to high concentration of rejected ions in the boundary layer that resulted in increased diffusion of NaCl across the membrane and a deterioration of permeate quality.

The retention of the membrane (Figure 6.5G) was lower than the expected value according to the manufacturer [49] as a result of the chosen set-point (lower pressure, feed flowrate and temperature) and the age of the membrane. The membrane was used for field trials in Australia in 2005 [60, 94] and extensive laboratory testing since 2008. While the flux was consistent with the expected values and previous experimentation, the retention under these operating conditions has reduced from 96 % to 92 % over the lifetime of the membrane [192]. Note that retention > 82 % is sufficient to produce permeate within the WHO guidelines (< 1000 mg/L) [12] from a feed water of 5500 mg/L NaCl, which is why the membrane continues to be used. Experimental analysis of a new BW30 membrane showed retention of 97 % at the set-point. In comparison to the new membrane, the flux of the aged membrane was ~ 12 % higher, resulting in increased recovery (~ 6 %) and reduced SEC (~ 18 %). Note however that this variation in flux was within the ± 20 % range for individual modules as given by the manufacturer [49].

The SEC is a measure of the energy required to produce a unit of clean water and is useful for determining efficiency in terms of energy requirements and water productivity. The energy required varied according to the operating conditions (pressure, flowrate, salt concentration) and exhibited a close relationship to the recovery of the system. For example, at low power the SEC was high because most of the energy was used to overcome the osmotic pressure due to the salinity difference across the

membrane (~ 4 bar), resulting in low recovery. The SEC obtained for this system under the chosen operating conditions was 2.7 kWh/m³ (Figure 6.5H).

The UI shows the combined impact of fluctuations on the flux (Figure 6.5F) and the permeate quality or retention (Figure 6.5G). The UI (Figure 6.5H) exhibited steady-state conditions throughout periods of intermittency up until the point when the supercapacitors were discharged. Once the supercapacitor SOC reached the unusable threshold (5 min), there was no more usable energy and the membrane system shut down (Figure 6.5E). Apart from buffering the intermittent periods up to 4 min, this highlights another advantage of using supercapacitors as they can be charged while the membrane system is turned off and therefore supply a sufficiently large amount of power to re-start the pump motor. This is useful both for overcoming the static friction of the pump and reducing the impact of intermittency on the average permeate quality. By using the supercapacitors to provide high power and therefore flux, the membrane can be rapidly purged of the of poor quality permeate produced by diffusion (measured as 2 L ± 10 % depending on operating conditions). The effectiveness of the supercapacitors in buffering short term wind intermittency is highlighted by comparing the system performance without any energy storage. By using the 4x3 supercapacitor bank to provide constant power over one hour with six intermittent periods of 3 min, there was a 40 % increase in the average flux and 15 % improvement in overall permeate quality when compared to the same experiment without energy storage (Section 5.3). This was a result of the supercapacitor bank providing constant power over this period, while the system without energy storage had zero flux during the off-time and poor quality permeate produced upon re-starting the system due to diffusion of NaCl. The increased performance was dependent on the amount of energy stored in the supercapacitors, which was a function of the size of supercapacitor bank and the SOC. Therefore, the performance increase was lower with wind speeds <7 m/s, longer off-time and smaller supercapacitor banks as a result of the reduced amount of energy stored. Overall, the supercapacitors were able to improve the performance (average flux and permeate quality) of the wind-membrane system by providing power during short-term intermittent periods and reducing the impact of longer-term intermittency on the recovery time and average permeate quality.

6.2.1 Discussion on choice of membrane set-point

A method of improving the performance of the supercapacitor bank by increasing the discharge time and decreasing the wind speed required for charging would be to reduce the amount of power required by changing the set-point of the membrane system. This set-point (10 bar at 250 L/h feed flowrate and 240 W power) was established in previous work to provide high flux and retention with low SEC and water recovery within the operating limits of the wind-membrane system. High water recovery coupled with low crossflow velocity causes concentration polarisation, resulting in lower flux and increased salt diffusion. In feed waters with sparingly soluble salts (i.e. calcium carbonate, calcium sulfate and silica) high water recovery can also cause increased risk of scaling [49]. Operation of small membrane systems at low recovery (~ 25 %) with regular forward flushing is a recognised method of preventative cleaning to avoid scaling thereby enhancing membrane performance and lifetime [49]. Reducing the maximum motor speed and therefore power drawn by the membrane system would result in lower SEC with the consequence of reduced performance in terms of flux and retention due to lower TMP. At low pressure, the permeate flux and recovery are controlled by mass transfer and therefore directly proportional to the TMP which is the driving force [52]. Hence, changing the set-point of the membrane system may result in more buffer time from the supercapacitor bank, but this would be at the expense of membrane system performance.

There are unique design criteria required for developing membrane systems to operate in remote regions with renewable energy. Designing systems with a focus on low energy consumption and robust long term membrane operation can be achieved by sacrificing efficiency in terms of high TMP, flux, recovery and salt rejection [58]. For example, to operate the membrane system at the test conditions given by the manufacturer (TMP of 15.5 bar, feed flowrate 1750 L/h with 5500 mg/L) [49], the power consumption would be 1840 W (Table 3.1). This would require a pump approximately six times the size of the existing one (300 W). While a larger pump may have increased efficiency (pump used here had efficiency 25 – 50 % depending on operating conditions), smaller pumps have lower energy requirements which determine the capital cost of the system by reducing the size of renewable energy generator required. In order to prolong the lifetime of the membrane, the recovery should be set to

~ 25 % (Figure 6.5G) and adequate pretreatment (such as UF) used to minimise the effects of fouling, particularly under intermittent operation [93, 197].

6.3 Effect of wind speed fluctuations on supercapacitor system performance

Controlled sinusoidal wind speed fluctuations were used to determine whether supercapacitors could improve the quality of power delivered to the membrane system and improve the overall system performance. Simulated fluctuations were examined over a range of periods of oscillation from 15 s – 20 min to cover the maximum range of short term wind speed fluctuations [67]. Previous experimentation without energy storage (Chapter 4) showed that the system performance deteriorated significantly with longer periods of oscillation (>60 s) at high turbulence intensity due to a combination of high loading from the pump motor and insufficient power to achieve system pressure, resulting in the power switching off. Figure 6.6 shows the wind-membrane system operating with the smallest supercapacitor bank (4x1) under a wide oscillating wind speed range 3 – 11 m/s with periods of oscillation 15 and 20 min. This data was used to demonstrate the system performance as it showed the operating limits of the 4x1 supercapacitor bank.

By buffering the periods of low wind speed (Figure 6.6A-D) and providing power to the pump motor, the supercapacitor bank was able to provide constant power during long periods of oscillation at high turbulence intensity (0.4) with no detrimental effect on the performance of the membrane system (Figure 6.6E-H). The performance of the membrane system was as under steady-state conditions as described above. Shorter periods of oscillation (15 s – 10 min) had less effect on the SOC, as did increasing the size of supercapacitor bank. The SOC (Figure 6.6D) showed the supercapacitor bank absorbing the fluctuations in power whilst operating at the limit of the available voltage range (Figure 6.6C). Note that while the membrane system did not shut down with the maximum oscillation period of 20 min, if the maximum supercapacitor voltage was limited to 60 V_{DC} then these fluctuations would have caused the SOC to reach the threshold value for the 4x1 supercapacitor bank, and it would have shut down.

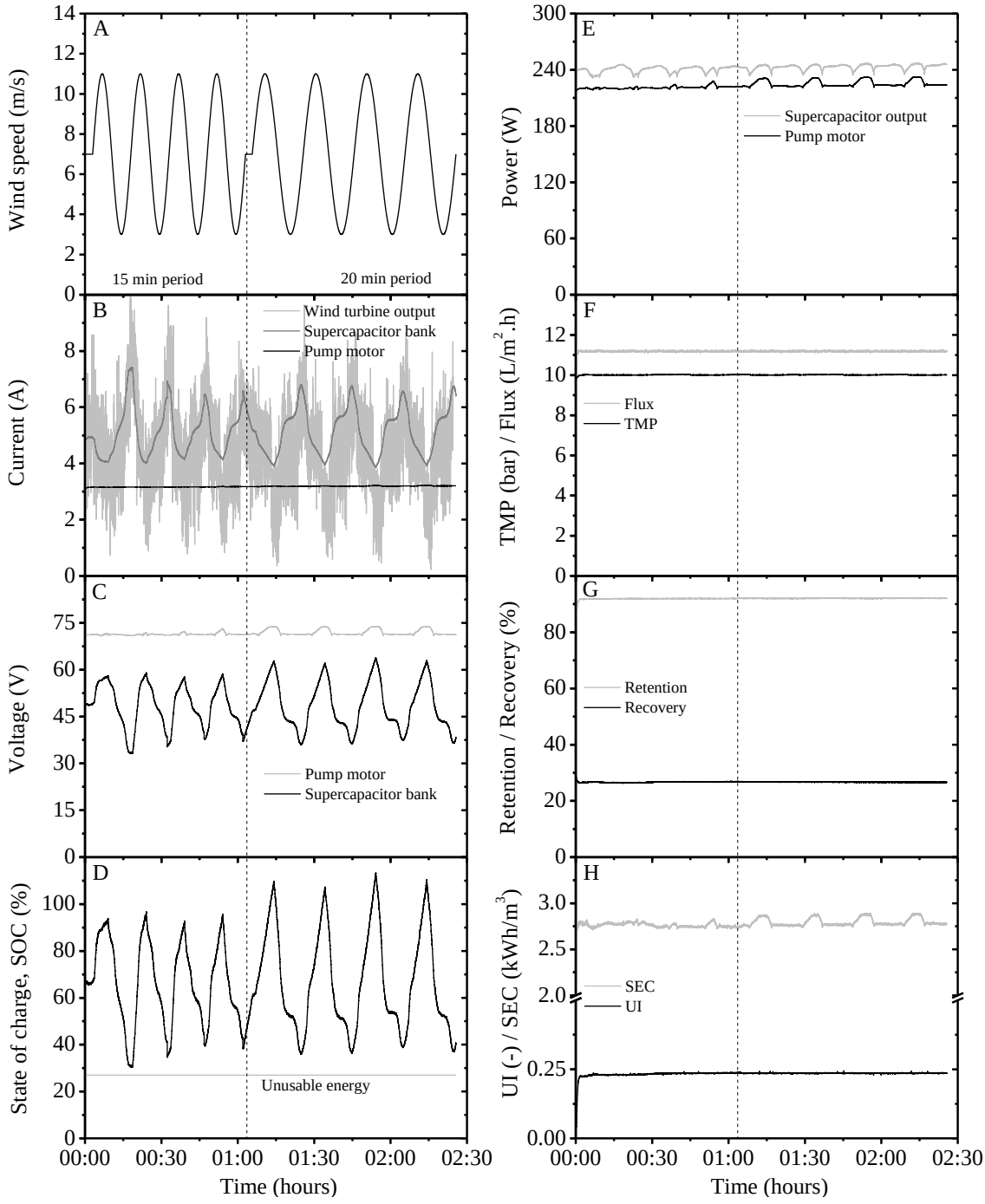

Figure 6.6: Wind-membrane system performance using 4x1 supercapacitor bank under oscillating wind speed fluctuations (average 7 m/s) with periods 15 and 20 min and feed water concentration 5500 mg/L.

When compared to the directly-driven system without energy storage (Section 4.2), the use of supercapacitors to buffer these wind fluctuations (Figure 6.6) with a 1 min period of oscillation resulted in an 85 % increase in average flux and 40 % improvement in the quality of permeate produced over 10 min. This was a result of the improved power

quality supplied to the membrane system as a result of the supercapacitors buffering the fluctuations and providing constant power. Note that turbulent wind speed fluctuations most commonly occur with a 1 min period of oscillation [67], which highlights the effectiveness of using supercapacitors for this purpose. The use of supercapacitors enabled the membrane system to produce permeate with retention ≥ 89 % at any wind speed where the SOC of the supercapacitor bank was above the unusable limit (27 %), compared to wind speeds of ~ 9 m/s required without energy storage. However wind speeds of >7 m/s were required for charging of the supercapacitor bank, therefore lower wind speeds were not sufficient for operating the system for more than ~ 5 min (Figure 6.4). While the smallest supercapacitor bank was adequate for absorbing the whole range of short term wind fluctuations over the operating range of this system, increasing the size of supercapacitor storage would provide power for longer periods of intermittency. This would be a trade-off between the benefits of increasing the storage time versus the added cost of supercapacitor capacity and would depend on the particular system and wind resource.

As the above results have demonstrated, the use of supercapacitors to buffer intermittency and fluctuations could reduce the power fluctuations experienced by the pump motor and the pressure and flowrate fluctuations experienced by the membrane. This would certainly decrease the mechanical stresses on these components, and may help to extend their lifetime. However, as described previously in Chapter 4 and Chapter 5, there is little to no data available on the impact of fluctuations or intermittency on the lifetime of components. This would require long-term testing of these systems with data logging and detailed analysis of the results. As most research projects and pilot tests are relatively short-term, on the order of a few months to years, this important information is generally overlooked.

The robustness of the various components of the wind-membrane system and the ability to provide relatively long-term operation with straightforward or minimal maintenance would be necessary to make these systems affordable and effective in remote communities [7, 58]. The robustness of small-scale wind turbines is certainly a concern, with some wind turbines failing after less than a year as highlighted in Section 1.3. However, it is hoped that the new MCS accreditation scheme launched in 2010 will help to improve the reliability issues in the design and manufacture of small wind

turbines [70]. The expected operational lifetime of the FuturEnergy wind turbine used for this work is unknown. The expected operational lifetime for larger wind turbines is 20 years, with the first wind farms installed in the UK now achieving this target [198]. According to the FuturEnergy manufacturer, the design is based on 2 years of testing in Warwickshire and the Scottish highlands, which may be linked to the 2 year guarantee provided against defective parts or workmanship [171]. The manufacturer recommends that an annual inspection of the blades, bolts and electrical connections be made to check for any damage or loose fittings. In addition, grease should be applied to the hinge mechanism required for furling. Assuming there are no problems with the blades or the permanent magnet generator, these maintenance requirements should be relatively straightforward to carry out.

The expected operational lifetime for the pump motor and the membrane modules subject to fluctuations and intermittency are also unknown. The study on solar PV-powered pumping systems described in Section 1.4.2 showed that a progressive cavity pump operated continuously for 3 years without any maintenance or deterioration in performance, however diaphragm pumps failed after only 1 – 2 years without maintenance [80]. Expected operational lifetimes for the membranes on stand-alone systems range from 1 – 3 years [30, 58, 111], however none of these predictions are based on long-term studies. The membrane manufacturer quotes an operational lifetime of 1 – 2 years for membranes operated at low recovery (< 30 %) with preventative cleaning by regular flushing of the membranes using the regulating valve on the concentrate stream [49]. The membranes in large-scale brackish water RO plants typically have an operational lifetime of 5 – 7 years, with the longest lifetimes in systems with lower feed water concentrations due to less fouling and lower pressure operation [29]. Therefore, the issue of robustness of components in the wind-membrane system is still relatively unknown, and longer-term studies are required to determine the feasibility of these systems in remote locations.

6.4 Conclusions

The suitability of supercapacitors to expand the safe operating window of the wind-membrane system was examined in a systematic manner. The supercapacitors were able to provide sufficient energy during periods of no wind (intermittency) and enhance the

power quality delivered to the membrane by absorbing turbulent wind (fluctuations). As a result, system shut-down and compromised permeate quality due to reduced TMP were avoided. The use of supercapacitors to provide constant power resulted in a 40 % increase in the average flux and 15 % increase in permeate quality under intermittent operation over one hour. The improvements in the average flux and permeate quality under fluctuating conditions due to increased power quality were 85 % and 40 %, respectively. While the SOC of the supercapacitor bank was above the minimum threshold value of 27 %, the membrane system operated as under steady-state conditions regardless of the wind speed and power output from the wind turbine. Once the threshold SOC was reached then the supercapacitors were no longer providing power and the membrane system either shut down or was directly subjected to the wind speed fluctuations from the wind turbine.

Wind speeds of >7 m/s were required to provide a net surplus of energy and increase the SOC of the supercapacitor banks when the membrane system was operating, otherwise the energy was gradually discharged. The length of run-time provided by the supercapacitors during intermittent periods was dependent upon the size and therefore the capacitance of the supercapacitor bank. The maximum period of intermittency that could be buffered was 4 min by the largest bank. More storage could be provided by adding further rows in parallel, but this would not be the optimum use for supercapacitors as they are a cheap and efficient source of power but an expensive source of energy. The supercapacitors were very effective at absorbing oscillations over a wide range (15 s – 20 min) and are therefore considered to be ideal for integration into membrane systems powered by renewable energies for reducing the number of system re-starts and providing higher average water quality and quantity.

The following chapter examines the effect of real wind speed data on the wind-membrane system performance with and without supercapacitors and the overall improvements in water quality and quantity. Testing under actual wind conditions is necessary to establish the optimum operating strategy and the most suitable size of supercapacitor bank for this system. This is also the best way to determine the effectiveness of supercapacitors at improving the short-term performance of the wind-membrane system.

Chapter 7

Wind-membrane system optimisation

Detailed knowledge of the safe operating window and the key constraints to safe operation are essential to optimise the performance of RE-membrane systems for operation with fluctuating and intermittent power. By mapping out the performance of the membrane system over the whole operating range in terms of power and pressure (using the regulating valve on the concentrate stream), the safe operating window for several membrane modules and feed water concentrations was determined. This provided a basis for examining the different operating strategies that could be used to maximise the short-term performance of the membrane system within the safe operating window. Operation at constant recovery was found to be the optimum operating strategy in terms of productivity and energy consumption. To conclude the research on the wind-membrane system and provide a basis for comparison with existing systems and future development, the performance was tested over 24 hours using real wind speed data. The experiments were performed with and without the use of supercapacitors to determine their ability to improve the performance of the wind-membrane system under real wind conditions.

7.1 Determining the safe operating window

7.1.1 Performance variation with membrane system set-point

The purpose of this research was to determine the safe operating window for the directly-driven wind-membrane system to optimise its performance with fluctuating and

intermittent power. Because of the transient nature of the wind resource and the lack of any energy storage device, directly-connected RE-membrane systems are required to operate over a wide power range. In order to optimise their performance, the hydraulic inputs in terms of feed pressure and flowrate need to be controlled to optimise the performance of the membrane system according to the available power over the whole power range. By mapping out the safe operating window and determining the main constraints to safe operation (both physical and performance based), the best method for operating the membrane system can be determined. The concept of the safe operating window was first described mathematically by Feron [96] in the 1980s for transient operation of RO plants with wind power, as detailed in Section 1.6.2. However, apart from a recent modelling analysis by Pohl *et al.* [97], there has been very little investigation of this concept and it has never been examined experimentally. The rigorous analysis used to optimise the performance of this wind-membrane system could be applied to the design and performance of future RE-membrane systems.

To determine what a safe operating window actually entails and what the defining constraints are requires knowledge of all of the possible operating scenarios for the membrane system. This is because the power input from the renewable energy generator could vary over the whole operating range with fluctuations and intermittency as shown in Chapter 4 and Chapter 5. As the inputs to the membrane system are in terms of feed pressure and flowrate (hydraulic power), these input parameters and the corresponding performance outputs must be determined. The performance of the membrane system is measured in terms of productivity (flux and recovery) and desalination efficiency (retention and energy requirements). Therefore, analysis of the safe operating window requires these performance parameters to be mapped out according to each combination of feed pressure and flowrate. The performance of the membrane system, and therefore the operating window, will of course depend on the specific membrane module and characteristics of the feed water in terms of concentration and temperature.

A systematic experimental procedure was designed to map out the whole operating range of the wind-membrane system in terms of the key input parameters of power, feed pressure and feed flowrate. The input power was varied over the whole operating range for each experiment using the step function methodology described in Section 2.5.1 and used previously in Chapter 3. This step function experiment was performed over the

whole range of feed pressures and flowrates by adjusting the set-point pressure according to the regulating valve on the concentrate stream at the start of each experiment as described in Section 2.1.7. Note that all of the work in the previous chapters utilised a constant set-point pressure of 10 bar at 240 W input power which gave a corresponding feed flowrate of 250 L/h. The use of a constant set-point was necessary to investigate the impact of fluctuations and intermittency by providing constant conditions for comparison of the results. For the following experiments, step function experiments were carried out with variables of i) increasing power from 45 W to 280 W (10 steps) and ii) regulating valve set-point pressure from 4 to 12 bar (or within the maximum bounds of operation). Conditions were held constant for 20 min at each level of power to achieve steady state conditions. These results were then used to determine the whole operating range of the wind membrane system according to the TMP in Figure 7.1 – Figure 7.5. Based on this operating range, the safe operating window was determined (Figure 7.6 – Figure 7.9) according to the performance constraints (flux, retention and recovery) and the physical constraints of the membrane module (pressure and flowrate).

The following combinations of membrane module and feed water concentration were examined:

i. BW30-4040 module with feed concentration 5500 mg/L NaCl;
ii. BW30-4040 module with feed concentration 10,000 mg/L NaCl;
iii. aged BW30-4040 module with feed concentration 5500 mg/L NaCl;
iv. NF90-4040 module with feed concentration 5500 mg/L NaCl; and
v. NF90-4040 module with feed concentration 2750 mg/L NaCl.

In small-scale membrane systems it is common to use one or two membrane modules to provide the necessary water demand. As these are generally sited in remote areas, regular maintenance of membrane modules can be difficult, especially if it involves the use of chemicals. For these reasons, it is common to use preventative membrane cleaning on these small-scale plants by using a low recovery (< 30 %) to prevent membrane scaling and the need to used scaling inhibitors [49]. Excessive recovery (> 30 %) can cause the build-up of high concentrations of salt in the boundary layer and increased osmotic pressure which reduces the net driving pressure across the membrane, thereby reducing flux and increasing the diffusion of salt. In addition, the high

concentration of solutes increases the risk of scaling in feed waters with sparingly soluble salts (Section 1.2.3). The maximum recovery to avoid scaling depends on the concentration of sparingly soluble salts as well as the temperature and pH of the water. Although there were no sparingly soluble salts in the NaCl solution used for these experiments, the maximum recommended recovery of 30 % was used to represent the wind-membrane system operating with real brackish feed water. Although this is essentially an arbitrary value that depends entirely on the feed water characteristics, it provides a basis for comparison and discussion of the results.

The steady-state performance characteristics resulting from the step function input power experiments were mapped out for each membrane module and feed water concentration as a function of TMP as shown in Figure 7.1 – Figure 7.5. These results were then used to compile the safe operating windows in Figure 7.6 – Figure 7.9. The results from the BW30 membrane module with a feed water concentration of 5500 mg/L (Figure 7.1) are used to explain the important trends; thereafter the differences resulting from changing the membrane module and feed water concentration are described in Figure 7.2 – Figure 7.5.

The feed flowrate increased linearly with the TMP (Figure 7.1A) due to increasing pump motor power, as the power was proportional to the square of the TMP. Each line in Figure 7.1A shows the variation of TMP and feed flowrate over the whole operating range by varying the power from 45 W to 280 W. The set-point pressures are given at 240 W as described in Section 2.1.7. Increasing the set-point pressure of the regulating valve resulted in reduced feed flowrate and increased pressure. This was because the positive displacement pump could not maintain high flowrates at high operating pressures. There was a trade-off to be made between voltage and current which were proportional to flowrate and pressure, respectively. When the pumping load (required pressure) increased due to the restriction of the regulating valve, the pump drew more current at constant power, therefore resulting in reduced voltage (flowrate). This had important implications for the operation of the membrane system that are detailed below.

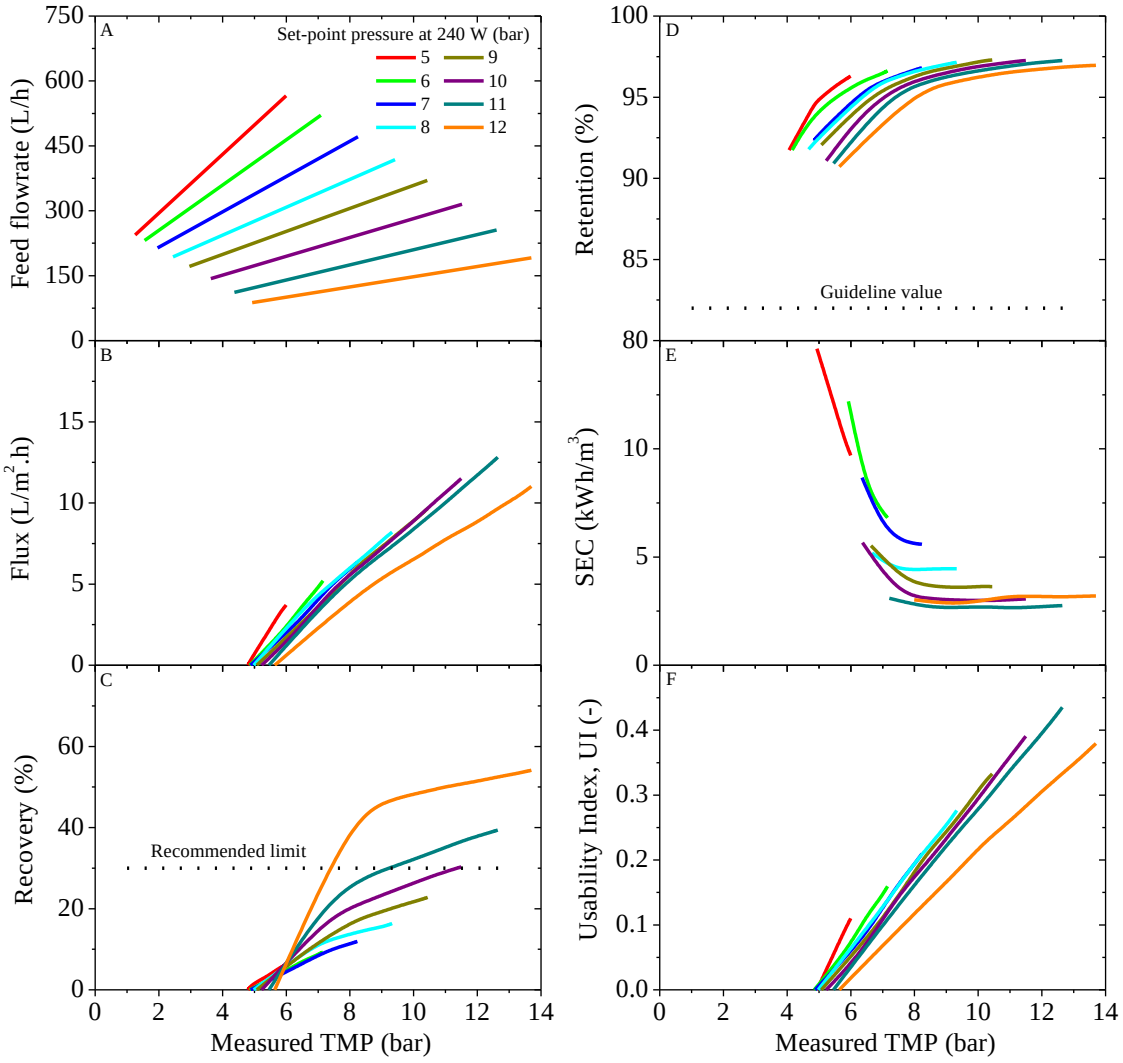

Figure 7.1: Steady-state performance of membrane system mapped out over whole operating range according to position of regulating valve on concentrate stream using BW30-4040 module with feed water concentration 5500 mg/L NaCl.

The flux (Figure 7.1B) increased linearly according to the TMP with some concentration polarisation occurring at high TMP for set-point pressures of 11 and 12 bar, shown by the departure from the linear relationship. Apart from the 12 bar set-point pressure, the maximum flux for each set-point line (Figure 7.1B) was limited by the maximum TMP achieved (Figure 7.1A). For example, at 5 bar set-point pressure, the maximum flux was 3.7 L/m^2.h due to the low TMP of 6 bar, which was not sufficient to produce much flux compared to the 4.4 bar bulk osmotic pressure of the feed water. The highest flux of 12.8 L/m^2.h occurred with the 11 bar set-point pressure at a TMP of 12.6 bar. However, this flux was achieved at recovery of 40 %, and

concentration polarisation started occurring at recovery > 30 % (Figure 7.1C). The 10 bar set-point line yielded the second highest flux of 11.5 L/m^2.h at TMP of 11.5 bar, which was produced with recovery of 30 %. Therefore, this could be a better set-point pressure at which to operate the system.

Concentration polarisation occurred with set-point pressures of 11 and 12 bar due to the combination of high TMP and low feed flowrate, causing increased concentration of salts in the boundary layer and reduced tangential flow across the membrane. This was directly linked to the operating characteristics of the progressive cavity pump as described above, where operating pressure is gained at the expense of feed flowrate. The concentration polarisation occurred for the 11 and 12 bar set-point lines at high recovery of > 30 % as shown in Figure 7.1C. The methodology for calculating the concentration polarisation modulus (β) is given in Section 2.1.6. By following this technique, the maximum β modulus was calculated as 1.9, 2.1 and 2.5 for the 10, 11 and 12 bar set-point lines, respectively. This highlights the significant increase in the β modulus by increasing the set-point pressure above 10 bar. The flux for the 12 bar set-point line decreased significantly compared to the 11 bar set-point, as the regulating valve was almost completely closed and the pump was approaching its limit in terms of the maximum discharge pressure of 15 bar (Table 2.2). The impact of high recovery on performance was particularly noticeable with the BW30 membrane module compared to the others tested, as it had the highest retention (Figure 7.1D), which resulted in the highest concentrate concentration, and therefore more osmotic pressure build-up in the boundary layer.

The retention (Figure 7.1D) of NaCl was sufficient to be within the WHO guideline value over the whole operating range and increased with TMP to an upper limit of 97.3 % achieved by the 9, 10 and 11 bar set-point pressure lines. The impact of concentration polarisation was seen again by the reduction in the maximum retention to 97 % in the 12 bar set-point pressure line (Figure 7.1D), which was the same maximum retention achieved with the 7 bar set-point line. The SEC (Figure 7.1E) decreased with increasing TMP to a minimum value of 2.6 kWh/m^3 with the 11 bar set-point pressure line at TMP of 8.4 bar, feed flowrate of 155 L/h and recovery of 28 %. Higher pressure resulted in increased SEC up to 2.8 kWh/m^3 at the maximum TMP of 12.6 bar due to the reduced flux caused by concentration polarisation. The 10 bar set-point line yielded

the second best performance in terms of SEC, achieving a minimum of 3 kWh/m^3 at a TMP of 8.5 bar, and remaining at this value at increased pressure. The 12 bar set-point line caused reduced SEC compared to the 10 and 11 bar set-point lines over the majority of the operating range, further highlighting the reduced performance at this combination of high pressure and low feed flowrate.

Although the 11 bar set-point line yielded the best overall performance in terms of the UI (Figure 7.1F), the set-point pressure of 10 bar provided the highest UI within the recommended recovery limit of 30 % (Figure 7.1C) and did not show reduced performance due to concentration polarisation. Therefore, this would be the optimum set-point for the membrane system to maximise the performance within the guideline limitations with this particular membrane and feed water. Figure 7.1F also demonstrates the effect of high recovery on the performance of the membrane system as shown by poor overall performance with the 12 bar set-point.

By increasing the feed water concentration from 5500 mg/L NaCl in Figure 7.1 to 10,000 mg/L in Figure 7.2, the bulk osmotic pressure of the feed water increased from 4.4 bar to 8 bar. This resulted in a smaller operating range for the BW30 module due to the minimum TMP required to produce flux. This is demonstrated by the minimum set-point pressure line of 7 bar (Figure 7.2A) compared to 5 bar in Figure 7.1A. As would be expected, the higher osmotic pressure resulted in poorer operational performance. The maximum flux of 10.1 L/m^2.h was achieved with a set-point pressure of 12 bar, however there were no visible effects of concentration polarisation due to the relatively low recovery (Figure 7.2C) compared to the values in Figure 7.1C. The maximum retention of 97 % was achieved by the 11 bar set-point pressure line at TMP of 12.6 bar and feed flowrate of 256 L/h. However, the minimum SEC with the 11 bar set-point line was 4.6 kWh/m^3 which was higher than the minimum of 3.8 kWh/m^3 achieved with the 12 bar set-point line. This demonstrates that higher feed flowrates are necessary to optimise the retention, while higher TMP at the expense of feed flowrate is required to optimise the flux and SEC. However, optimising the flux and SEC is done at the risk of higher recovery (35 – 40 % compared to 20 – 25 %), which could increase the risk of scaling, and would need to be managed according to the feed water characteristics.

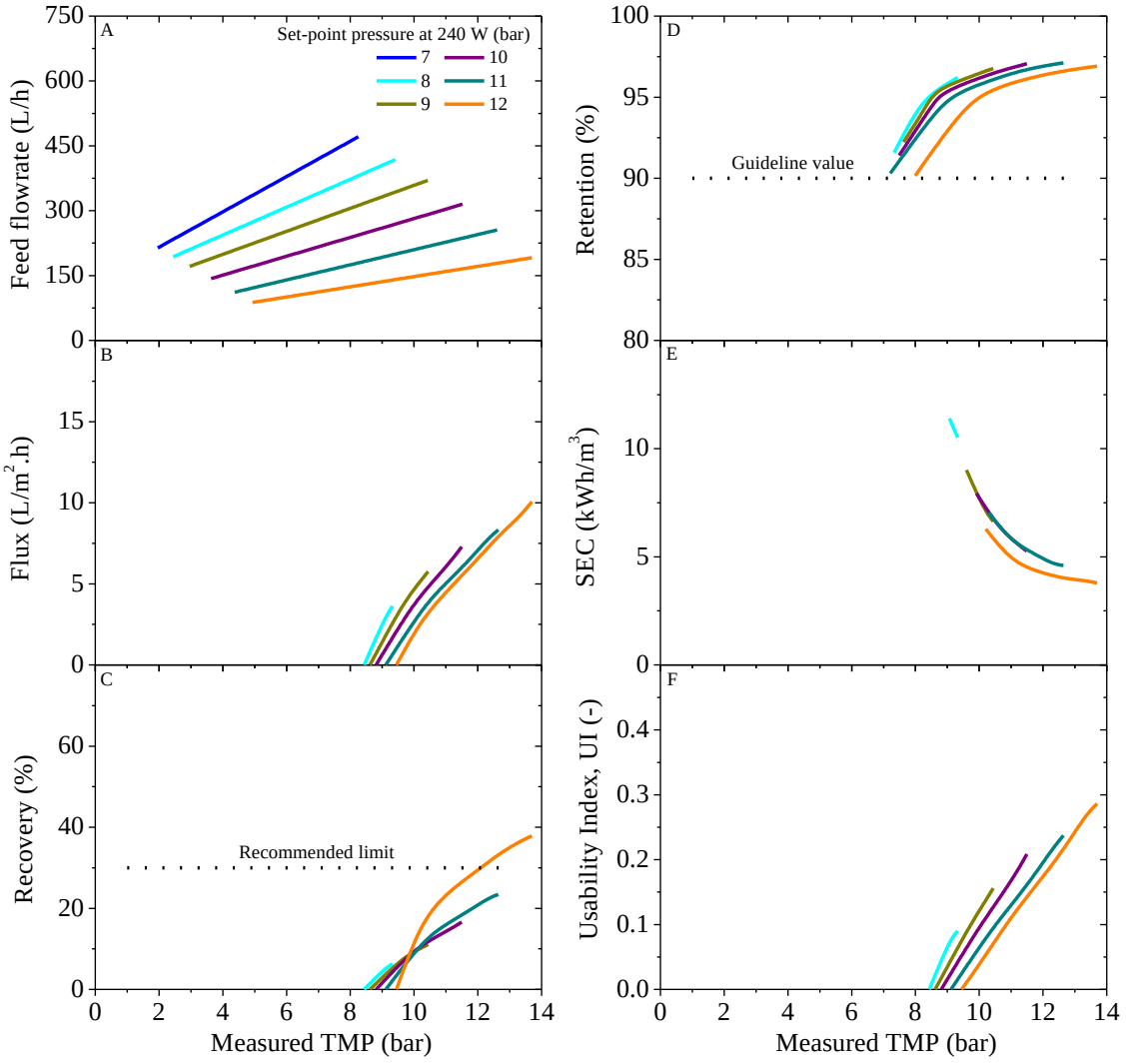

Figure 7.2: Steady-state performance of membrane system mapped out over whole operating range according to position of regulating valve on concentrate stream using the BW30-4040 module with feed water concentration of 10,000 mg/L NaCl.

The aged BW30 module had a wider operating range (Figure 7.3A) with the 5500 mg/L NaCl feed water than the new BW30 module (Figure 7.1A). This is shown by the 4 bar set-point pressure line (Figure 7.3A) that was possible with the aged BW30 due to lower osmotic pressure and resistance to flow. The maximum flux (Figure 7.3B) of 15.4 L/m^2.h, achieved with the 10 bar set-point pressure line, was 20 % higher than the flux achieved with the new module (Figure 7.1B). The maximum retention of 92.8 % (Figure 7.3D) achieved with the 7 and 8 bar set-point pressure lines was significantly lower than the retention of 97.3 % achieved with the new module, however the minimum SEC of 2.4 kWh/m^3 was 23 % lower.

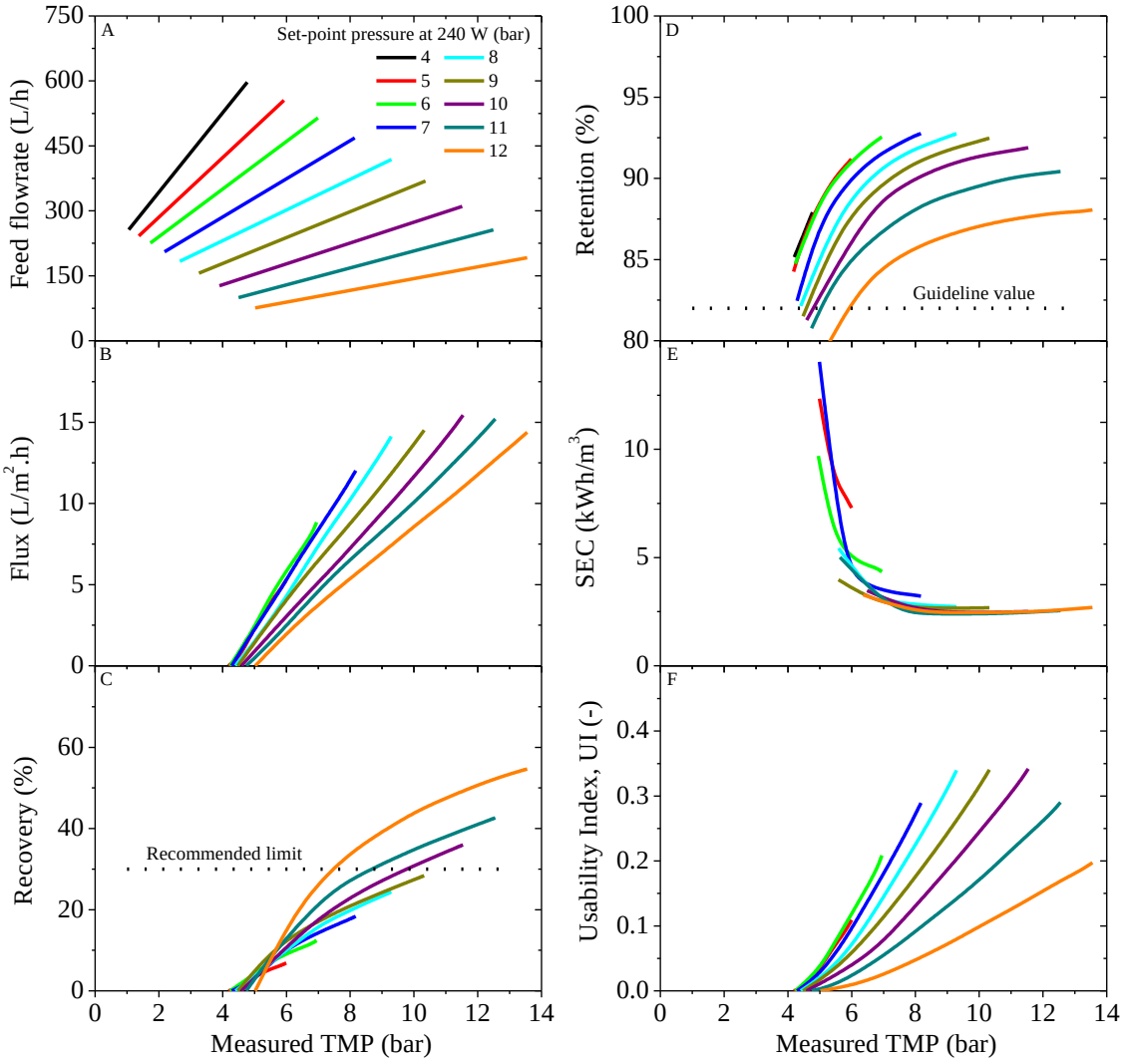

Figure 7.3: Steady-state performance of membrane system mapped out over whole operating range according to position of regulating valve on concentrate stream using the aged BW30-4040 module with feed water concentration of 5500 mg/L NaCl.

The productivity of the NF90 membrane module (Figure 7.4) was significantly higher than with the BW30 (Figure 7.1) for the same feed water concentration (5500 mg/L NaCl). This is shown by the maximum flux of 21.6 L/m^2.h (Figure 7.4B) achieved with the 9 bar set-point pressure line, compared to 12.8 L/m^2.h with the BW30 module (Figure 7.1B). The maximum recovery reached 58 % (Figure 7.4C) due to the higher productivity of the NF90 module. The maximum retention of 94.2 % (Figure 7.4D) was achieved with a set-point pressure of 7 bar, highlighting the lower operating pressure range required for this membrane. The minimum SEC of 1.6 kWh/m^3 (Figure 7.4E), was significantly lower than 2.6 kWh/m^3 with the BW30.

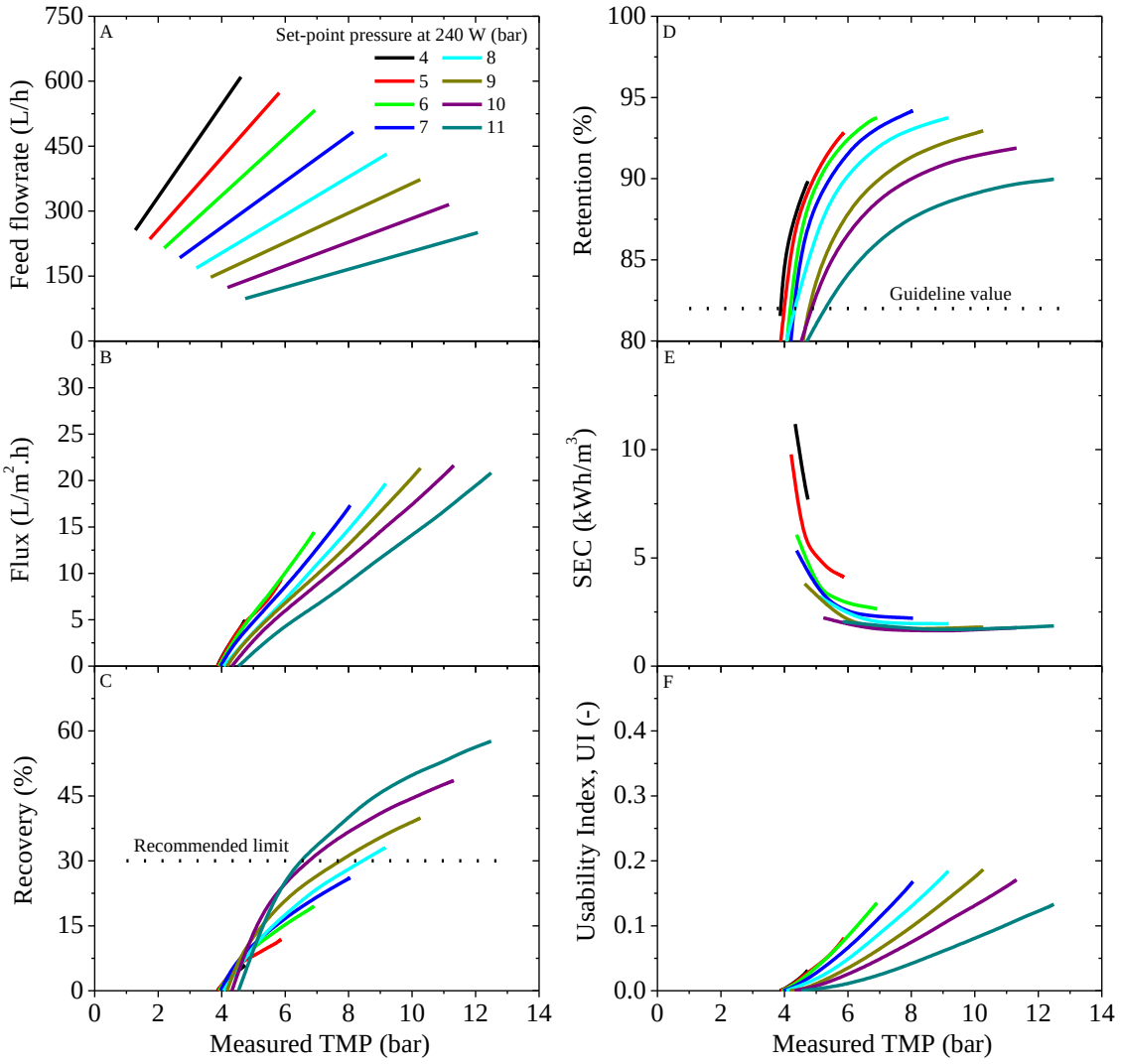

Figure 7.4: Steady-state performance of membrane system mapped out over whole operating range according to position of regulating valve on concentrate stream using the NF90-4040 module with feed water concentration of 5500 mg/L NaCl.

As would be expected, the productivity of the NF90 increased significantly by halving the feed water concentration from 5500 mg/L (Figure 7.4) to 2750 mg/L NaCl (Figure 7.5) due to reduced osmotic pressure. The maximum flux of 33 L/m^2.h (Figure 7.5B), achieved with a 9 bar set-point pressure line, was 53 % higher than with the 5500 mg/L NaCl feed water. The lower osmotic pressure of the feed water allowed high recovery up to a maximum of 74 % (Figure 7.5C). The maximum retention of 95.5 % was achieved with the 6 bar set-point pressure line (Figure 7.5D), and the minimum SEC of 0.77 kWh/m^3 with the 10 bar set-point line (Figure 7.5E).

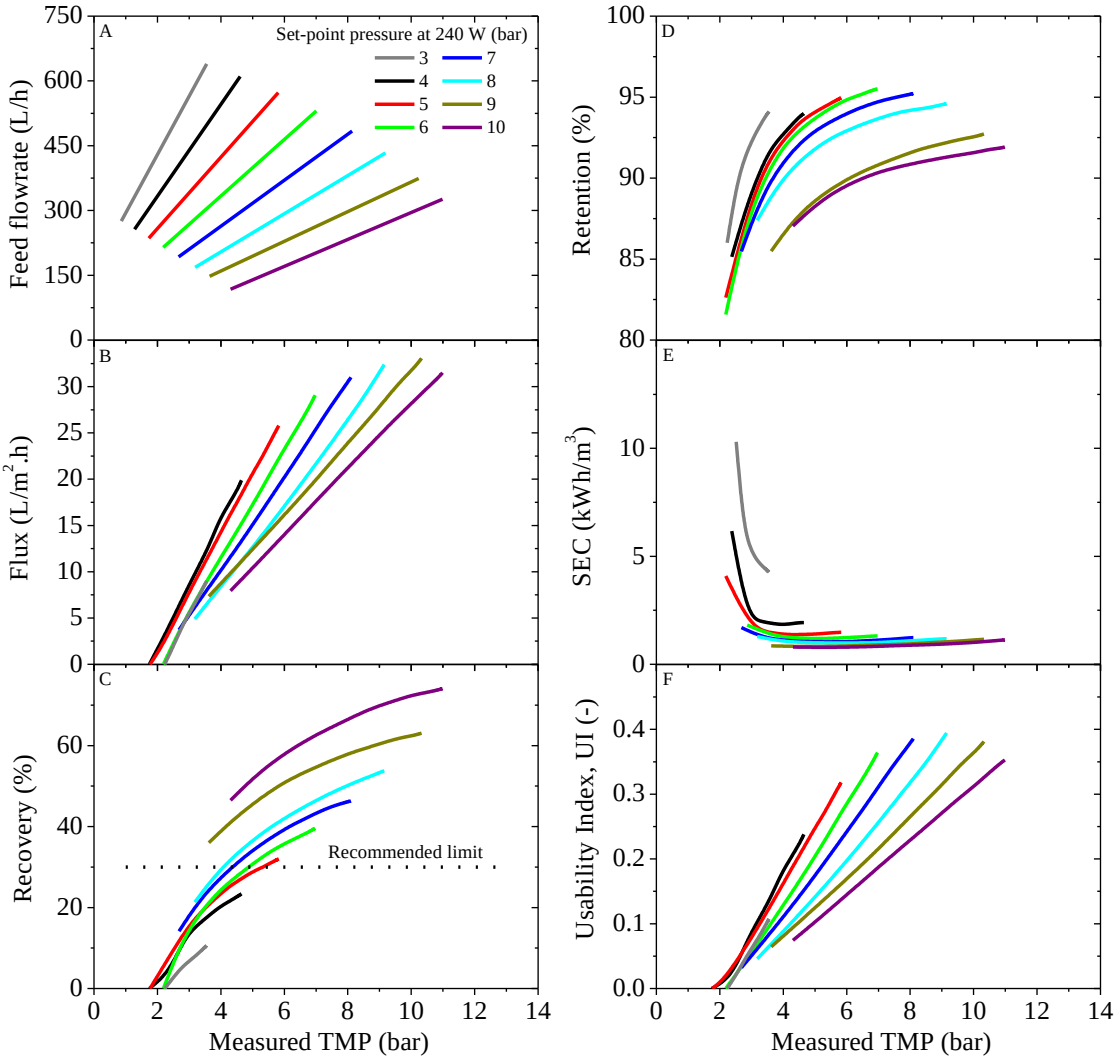

Figure 7.5: Steady-state performance of membrane system mapped out over whole operating range according to position of regulating valve on concentrate stream using the NF90-4040 module with feed water concentration of 2750 mg/L NaCl.

The general trend of the results in Figure 7.1 – Figure 7.5 showed that the maximum flux and minimum SEC were generally achieved under similar conditions of TMP and feed flowrate for each membrane module and feed water concentration. This is highlighted by the fact that the set-point lines that achieved maximum performance in terms of flux and SEC were all in the range 9 – 12 bar. However, the maximum retention was generally achieved at lower TMP and higher feed flowrates with set-point pressure lines of 6 – 9 bar. This highlights the trade-off that needs to be made between maximising the retention versus operating at higher flux and SEC with slightly lower retention. Undoubtedly, this decision would depend on the feed water characteristics.

7.1.2 Safe operating window according to membrane and feed water

The data shown in Figure 7.1 – Figure 7.5 was used to determine the safe operating window for each membrane and feed water concentration. The operating window for the BW30 membrane module with feed water concentration of 5500 mg/L NaCl was mapped out as shown in Figure 7.6 in terms of TMP and feed flowrate as these are the two variable parameters that define the operating characteristics of the membrane system. The main objective was to determine the main constraints for the safe operating window (Figure 7.6) and the effects of varying the feed water concentration and membrane module (Figure 7.7 – Figure 7.10). The safe operating window was then used to optimise the performance of the wind-membrane system and to determine the optimum operating strategy for operation with fluctuating and intermittent energy, as shown in Section 7.2.3.

The methodology for determining the safe operating window shown in Figure 7.6 could be used for optimising the performance of any RE-membrane system, and was carried out as follows:

i. Experiments were performed to map out the whole operating range of the wind-membrane system in terms of the key input parameters of power, feed pressure and feed flowrate as described above and shown in Figure 7.1.
ii. The operating range of the membrane system was plotted according to the input parameters of TMP and feed flowrate (shown in Figure 7.1A) to form the basis of the safe operating window in Figure 7.6. The most straightforward method of plotting the operating window was to use the lines of constant set-point to relate the TMP to the feed flowrate, providing a platform to plot other lines on top.
iii. Lines corresponding to the limitations of the pump power on the TMP and feed flowrate range were plotted onto the operating window in Figure 7.6.

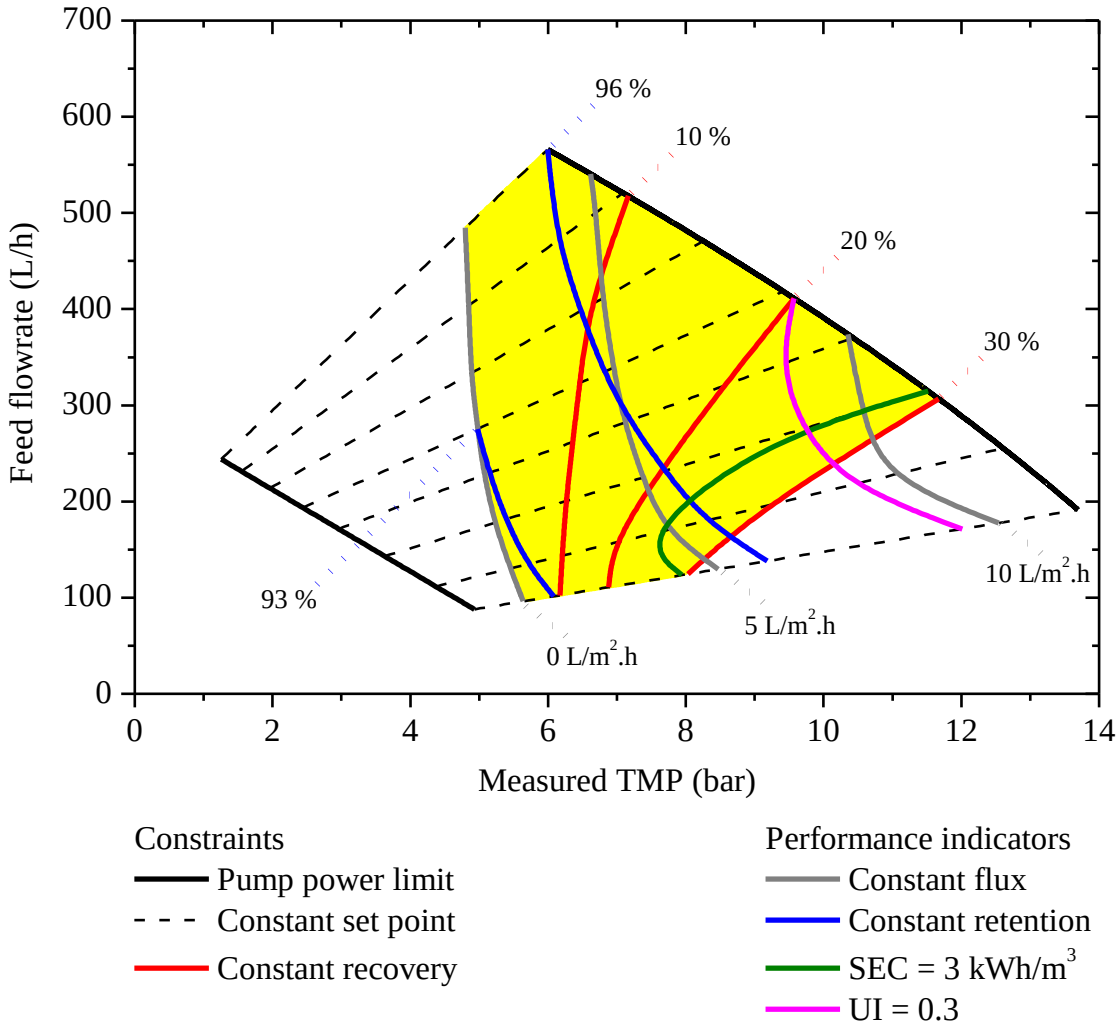

Figure 7.6: Safe operating window for the membrane system (shaded in yellow) using BW30-4040 module with feed water concentration of 5500 mg/L NaCl showing constraints to safe operation and performance indicators. The experimental data used to construct the safe operating window is shown in Figure 7.1.

iv. Based on the relationship of the recovery to the TMP and set-point pressure in Figure 7.1C, lines of constant recovery were added to Figure 7.6. For example, to plot the 30 % recovery line, the 10, 11 and 12 bar set-point lines in Figure 7.1C were used to find the TMP at 30 % recovery. This was then plotted onto the safe operating window using the TMP and corresponding set-point line.

v. The relationships of flux, retention, SEC and UI to TMP and set-point pressure were used to add constant lines to the safe operating window as described above for the recovery.

vi. The boundaries of the safe operating window in terms of pump power, zero flux, 30 % recovery and the maximum and minimum set-point pressure lines were used to determine the safe operating window shaded in yellow (Figure 7.6).

The main aim of determining the safe operating window was to highlight the physical constraints to the safe operation of the membrane system. The knowledge of these constraints and how they impact on performance are useful for designing effective control systems and ensuring efficient operation of RE-membrane systems. The constraints to the safe operating window, as illustrated in Figure 7.6, were as follows:

i. Pump power: limited both the maximum and minimum values of TMP and feed flowrate achievable. The type of pump also determines the relationship between the TMP and the feed flowrate as shown by the constant set-point lines in Figure 7.6. This is the same relationship used by manufacturers for plotting pump curves, as shown in Figure 2.4. The pump used for this research had a maximum rated power of 300 W and the minimum power required to start the system was 45 W. The operating limits of the pump restricted the range of TMP to 1.4 – 13.7 bar and the feed flowrate to 90 – 570 L/h.

ii. Osmotic pressure: the osmotic pressure that must be overcome by the pump to produce flux depends on the feed water concentration, membrane module and the recovery. Higher feed water concentrations, tighter membrane modules and increased recovery all result in increased osmotic pressure. The minimum TMP required for overcoming the osmotic pressure and producing flux for the BW30 module with feed water of 5500 mg/L NaCl is shown by the zero flux line in Figure 7.6. The impact of increasing the recovery on the osmotic pressure is demonstrated by the increased TMP required to produce flux at low feed flowrates. By increasing the feed water concentration from 5500 mg/L (Figure 7.6) to 10,000 mg/L (Figure 7.7), the minimum TMP required to produce flux also increased from 4.8 bar to 8.4 bar (75 % higher) due to higher osmotic pressure. Furthermore, when the membrane module was changed to the NF90, the minimum TMP required to produce flux was only 3.9 bar (Figure 7.9), a decrease of almost 20 % compared to the BW30 module. This highlights the impact of reduced osmotic pressure when using membranes with increased permeability.

iii. Feed water characteristics: the concentration of the feed water determines the osmotic pressure as well as the minimum retention required to remove the solutes to provide permeate concentrations within the WHO guidelines [12]. This ability to achieve the minimum retention is dependent on the type of membrane module and operating conditions. The retention was not a constraint for the BW30 membrane with the 5500 mg/L NaCl feed water (Figure 7.1). However, for the aged BW30 (Figure 7.8) and NF90 (Figure 7.9), the safe operating window was constrained at low pressure and feed flowrate (high recovery) by the minimum retention (88 %) required to produce permeate within the WHO guidelines [12].

The other constraint caused by the characteristics of the feed water is the potential for scaling due to the presence of sparingly soluble salts (i.e. calcium carbonate, calcium sulphate and silica) [49]. In the case of small-scale systems designed to operate without chemical additions, this limits the maximum recovery to prevent scaling to a recommended value of ≤ 30 % [49]. As shown in Figure 7.6, the maximum recovery restricted the operating window at high pressure and low flowrate. While a recovery limitation of 30 % was an arbitrary value for this synthetic NaCl feed water, it was used to highlight the impact of having a limiting recovery. Although there was little impact of the limiting recovery on the operating windows with the BW30 module (Figure 7.6 and Figure 7.7), when the permeability of the membrane was increased (Figure 7.8 and Figure 7.9), or the feed water concentration decreased (Figure 7.10), the limiting recovery had a significant impact on the safe operating window. The main impact of the limiting recovery was the reduced flux that could be achieved (Figure 7.8 – Figure 7.10) due to unsafe operation at the highest TMP range. In a small-community based system, this would impact the volume and cost of the potable water produced. Therefore, a detailed study of the specific feed water characteristics would be essential before the limiting recovery was determined and implemented.

iv. The mechanical limitations of the membrane: restrict the maximum hydraulic loads (feed pressure and flowrate) due to telescoping and mechanical damage caused by excessive mechanical stresses on the membrane module [49]. Telescoping is the unravelling of the outer layers of the membrane due to excessive feed flowrates resulting in the outer layers extending downstream and potential rupturing of the

membrane. The maximum operating conditions for the BW30 module specified by the manufacturer were feed water pressure of 41 bar, feed flowrate of 3600 L/h and pressure drop of 1 bar [49]. These restrictions were outside the operating window for the small pump used for these experiments and therefore did not need to be included.

Figure 7.6 shows lines that correspond to the operating constraints (pump power limit, recovery limit and constant set-point line relating TMP to flowrate) and lines that correspond to performance (constant flux, constant retention, SEC and UI). The performance lines were included for several reasons: i) to illustrate the impact of TMP and feed flowrate on performance; ii) to show the best operating region within the safe operating window and iii) to allow performance comparison between the different operating windows in Figure 7.6 – Figure 7.10.

Increasing the feed water concentration from 5500 mg/L NaCl (Figure 7.6) to 10,000 mg/L (Figure 7.7) resulted in the safe operating window shifting to higher TMP as a result of the higher osmotic pressure of the feed water. The increased osmotic pressure also reduced the impact of the maximum recovery constraint on the operating window due to lower flux over the operating range. The BW30 module was able to produce water within the WHO guidelines even with the high feed water concentration and low pressure operation. However, the pressure limitations of the pump were shown by the relatively high SEC and low UI caused by low flux, in comparison to the 5500 mg/L NaCl feed water (Figure 7.6).

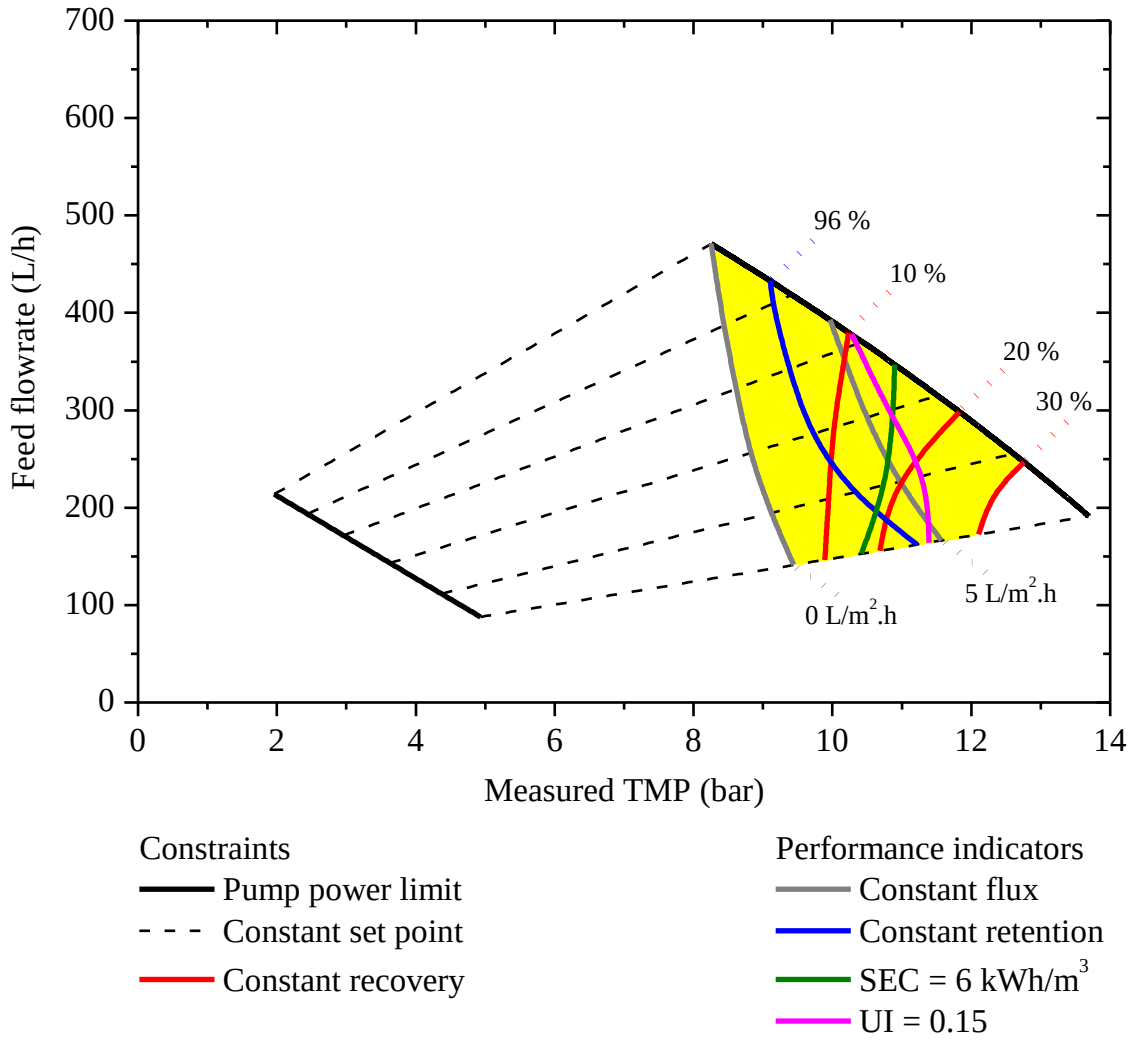

Figure 7.7: Safe operating window for the membrane system (shaded in yellow) using the BW30-4040 module with feed water concentration of 10,000 mg/L NaCl showing constraints to safe operation and performance indicators. The experimental data used to construct the safe operating window is shown in Figure 7.2.

The operating window for the aged BW30 membrane module (Figure 7.8) was restricted by retention at low values of TMP and feed flowrate due to the minimum retention required to achieve the WHO guidelines. Overall, the retention was reduced over the whole operating range compared to the new BW30 (Figure 7.6) with the 5500 mg/L NaCl feed water. The flux of the aged BW30 was slightly higher than the new BW30, which may indicate that there has been some mechanical damage to the membrane module [49]. The increased flux also resulted in higher recovery, SEC and UI over the operating range in comparison to the new BW30 module (Figure 7.6).

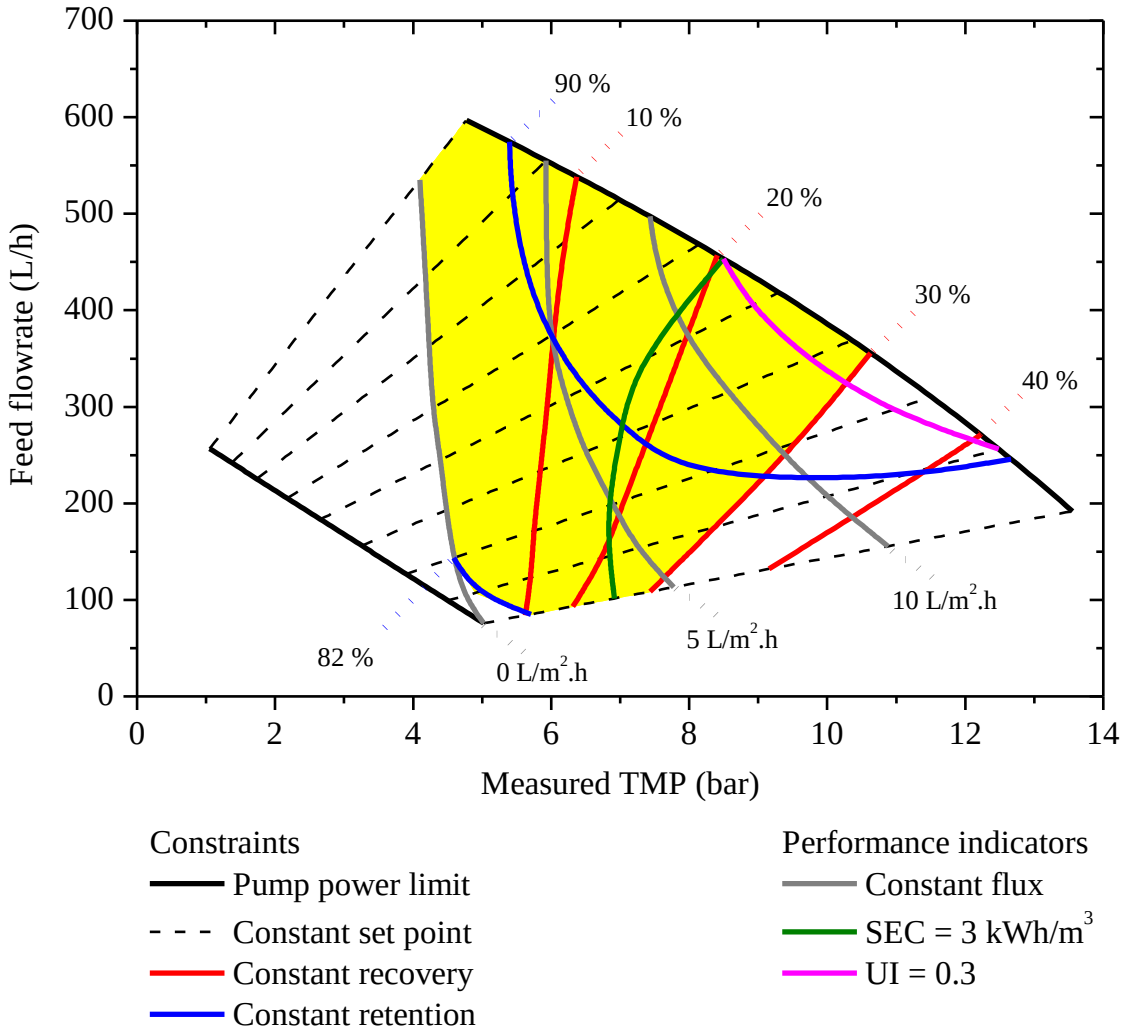

Figure 7.8: Safe operating window for the membrane system (shaded in yellow) using the aged BW30-4040 module with feed water concentration of 5500 mg/L NaCl showing constraints to safe operation and performance indicators. The experimental data used to construct the safe operating window is shown in Figure 7.3.

The operating window for the NF90 membrane module with the 5500 mg/L NaCl feed water (Figure 7.9) was also restricted by the minimum retention (82 %) required to achieve the WHO guidelines. Due to the higher permeability of the NF90 in comparison to the BW30 (Figure 7.6), the operating window was much narrower because of the maximum recovery limitation. The operating limits of the pump in terms of feed flowrate meant that high crossflow velocity could not be maintained at high pressure, resulting in high recovery with the NF90. The NF90 could be used for increased flux and lower SEC than the BW30, as long as the retention at low TMP/flowrate could be controlled or avoided and the high recovery would not cause scaling.

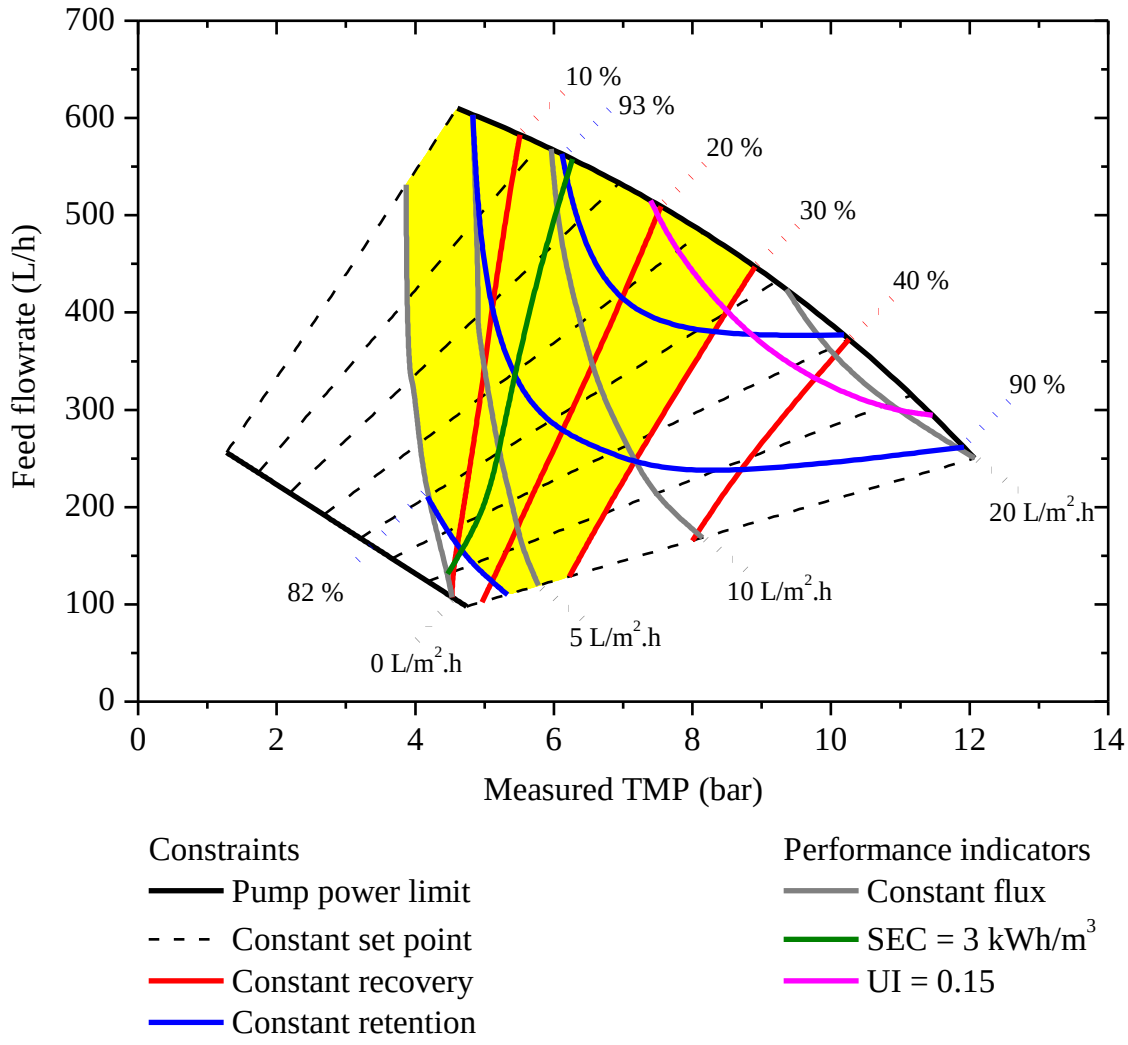

Figure 7.9: Safe operating window for the membrane system (shaded in yellow) using the NF90-4040 module with feed water concentration of 5500 mg/L NaCl showing constraints to safe operation and performance indicators. The experimental data used to construct the safe operating window is shown in Figure 7.4.

The safe operating window for the NF90 membrane module with 2750 mg/L NaCl feed water (Figure 7.10) was much narrower than with the 5500 mg/L feed water (Figure 7.9). This was a result of lower osmotic pressure of the feed water allowing increased flux and therefore recovery. Once again, the maximum flowrate limitation of the pump at increased pressure could not provide the feed flowrate required to obtain low recovery (≤ 30 %) with the NF90 module and the low feed water concentration.

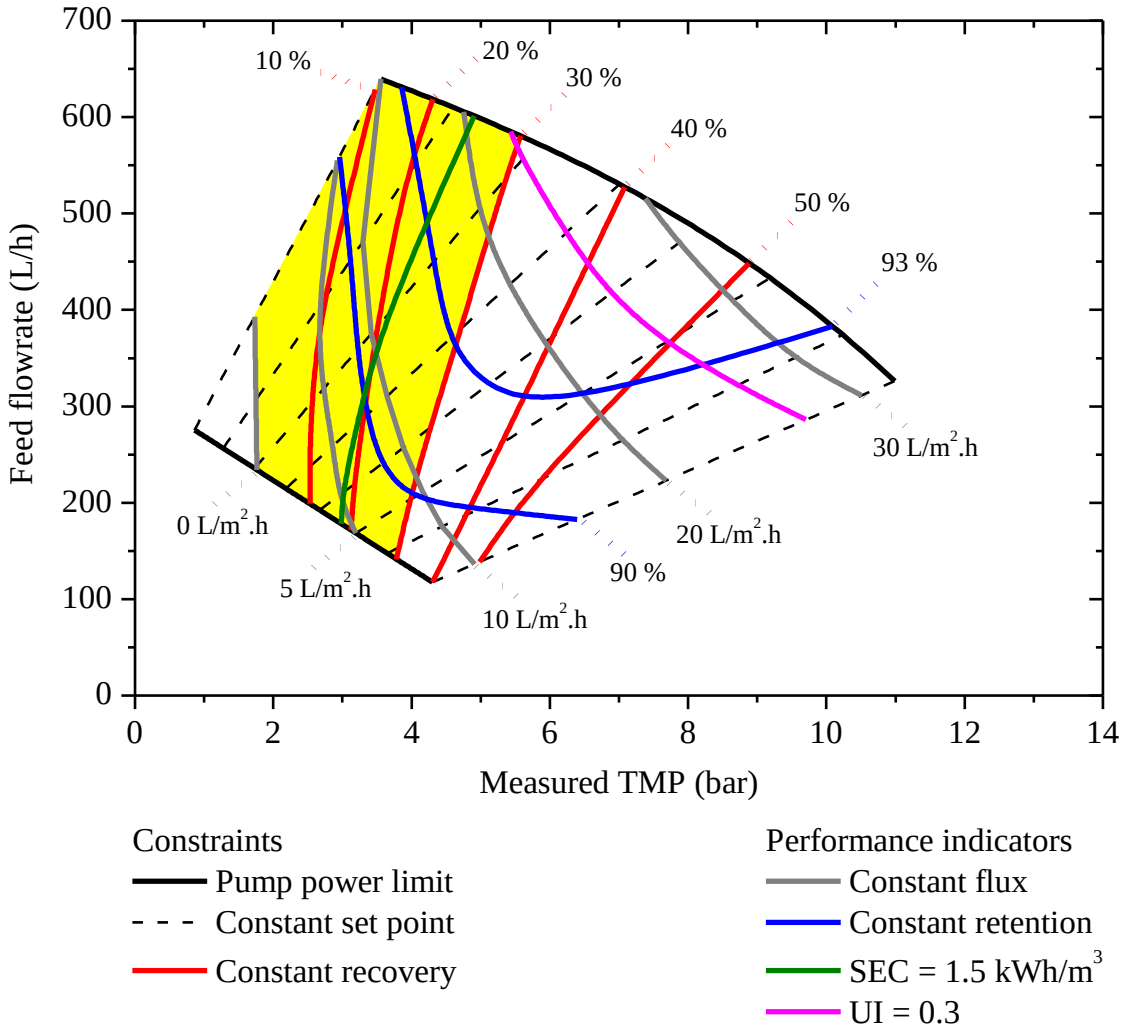

Figure 7.10: Safe operating window for the membrane system (shaded in yellow) using the NF90-4040 module with feed water concentration of 2750 mg/L NaCl showing constraints to safe operation and performance indicators. The experimental data used to construct the safe operating window is shown in Figure 7.5.

As described in Section 1.6.2, the concept of the safe operating window was first proposed by Feron [96]. Since then, Pohl *et al.* [97] performed modelling work using ROSA to investigate the use of four different operating strategies for transient operation within a safe operating window. The results of the safe operating windows in Figure 7.6 – Figure 7.10 were similar to these modelled results, however there were some key differences that require further discussion. The results presented by Feron [96] and Pohl *et al.* [97] were modelled based on the membrane alone, without any consideration of the possible constraints of a pumping system. As shown by the results in Figure 7.6 – Figure 7.10, the choice of pump and the resulting TMP and feed flowrate range can be

the main restrictions for the safe operating window. Even for pumping systems that were sized to provide the maximum range of TMP and feed flowrate provided by the membrane, the wide operating range would certainly impact the efficiency of the pump, as discussed in Section 1.4. Therefore, the SEC would need to be included in any detailed analysis of the safe operating window for a RE-membrane system.

The safe operating windows described previously were determined for large-scale seawater RO systems operating at high pressure (30 – 70 bar) and high feed flowrates (5000 – 10,000 L/h) [96, 97]. By comparison, the wind-membrane system was designed for brackish feed water with low pressure (1.4 – 13.7 bar) and feed flowrates (100 – 600 L/h). The difference in these operating ranges had some interesting effects on the safe operating window. The operational limits of the membrane determined by the mechanical strength limitations would be similar for any membrane system. However, as shown above in Figure 7.6 – Figure 7.10, small-scale systems are often operated at much lower TMP and feed flowrate to reduce the power requirements of the membrane system. Therefore, the pump limitations dictated the outer bounds of the safe operating window rather than the maximum pressure and flowrate restrictions of the membrane.

The safe operating windows for the large-scale systems showed that the operating constraint at low TMP and feed flowrate was due to the maximum allowable permeate concentration to remain within the WHO guidelines [96, 97]. The minimum retention required to remain within the WHO guidelines was a restriction for the aged BW30 (Figure 7.8) and the NF90 (Figure 7.9) membranes with the 5500 mg/L NaCl feed water. However, the retention was only a constraint in these examples at the minimum range of TMP and feed flowrate. The main restriction at low TMP was the minimum osmotic pressure required to produce flux, shown by the zero flux curve (Figure 7.6 – Figure 7.10). This difference is most likely a result of the increase retention of > 97 % required to desalinate seawater to meet the WHO guidelines, compared to > 82 % required to adequately desalinate brackish feed water of 5500 mg/L NaCl. This presents an interesting design challenge for small-scale brackish water systems. Namely, it may be advantageous to use a membrane with higher permeability at the risk of exceeding the retention limitation at low TMP and flowrate. This would allow operation at lower pressure with increased flux and lower SEC, for example the NF90 (Figure 7.9). The membrane system could be controlled so that it does not exceed the minimum retention

by ensuring that the feed flowrate is sufficiently high to avoid operating outside the safe operating window.

7.2 Optimum operating strategy for the membrane system

7.2.1 Optimum set-point operation

To demonstrate the use of the safe operating window, the performance of the wind-membrane system was optimised using the existing operating strategy, defined as constant set-point operation. This name is because the membrane system operates along one of the set-point lines shown in the operating window (Figure 7.6 – Figure 7.10) according to the available power and the position of the regulating valve on the concentrate stream, which is set at the start of operation. To determine the optimum performance first required a clear definition of the desirable performance attributes. The optimum performance was taken to be:

i. operation within the bounds of the safe operating window over the whole range of TMP and feed flowrate; and
ii. production of the maximum flux and minimum SEC within the bounds of the safe operating window.

With the safe operating window already plotted, by optimising the performance according to the maximum flux and minimum SEC within the operating window, the other criteria of adequate retention and recovery limitations have already been accounted for. The most straightforward method of highlighting the optimum set-point line for each combination of membrane module and feed water concentration was to use the UI as shown Figure 7.11. Note that there is no graph included for the aged BW30 membrane with 10,000 mg/L NaCl feed water as it functioned outside the safe operating window over the whole range due to inadequate permeate quality.

The optimum set-point line was found to be a function of the permeability of the membrane and the feed water concentration. With a feed water of 5500 mg/L the BW30 performance was highest within the safe operating window when operated at a set-point of 10 bar (Figure 7.11A). In comparison, the optimum set-point for the aged BW30 and the NF90 was 9 bar 8 bar, respectively. The aged BW30 and NF90 have a lower resistance and therefore higher permeability relative to the BW30, therefore reaching

the maximum recovery at lower TMP and limiting the maximum set-point. However, this did not prevent the system from achieving the maximum UI and demonstrates that these membranes are a good match for the pump with moderate salinity brackish water.

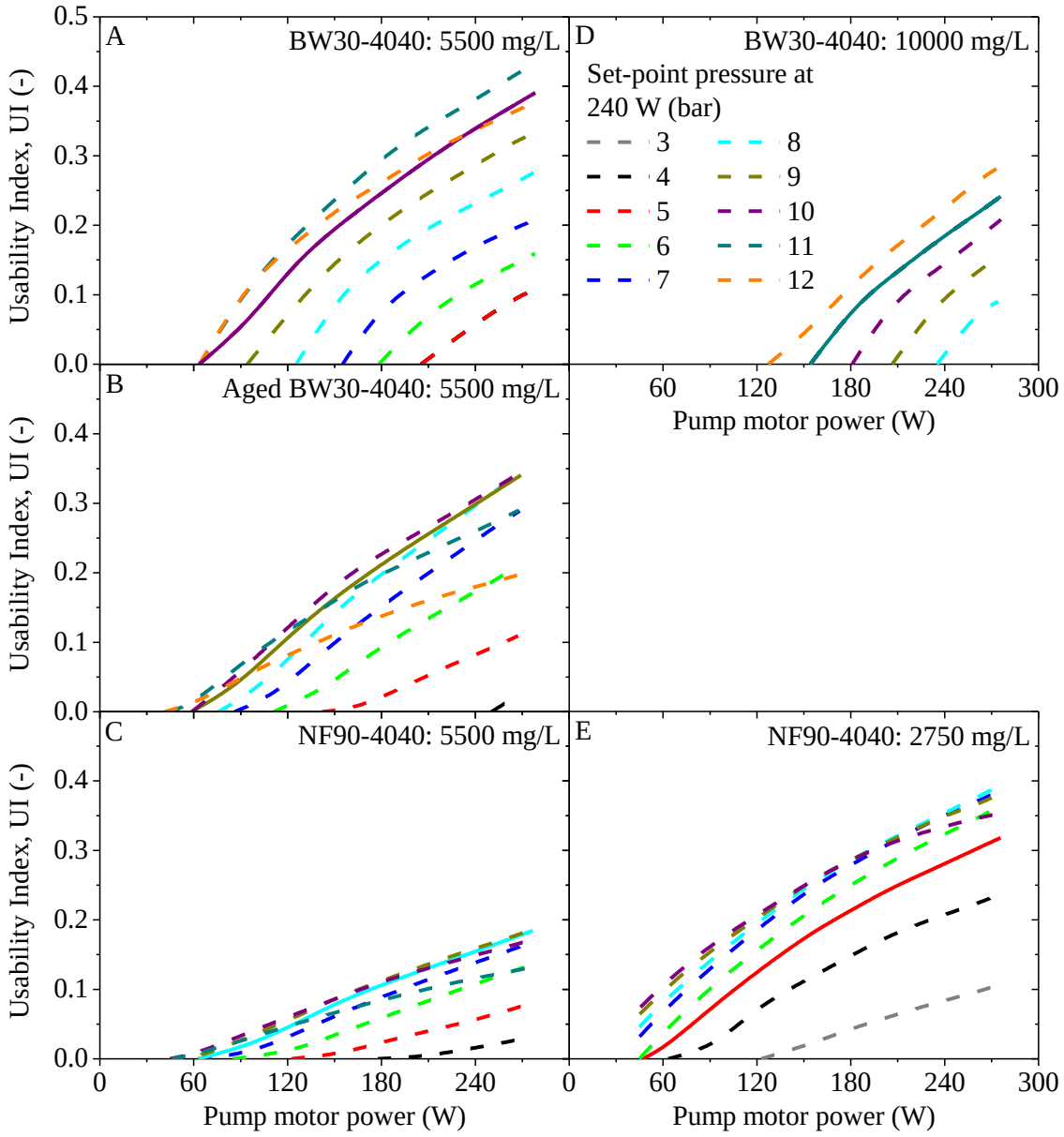

Figure 7.11: Optimising the set-point operation of the membrane system (optimised line in bold) using the usability index (UI) within the safe operating window for the range membrane modules and feed water concentrations.

The optimum set-point lines in Figure 7.11D and Figure 7.11E show the pump motor operating close to its limits in terms of efficient operation with salt concentrations of

10,000 mg/L and 2750 mg/L, respectively. With a feed water of 10,000 mg/L, the optimum set-point of the BW30 was 11 bar in order to remain within the safe operating window. As a result of the high osmotic pressure, there was no permeate produced below a pump motor power of 155 W with this set-point. The minimum pressure could be reduced to 125 W with a 12 bar set-point but would be at the risk of high recovery. In real operating terms, this would be the difference between producing water at an average wind speed of 6.3 m/s versus 7.3 m/s for the 11 bar set-point. Therefore, the wind speed characteristics for the specific site would have to be taken into account for this choice to be made.

When the NF90 membrane was used with 2750 mg/L feed water, the optimum set-point was 5 bar (Figure 7.11E). As a result of the low salinity feed water and high permeability of the membrane, the maximum recovery was achieved at a TMP of only 4 bar and a feed flowrate of 180 L/h with an 8 bar set-point. This indicates the importance of determining the feed water characteristics prior to system design. For lower salinity feed waters it could be more beneficial to use an NF90 membrane with a pump that provides lower pressure and higher flowrate in order to increase the flux and reduce the maximum recovery. This would depend entirely on the feed water characteristics and the type of contaminants that required removal. In terms of the renewable energy generator, this may require increasing the voltage output to accommodate a higher flowrate pump motor.

7.2.2 Choice of operating strategy

The previous Section 7.2.1 described the optimum set-point for operating the membrane system within the safe operating window. This type of operation where the valve was set at the start of the experiment has been termed as constant set-point operation and is the method that has been used to date. However, there are other possible operating strategies that could be more beneficial for maximising the performance for variable power operation and these must be investigated.

Figure 7.12 shows the various possible operating strategies for the BW30 membrane with 5500 mg/L NaCl feed water. The safe operating window from Figure 7.6 has been re-plotted as a function of power to better understand the implications for the renewable

energy generator. These strategies could be used for any of the membrane and feed water setups. Each of the operating strategies was designed to optimise the performance of the membrane system according to the parameters of high flux and low SEC as described in Section 7.2.1. To allow comparison between the various operating strategies, they were all made to pass through the standard set-point used in earlier experimental work (Chapter 3 – Chapter 6) of 240 W power, 10 bar TMP and 250 L/h feed flowrate.

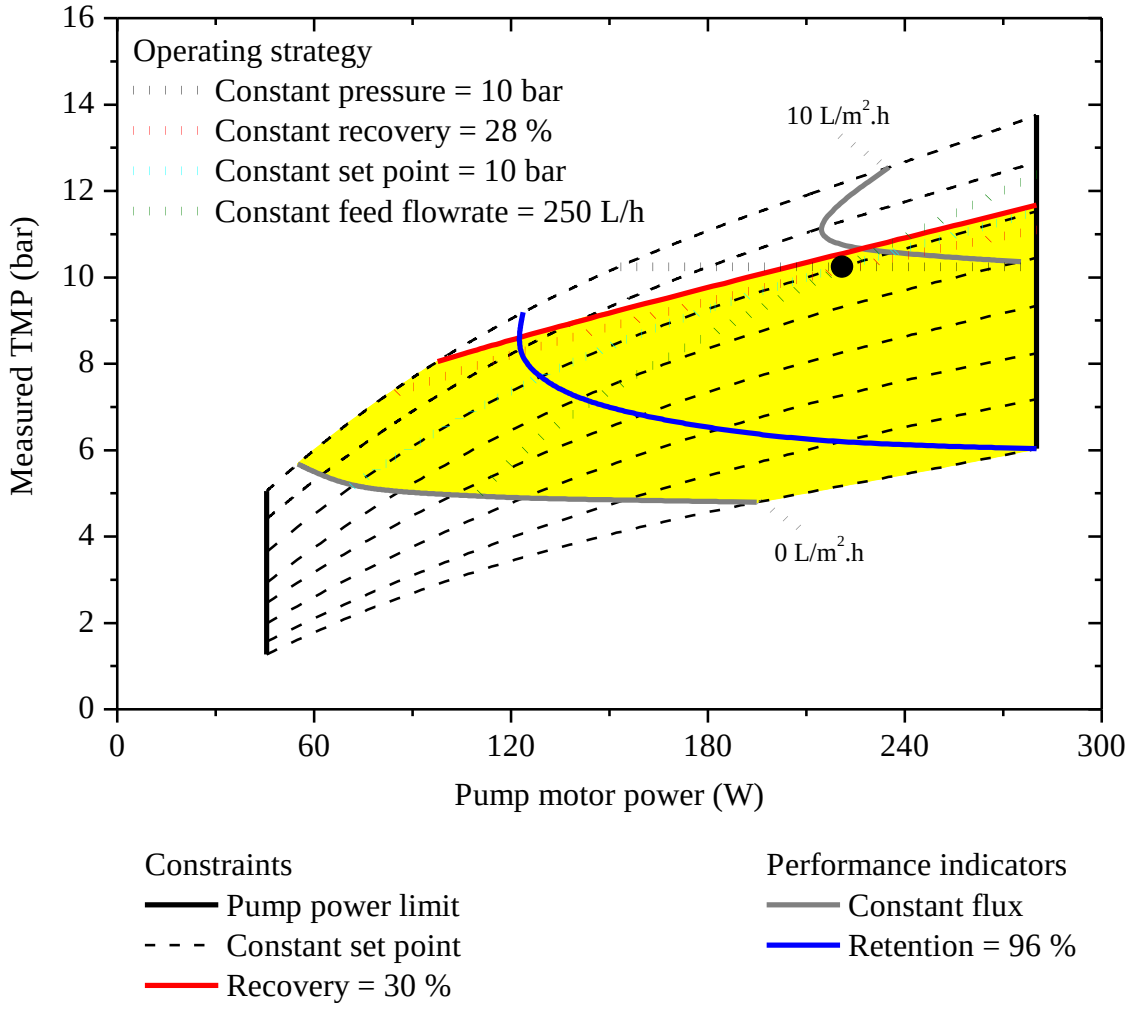

Figure 7.12: Safe operating window (shaded in yellow) for the membrane system with BW30-4040 module and feed water concentration of 5500 mg/L NaCl plotted against pump motor power. Diagram shows the various operating strategies that could be used for transient operation in order to maximise flux and retention.

The potential operating strategies shown in Figure 7.12 are as follows:

Constant pressure (10 bar): implemented by varying the feed flowrate. This would involve operating the system at relatively constant current (3.1 – 3.3 A) by varying the voltage and the regulating valve on the concentrate stream. This could be achieved using automatically actuated valves or a hydraulic accumulator [58, 93, 100]. Operation of the system with constant pressure is more consistent with conventional RO plants than the other options. This operating strategy would be difficult to implement within the constraints of the safe operating window while maximising system performance.

Constant recovery (28 %): achieved using a positive displacement pump that provided a fixed ratio of feed and concentrate flow and hydraulic energy recovery [101, 124].

Constant set-point: the operating strategy that has been previously described and is currently used for this system. A set-point of 10 bar at 240 W and 250 L/h would be set using the regulating valve on the concentrate stream using this membrane and feed water.

Constant feed flowrate (250 L/h): implemented by varying the pressure. This would involve keeping the voltage in a relatively narrow range (50 – 70 V_{DC}) and varying the current and the regulating valve on the concentrate stream. Operation would exceed the bounds of the safe operating window at high power (>250 W).

With the potential operating strategies defined, the choice of the optimal strategy should satisfy the following criteria:

i. allow the membrane system to operate within the safe operating window;
ii. optimise the performance in terms of the maximum possible flux and retention at low SEC;
iii. operate over a wide power range to utilise the power output from the wind turbine efficiently; and
iv. be robust, cheap and simple to implement.

7.2.3 Performance comparison of different operating strategies

A performance comparison of the operating strategies (taken from Figure 7.12) are shown in terms of the SEC (Figure 7.13A) and the UI (Figure 7.13B) over the whole

operating range. The SEC and UI are two of the most important criteria for maximising the system performance and reducing the overall cost of water. The best overall performance was found using the constant recovery operating strategy. The use of constant recovery resulted in a low SEC (~ 3 kWh/m^3) and high UI over the whole operating range. In addition, this strategy fulfilled the desired criteria by having a wide power range (80 – 280 W) and narrow pressure range (7 – 11 bar).

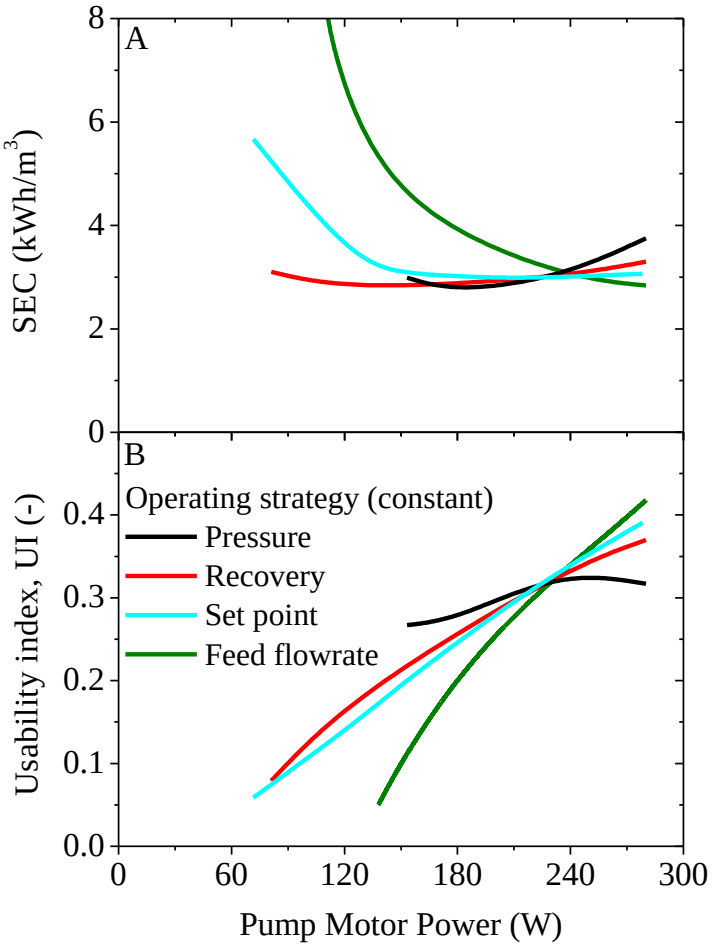

Figure 7.13: Performance comparison of operating strategies over the whole operating range plotted as (A) specific energy consumption (SEC) and (B) usability index (UI).

Constant TMP operation had a relatively low SEC and average UI but was limited by the load range as the power must be >150 W to achieve 10 bar. This strategy also resulted in operation outside the safe operating window below 210 W and would therefore result in poor overall performance. While this type of operation may be used

for large-scale systems operated with constant power, it would result in poor performance with fluctuating power.

Constant feed flowrate operation showed relatively poor SEC and UI over the majority of the power range due to low TMP and therefore flux. This operating strategy would result in a relatively narrow power range (110 – 280 W) with a wide pressure range 5 – 12.5 bar and therefore falls short of the desired criteria.

Constant set-point operation exhibited low SEC (~ 3 kWh/m^3) above 150 W and high UI over the whole operating range. High SEC (3 – 6 kWh/m^3) was observed at low power due to the relatively low TMP (5 – 7.5 bar). This strategy would have a wide power range 70 – 280 W and pressure range 5 – 11.5 bar and therefore fulfilled the desired criteria for the operating strategy

Constant recovery operation would require a different pump or a dedicated control system to actuate the regulating valve on the concentrate stream according to fluctuations in power. Apart from additional cost and complexity, the response rate of the valve may result in reduced energy efficiency [97]. For these reasons, the constant set-point operating strategy was considered to be a good operating strategy for the current system. This meant sacrificing SEC at low power and accepting an additional 2.5 bar variation to the maximum pressure range when compared to constant recovery operation. However there was no reduction in the average UI and slightly increased performance from the minor reduction of 10 W in the power required to initiate permeate flow.

7.2.4 Set-point performance comparison within safe operating window

Having decided that constant set-point operation was the most appropriate operating strategy (Section 7.2.2) for the wind-membrane system to maximise performance within the safe operating window, the expected productivity according to the average wind speed could be determined. This is important to determine the feasibility of operating the wind-membrane system in a specific location according to the available wind resource and feed water concentration.

Figure 7.14 shows the predicted water productivity, permeate NaCl and SEC of the wind-membrane system based on steady-state conditions according to the available wind speed. Performance criteria for each membrane are given according to the optimum set-point within the safe operating window depending on the feed water concentration as previously described in Section 7.2.1.

With 5500 mg/L NaCl feed water, the NF90 membrane produced 70 % more water (Figure 7.14A) at 35 % lower SEC (Figure 7.14B) than the BW30 over the whole range of operation, but this was at the expense of permeate quality (Figure 7.14C). The permeate concentration with the NF90 was double that of the BW30 due to its increased permeability. The choice of membrane module with this feed water concentration would therefore depend upon the other contaminants present in the local water supply. With NaCl as the main solute being removed, the NF90 would provide lower water costs due to the increased productivity and this would be within the safe operating window. However if there were high concentrations of salts with monovalent ions in the feed water, then the BW30 may need to be used to increase the retention to within the guideline value according to the particular contaminant being removed [49].

At moderate average wind speeds of 7 m/s, the BW30 could produce 1 m^3 of permeate with concentration of 200 mg/L at an average SEC of 3 kWh/m^3 (Figure 7.14). By comparison, the NF90 could produce 1.8 m^3 at an average of 450 mg/L and SEC of 2 kWh/m^3. The aged BW30 has increased productivity (~ 25 %) and therefore SEC (13 %) compared to the new BW30, but has seen a significant reduction in the permeate quality which has a concentration more than double its original performance [192]. However, for most of the operating range, the aged BW30 produced water within the safe operating window and therefore continues to be used.

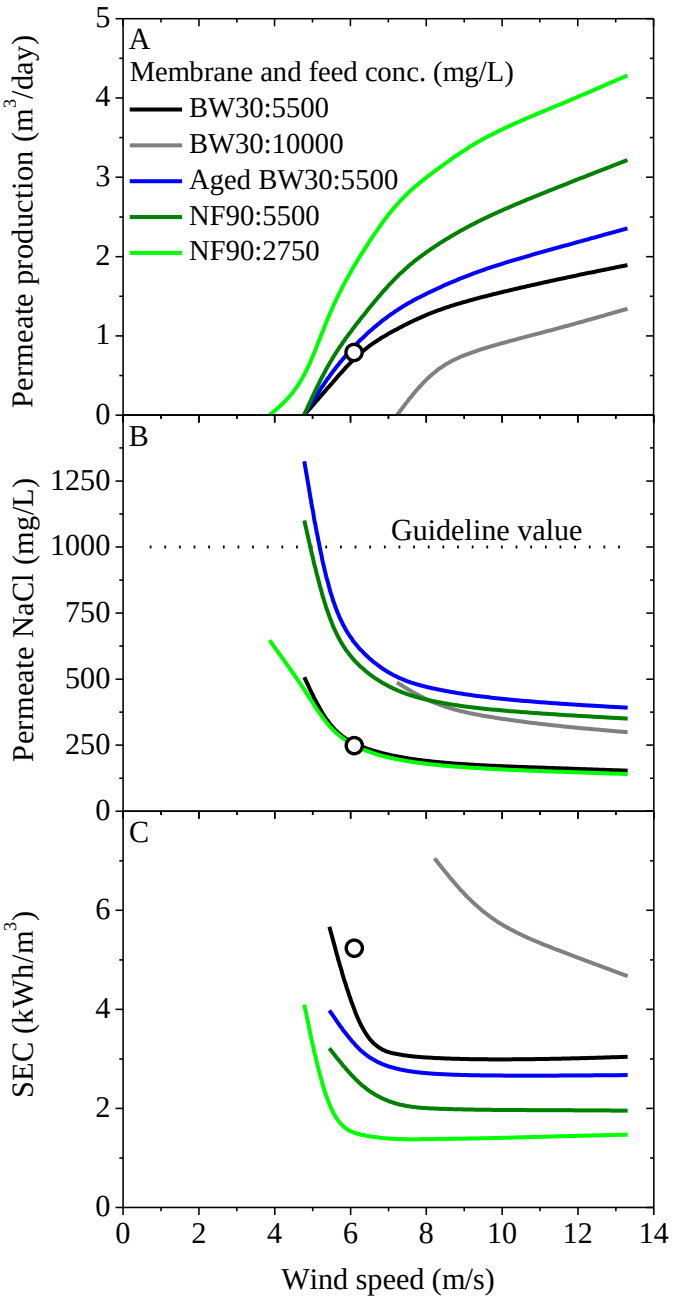

Figure 7.14: Performance of wind-membrane system using optimum set-point within safe operating window for various membrane modules and feed water concentrations plotted as (A) permeate production; (B) permeate NaCl and (C) specific energy consumption (SEC). The black circle represents the real wind speed performance and is discussed in Section 7.3.2.

7.3 System performance over wind days

7.3.1 Effect of membrane system set-point and supercapacitor energy storage

The final objective of this research was to examine the operation of the wind-membrane system over 24 hours using real wind speed data. This would serve several purposes:

i. verify the impact of real wind fluctuations and intermittency on performance;
ii. determine the actual productivity of the optimised wind-membrane system and allow comparison with the steady-state values obtained in Section 7.2.4; and
iii. determine the effectiveness of supercapacitors in improving the overall system performance and decide what size of bank would be optimal for this system.

The experiments were conducted using the wind turbine simulator (described in Section 2.3) directly-connected to the membrane system. Real wind speed data (taken at Emden, Germany [68]) was corrected for the wind turbine hub height from 20 m to 8 m and used as the input to the simulator. Further details of the real wind data for these experiments can be found in Section 2.5.4. Four wind experiments were performed with the BW30 module and feed water concentration 5500 mg/L NaCl using the following configurations:

i. 7 bar set-point (to illustrate poor system performance);
ii. 10 bar set-point (optimised set-point performance);
iii. 4x1 supercapacitor bank and 10 bar set-point (smallest supercapacitor bank); and
iv. 4x3 supercapacitor bank and 10 bar set-point (largest supercapacitor bank).

Figure 7.15 shows the operating performance of the wind-membrane system in terms of pump motor power, flux and permeate NaCl for each of the system setups over the full 24 hour period.

The average wind speed over the 24 hour period was 6 m/s with a wide range from 0 – 20 m/s (Figure 7.15A). Based on the average wind speed and hub height of 8 m, this would be categorised as a class 4 – 5 wind resource, which would generally be considered suitable for wind energy production [113]. The wind speed input (Figure 7.15A) exhibited both fluctuations and intermittency, where intermittency was taken to be any period of time where the system shut down due to insufficient power. This occurred at wind speeds ≤ 3 m/s where the pump motor power decreased below

40 W, which was consistent with previous experiments using simulated wind speed fluctuations (Section 4.1).

There was relatively poor performance with the 7 bar set-point compared to 10 bar as would be expected from the safe operating window analysis (Section 7.1.2). The maximum flux (Figure 7.15C) was only 7.5 $L/m^2.h$ compared to 15 $L/m^2.h$ with the 10 bar set-point as a result of the reduced TMP. This also caused significantly increased permeate NaCl due to the high rate of salt diffusion with relatively low water flux. The permeate NaCl exceeded the guideline value with the 7 bar set-point when the wind speed dropped below 4 m/s. With the 10 bar set-point, the guideline value was only exceeded for very short periods of time when the system was restarted after a period of intermittency as observed previously (Section 5.1).

The pump motor power (Figure 7.15B) illustrates how the supercapacitors buffered the fluctuating power output from the wind turbine and provided constant power for the first five hours while the average wind speed was > 7 m/s. Once the wind speed dropped below this value the supercapacitor state of charge (SOC) reduced to the threshold for usable energy and the wind speed fluctuations started to impact on the performance. This is consistent with the experimental results on the supercapacitor performance described in Section 6.1.3.

The use of supercapacitor energy storage resulted in improved flux (Figure 7.15C) and reduced permeate NaCl (Figure 7.15D) due to the buffering of power fluctuations and the provision of increased power quality to the pump motor. While steady-state power was only provided for the first five hours, performance was improved over the whole 24 hour period.

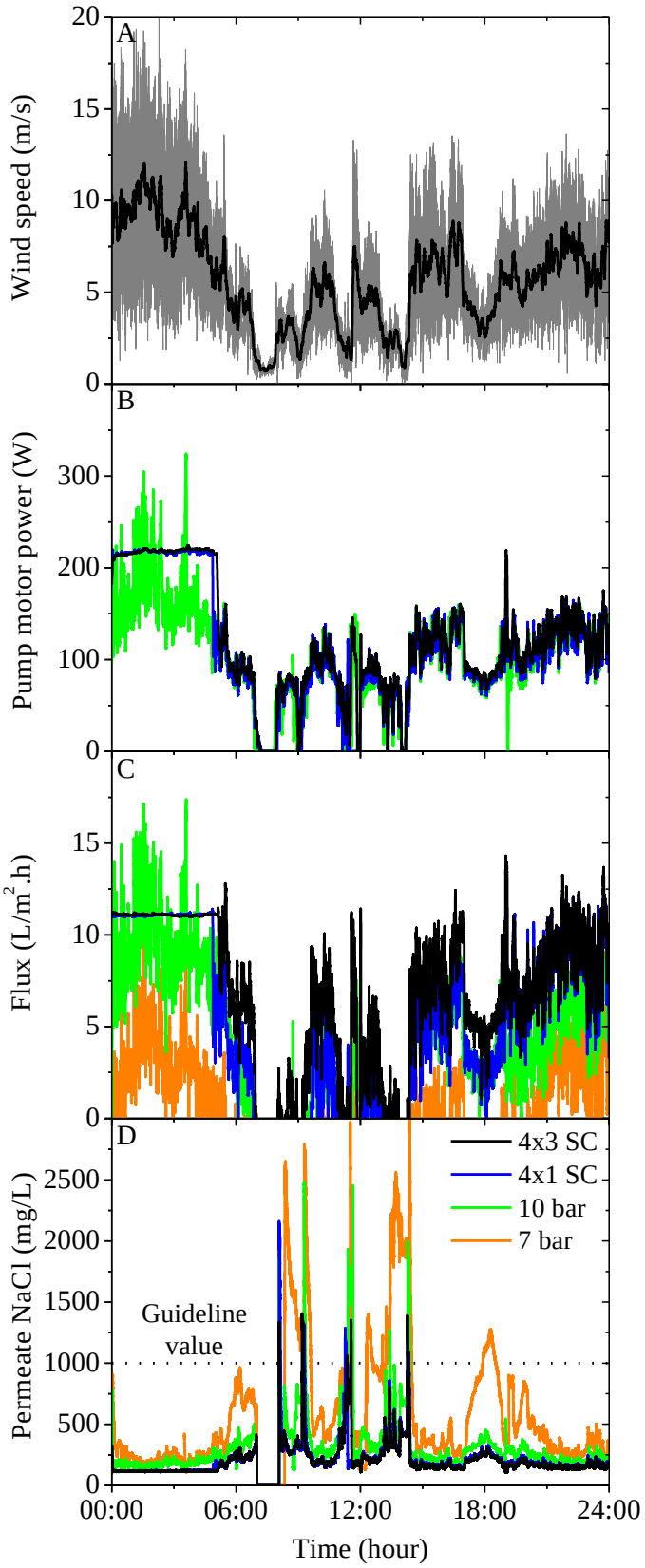

Figure 7.15: Performance of the wind-membrane system (BW30-4040 and feed water concentration 5500 mg/L) over 24 hours using real wind speed data with and without supercapacitor storage.

An important point that has not been addressed previously is the potential for short-term pressure fluctuations to damage the membrane module. The membrane manufacturer states that a 'soft' start should be used to prevent possible damage caused by excessive pressure or flowrates and hydraulic shock [49]. If the feed pressure and flowrate are ramped up too rapidly, excessive radial or longitudinal forces can damage the membrane, particularly if there is air in the system. To achieve a 'soft' start, the rate of feed pressure increase should be less than 0.7 bar/s [49]. Analysis of the TMP from the 24 hour experiments showed that with a 10 bar set-point, the maximum pressure change was 0.7 bar/s with an average value of 0.3 bar/s. Therefore, even with extreme wind speed fluctuations, the maximum rate of pressure change was within the allowable region for a soft start and should not be a cause for concern during long term operation. The addition of supercapacitor energy storage resulted in a reduction of the maximum pressure change to 0.5 bar/s with an average of 0.2 bar/s.

7.3.2 Average system performance with real wind speed fluctuations

While the instantaneous performance (Figure 7.15) is important for understanding the impact of real wind on the operating characteristics of the wind-membrane system, the most important performance indicators are the quantity and quality of potable water produced over the course of a typical day. Figure 7.16 illustrates the potable water production and NaCl concentration over the 24 hour period for the 4 different experimental setups shown in Figure 7.15.

For the first five hours while the average wind speed was > 7 m/s (Figure 7.15A), there was a high rate of water production (Figure 7.16A) while the concentration (Figure 7.16B) reduced from the initially high value produced when the membrane system was turned on. Once the wind speed dropped below 7 m/s, the rate of water production was lower and the concentration increased gradually over the rest of the day. All four of the system setups produced low permeate concentrations of < 300 mg/L NaCl at the end of the day and at no point did the concentration go above the guideline value even during the periods of intermittency. This highlights the importance of having an adequate average wind speed (≥ 6 m/s) to produce sufficient flux to increase productivity and maintain adequate permeate quality.

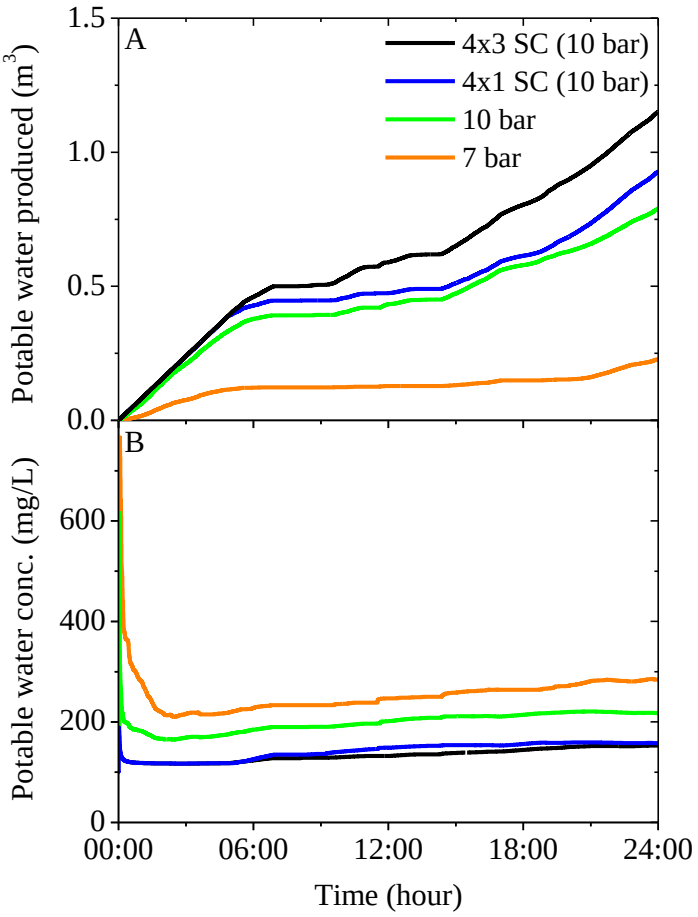

Figure 7.16: Real-time performance of wind-membrane system over 24 hour period in terms of (A) potable water produced and (B) potable water concentration.

The average performance values over the 24 hour period are summarised in Table 7.1 for further comparison. The impact of changing the set-point from 7 to 10 bar is shown particularly in the permeate production which increased from 0.23 to 0.79 m^3. To allow comparison with the steady-state values, the average values from Table 7.1 for the 10 bar set-point have been included in Figure 7.14 (shown by ○ with steady-state values shown by black line). The real wind speed results showed excellent correlation with the steady-state values, highlighting that the steady-state performance can be used to predict the productivity according to the average wind speed. The marginal difference observed in the SEC (Figure 7.14C) was most probably a result of the reduced power quality caused by the wind speed fluctuations.

Table 7.1: Performance parameters of the wind-membrane system averaged over a 24 hour period with real wind speed fluctuations as shown in Figure 7.15.

Membrane system setup	Avg. Power (W)	Avg. TMP (bar)	Permeate produced* (m^3)	Permeate NaCl* (mg/L)	Avg. SEC (kWh/m^3)	Avg. UI (-)
7 bar	103	4.0	0.23	280	6.2	0.04
10 bar	107	6.3	0.79	240	5.2	0.14
4x1 supercapacitor bank (10 bar)	115	6.6	0.93	170	3.2	0.18
4x3 supercapacitor bank (10 bar)	121	6.9	1.15	160	3.1	0.22

*Values given at end of 24 hour period as shown in Figure 7.16.

The use of supercapacitor energy storage (4x1) resulted in an 18 % increase in permeate production and a reduction in the average SEC from 5.2 to 3.2 kWh/m^3. There was only a marginal performance increase observed by increasing the size of the supercapacitor bank from 4x1 to 4x3. This highlights the inherent characteristics of supercapacitors, that they provide an excellent source of power but a poor source of energy, even at increased capacity. Therefore, the 4x1 size of supercapacitor bank is considered to be the optimal size for improving the performance of this particular system by buffering the most common short-term wind fluctuations and intermittency (up to 1 min long).

The expected lifetime of the supercapacitor banks is important, as any improvements in short-term performance should not be made at the expense of increased maintenance and cost of water. The performance of supercapacitors degrades over time according to the variation of voltage and the ambient temperature [182]. This degradation follows an exponential decay rather than a failure to indicate the end of lifetime. The standard lifetime measurement used in industry is a 20 % decrease in capacitance and/or a 200 % increase in the internal resistance of the supercapacitor. The cycle lifetime for these supercapacitors was given as 500,000 cycles (at 25 °C), measured as cycles from the

rated voltage (60 V_{DC}) to half of the rated voltage, resulting in a 20 % decrease in capacitance (Table 2.7).

To give an indication of the expected lifetime of the supercapacitors, the number of cycles was calculated over the 24 hour period shown in Figure 7.15. One cycle was taken to be a round trip voltage change of 60 V_{DC}, and this was averaged over two experiments, as the 24 hour experiment was repeated. The 4x1 supercapacitor bank underwent 156 cycles and the 4x3 supercapacitor experienced 112 cycles over the 24 hour period, giving a lifetime range of 8.8 – 12.2 years. These figures are based on a single 24 hour period and due to the inherent variability in wind, can only serve as a rough estimate. However, these values do correspond well with the literature, where typical lifetimes of 8 – 12 years have been given for supercapacitors used in wind energy applications [134, 142].

7.4 Conclusions

The safe operating window for the wind-membrane system was determined for BW30, aged BW30 and NF90 membrane modules and feed water concentrations of 2750 mg/L, 5500 mg/L and 10,000 mg/L NaCl over the whole range of operation. The main constraints to the operating window were from the pump motor (minimum start-up power 45 W and maximum power 300 W) and the maximum recommended recovery (30 %). The use of a larger pump could provide increased flowrate and pressure which would increase the size of the safe operating window, but this would require a larger renewable energy generator. The physical limitations of the membrane (feed water pressure, flowrate and pressure drop across membrane) were outside the bounds of the operating window using this small pump motor.

The minimum pressure required to produce permeate flux was the other factor that determined the size of the operating window. This was largely dependent upon the osmotic pressure of the feed water. When using the BW30 membrane, flux was produced at 4.8 bar with 5500 mg/L NaCl feed water and at 8.4 bar with 10,000 mg/L. The resistance of the membrane also played a role with the NF90 able to produce water at TMP of 3.9 bar with 5500 mg/L feed water due to its higher permeability. The

minimum retention was only a constraint for the aged BW30 and the NF90 with 5500 mg/L feed water at low pressure and feed flowrate.

The optimum operating strategy was chosen to operate the membrane system within the safe operating window with the maximum flux and retention at low SEC over a wide power range to fully utilise the power output from the wind turbine. A narrow pressure range was also desirable to reduce the potential for mechanical fatigue that may reduce membrane lifetime and performance. Constant recovery was shown to be the optimum operating strategy but constant set-point operation was chosen for the current system as it was considered to be robust, cheap and simple to implement. Compared to operation at constant recovery there was a small reduction in performance caused by the higher SEC at low power and an additional 2.5 bar variation in the maximum pressure range. However the average UI was the same and there was slightly increased performance from the wider power range (10 W increase).

The optimum set-point for the membrane system was determined for each membrane and feed water combination to maximise the UI within the safe operating window. This was dictated by the permeability of the membrane and the osmotic pressure of the feed water. The optimum set-point for the BW30 membrane with a feed water of 5500 mg/L was 10 bar, while the aged BW30 and the NF90 were 9 bar and 8 bar, respectively. This was a result of the recovery reaching the maximum recommended threshold at lower TMP which limited the maximum set-point.

By increasing the feed water to 10,000 mg/L the optimum set-point could be increased to 11 bar within the safe operating window. This was due to the increased osmotic pressure of the feed water and therefore reduced recovery over the whole operating range. The membrane system could be operated at a 12 bar set-point but this would cause the recovery to exceed the recommended limit at high power. However, if the average wind speed resource was low for the site then this could be an allowable risk to improve the system productivity. The choice of operating point should therefore be chosen according the feed water and membrane as well as the wind resource for the specific site.

A comparison of the wind-membrane system was performed over 24 hours using real wind speed data (average 6 m/s) with the BW30 membrane and 5500 mg/L NaCl feed water. Experimental setups included a comparison of 7 bar and 10 bar set-points and the impact of two different sized supercapacitor banks (4x1 and 4x3) on the membrane performance. Examining the productivity of the membrane system over the course of a day showed the effect of the average wind speed on the overall permeate production and concentration. When the average wind speed was high (> 7 m/s), there was an increased rate of water production while the concentration reduced from the initially high value produced when the system started up. Once the wind speed dropped below 7 m/s, the rate of water production was lower and the concentration increased gradually over the rest of the day. The overall permeate quality was excellent for all system setups and at no point approached the guideline value.

With a 10 bar set-point the wind-membrane system produced 0.78 m^3 of water with a final concentration of 240 mg/L NaCl and average SEC of 5.2 kWh/m^3. This illustrates the potential for wind-membrane systems to operate without energy storage in areas with an adequate wind resource. For this particular system an average wind speed of $\geq$ 6 m/s is recommended.

With the addition of supercapacitor storage, the system performance improved with 0.93 m^3 of water produced and a final concentration of 170 mg/L NaCl at average SEC of 3.2 kWh/m^3. By buffering the wind speed fluctuations and providing power during periods of intermittency, the supercapacitors increased the quality of power delivered to the pump motor. Steady-state power was provided to the pump motor while the supercapacitor SOC was above the unusable threshold at wind speeds > 7 m/s, and the average performance was increased over the whole 24 hour period. Based on this study, the recommended size of supercapacitor bank for this system is the smaller sized 4x1. While increasing the size of storage resulted in improved performance, it was a marginal increase and would not be worthwhile for the additional cost. This reinforces the previous observation that supercapacitors are a cheap and efficient source of power but an expensive source of energy.

In the thesis objectives (Section 1.8), the key technical barriers to the wide-scale deployment of RE-membrane systems highlighted by the ProDes project were summarised as follows [28]:

i. the majority of RE-membrane systems are combinations of components that are developed independently resulting in poor reliability and increased water costs;
ii. the development of desalination focuses on large-scale systems resulting in a lack of appropriate technology for small-scale systems;
iii. desalination technology has been designed for constant power usage which could result in increased capital and maintenance costs for RE-membrane systems due to frequent replacement of membrane modules; and
iv. RE-membrane systems are considered to be more suitable for small-scale community led projects and are therefore not being commissioned by water authorities who consistently use centralised and familiar technologies.

These barriers emphasised the lack of detailed design knowledge, technical experience and experimental data from RE-membrane systems within the wider desalination community. The main aim of this PhD research was to systematically examine the challenges and performance issues associated with a wind-membrane system, and in doing so help to address this shortage of knowledge and experience. The above conclusions on the coupling of the wind turbine to the membrane system; the effect of wind speed fluctuations and intermittency; the potential of supercapacitors to buffer wind variability; the safe operating window and the optimum operating strategy address many of the technical barriers faced by RE-membrane systems. It is hoped that this knowledge can be used to improve the feasibility for the wide-scale implementation of this technology by laying the foundations for further studies on control systems, energy buffering and field testing of prototype plants.

Chapter 8

Conclusions

8.1 Summary

The main aim of this PhD thesis was to examine the feasibility, challenges and performance issues associated with the direct-connection of a wind turbine to a RO/NF membrane system. By helping to address the lack of knowledge, design experience and experimental data on wind-membrane systems within the wider desalination community, this research should assist in generating enthusiasm and confidence in the implementation of this important technology. The significant findings from this research are summarised below.

Coupling the wind turbine to the membrane system

An essential part of the initial design process was the choice of an appropriate wind turbine to provide the necessary power for the membrane system. The key challenge for the direct-coupling of these technologies is the provision of sufficient power to the membrane system with the appropriate current and voltage characteristics at achievable average wind speeds. As the wind turbine power curves provided by the manufacturer are often very different to real conditions, it is essential to accurately determine the power curve over a range of resistance loads before coupling with the membrane system or any other directly-powered application. A relatively high power output from the wind turbine at low average wind speeds (~ 6 m/s) is a distinct advantage for improving the performance of a wind-membrane system in realistic wind regimes. The use of a five-bladed wind turbine to provide additional torque at low wind speeds proved to be

beneficial for this purpose. Using the design procedure outlined in this thesis for sizing wind-membrane systems will result in more efficient operation by maximising the use of power from the wind turbine and allowing the membrane system to be operated over the optimum range of pressure and flowrate.

Effect of wind speed fluctuations

The impact of transient operation of membrane systems was not previously well understood and there has been little detailed research performed in this area. A systematic experimental investigation showed that the operating characteristics of the membrane system were influenced by the average wind speed as well as the TI (directly related to the amplitude of fluctuations) and the period of oscillation. However, at average wind speeds of 7.0 m/s or higher the performance was independent of the period of oscillation up to a TI of 0.4. In addition, within this operating range the system performance was the same under fluctuations as under steady-state conditions. The system performance was seen to deteriorate most under fluctuations that occurred at low average wind speeds with high TI and long periods of oscillation. Therefore, the main challenge associated with direct-connection to renewable energy supplies is not the size of the fluctuations but the effect of the power switching off which causes reduced flux and permeate quality.

Effect of wind intermittency

To determine the impact of wind intermittency on the average quality and quantity of potable water produced, experiments were performed over one hour intervals with intermittent periods from 0.5 – 3 min. The membrane system showed good resilience to intermittency in terms of permeate quality by producing potable water for all of the conditions except with a high feed concentration at low power (5500 mg/L NaCl at 60 W). The amount of power available to re-start the system after a period of intermittency was important for the average permeate concentration as it determined the TMP, flowrate and flux which purged the system of high salinity permeate. Due to the concentration gradient being highest when the power was initially turned off, the increase in permeate concentration was highest at off-times up to 60 s, which highlights the potential for short-term energy buffering to improve performance.

Potential of supercapacitors to buffer wind variability

The potential of supercapacitors to expand the safe operating window of the wind-membrane system by buffering short-term fluctuations and intermittency was examined systematically. The supercapacitors were able to provide sufficient energy during periods of no wind (intermittency) and enhance the power quality delivered to the membrane by absorbing the effects of turbulent wind (fluctuations). As a result, system shut-down and compromised permeate quality due to reduced TMP were avoided. The use of supercapacitors to provide constant power resulted in a 40 % increase in the average flux and a 15 % increase in permeate quality under intermittent operation over one hour. The improvements in the average flux and permeate quality under fluctuating conditions due to increased power quality were 85 % and 40 %, respectively. The supercapacitors were very effective at absorbing oscillations over a wide range (15 s – 20 min) and are therefore considered to be ideal for integration into RE-membrane systems to provide higher average water quality and quantity.

Safe operating window

The safe operating window for the wind-membrane system was determined for the BW30, aged BW30 and NF90 membrane modules with feed water concentrations of 2750 mg/L, 5500 mg/L and 10,000 mg/L NaCl over the whole range of operation. The main constraints to the operating window were from the pump motor power (minimum start-up power of 45 W and maximum power of 300 W) and the maximum recommended recovery (30 %). The osmotic pressure of the feed water was also a constraint as it determined the minimum pressure required to produce permeate flux. The minimum retention required to produce adequate permeate quality was a constraint for the aged BW30 and the NF90 with a feed water concentration of 5500 mg/L NaCl at low pressure and feed flowrate. The physical limitations of the membrane (feed water pressure, flowrate and pressure drop across membrane) were outside the bounds of the operating window using this small pump motor. The use of a larger pump could provide increased flowrate and pressure which would increase the size of the safe operating window, but this would require a larger renewable energy generator.

Optimum operating strategy

The optimum operating strategy was chosen to operate the membrane system within the safe operating window with the maximum flux and retention at low SEC over a wide power range to fully utilise the power output from the wind turbine. A narrow pressure range was also desirable to reduce the potential for mechanical fatigue that may reduce membrane lifetime and performance. Constant recovery was shown to be the optimum operating strategy but constant set-point operation was chosen for this system as it was considered to be robust, cheap and simple to implement. Compared to operation at constant recovery, there was a small reduction in performance caused by high SEC at low power and an additional 2.5 bar variation in the maximum pressure range. However the average UI was the same and there was slightly increased performance from the wider power range (10 W increase).

Wind-membrane performance over real wind days

A comparison of pressure settings and size of supercapacitor banks was performed over 24 hours using real wind speed data (average 6 m/s) with the BW30 membrane and 5500 mg/L NaCl feed water. Experimental setups included a comparison of 7 bar and 10 bar set-points and the impact of two different sized supercapacitor banks (4x1 and 4x3) on the membrane performance. With a 10 bar set-point the wind-membrane system produced 0.78 m^3 of water with a final concentration of 240 mg/L NaCl and average SEC of 5.2 kWh/m^3. With the addition of supercapacitor storage, the system performance improved significantly with 0.93 m^3 of water produced and a final concentration of 170 mg/L NaCl at average SEC of 3.2 kWh/m^3. These final experimental results illustrate the potential for wind-membrane systems to operate in areas with an adequate wind resource. For this particular system an average wind speed of ≥ 6 m/s is recommended and the optimum supercapacitor bank is the smaller sized, 4x1. While increasing the size of storage resulted in improved performance, it was a marginal increase and would not be worthwhile for the additional cost.

8.2 Suggestions for further research

A number of interesting research topics that were outside the scope of this PhD research but would benefit from further investigation are outlined below.

The impact of transient operation on the long-term performance and lifetime of the membrane module and other components is still unknown. This would require a pilot plant to be set up with a real brackish water source and detailed performance measurements taken over several years. Now that the technical challenges associated with coupling the wind turbine to the membrane system and determination of the safe operating window have been addressed, this next phase of testing can begin.

This research used a saline solution to represent brackish water, however real brackish groundwater is much more complex and variable, being composed of nine major chemicals and a wide number of other trace contaminants according to location (as detailed in Section 1.1.1). The impact of pH and energy fluctuations on the retention of a range of trace contaminants has been analysed by Richards *et al.* [26]. However, further similar studies using RE-membrane systems with a wide variety of real brackish groundwaters would be required to form a more comprehensive overview.

The performance decline of the aged BW30-4040 membrane module was compared to that of a new module in Chapter 7. The aged module was used for field trials in Australia in 2005 [60, 94] and then used for extensive laboratory testing from 2008 to the present date. It exhibited a significant reduction in retention and an increase in permeate flowrate and recovery. It would be interesting to compare this change in performance with a module taken from a full-scale membrane plant or used for long-term testing with real brackish groundwater to examine the difference in membrane degradation.

In the discussion in Section 3.2.1, the potential for improving the performance of the membrane system using 2.5 inch modules was highlighted. By using three 2.5 inch modules in series as opposed to a single 4 inch module, the detrimental effects of concentration polarisation could be reduced. This would provide higher flux while reducing both the likelihood of scaling and the energy consumption of the plant. It would be interesting to investigate the use of 2.5 inch modules in series, particularly with respect to the impact of fluctuating pressure and flowrate from renewable energy generators. The improvement in the overall performance with additional modules would have to be weighed against the added complexity of the plant, particularly with respect to plant operation and maintenance in remote areas.

A cost estimate for water produced by the RE-membrane system when powered by solar PV was calculated as 3.70 £/m^3 based on a capital cost of £ 9940 and potable water production of 1 m^3/day [199]. This is an approximate value as the productivity of the RE-membrane system over time periods of more than several days is still estimated and the costs associated with a prototype system in development are always considerably higher. Additionally, the lifetime of membrane modules and other components including the pump motor are still unknown. The accuracy of this calculation could therefore be improved with further experience and operation of the pilot plant.

The literature review on transient operation of wind-membrane systems (Section 1.6) highlighted that constant recovery operation was the optimum strategy for coupling membrane systems with renewable energy. This observation was confirmed by the experimental analysis on operating strategies performed in Section 7.2. Therefore, it would be interesting to try and implement this control strategy using control of the pressure and flowrate from the pump. This could be done using a control system with solenoid valves; however the response rate of the valve to wind fluctuations would have to be carefully controlled. Some sort of energy recovery device could also be used to control the recovery, similar to the Clark pump or Danfoss energy recovery system (described in Section 1.6.2). However, there is currently no pressure recovery system that can operate down to the low pressures used for brackish water desalination.

Bibliography

[1] M.D. Villiers, Water: The Fate of Our Most Precious Resource, Houghton Mifflin Harcourt, (2001).

[2] United Nations Water, International Decade for Action, Water for Life, 2005-2015, (2006).

[3] Department of Economic and Social Affairs, The Millennium Development Goals Report, United Nations, New York, (2011), pp. 53-54.

[4] World Health Organisation, First Consultation on Post-2015 Monitoring of Drinking-Water and Sanitation, WHO/UNICEF Joint Monitoring Programme for Water Supply and Sanitation, (2011).

[5] J. Bartram, K. Lewis, R. Lenton, A. Wright, Focusing on Improved Water and Sanitation for Health, Lancet, 365 (2005) 810-812.

[6] H. Ahlenius, Access to Safe Drinking Water, UNEP/GRID-Arendal, (2008). http://www.grida.no/graphicslib/detail/access-to-safe-drinking-water_de64 (25/04/2012).

[7] M. Peter-Varbanets, C. Zurbrügg, C. Swartz, W. Pronk, Decentralised Systems for Potable Water and the Potential of Membrane Technology, Water Research, 43 (2009) 245-265.

[8] A. Gadgil, Drinking Water in Developing Countries, Annual Review of Energy and the Environment, 23 (1998) 253-286.

[9] A. Niez, Comparitive Study on Rural Electrification Policies in Emerging Economies, International Energy Agency, (2010).

[10] M.A. Montgomery, M. Elimelech, Water And Sanitation in Developing Countries: Including Health in the Equation, Environmental Science and Technology, 41 (2007) 17-24.

[11] A.M. MacDonald, R.C. Calow, Developing Groundwater for Secure Rural Water Supplies in Africa, Desalination, 248 (2009) 546-556.

[12] World Health Organisation, Guidelines for Drinking-Water Quality, Fourth Edition, WHO press, (2011).
http://whqlibdoc.who.int/publications/2011/9789241548151_eng.pdf (25/04/2012).

[13] J.M. Arnal Arnal, M. Sancho Fernández, G. Martín Verdú, J. Lora García, Design of a Membrane Facility for Water Potabilisation and its Application to Third World Countries, Desalination, 137 (2001) 63-69.

[14] Meenakshi, R.C. Maheshwari, Fluoride in Drinking Water and its Removal, Journal of Hazardous Materials, 137 (2006) 456-463.

[15] O. Schmoll, G. Howard, J. Chilton, I. Chorus, Protecting Groundwater for Health: Managing the Quality of Drinking-Water Sources, World Health Organisation, (2006).
http://www.who.int/water_sanitation_health/publications/PGWsection1.pdf
(25/04/2012).

[16] T. Shah, D. Molden, R. Sakthivadivel, D. Seckler, Global Groundwater Situation: Opportunities and Challenges, Economic and Political Weekly, 36 (2001) 4142-4150.

[17] R. Helmer, Water Quality and Health, The Environmentalist, 19 (1999) 11-16.

[18] International Groundwater Resources Assessment Centre, Global Overview of Saline Groundwater Occurrence and Genesis, IGRAC maps, (2009).
http://www.un-igrac.org/publications/329 (25/04/2012).

[19] World Health Organisation, Water, Sanitation and Hygiene Links to Health. Facts and Figures, (2004).
http://www.who.int/water_sanitation_health/factsfigures2005.pdf (25/04/2012).

[20] SBI Energy, Global Desalination Market will Grow 320.3 % by 2020, Driven by Reverse Osmosis, (2011).
http://www.sbireports.com/about/release.asp?id=2267 (25/04/2012).

[21] T.R. Green, M. Taniguchi, H. Kooi, J.J. Gurdak, D.M. Allen, K.M. Hiscock, H. Treidel, A. Aureli, Beneath the Surface of Global Change: Impacts of Climate Change on Groundwater, Journal of Hydrology, 405 (2011) 532-560.

[22] R.L. McGinnis, M. Elimelech, Global Challenges in Energy and Water Supply: The Promise of Engineered Osmosis, Environmental Science and Technology, 42 (2008) 8625-8629.

[23] E. Mathioulakis, V. Belessiotis, E. Delyannis, Desalination by using Alternative Energy: Review and State-of-the-Art, Desalination, 203 (2007) 346-365.

[24] J.M. Wellington, A.Y. Ku, Opportunities for Membranes in Sustainable Energy, Journal of Membrane Science, 373 (2011) 1-4.

[25] R.G. Raluy, L. Serra, J. Uche, Life Cycle Assessment of Desalination Technologies Integrated with Renewable Energies, Desalination, 183 (2005) 81-93.

[26] L.A. Richards, B.S. Richards, A.I. Schäfer, Renewable Energy Powered Membrane Technology: Salt and Inorganic Contaminant Removal by Nanofiltration/Reverse Osmosis, Journal of Membrane Science, 369 (2011) 188-195.

[27] M.A. Shannon, P.W. Bohn, M. Elimelech, J.G. Georgiadis, B.J. Marinas, A.M. Mayes, Science and Technology for Water Purification in the Coming Decades, Nature, 452 (2008) 301-310.

[28] M. Papapetrou, M. Wieghaus, C. Biercamp, Roadmap for the Development of Desalination Powered by Renewable Energy, ProDes Project: Promotion of Renewable Energy for Water Production through Desalination, Deliverable 2.2 (2010). http://www.prodes-project.org/index.php?id=45 (25/04/2012).

[29] L.F. Greenlee, D.F. Lawler, B.D. Freeman, B. Marrot, P. Moulin, Reverse Osmosis Desalination: Water Sources, Technology, and Today's Challenges, Water Research, 43 (2009) 2317-2348.

[30] C.C.K. Liu, Wind-Powered Reverse Osmosis Water Desalination for Pacific Islands and Remote Coastal Communities, Desalination and Water Purification Research and Development Program Report No.128, U.S. Department of the Interior (Bureau of Reclamation) (2009).

[31] M.A. Eltawil, Z. Zhengming, L. Yuan, A Review of Renewable Energy Technologies Integrated with Desalination Systems, Renewable and Sustainable Energy Reviews, 13 (2009) 2245-2262.

[32] G. Papadakis, E.S. Mohamed, D. Manolakos, Small Autonomous RO Desalination Systems Powered by Renewable Energies. Technological Advances and Economics, Solar Desalination for the 21st Century, Springer, (2007), pp. 293-303.

[33] R. Semiat, Energy Issues in Desalination Processes, Environmental Science and Technology, 42 (2008) 8193-8201.

[34] M. Werner, A.I. Schäfer, Social Aspects of a Solar-Powered Desalination Unit for Remote Australian Communities, Desalination, 203 (2007) 375-393.

[35] A. Subramani, M. Badruzzaman, J. Oppenheimer, J.G. Jacangelo, Energy Minimisation Strategies and Renewable Energy Utilisation for Desalination: A Review, Water Research, 45 (2011) 1907-1920.

[36] A.M. Bilton, R. Wiesman, A.F.M. Arif, S.M. Zubair, S. Dubowsky, On the Feasibility of Community-Scale Photovoltaic-Powered Reverse Osmosis Desalination Systems for Remote Locations, Renewable Energy, 36 (2011) 3246-3256.

[37] C. Catherine, A Review of Membrane Processes and Renewable Energies for Desalination, Desalination, 245 (2009) 214-231.

[38] C.T. Kiranoudis, N.G. Voros, Z.B. Maroulis, Wind Energy Exploitation for Reverse Osmosis Desalination Plants, Desalination, 109 (1997) 195-209.

[39] M.A. Alghoul, P. Poovanaesvaran, K. Sopian, M.Y. Sulaiman, Review of Brackish Water Reverse Osmosis (BWRO) System Designs, Renewable and Sustainable Energy Reviews, 13 (2009) 2661-2667.

[40] Q. Ma, H. Lu, Wind Energy Technologies Integrated with Desalination Systems: Review and State-of-the-Art, Desalination, 277 (2011) 274-280.

[41] S.A. Kalogirou, Seawater Desalination using Renewable Energy Sources, Progress in Energy and Combustion Science, 31 (2005) 242-281.

[42] M. Forstmeier, F. Mannerheim, F. D'Amato, M. Shah, Y. Liu, M. Baldea, A. Stella, Feasibility Study on Wind-Powered Desalination, Desalination, 203 (2007) 463-470.

[43] L. Garcia-Rodriguez, V. Romero-Ternero, C. Gomez-Camacho, Economic Analysis of Wind-Powered Desalination, Desalination, 137 (2001) 259-265.

[44] 3TIER, Global Mean Wind Speed Map at 80 m, 3TIER Resource Maps, (2011). http://www.3tier.com/en/support/resource-maps/ (25/04/2012).

[45] B. Van der Bruggen, C. Vandecasteele, Removal of Pollutants from Surface Water and Groundwater by Nanofiltration: Overview of Possible Applications in the Drinking Water Industry, Environmental Pollution, 122 (2003) 435-445.

[46] P. Eriksson, Nanofiltration Extends the Range of Membrane Filtration, Environmental Progress, 7 (1988) 58-62.

[47] E.M.V. Hoek, J. Allred, T. Knoell, B.-H. Jeong, Modeling the Effects of Fouling on Full-Scale Reverse Osmosis Processes, Journal of Membrane Science, 314 (2008) 33-49.

[48] D.R. Paul, Reformulation of the Solution-Diffusion Theory of Reverse Osmosis, Journal of Membrane Science, 241 (2004) 371-386.

[49] Dow Water and Process Solutions, FILMTEC Reverse Osmosis Membranes Technical Manual - Form No. 609-00071-1009, http://www.dowwaterandprocess.com/support_training/literature_manuals/prod_manuals.htm (25/04/2012).

[50] R.H. Perry, D.W. Green, Perry's Chemical Engineers' Handbook, McGraw Hill, New York, (1997).

[51] J. Schwinge, P.R. Neal, D.E. Wiley, D.F. Fletcher, A.G. Fane, Spiral Wound Modules and Spacers: Review and Analysis, Journal of Membrane Science, 242 (2004) 129-153.

[52] L. Song, J.Y. Hu, S.L. Ong, W.J. Ng, M. Elimelech, M. Wilf, Performance Limitation of the Full-Scale Reverse Osmosis Process, Journal of Membrane Science, 214 (2003) 239-244.

[53] M. Takeshi, Progress in Membrane Science and Technology for Seawater Desalination — A Review, Desalination, 134 (2001) 47-54.

[54] V. Yangali-Quintanilla, S.K. Maeng, T. Fujioka, M. Kennedy, G. Amy, Proposing Nanofiltration as Acceptable Barrier for Organic Contaminants in Water Reuse, Journal of Membrane Science, 362 (2010) 334-345.

[55] S. El-Manharawy, A. Hafez, Water Type and Guidelines for RO System Design, Desalination, 139 (2001) 97-113.

[56] A. Abderrahim, Simulation and Analysis of an Industrial Water Desalination Plant, Chemical Engineering and Processing: Process Intensification, 44 (2005) 999-1004.

[57] J.H. van't Hoff, The Function of Osmotic Pressure in the Analogy between Solutions and Gases, Proceedings of the Physical Society of London, 9 (1887) 307.

[58] R. Robinson, G. Ho, K. Mathew, Development of a Reliable Low-Cost Reverse Osmosis Desalination Unit for Remote Communities, Desalination, 86 (1992) 9-26.

[59] H. Klaus, Removal of Particles, Bacteria and Parasites with Ultrafiltration for Drinking Water Treatment, Desalination, 119 (1998) 85-91.

[60] A.I. Schäfer, A. Broeckmann, B.S. Richards, Renewable Energy Powered Membrane Technology. 1. Development and Characterisation of a Photovoltaic Hybrid Membrane System, Environmental Science and Technology, 41 (2007) 998-1003.

[61] C.A.C. van de Lisdonk, B.M. Rietman, S.G.J. Heijman, G.R. Sterk, J.C. Schippers, Prediction of Supersaturation and Monitoring of Scaling in Reverse Osmosis and Nanofiltration Membrane Systems, Desalination, 138 (2001) 259-270.

[62] W. Zhou, L. Song, T.K. Guan, A Numerical Study on Concentration Polarisation and System Performance of Spiral Wound RO Membrane Modules, Journal of Membrane Science, 271 (2006) 38-46.

[63] F. Macedonio, L. Katzir, N. Geisma, S. Simone, E. Drioli, J. Gilron, Wind-Aided Intensified eVaporation (WAIV) and Membrane Crystallizer (MCr) Integrated Brackish Water Desalination Process: Advantages and Drawbacks, Desalination, 273 (2011) 127-135.

[64] J. Gilron, Y. Folkman, R. Savliev, M. Waisman, O. Kedem, WAIV — Wind Aided Intensified Evaporation for Reduction of Desalination Brine Volume, Desalination, 158 (2003) 205-214.

[65] T. Ackermann, L. Söder, An Overview of Wind Energy-Status 2002, Renewable and Sustainable Energy Reviews, 6 (2002) 67-127.

[66] T. Burton, D. Sharpe, N. Jenkins, E. Bossanyi, Wind Energy Handbook, John Wiley & Sons Ltd, (2001).

[67] I. Van der Hoven, Power Spectrum of Horizontal Wind Speed in the Frequency Range from 0.0007 to 900 Cycles Per Hour, Journal of Meteorology, 14 (1957) 160-164.

[68] J. Peinke, S. Barth, F. Böttcher, D. Heinemann, B. Lange, Turbulence, A Challenging Problem for Wind Energy, Physica A: Statistical Mechanics and its Applications, 338 (2004) 187-193.

[69] P.A.B. James, M.F. Sissons, J. Bradford, L.E. Myers, A.S. Bahaj, A. Anwar, S. Green, Implications of the UK Field Trial of Building Mounted Horizontal Axis Micro-Wind Turbines, Energy Policy, 38 (2010) 6130-6144.

[70] The Microgeneration Certification Scheme, (2010).
http://www.microgenerationcertification.org/ (25/04/2012).

[71] Z. Maung, The Guardian, Feed-in Tariff 'Killing Off' Burgeoning UK Small Turbine Industry, Environment - Feed-in Tariffs, (2010).
http://www.guardian.co.uk/environment/2010/mar/10/feed-in-tariffs-turbine-solar (25/04/2012).

[72] K. De Decker, Real-World Tests of Small Wind Turbines in Netherlands and the UK, Energy Bulletin, (2010).
http://www.energybulletin.net/stories/2010-09-16/real-world-tests-small-wind-turbines-netherlands-and-uk (25/04/2012).

[73] Encraft, Microwind - A Catalyst for Change in UK Energy Culture?, Warwick Microwind Trial Project, (2009).
http://www.warwickwindtrials.org.uk/index.html (25/04/2012).

[74] ADU-RES, Co-ordination Action for Autonomous Desalination Units based on Renewable Energy Systems. WP-4: Cost Reduction Strategies, Report on Techno-Economic Performance and Cost Reduction Potential, (2006).
http://www.adu-res.org/ (25/04/2012).

[75] B.D. Vick, R.N. Clark, Determining the Optimum Solar Water Pumping System for Domestic Use, Livestock Watering or Irrigation, Proceedings of American Solar Energy Society, (2009). http://hdl.handle.net/10113/46008 (25/04/2012).

[76] G.R. Whitfield, J.D. Burton, Increasing the Cost-Effectiveness of Small Solar Photovoltaic Pumping Systems, Renewable Energy, 5 (1994) 342-344.

[77] C. Protogeropoulos, S. Pearce, Laboratory Evaluation and System Sizing Charts for a 'Second Generation' Direct PV-Powered, Low Cost Submersible Solar Pump, Solar Energy, 68 (2000) 453-474.

[78] B. Nesbitt, Pumping Manual International - Handbook of Pumps and Pumping, Elsevier, (2006).

[79] Mono Pumps Australia Pty. Ltd., Operating and Maintenance Instructions - Sun-Sub Solar Water Pumping Systems MPA573/5 (2002). http://www.monopumps.com.au/en-au/sunsub?productid=875 (25/04/2012).

[80] B.D. Vick, R.N. Clark, Experimental Investigation of Solar Powered Diaphragm and Helical Pumps, Solar Energy, 85 (2011) 945-954.

[81] D. Langridge, W. Lawrance, B. Wichert, Development of a Photovoltaic Pumping System using a Brushless D.C. Motor and Helical Rotor Pump, Solar Energy, 56 (1996) 151-160.

[82] J.S. Ramos, H.M. Ramos, Solar Powered Pumps to Supply Water for Rural or Isolated Zones: A Case Study, Energy for Sustainable Development, 13 (2009) 151-158.

[83] Engineering Diggest, Pumps: Centrifugal Pumps, (2011). http://engineeringdiggest.com/pumps/centrifugal-pumps/ (25/04/2012).

[84] B.D. Vick, R.N. Clark, Solar-PV Water Pumping with Fixed and Passive Tracking Panels, American Solar Energy Society, Reno, Nevada, (2002). http://www.ars.usda.gov/research/publications/publications.htm?seq_no_115=133920 (25/04/2012).

[85] N. Argaw, R. Foster, A. Ellis, Renewable Energy for Water Pumping Applications in Rural Villages, National Renewable Energy Laboratory, NREL/SR-500-30361, (2003). http://www.nrel.gov/docs/fy03osti/30361.pdf (25/04/2012).

[86] ADU-RES, Co-ordination Action for Autonomous Desalination Units Based on Renewable Energy Systems. WP-6: Further Development of Integrated Plant Design, Energy Consumption Modelling, (2006). http://www.adu-res.org/ (25/04/2012).

[87] J. Ayoub, R. Alward, Water Requirements and Remote Arid Areas: The Need for Small-Scale Desalination, Desalination, 107 (1996) 131-147.

[88] D. Infield, Performance Analysis of a Small Wind Powered Reverse Osmosis Plant, Solar Energy, 61 (1997) 415-421.

[89] E.S. Mohamed, G. Papadakis, Design, Simulation and Economic Analysis of a Stand-Alone Reverse Osmosis Desalination Unit Powered by Wind Turbines and Photovoltaics, Desalination, 164 (2004) 87-97.

[90] G. Petersen, S. Fries, J. Mohn, A. Muller, Wind and Solar Powered Reverse Osmosis Desalination Units - Design, Start up, Operating Experience, Desalination, 39 (1981) 125-135.

[91] E. Tzen, D. Theofilloyianakos, M. Sigalas, K. Karamanis, Design and Development of a Hybrid Autonomous System for Seawater Desalination, Desalination, 166 (2004) 267-274.

[92] D. Weiner, D. Fisher, E.J. Moses, B. Katz, G. Meron, Operation Experience of a Solar- and Wind-Powered Desalination Demonstration Plant, Desalination, 137 (2001) 7-13.

[93] C.C.K. Liu, P. Jae-Woo, R. Migita, Q. Gang, Experiments of a Prototype Wind-Driven Reverse Osmosis Desalination System with Feedback Control, Desalination, 150 (2002) 277-287.

[94] B.S. Richards, D.P.S. Capão, A.I. Schäfer, Renewable Energy Powered Membrane Technology. 2. The Effect of Energy Fluctuations on Performance of a Photovoltaic Hybrid Membrane System, Environmental Science and Technology, 42 (2008) 4563-4569.

[95] M. Thomson, M.S. Miranda, D. Infield, A Small-Scale Seawater Reverse-Osmosis System with Excellent Energy Efficiency over a Wide Operating Range, Desalination, 153 (2003) 229-236.

[96] P. Feron, The Use of Windpower in Autonomous Reverse Osmosis Seawater Desalination, Wind Engineering, 9 (1985) 180-199.

[97] R. Pohl, M. Kaltschmitt, R. Holländer, Investigation of Different Operational Strategies for the Variable Operation of a Simple Reverse Osmosis Unit, Desalination, 249 (2009) 1280-1287.

[98] E.R. Lising, R. Alward, Unsteady State Operation of a Reverse-Osmosis Desalination Unit, Desalination, 11 (1972) 261-268.

[99] F. Moreno, A. Pinilla, Preliminary Experimental Study of a Small Reverse Osmosis Wind-Powered Desalination Plant, Desalination, 171 (2005) 257-265.

[100] I. de la Nuez Pestana, F. Javier Garcia Latorre, C. Argudo Espinoza, A. Gomez Gotor, Optimisation of RO Desalination Systems Powered by Renewable Energies. Part I: Wind Energy, Desalination, 160 (2004) 293-299.

[101] M.S. Miranda, D. Infield, A Wind-Powered Seawater Reverse-Osmosis System Without Batteries, Desalination, 153 (2003) 9-16.

[102] S.G.J. Heijman, E. Rabinovitch, F. Bos, N. Olthof, J.C. van Dijk, Sustainable Seawater Desalination: Stand-Alone Small Scale Windmill and Reverse Osmosis System, Desalination, 248 (2009) 114-117.

[103] J.A. Carta, J. Gonzalez, V. Subiela, The SDAWES Project: An Ambitious R&D Prototype for Wind-Powered Desalination, Desalination, 161 (2004) 33-48.

[104] J.A. Carta, J. Gonzalez, V. Subiela, Operational Analysis of an Innovative Wind Powered Reverse Osmosis System Installed in the Canary Islands, Solar Energy, 75 (2003) 153-168.

[105] V.J. Subiela, J.A. Carta, J. Gonzalez, The SDAWES Project: Lessons Learnt from an Innovative Project, Desalination, 168 (2004) 39-47.

[106] E. Rabinovitch, Drinking with the Wind: Small Scale SWRO-Installation Mechanically Driven by Wind Energy, MSc Thesis, Delft University of Technology, (2008). http://citg.tudelft.nl/index.php?id=20829&L=1 (25/04/2012).

[107] M.S. Miranda, Small-scale Wind-Powered Seawater Desalination Without Batteries, PhD Thesis, Loughborough University, (2003). http://staff.bath.ac.uk/eesmm/Marcos%20Miranda%20Thesis.pdf (25/04/2012).

[108] K. Paulsen, F. Hensel, Design of an Autarkic Water and Energy Supply Driven by Renewable Energy using Commercially Available Components, Desalination, 203 (2007) 455-462.

[109] A. Ghermandi, R. Messalem, Solar-Driven Desalination with Reverse Omosis: The State of the Art, Desalination and Water Treatment, 7 (2009) 285-296.

[110] H.M.A. Rossiter, P.A. Owusu, E. Awuah, A.M. MacDonald, A.I. Schäfer, Chemical Drinking Water Quality in Ghana: Water Costs and Scope for Advanced Treatment, Science of The Total Environment, 408 (2010) 2378-2386.

[111] M. Thomson, D. Infield, A Photovoltaic-Powered Seawater Reverse-Osmosis System Without Batteries, Desalination, 153 (2003) 1-8.

[112] E. Tzen, D. Theofilloyianakos, Z. Kologios, Autonomous Reverse Osmosis Units Driven by RE Sources Experiences and Lessons Learned, Desalination, 221 (2008) 29-36.

[113] J.F. Manwell, Wind Energy Explained: Theory, Design and Application, John Wiley & Sons Ltd, (2002).

[114] Dow Water and Process Solutions, Membrane datasheet Filmtec BW30-4040. http://www.dowwaterandprocess.com/products/membranes/bw30_4040.htm (25/04/2012).

[115] Z. Rahal, D.G. Infield, Wind Powered Stand Alone Desalination, European Wind Energy Conference, Dublin Castle, Ireland, (1997), pp. 802-806.

[116] R. McBride, R. Morris, W. Hanbury, Wind Power A Reliable Source for Desalination, Desalination, 67 (1987) 559-564.

[117] M. Thomson, D. Infield, Laboratory Demonstration of a Photovoltaic-Powered Seawater Reverse-Osmosis System Without Batteries, Desalination, 183 (2005) 105-111.

[118] W. Gocht, A. Sommerfeld, R. Rautenbach, T. Melin, L. Eilers, A. Neskakis, D. Herold, V. Horstmann, M. Kabariti, A. Muhaidat, Decentralised Desalination of Brackish Water by a Directly Coupled Reverse-Osmosis-Photovoltaic-System - A Pilot Plant Study in Jordan, Renewable Energy, 14 (1998) 287-292.

[119] H.B. Winzeler, G. Belfort, Enhanced Performance for Pressure-Driven Membrane Processes: The Argument for Fluid Instabilities, Journal of Membrane Science, 80 (1993) 35-47.

[120] N. Al-Bastaki, A. Abbas, Use of Fluid Instabilities to Enhance Membrane Performance: A Review, Desalination, 136 (2001) 255-262.

[121] N.M. Al-Bastaki, A. Abbas, Periodic Operation of a Reverse Osmosis Water Desalination Unit, Separation Science and Technology, 33 (1998) 2531 - 2540.

[122] E. Godin, D. Broad, How to Deal with Pre-Charge Loss in Bladder Accumulators Due to Gas Permeation, Hydraulic Accumulator Division - Parker Hannifin Corporation, (2007). http://www.parker.com/literature/Hydraulic%20Accumulator/News%20Releases/Bladder_Accum_-_Gas_Permeation.pdf (25/04/2012).

[123] S.V. Angadi, R.L. Jackson, S.-y. Choe, G.T. Flowers, J.C. Suhling, Y.-K. Chang, J.-K. Ham, J.-i. Bae, Reliability and Life Study of Hydraulic Solenoid Valve. Part 2: Experimental Study, Engineering Failure Analysis, 16 (2009) 944-963.

[124] B.G. Keefer, R.D. Hembree, F.C. Schrack, Optimised Matching of Solar Photovoltaic Power with Reverse Osmosis Desalination, Desalination, 54 (1985) 89-103.

[125] K. Paulsen, F. Hensel, Introduction of a New Energy Recovery System - Optimised for the Combination with Renewable Energy, Desalination, 184 (2005) 211-215.

[126] S. Dallas, N. Sumiyoshi, J. Kirk, K. Mathew, N. Wilmot, Efficiency Analysis of the Solarflow – An Innovative Solar-Powered Desalination Unit for Treating Brackish Water, Renewable Energy, 34 (2009) 397-400.

[127] A.M. Thomson, Reverse-Osmosis Desalination of Seawater Powered by Photovoltaics Without Batteries, PhD Thesis, Loughborough University, (2003). http://www-staff.lboro.ac.uk/~elmt/Murray%20Thomson%20Thesis.pdf (25/04/2012).

[128] K. Mathew, S. Dallas, G.E. Ho, M. Anda, Chapter 439 - A Solar-Powered Village Water Supply System from Brackish Water, World Renewable Energy Congress VI, Pergamon, Oxford, (2000), pp. 2061-2064.

[129] D.G Infield, An Overview of Renewable Energy Technologies with a View to Stand Alone Power Generation and Water Provision, Desalination, 248 (2009) 494-499.

[130] M. Perrin, Y.M. Saint-Drenan, F. Mattera, P. Malbranche, Lead-Acid Batteries in Stationary Applications: Competitors and New Markets for Large Penetration of Renewable Energies, Journal of Power Sources, 144 (2005) 402-410.

[131] B. Willer, Investigation on Storage Technologies for Intermittent Renewable Energies: Evaluation and Recommended R&D Strategy. Supercaps Report, INVESTIRE NETWORK, Deliverable No. 5 (ENK5-CT-2000-20336) (2003).

[132] Y. Kim, N. Chang, Y. Wang, M. Pedram, Maximum Power Transfer Tracking for a Photovoltaic-Supercapacitor Energy System, ACM/IEEE International Symposium on Low-Power Electronics and Design, ISLPED (2010).

[133] I. Hadjipaschalis, A. Poullikkas, V. Efthimiou, Overview of Current and Future Energy Storage Technologies for Electric Power Applications, Renewable and Sustainable Energy Reviews, 13 (2009) 1513-1522.

[134] M. Beaudin, H. Zareipour, A. Schellenberglabe, W. Rosehart, Energy Storage for Mitigating the Variability of Renewable Electricity Sources: An Updated Review, Energy for Sustainable Development, 14 (2010) 302-314.

[135] M.E. Glavin, P.K.W. Chan, S. Armstrong, W.G. Hurley, A Stand-Alone Photovoltaic Supercapacitor Battery Hybrid Energy Storage System, 13th Power Electronics and Motion Control Conference, EPE-PEMC (2008), pp. 1688-1695.

[136] P.J. Hall, E.J. Bain, Energy-Storage Technologies and Electricity Generation, Energy Policy, 36 (2008) 4352-4355.

[137] P.D. Lund, J.V. Paatero, Energy Storage Options for Improving Wind Power Quality, Nordic Wind Power Conference, Espoo, Finland (2006).

[138] Maxwell Technologies, Maxwell BOOSTCAP Ultracapacitors - Small Module Technical Papers. http://www.maxwell.com/products/ultracapacitors/ (25/04/2012).

[139] C. Abbey, G. Joos, Supercapacitor Energy Storage for Wind Energy Applications, IEEE Transactions on Industry Applications, 43 (2007) 769-776.

[140] A. Burke, R&D Considerations for the Performance and Application of Electrochemical Capacitors, Electrochimica Acta, 53 (2007) 1083-1091.

[141] Z. Yun, Z. Jiancheng, L. Gengyin, L. Aiguo, Research on Energy Efficiency of Supercapacitor Energy Storage System, International Conference on Power System Technology, PowerCon (2006), pp. 1-4.

[142] J.P. Barton, D.G. Infield, Energy Storage and its Use with Intermittent Renewable Energy, IEEE Transactions on Energy Conversion, 19 (2004) 441-448.

[143] W. Henson, Optimal Battery/Ultracapacitor Storage Combination, Journal of Power Sources, 179 (2008) 417-423.

[144] H. Bludszuweit, J.M. Fandos, J.A. Domínguez, A. Llombart, J. Sanz, Simulation of a Hybrid System Wind Turbine - Battery - Ultracapacitor, ICREPQ, Zaragoza, Spain (2005).

[145] S.Y. Kan, M. Verwaal, H. Broekhuizen, The Use of Battery-Capacitor Combinations in Photovoltaic Powered Products, Journal of Power Sources, 162 (2006) 971-974.

[146] A.M. van Voorden, L.M.R. Elizondo, G.C. Paap, J. Verboomen, L. van der Sluis, The Application of Supercapacitors to Relieve Battery-Storage Systems in Autonomous Renewable Energy Systems, Power Tech, IEEE Lausanne (2007), pp. 479-484.

[147] D.B. Murray, M.G. Egan, J.G. Hayes, D.L. O'Sullivan, Applications of Supercapacitor Energy Storage for a Wave Energy Converter System, 8th European Wave and Tidal Energy Conference, Uppsala, Sweden (2009).

[148] S. Breban, M. Nasser, A. Vergnol, B. Robyns, M.M. Radulescu, Hybrid Wind/Microhydro Power System Associated with a Supercapacitor Energy Storage Device - Experimental Results, 18th International Conference on Electrical Machines, ICEM (2008).

[149] M. Nitta, S. Hashimoto, N. Sekiguchi, Y. Kouchi, T. Yachi, T. Tani, Experimental Study for Wind Power - Hydrogen Energy System with Energy Capacitor System, The 25th International Telecommunications Energy Conference, INTELEC (2003), pp. 451-456.

[150] Omega, Low Flow Turbine Meters - FTB 9500 Series. http://www.omega.com/toc_asp/frameset.html?book=Green&file=FTB9500&flag=1 (25/04/2012).

[151] G. Fischer, Signet 2818-2823 Conductivity/Resistivity Electrodes. http://www.gfsignet.com/go/BB04361419993E1D4BD2044DF9B3C872 (25/04/2012).

[152] Burkert, 8323 Pressure Transmitter for General Applications, 0-25 bar. http://www.burkert.co.uk/ENG/buerkert_datasheets.php?type=8323 (25/04/2012).

[153] Omega, DC and AC Voltage Input Signal Conditioners. http://www.omega.co.uk/ppt/pptsc.asp?ref=DRF-VDC_VAC&flag=1 (25/04/2012).

[154] Omega, DC and AC Current Input Signal Conditioners. http://www.omega.co.uk/ppt/pptsc.asp?ref=DRF-IDC_IAC&flag=1 (25/04/2012).

[155] G. Fischer, Signet 2714-2717 Twist-Lock ph/ORP Electrodes. http://www.gfsignet.com/go/002767CA2557B9318F4A42E9766B40E7 (25/04/2012).

[156] Omega, Molded Thermocouple Transition Joint Probes with PFA Insulated Wire. http://www.omega.co.uk/ppt/pptsc.asp?ref=KTSS_JTSS_chb&flag=1 (25/04/2012).

[157] B.S. Richards, A.I. Schäfer, Photovoltaic-Powered Desalination System for Remote Australian Communities, Renewable Energy, 28 (2003) 2013-2022.

[158] A.I. Schäfer, C. Remy, B.S. Richards, Performance of a Small Solar-Powered Hybrid Membrane System for Remote Communities Under Varying Feed water Salinities, Water Science and Technology: Water Supply, 4 (2004) 233-243.

[159] R.C. Heath, Basic Ground-Water Hydrology, U.S. Geological Survey Water-Supply Paper 2220, (1983).

[160] G.R. Garbarini, R.F. Eaton, T.K. Kwei, A.V. Tobolsb, Diffusion and Reverse Osmosis Through Polymer Membranes, Journal of Chemical Education, 48 (1971) 226.

[161] M. Mulder, Basic Principles of Membrane Technology, Kluwer Academic Publishers, (1996).

[162] A.S. Michaels, New Separation Technique for the Chemical Process Industries, Chemical Engineering Progress, 64 (1968) 31-43.

[163] I. Sutzkover, D. Hasson, R. Semiat, Simple Technique for Measuring the Concentration Polarization Level in a Reverse Osmosis System, Desalination, 131 (2000) 117-127.

[164] S. Kim, E.M.V. Hoek, Modeling Concentration Polarization in Reverse Osmosis Processes, Desalination, 186 (2005) 111-128.

[165] S.S. Sablani, M.F.A. Goosen, R. Al-Belushi, M. Wilf, Concentration Polarization in Ultrafiltration and Reverse Osmosis: A Critical Review, Desalination, 141 (2001) 269-289.

[166] Integrated Social Development Centre, Report of the International Fact-Finding Mission on Water Sector Reform in Ghana, (2002).
http://cesr.org/downloads/factfindingmissionGhana.pdf (25/04/2012).

[167] P.L. Smedley, Arsenic in Rural Groundwater in Ghana : Part Special Issue: Hydrogeochemical Studies in Sub-Saharan Africa, Journal of African Earth Sciences, 22 (1996) 459-470.

[168] A.I. Schäfer, Physio-Chemical Water Quality in Ghana: Prospects for Water Supply Technology Implemenation, Proceedings of 'Water and Sanitation in International Development and Disaster Relief', Edinburgh, Scotland, 2008, pp. 213-223.

[169] Solar Energy Centre Denmark, Ghanaian Weather Data for Simulation Purposes, (2001). http://www.solenergi.dk/SEC/rapporter/sec-r-5.pdf (25/04/2012).

[170] Intelligent Energy Europe Programme, Catalogue of European Urban Wind Turbine Manufacturer's.
http://www.urbanwind.net/pdf/CATALOGUE_V2.pdf (25/04/2012).

[171] FutureEnergy Ltd, Wind Turbine Performance Data for 48 V 1 kW Upwind Turbine (2008).
http://www.futurenergy.co.uk/pdf_doc/FE1048U%20(408).pdf (25/04/2012).

[172] International Electrotechnical Commission, IEC 61400-12-1 Wind Turbines: Power Performance Measurements of Electricity Producing Wind Turbines, Geneva, Switzerland, (2005).

[173] W. Irshad, G. Keng, J. Kubie, Wind Resource Assessment in the Edinburgh Region, World Non-Grid-Connected Wind Power and Energy Conference, (2009), pp. 1-5.

[174] Vector Instruments, A100L2 Low Power Anemometer.
http://www.windspeed.co.uk/ws/index.php?option=displaypage&Itemid=49&op=page&SubMenu (25/04/2012).

[175] Vector Instruments, W200P Potentiometer Windvane.
http://www.windspeed.co.uk/ws/index.php?option=displaypage&op=page&Itemid=61#downloads (25/04/2012).

[176] Powertek, DC Current Sensors, Current Transducers, Current Probes.
http://www.powertekuk.com/dcasensor.htm (25/04/2012).

[177] Campbell Scientific, CS100 Barometric Pressure Sensor.
http://www.campbellsci.com/cs100 (25/04/2012).

[178] Campbell Scientific, HMP50 Temperature and Relative Humidity Probe.
ftp://ftp.campbellsci.com/pub/csl/outgoing/uk/leaflets/hmp50.pdf (25/04/2012).

[179] S. Reid, Reductions of Power Fluctuations in a Small Wind Turbine, MEng Thesis, School of Engineering and Physical Sciences, Heriot-Watt University, Edinburgh, (2010).

[180] K. Bradbury, Energy Storage Technology Review, Duke University, Durham, North Carolina (2010).
http://www.duke.edu/~kjb17/tutorials/Energy_Storage_Technologies.pdf (25/04/2012).

[181] S.M. Schoenung, W.V. Hassenzahl, Long- vs. Short-Term Energy Storage Technologies Analysis. A Life-cycle Cost Study for the DOE Energy Storage Systems Program, Sandia National Laboratories Report, SAND2003-2783 (2003).
http://prod.sandia.gov/techlib/access-control.cgi/2003/032783.pdf (25/04/2012).

[182] Maxwell Technologies, Product Guide - Maxwell Technologies BOOSTCAP Ultracapacitors - Doc. No. 10146271 (2009).
http://about.maxwell.com/pdf/1014627_BOOSTCAP_Product_Guide.pdf (25/04/2012).

[183] O.C. Onar, M. Uzunoglu, M.S. Alam, Modeling, Control and Simulation of an Autonomous Wind Turbine/Photovoltaic/Fuel Cell/Ultra-Capacitor Hybrid Power System, Journal of Power Sources, 185 (2008) 1273-1283.

[184] J.V. Paatero, P.D. Lund, Effect of Energy Storage on Variations in Wind Power, Wind Energy, 8 (2005) 421-441.

[185] Maxwell Technologies, Cell Balancing in Low Duty Cycle Applications.
http://www.maxwell.com/products/ultracapacitors/docs/AN-002_CELL_BALANCING.PDF (25/04/2012).

[186] Maxwell Technologies, BOOSTCAP Energy Storage Modules. User Manual for 15 V Modules (2007).
http://about.maxwell.com/pdf/uc/manuals/1007108.7_UserManual_15V.pdf (25/04/2012).

[187] Maxwell Technologies, Data Sheet for BPAK Energy Series 15V BOOSTCAP Ultracapacitors.
http://www.tecategroup.com/capacitors/datasheets/maxwell/archive/BPAK0058-15V.pdf (25/04/2012).

[188] Maxwell Technologies, How to Determine the Appropriate Size Ultracapacitor for Your Application - Doc. No. 1007236 Rev 2 (2004).
http://files.energiatehnika.ee/Datasheets/Maxwell_General_Sizing.pdf (25/04/2012).

[189] Maxwell Technologies, Charging of Ultracapacitors - Document 1008981. http://www.maxwell.com/docs/AN-010_CHARGING_ULTRACAPS.PDF (25/04/2012).

[190] A. Rosen, Y. Sheinman, The Power Fluctuations of a Wind Turbine, Journal of Wind Engineering and Industrial Aerodynamics, 59 (1996) 51-68.

[191] L. Masson, B.S. Richards, A.I. Schäfer, System Design and Performance Testing of a Hybrid Membrane -- Photovoltaic Desalination System, Desalination, 179 (2005) 51-59.

[192] M.F.A. Goosen, S.S. Sablani, S.S. Al-Maskari, R.H. Al-Belushi, M. Wilf, Effect of Feed Temperature on Permeate Flux and Mass Transfer Coefficient in Spiral-Wound Reverse Osmosis Systems, Desalination, 144 (2002) 367-372.

[193] A. Joyce, D. Loureiro, C. Rodrigues, S. Castro, Small Reverse Osmosis Units using PV Systems for Water Purification in Rural Places, Desalination, 137 (2001) 39-44.

[194] Z. Al Suleimani, V.R. Nair, Desalination by Solar-Powered Reverse Osmosis in a Remote Area of the Sultanate of Oman, Applied Energy, 65 (2000) 367-380.

[195] E. Badreddin, A. Gambier, F. Aboul-Fotouh, Laboratory Set-Up for Education and Research on Automation of Reverse Osmosis Plants Employing a Sustainable Energy Source, Desalination, 166 (2004) 307-314.

[196] J.A. Redondo, Brackish-, Sea- and Wastewater Desalination, Desalination, 138 (2001) 29-40.

[197] Delabole Windfarm, Delabole Windfarm: The First Commercial Windfarm in the United Kingdom, (2010). http://www.delabole.com/windfarm.html (25/04/2012).

[198] H.A. Cope, A.I. Schäfer, Renewable Energy Powered Membrane Technology: A Leapfrog Approach to Rural Water Supply Technologies in Developing Countries?, (In Preparation), (2011).